CRCLEME
Cooperative Research Centre for Landscape Evolution & Mineral Exploration

CSIRO
EXPLORATION AND MINING

AMIRA
Australian Mineral Industries Research Association Limited ACN 004 448 266

OPEN FILE REPORT SERIES

REGOLITH-LANDFORM DEVELOPMENT AND CONSEQUENCES ON THE MINERALOGICAL AND GEOCHEMICAL CHARACTERISTICS OF REGOLITH UNITS, LAWLERS DISTRICT WESTERN AUSTRALIA

R.R Anand, H.M. Churchward, R.E. Smith and E.C. Grunsky

CRC LEME OPEN FILE REPORT 62

November 1998

(CSIRO Division of Exploration Geoscience Report 166R, 1991. Second impression 1998)

CRC LEME is an unincorporated joint venture between The Australian National University, University of Canberra, Australian Geological Survey Organisation and CSIRO Exploration and Mining, established and supported under the Australian Government's Cooperative Research Centres Program.

CRC AUSTRALIA

REGOLITH-LANDFORM DEVELOPMENT AND CONSEQUENCES ON THE MINERALOGICAL AND GEOCHEMICAL CHARACTERISTICS OF REGOLITH UNITS, LAWLERS DISTRICT WESTERN AUSTRALIA

R.R Anand, H.M. Churchward, R.E. Smith and E.C. Grunsky

CRC LEME OPEN FILE REPORT 62

November 1998

(CSIRO Division of Exploration Geoscience Report 166R, 1991.
Second impression 1998)

CRC LEME is an unincorporated joint venture between The Australian National University,
University of Canberra, Australian Geological Survey Organisation and CSIRO Exploration and Mining
Headquarters: CRC LEME c/o CSIRO Exploration and Mining, Private Bag, PO Wembley, Western Australia, 6014

RESEARCH ARISING FROM CSIRO/AMIRA REGOLITH GEOCHEMISTRY PROJECTS 1987-1993

In 1987, CSIRO commenced a series of multi-client research projects in regolith geology and geochemistry which were sponsored by companies in the Australian mining industry, through the Australian Mineral Industries Research Association Limited (AMIRA). The initial research program, "Exploration for concealed gold deposits, Yilgarn Block, Western Australia" (1987-1993) had the aim of developing improved geological, geochemical and geophysical methods for mineral exploration that would facilitate the location of blind, buried or deeply weathered gold deposits. The program included the following projects:

P240: Laterite geochemistry for detecting concealed mineral deposits (1987-1991). Leader: Dr R.E. Smith. Its scope was development of methods for sampling and interpretation of multi-element laterite geochemistry data and application of multi-element techniques to gold and polymetallic mineral exploration in weathered terrain. The project emphasised viewing laterite geochemical dispersion patterns in their regolith-landform context at local and district scales. It was supported by 30 companies.

P241: Gold and associated elements in the regolith - dispersion processes and implications for exploration (1987-1991). Leader: Dr C.R.M. Butt. The project investigated the distribution of ore and indicator elements in the regolith. It included studies of the mineralogical and geochemical characteristics of weathered ore deposits and wall rocks, and the chemical controls on element dispersion and concentration during regolith evolution. This was to increase the effectiveness of geochemical exploration in weathered terrain through improved understanding of weathering processes. It was supported by 26 companies.

These projects represented "an opportunity for the mineral industry to participate in a multi-disciplinary program of geoscience research aimed at developing new geological, geochemical and geophysical methods for exploration in deeply weathered Archaean terrains". This initiative recognised the unique opportunities, created by exploration and open-cut mining, to conduct detailed studies of the weathered zone, with particular emphasis on the near-surface expression of gold mineralisation. The skills of existing and specially recruited research staff from the Floreat Park and North Ryde laboratories (of the then Divisions of Minerals and Geochemistry, and Mineral Physics and Mineralogy, subsequently Exploration Geoscience and later Exploration and Mining) were integrated to form a task force with expertise in geology, mineralogy, geochemistry and geophysics. Several staff participated in more than one project. Following completion of the original projects, two continuation projects were developed.

P240A: Geochemical exploration in complex lateritic environments of the Yilgarn Craton, Western Australia (1991-1993). Leaders: Drs R.E. Smith and R.R. Anand. The approach of viewing geochemical dispersion within a well-controlled and well-understood regolith-landform and bedrock framework at detailed and district scales continued. In this extension, focus was particularly on areas of transported cover and on more complex lateritic environments typified by the Kalgoorlie regional study. This was supported by 17 companies.

P241A: Gold and associated elements in the regolith - dispersion processes and implications for exploration. Leader: Dr. C.R.M. Butt. The significance of gold mobilisation under present-day conditions, particularly the important relationship with pedogenic carbonate, was investigated further. In addition, attention was focussed on the recognition of primary lithologies from their weathered equivalents. This project was supported by 14 companies.

Although the confidentiality periods of the research reports have expired, the last in December 1994, they have not been made public until now. Publishing the reports through the CRC LEME Report Series is seen as an appropriate means of doing this. By making available the results of the research and the authors' interpretations, it is hoped that the reports will provide source data for future research and be useful for teaching. CRC LEME acknowledges the Australian Mineral Industries Research Association and CSIRO Division of Exploration and Mining for authorisation to publish these reports. It is intended that publication of the reports will be a substantial additional factor in transferring technology to aid the Australian Mineral Industry.

This report (CRC LEME Open File Report 62) is a Second impression (second printing) of CSIRO, Division of Exploration Geoscience Restricted Report 166R, first issued in 1991, which formed part of the CSIRO/AMIRA Project P240.

Copies of this publication can be obtained from:
The Publication Officer, c/- CRC LEME, CSIRO Exploration and Mining, PMB, Wembley, WA 6014, Australia. Information on other publications in this series may be obtained from the above or from http://leme.anu.edu.au/

Cataloguing-in-Publication:

Regolith-landform development and consequences on the mineralogical and geochemical characteristics of regolith units, Lawlers District, Western Australia
ISBN 0 642 28267 6
1. Geochemistry - Western Australia 2. Weathering 3. Laterites
I. Anand, R.R. II. Title
CRC LEME Open File Report 62.
ISSN 1329-4768

EXECUTIVE SUMMARY

Regolith-landform Relationships

The regolith patterns observed in the Lawlers district are explained in terms of the distribution of (a) regimes of erosion of the laterite profile to the level of saprolite/saprock/bedrock resulting in terrain characterized by low hills, (b) regimes where the essentially-complete laterite profile is preserved, commonly forming gentle ridge crests and backslopes, and (c) regimes characterized by depositional accumulations of detritus derived by erosion of the laterite profile, burying the partly-truncated, and in places complete, laterite profile in the lower slopes of colluvial/alluvial outwash plains. In the depositional areas, the sediments reach up to 30 m in thickness. It is now well established that buried residual laterite profiles are widespread beneath the colluvium and alluvium.

Studies in three type areas (the Agnew-McCaffery, Meatoa, and Brilliant areas) provide an understanding of regolith relationships, regolith stratigraphy, and the origin of regolith units. Criteria are established for distinguishing residual regolith from transported regolith applicable to drill hole logging. A regolith-landform model for the Lawlers district presents relationships in terms of erosion and burial of complete and partly-truncated lateritic profiles.

Soils

The soils occurring within those truncated regimes which have mafic or ultramafic bedrock lithologies are predominantly red-coloured light clays and red sandy clay loams. They are often acidic and commonly are underlain by a red-brown hardpan. The red clays often contain pseudomorphic grains after amphiboles, further evidence of their mafic origin. The occurrence of pedogenic calcrete at shallow depths in the erosional regimes generally relates to a mafic lithology. Soils on felsic lithologies are acidic, yellowish-brown, sandy loams. Residual regimes are dominated by acidic, brown gravelly sandy loams and sandy clay loams and generally red-brown hardpan is not developed. The soils within the depositional regimes are developed in colluvium/alluvium and are acidic, gravelly sandy clay loams and light clays.

Lags

The distribution and characteristics of lag gravels have been placed within the regolith-landform framework established during this study. Black, ferruginous cobbles of iron segregations, fragments of ferruginous saprolite, and vein quartz occur largely on erosional areas (Units 2a, 2b). Lag of lateritic pisoliths and nodules occurs on residual areas (Units 1a, 1b) overlying complete or nearly-complete laterite profiles. The lag of mixed origin comprising lithic fragments, quartz, lateritic pisoliths and nodules, and fragments of ferruginous saprolite is abundant on colluvial/alluvial outwash plains.

Lateritic residuum

The top of the residual laterite profile is composed of a layer of lateritic residuum averaging some 3 to 8 m in thickness comprising a sub-unit of loose pisoliths and nodules which may be underlain by a sub-unit of nodular duricrust. A zone of ferruginous saprolite characterized by bodies of iron segregations generally underlies the lateritic residuum. It is established that ferruginous saprolite forms a blanket deposit up to several metres thick in many areas in the Lawlers district and is preferentially developed over mafic and ultramafic lithologies. In turn, ferruginous saprolite grades into a thick saprolite zone, which extends to vertical depths of 50 to 70 m.

Development of many nodules and pisoliths in lateritic residuum is associated with fragmentation of ferruginous saprolite. Fragmentation of bodies of iron segregations can also yield nodules and pisoliths which become incorporated within the lateritic residuum.

Investigation suggests that the Fe-rich duricrusts are probably formed by absolute accumulation of Fe. One possible explanation is that Fe originally impregnated the soils/sediments in local valleys which now occur as ridge crests in the present landscape because of inversion of relief.

Hardpan

At Lawlers, hardpan has developed within *in situ* regolith and detritus resulting from the erosional modification of the old surface. Cementation of these materials by Si and Fe to form the hardpan is a relatively recent process.

Discrimination between sample types

The 181 samples collected from the McCaffery-North Pit area were separated into four broad groups based mainly upon their morphological characteristics and regolith-landform framework. These include materials from both surface and sub-surface units of the weathering profiles. The four groups recognized are: colluvium, lateritic residuum, ferruginous saprolite, and iron segregations. These four groups are shown to have different morphological, mineralogical, and geochemical characteristics. Iron segregations can be recognized by their irregular, black, non-magnetic pitted surfaces. Internal surfaces of iron segregations may show goethite/hematite pseudomorphs after sulphides. Lateritic pisoliths/nodules of lateritic residuum typically have 1 to 2-mm thick yellowish-brown/greenish cutans around black/red nuclei. The presence of cutans may be used to recognize nodules and pisoliths derived from the breakdown of lateritic residuum.

Mineralogy has been shown to give valuable information concerning which part of the weathering profile is exposed at the surface. Iron segregations differ from lateritic residuum by having abundant goethite and less hematite and kaolinite. Maghemite is typically absent in iron segregations. Lateritic residuum can be distinguished from ferruginous saprolite by having abundant hematite and less kaolinite. Colluvium differs from the other groups in having abundant quartz, kaolinite, and some heavy minerals.

The four sample media also show differences in the degree of Al-substitution in goethite which appears to be related to the maturity of the regolith, level of truncation, and may also reflect the environments in which the particular regolith unit has formed. Evaluation and identification of various sample media by the degree of Al substitution in goethite looks to be very promising.

Iron segregations are dominated by Fe_2O_3, Mn, Zn, Co, Ba, and goethite and these elements can be used to discriminate iron segregations from lateritic residuum, ferruginous saprolite, and colluvium. Many of the chalcophile elements and Au exhibit lower levels of abundances to those in lateritic residuum and ferruginous saprolite. However, the prominent regional distribution of iron segregations, often as scree on pediment surfaces in partly-stripped profiles, offers potential for use as a geochemical sampling medium.

Whilst the Fe_2O_3 contents of the ferruginous saprolite are comparable with those of the lateritic residuum, there are strong geochemical distinctions between the two types. Lateritic residuum has relatively-higher levels of Cr, V, Ni, As, and Pb. Conversely, ferruginous saprolite carries significantly-higher levels of Cu, Sb, Bi, and Au. The concentrations of SiO_2, MgO, TiO_2, Zr, and Nb are higher in colluvium than in lateritic residuum and ferruginous saprolite. These differences may be due to the degree of weathering, mineralization, mechanism of accumulation of the secondary weathering products, and origin.

The group separation using canonical variate analysis and all possible-subset calculations has indicated that effective separation of the four sampling media exists. A combination of 14 elements (Fe, Mn, Cr, V, Pb, Zn, Ni, Co, As, Sb, Bi, W, Zr, Nb) would seem to be the most useful for separation of the groups.

Siting and bonding of elements

Gold in lateritic nodules from the North Pit location occurs as (i) grains up to 15 μm in diameter, occurring in cracks, and (ii) relatively large dendritic Au grains, which reach 70 μm in diameter, attached to the surface of goethite. Both occurrences of Au appear to be secondary and are almost free from Ag ($<1\%$ Ag). In the lateritic nodules, As and Mn are strongly associated with Fe oxides, while Cu is associated with kaolinite.

CONTENTS

1.0 PROJECT LEADER'S PREFACE

R E Smith, 31 May 1991

The Lawlers district, an area of some 500 km^2, was chosen, for reasons given below, as the fourth in a series of multi-disciplinary district-scale orientation studies which form the foundations of the CSIRO/AMIRA Laterite Geochemistry Project. The other studies of this type are at Boddington, Mt. Gibson, and Bottle Creek. These studies focus on Au deposits in differing lateritic regolith-landform situations, covering a range of climatic types and geographic locations.

The Lawlers district exemplifies some important exploration problems in the Yilgarn Block and particularly in the Norseman-Wiluna Belt, namely exploration of extensive gravelly alluvial and colluvial plains and the associated partly-truncated uplands which are commonly characterized by cobbly ferruginous rubble.

The Lawlers district provides a type example for regolith relationships and regolith stratigraphy where uplands represent truncated lateritic profiles and are coupled with extensive plains where laterite profiles are buried beneath transported, sedimentary sequences reaching tens of metres in thickness. The sparse vegetation accompanying the arid climate allows us to see and interpret processes of regolith and landscape evolution not possible in thickly-vegetated, high-rainfall regions.

Because of the attributes of the area (Section 2.3) and the research and exploration carried out to date, it is likely that the Lawlers district will be used as a training ground for research into exploration methods for some time. Particularly relevant will be the testing of airborne geophysical methods and remote sensing. The Lawlers district also provides excellent opportunities for training explorationists in regolith geology.

2.0 INTRODUCTION

2.1 Previous Work

Geochemex Australia commenced a regolith-focussed geochemical exploration programme over the Lawlers district for Forsayth in 1987. An early phase of that work was a district-scale surface and near-surface laterite sampling programme. It was clear that regolith-landform control would be essential to guide the programme and for the interpretation of results. In order to provide this control, Geochemex carried out a regolith-landform programme for Forsayth in parallel with geochemical sampling from August 1988 until February 1989. The latter included sampling of soils for BLEG geochemistry of saprolitic areas, and laterite sampling where appropriate. Mapping of the regolith units was carried out at a 1:25,000 scale using colour air photography. Two maps were produced at this scale and cover the main parts of the district. The maps were included in a report by Butler *et al.* (February, 1989) which covered the regolith-landform relationships in the district, the regolith stratigraphy, description of the regolith units, and an initial synthesis.

The CSIRO research at Lawlers, which commenced in November 1988, provided an understanding of the regolith and this, along with the Geochemex studies, became an integral part of exploration by Forsayth. This included the mapping, regolith stratigraphy, and characterization of regolith units in type areas. All this provided the base for synthesis of regolith development and establishing a regolith-landform model for the Lawlers district.

A satisfying result of collaboration at Lawlers was the discovery of the Turrett and Waroonga Au deposits as a direct result of the experimental exploration programme. Both were discovered by drilling and recognizing buried geochemical haloes in laterite. In the case of the Waroonga deposit, the halo was beneath 7 m of hardpanized transported sediments. Open pit mining commenced at both these deposits in the latter half of 1990 and has provided exposure of both the cover sequences and the buried laterite profiles.

2.2 Objectives of the Lawlers District Study

The overall objectives of the Lawlers study were to provide a well-understood regolith-landform framework of reference over the district and, within this, to carry out multi-element, orientation, geochemical, dispersion studies about concealed Au deposits.

The main specific objectives were:

- to establish methods for reliable identification of laterite types and regolith stratigraphy from drill spoil;
- to carry out a concise orientation study at the concealed North Pit Au deposit;
- to characterize and establish the origin of various massive ironstones, ferruginous pods, and iron segregations which occur widely in the ferruginous saprolite, and occur as coarse ironstone lag in partly-truncated landform situations;
- to establish the relationships of lag type to regolith situations (in the Meatoa area); and
- to carry out pilot investigations into the siting and bonding of Au and chalcophile elements in samples from the laterite geochemical anomalies at the Turrett and North Pit deposits.

2.3 Attributes of the Lawlers District

The attributes of the Lawlers district relevant to the Laterite Geochemistry Project are:

- The supracrustal sequence is dominated by mafic and ultramafic lithologies (thus complementing the Mt. Gibson study where the sequence of interest consists of mafic and felsic schists).

- Buried, essentially-complete laterite profiles are common beneath the alluvial and colluvial plains, as revealed by reconnaissance regolith studies by Geochemex and CSIRO.

- Opportunities existed to carry out orientation studies of undisturbed Au ore deposits which were buried beneath colluvium and had essentially-complete laterite profiles.

- The district was ideal for testing an experimental approach to exploration (by Forsayth, Geochemex, and CSIRO) where concealed Au deposits would be sought by drilling for buried geochemical haloes in laterite.

- A substantial framework of knowledge of regolith relationships in the district was arising from the exploration activities being carried out at the time by Geochemex for Forsayth.

- There was growing knowledge of the distribution of bedrock types in the non-outcropping areas as drilling progressed.

2.4 Components of Research at Lawlers

During the course of the Laterite Geochemistry Project, research at Lawlers has been directed at the following components:

- establishing the regolith-landform framework of reference,

- characterizing relevant regolith materials,

- generalized models of regolith evolution,

- geochemical dispersion studies,

- classification and characterization of laterite types and associated ferruginous materials.

- the siting and bonding of elements.

This report covers the first, second, third and fifth and sixth components. A report on geochemical dispersion will be presented separately.

Because of the opportunities which became apparent from the mapping of regolith relationships at Lawlers by Geochemex and the Laterite Geochemistry Group, coupled with the sparseness of vegetation, the WA Remote Sensing group at CSIRO were invited to join the research collaboration in June 1989. This collaboration is ongoing and is focussed on developing methods for regolith mapping using remote sensing.

Another phase of current research at Lawlers, although outside the AMIRA study, concerns the application of geophysics, particularly ground geophysical methods, for defining and delineating regolith stratigraphy. This research is being carried out through collaboration with the Department of Geophysics at Curtin University (G Cant and V.C. Wilson).

Investigation of the airborne radiometric survey of the Lawlers district, which was used in support of the Geochemex regolith mapping, is planned, as is research on the merging of regolith, landform, bedrock, geochemical, geophysical, and remote sensing data sets and information. These phases of research will be collaborative between Forsayth and the CSIRO Laterite Geochemistry and Remote Sensing Groups.

2.5 Location

The Lawlers district lies some 300 km north of Kalgoorlie (Fig. 1) and spans the boundary between the Sir Samuel (SG-51-13) and Leonora (SH-51-01) 1:250,000 map sheets. Access is gained from the sealed Leonora-Leinster road or by the unsealed road from Sandstone to the Agnew townsite.

2.6 Climate

The study area has a hot, arid climate with a median annual rainfall of approximately 200 mm which is very unreliable. Rain can fall in both summer and winter, but the highest incidence tends to be in late summer resulting from rain-bearing depressions, dependent on cyclonic activity. The mean daily maximum temperature for January is 36° and that for July is 18° (Gentilli, 1971). Frosts are frequent in winter.

2.7 Vegetation

The area is characterized by sparse low acacia woodlands with mulga (*Acacia aneura*) being the dominant species. The shrub layer is dominated by poverty bush and turpentine (various *Eremophila sp*) and rattle bush (various *Cassia sp*). More shrubby examples of the same species dominate the hill tracts with their shallow, stony soil.

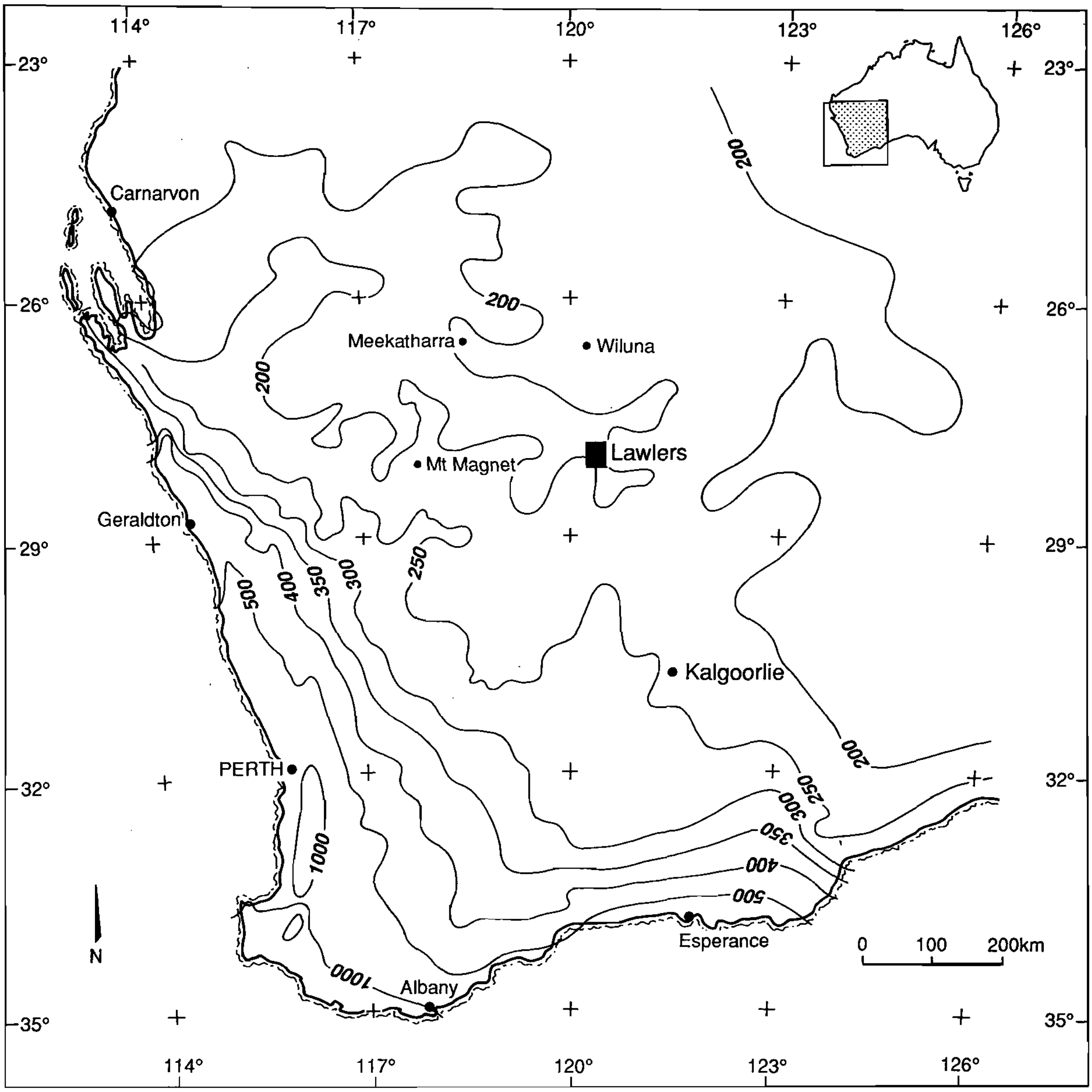

Fig.1. Location of the Lawlers orientation study area placed within the rainfall gradient for the south-west part of the continent.

3.0 REGIONAL SETTING OF LAWLERS DISTRICT

3.1 Regional Geology

The Lawlers district lies within the Agnew supracrustal belt in the Archaean Yilgarn sub-province. The Lawlers greenstone sequence is up to 3 km thick. It consists of interlayered basalt, high-Mg basalt, ultramafic rock, gabbro and differentiated gabbro-pyroxenite-peridotite sills, and thin fine-grained sedimentary and silicic volcanogenic layers (Platt *et al.*, 1978). Some ultramafic units show spinifex texture, the quench texture characteristic of ultramafic lava (Nesbitt, 1971). The gabbroic sills are up to 300 m thick; they are concordant and laterally very extensive. Volcanic and sedimentary units are interlayered with sills throughout. The sequence is intruded by tonalite. In this sequence is the most prominent structural feature in the area, a major north plunging upright fold, the Lawlers Anticline (Fig. 2). A later leucogranite has been mapped in the area (Partington, 1986) cutting both the tonalite and greenstones.

The Lawlers greenstone sequence is overlain on the west side of the Lawlers Anticline by the Scotty Creek sedimentary sequence (Fig. 2). This is about 1500 m thick and consists of basal conglomerate derived from mafic and ultramafic units within the Lawlers greenstone sequence (Platt *et al.*, 1978). The Scotty Creek sequence faces westwards and grades into quartz-felspathic sandstones with tonalitic clasts and sporadic chert and shale horizons.

North and E of Lawlers, the Lawlers greenstone sequence is also overlain by the Vivien sedimentary Sequence of sandstone, siltstone, shales, conglomerates, and cherts. Cudahy (Personal Communication) considers the Vivien clastic Sequence to be stratigraphically equivalent to the Scotty Creek Sequence. Partington (1986) and Eisenlohr (1989) have argued that the Scotty Creek Sequence has an angular unconformable relationship with the Lawlers greenstone succession.

West of the Scotty Creek Sequence lies the Waroonga Gneiss. The contact lies within a major ductite shear zone (Waroonga Shear zone), and the original relationship of the gneiss to the supracrustal sequence is not clear.

The mafic and sedimentary rocks of the Lawlers greenstone sequence have been metamorphosed to mineral assemblages suggesting upper greenschist and lower amphibolite facies conditions (Platt *et al.*, 1978). In the N of the area of Fig. 2, the mineral assemblages in mafic schist are blue green hornblende + plagioclase ± tremolite ± calcite ± biotite ± quartz ± opaque ore. In the SE, a possibly higher grade assemblage appears: green hornblende + plagioclase ± epidote ± quartz ± sphere. Ultramafic rocks, as exposed at the surface, have been largely serpentinized.

3.2 Mineralization

The Au deposits in the Lawlers district fall into the following broad categories.

i) Disseminated Au within alteration haloes ± quartz vein systems in shear zones (e.g. Great Eastern, McCaffery, and Weight Hill).
ii) Laminated Au-bearing quartz veins in fractures or shear zones (e.g. Donegal, Bellevue).
iii) Altered and sulphidic shoots with little or no quartz in major shear zones (e.g. Emu, Redeemer).

The characteristics of these deposits are as follows:

Type i) Most of these deposits occur in shear zones and are in excess of 100 m long and 100 m deep. The host rocks are commonly extensively affected by potassic metasomatism (resulting in sericitization, biotitization) and intense carbonatization. Centrally, pyrite ± arsenopyrite alteration is dominant but is restricted to 1-5 m from the shear zones. Gold is strongly concentrated in the pyritic alteration zones. The lithology and chemistry of the host rocks influence the position of the shear zone and the Au grade.

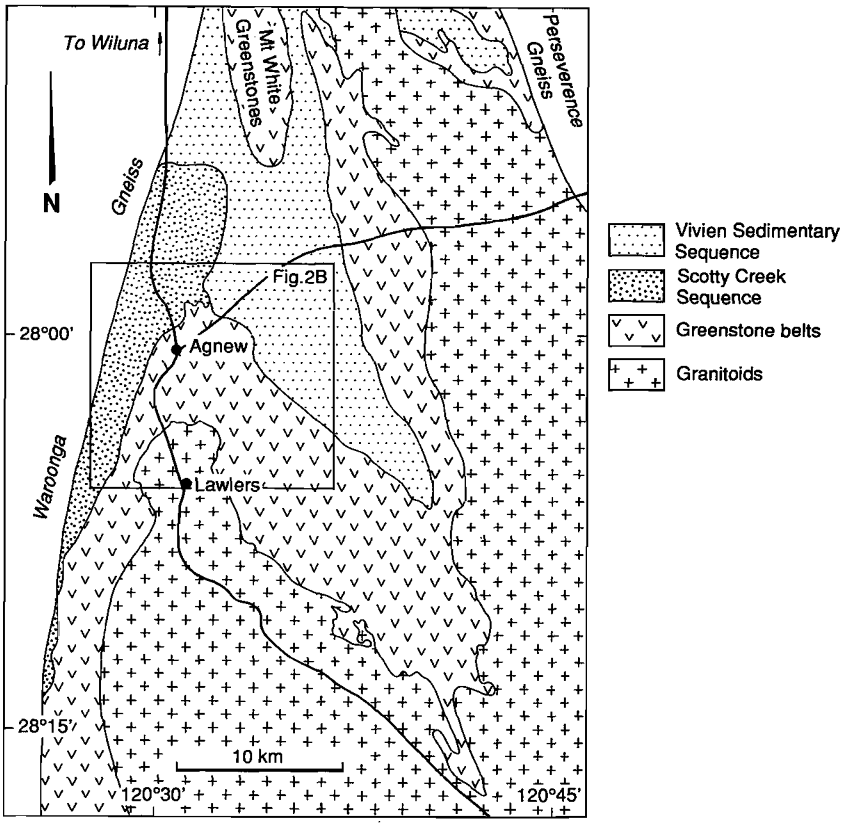

Fig.2A. Regional geology of the Lawlers region (after Platt *et al.*, 1978).

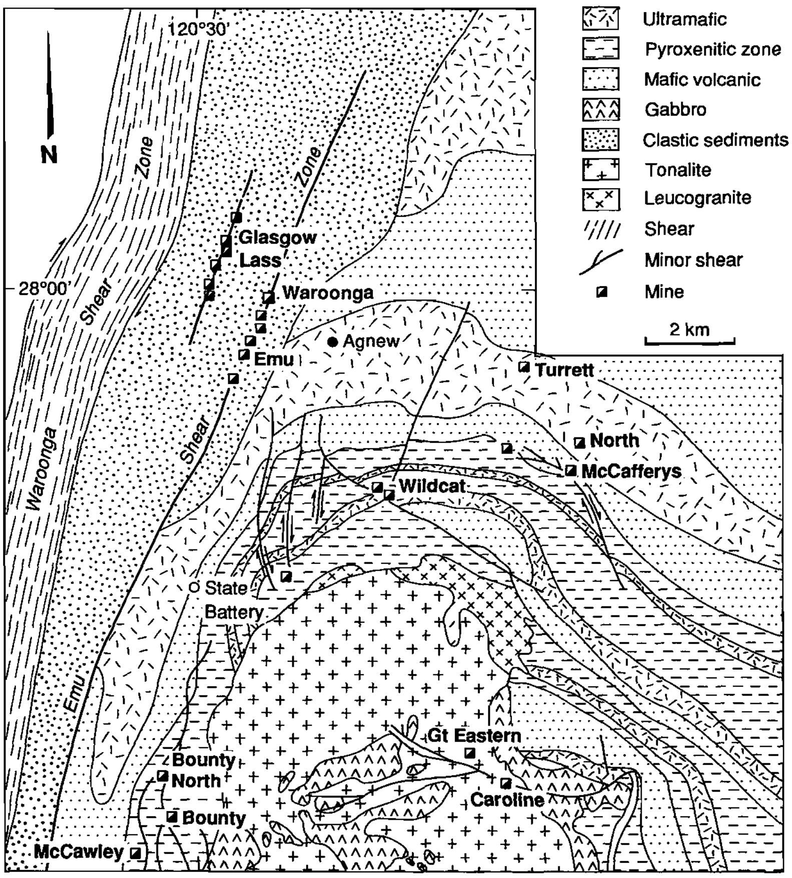

Fig.2B. Detailed geology in the vicinity of Agnew and Lawlers

Type ii) This type generally forms in tensional structures developed in brittle mafic host rocks associated with major movement along the Waroonga shear zone (Partington 1986). The quartz veins are persistent with 1-10-m veins extending over a strike length of over 1 km and to depths of over 250 m. The laminated veins consist almost exclusively of quartz with thin bands of chlorite and low concentration of Fe sulphides. Free Au may be present in the veins. The contained Au lodes are generally small in extent but rich in Au.

Type iii) The Au mineralization is confined to the major sheared contact (Waroonga shear) of the Scotty Creek Sequence and the underlying Lawlers greenstone sequence. There is almost a total absence of quartz veining and the higher Au grades may be associated with biotite alteration. Alteration assemblages are variable but include sulphides (pyrite, pyrrhotite, $\pm$ arsenopyrite), quartz, carbonate, actinolite, and chlorite. The Au is very fine grained at the Redeemer deposit and not associated with sulphides. Structural zones cross cutting the main Waroonga shear and the chemistry of the host rocks within the ductile shear zones are thought to be important influencing factors.

Gold sourced from any of the three primary categories has been redistributed and concentrated by secondary weathering effects into the saprolite and, in places, in the overlying lateritic residuum. This secondary Au mineralization is in effect a subcategory, but nevertheless, it is important as low to medium tonnages of low-grade Au resources can be defined. These are easily mined and processed, examples being the oxide ore at Lawlers and the lateritic ore at Mt Gibson.

3.3 Geomorphology and Drainage

The Lawlers district is situated on the Great Plateau of Western Australia (Jutson, 1950). It is a broadly-undulating terrain with scattered belts of hills providing some local relief. More detailed relief variation, such as at breakaway scarps, is the result of differential stripping of an extensive deeply-weathered mantle and by localized deposition of detritus resulting from this process.

This district straddles a divide between the Lake Raeside drainage to the S and that of Lake Miranda and Lake Darlot to the N. For much of its length, the NW oriented divide comprises the crests of prominent breakaways, the Agnew Bluff (see Fig. 3). Extensive erosional tracts extending S from these breakaways are first dominated by hill belts. Here strike ridges on the greenstone sequence contrast with the smooth, rounded domes and tors on granite outcrops. These hill belts give way, southwards, to gently-sloping pediments, thinly mantled by debris from the immediate hinterland. The pediments have, in general, been incised by S-trending streams, resulting in a series of very low broad, flat-crested spurs. These spurs are usually cored by weathered granite, sometimes with a cover of greenstone debris (Churchward, 1976) as at the Fourteen Mile Creek. The incising streams are flanked by a narrow body of alluvium which merges with the debris of the spur crests into extensive gently-graded alluvial plains that flank the saline environments of the Lake Raeside playa.

By way of contrast, N of the divide the topography is dominated by long, very gentle, smooth slopes. Many of these have their origin on the broadly-convex laterite-mantled crests, immediately above the Agnew breakaway and gradually merge down to broad alluvial floors of tributary valleys, and thence to the main drainage sumps of Lake Darlot and Lake Miranda. The direct length of this drainage is approximately 60 to 70 km while the southward drainage is from 20 to 30 km. Alluvial floors, often associated with a complex of minor meandering channels, are little incised below the main alluvial plain and the drainage often terminates on sandplain tracts over granitic rocks.

A topographic module of this ancient, deeply, weathered surface of subdued relief N of the major divide is provided by a minor valley that intersects the Leinster road 3.5 km E of Agnew. Its broad floor is flanked by smooth gentle slopes rising to broadly-convex crests. By way of contrast, the adjacent valley immediately adjacent to the W, with similar dimensions, has flanking slopes broken by lines of low breakaways. However, the most striking erosional modification of the N sector of the Lawlers district is limited to the differential stripping of the deeply-weathered mantle associated with a hill belt on greenstone that trends northward across the Leinster road, 15 km E of Agnew, in the vicinity of Brilliant.

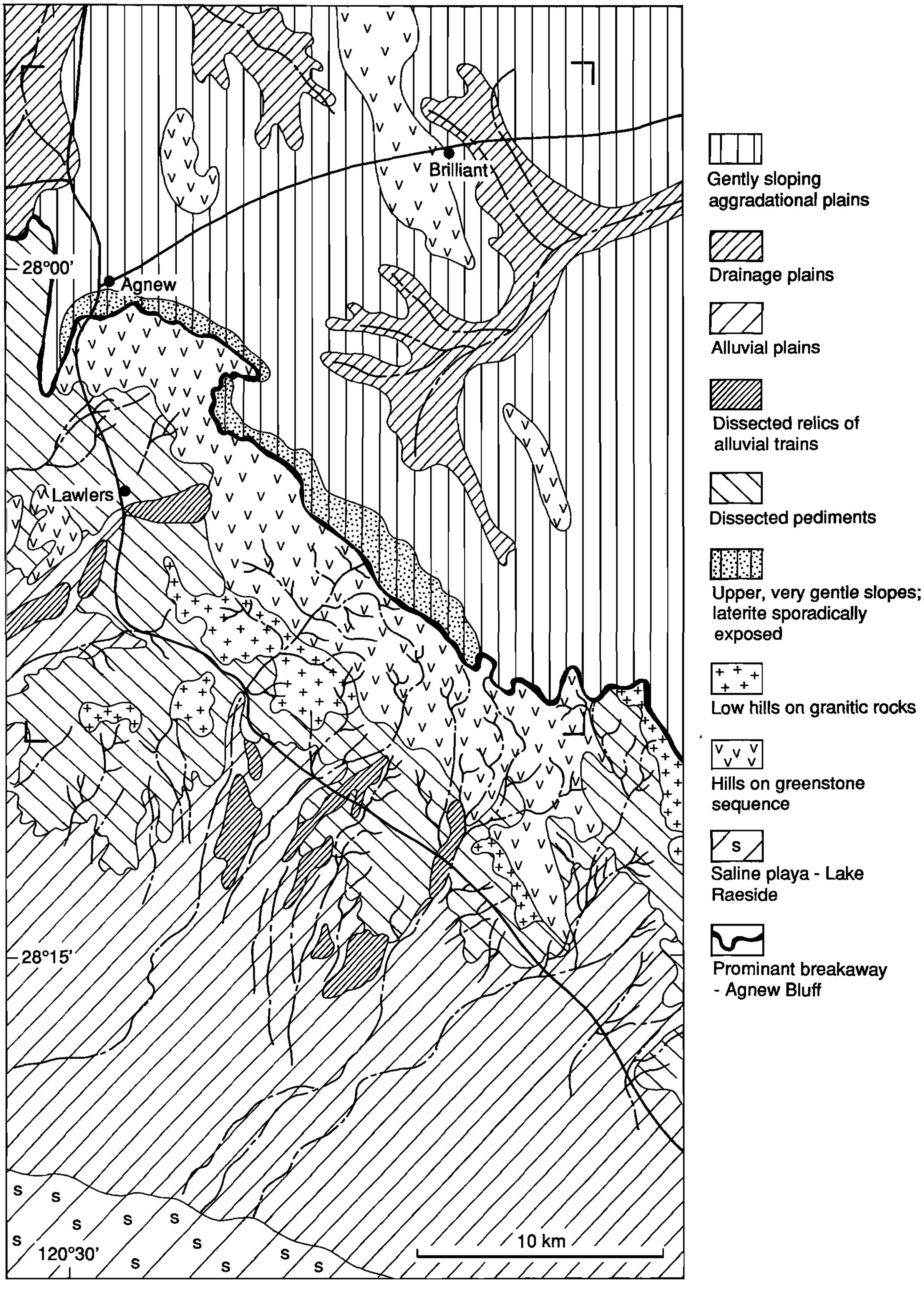

Fig.3. Generalized geomorphology of the Lawlers region. The outline of the district (Fig.4) forming the basis of this report is indicated by the corner symbols.

4.0 REGOLITH-LANDFORM RELATIONSHIPS IN THE LAWLERS DISTRICT

4.1 Introduction

This section deals with the regolith-landform relationships of the Lawlers district over a 30-by 30-km area focussing on the sector NE of the prominent diagonal breakaway marked by Agnew Bluff. Topics include the surface distribution of regolith units, establishing the regolith stratigraphy, characterization of regolith units, and compilation of a synthesis of regolith facies relationships. The overall aim is to provide, for the Lawlers district, a regolith-landform-based scientific framework within which various methods of exploration can be assessed. These include geochemical, remote sensing, and ground and airborne geophysical exploration methods. The regolith-landform framework will also be important in the merging of various data sets and information arising from the exploration methods, an activity which is collaborative between the Laterite Geochemistry and WA Remote Sensing Groups.

A fundamental aim of this section is to provide an understanding of the nature, distribution, and origin of the regolith units. This includes generating knowledge of the original lateritic weathering regime. It also involves a study of the subsequent partial dismantling of the lateritic weathering profile, the accompanying sedimentation which resulted in burial of the lateritic weathering profiles, and authigenic alteration and cementation of some of the regolith units.

4.2 Definitions

When exploring in lateritic terrain, it is useful to consider the landscape in terms of residual, erosional, and depositional regimes - where focus is on preservation and truncation of the lateritic residuum.

Residual regimes, by definition, are areas characterized by preservation of the lateritic residuum. Soils are generally residual and gravelly. *Erosional regimes* are those where erosion has removed the lateritic residuum to the level where the mottled zone, ferruginous saprolite, saprolite, saprock or fresh bedrock are either exposed, concealed beneath residual soils, or beneath a veneer of locally-derived sediments. *Depositional regimes* are characterized by sediments, the origin of which may range from local to distal, and the thickness of which can reach tens of metres. Soils in the depositional regimes are developed in colluvium/alluvium.

Iron segregations refer to dense, black, relatively-homogeneous bodies of weathered materials, which are very rich in Fe and may or may not have any recognisable relict textures. Iron-rich materials which show the preservation of relict textures after sulphides are referred to as *gossans*. Iron segregations may outcrop or, as seen in exposures in mine pits, occur as pods, lenses, or slabs in the upper part of the deeply-weathered regolith. *Ferruginous saprolite* is yellowish-brown to reddish-brown, low in Fe relative to iron segregation bodies, usually has relict textures and can have diffuse mottling and incipient nodular structures.

Other terms used are taken from the *Terminology, Classification and Atlas* of Anand *et al.* (August, 1989).

4.3 The Surface Distribution of Regolith Units

Figure 4 shows the distribution of regolith-landform units for the Lawlers district. This is based upon mapping using 1:25,000 scale colour air photography and a 1:50,000 colour photomosaic. It incorporates regolith mapping carried out by Geochemex for Forsayth (Butler *et al.*, 1989) which formed the basis of the Geochemex geochemical exploration programme of 1988 and 1989. The broad regolith-landform units which have been recognized in the Lawlers district are given in Table 1 together with their main characteristics. Two contrasting geomorphic provinces are recognized and are separated by a regional scarp marked by the NW-NE line of pronounced breakaways referred to in Section 3.3. On the NE upland side of the scarp, the focus of this report, the district is characterized by a partly-preserved, partly-eroded undulating lateritic terrain with areas of outcrop of both saprolitic and fresh mafic and ultramafic rocks, extensive colluvial and alluvial plains as well as minor pediments and pediplains formed on granitic lithologies.

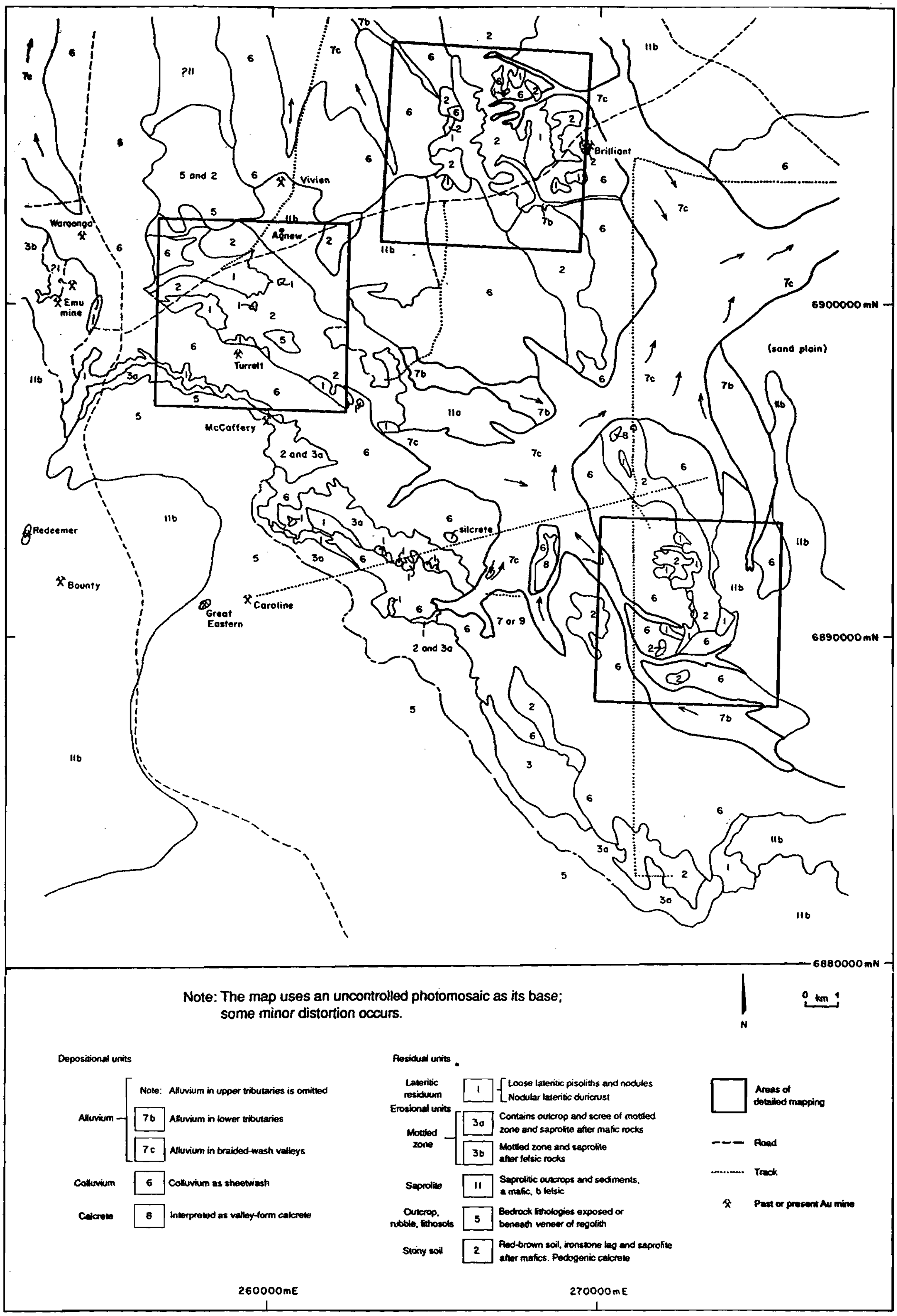

Fig.4. Map showing the surface distribution of regolith-landform units for the Lawlers district.

In order to develop an understanding of regolith relationships, regolith stratigraphy, and the origin of the regolith units, three areas were chosen for detailed study (Fig. 4). These are referred to as the Agnew-McCaffery, Meatoa, and Brilliant areas. The surface distribution of regolith units in these areas is shown in Figs. 5, 6, and 7 as an overlay to airphotos. The units delineated in the diagrams have been mapped onto three-times enlargements of the air photographs, that is, at a scale of 1:8333. (The air photography is by Kevron Aerial Services Pty Ltd for Forsayth; Run 4/9544 6.12.1988, Run 3/9505 6.12.1988 and Run 6/0133 4.1.1989). Some of the units mapped at district scale have been subdivided in the maps of the chosen areas.

Residual Regimes

Regolith Unit 1 occurs within the residual regimes and is characterized by a complete or nearly-complete laterite profile. It commonly occurs as topographically-higher parts of the area, and is a gently-undulating upland comprising broad crests flanked by long gentle slopes sometimes being components of broad concavities (often referred to as backslopes). Unit 1 has been subdivided largely on the basis of the surface expression, nature and size of lateritic gravels, and topographic characteristics. Unit 1a is mantled by Fe-rich pisolitic-nodular lateritic duricrust and coarse lateritic nodules and pisoliths, whereas Unit 1b is dominated by fine lateritic gravels. Unit 1b generally merges downslope into colluvium, Unit 6. Due to local truncation within Unit 1, patches of saprolite may be exposed, and in places the saprolite is partially c. Pockets of silcrete formed by silicification of saprolite may also occur.

Erosional Regimes

Erosional regimes comprise terrain within which varying degrees of erosion of the weathering profile has occurred, and has removed the lateritic residuum to the level where the mottled zone, saprolite, or fresh bedrock are either exposed, concealed beneath soils, or beneath locally derived patchy sediments. Erosional regimes comprise breakaways, low hills and broad convex hills. Units in the erosional regimes are dominated by largely residual soils on saprolite, lag derived from bodies of iron segregations, ferruginous saprolite, saprolite, and vein quartz. Patches of locally-derived sediments are also common. Lateritic lag comprising nodules and pisoliths is typically absent, exceptions being derived by lateral transportation from adjacent residual regimes.

Four units were mapped within the erosional regimes. They were further subdivided according to the surface expression of regolith and topographic characteristics. For example, Unit 2 has been subdivided into Unit 2a and 2b for the Meatoa and Brilliant areas. These units occupy the central zone of the Brilliant area (Fig. 7). There are flanked by residual Units 1a, 1b and depositional Units 6 and 7. This relationship was not observed in the Meatoa area where the Units 2a and 2b are flanked by exposures of the felsic bedrocks to the E and residual and depositional Units to the W (Fig. 6).

Unit 2a is characterized by local undulating saprolitic terrain, comprising low stony hills and local valleys within mostly mafic rocks and shallow red, light clay soils. A coarse lag of black ferruginous cobbles of iron segregations and vein quartz is common. Patches of pedogenic carbonate related to mafic rocks occur within Unit 2a. The calcrete comprises a mixture of powdery carbonate and calcrete nodules.

Unit 2b is characterized by terrain having long gentle slopes, often forming into wide amphitheatres with broad drainage floors. Colluvial mantles are extensive, comprising friable sandy clay loam derived locally from within Unit 2. The nature of lag is similar to that of Unit 2a, but is relatively less abundant.

Outcrops of mafic/ultramafic rocks forming low hills have been mapped as Unit 5 at the Agnew-McCaffery and Brilliant areas (Fig. 5, 7). These features are not prominent at Meatoa.

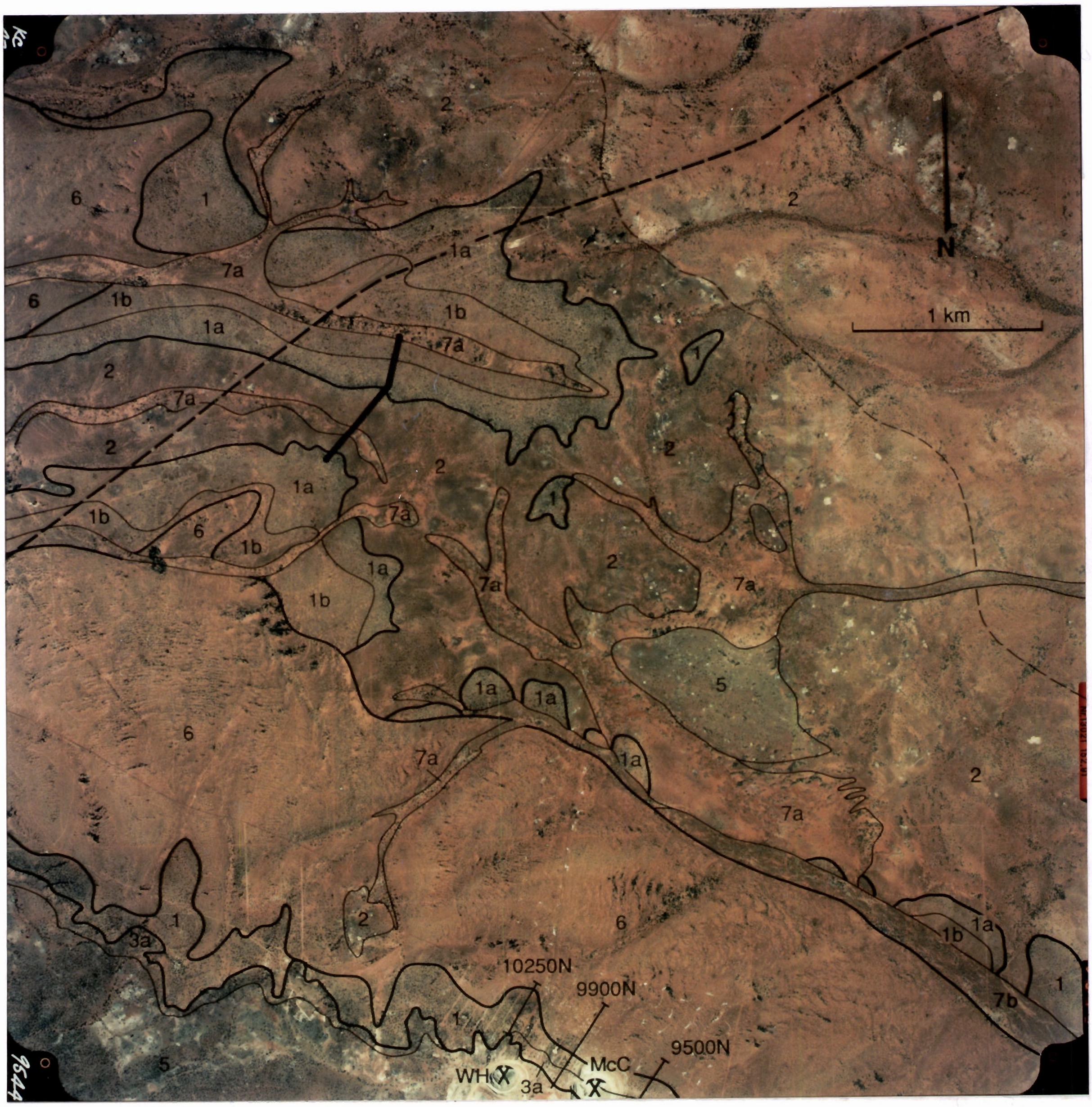

EROSIONAL REGIMES

2	Soil, lag, on saprolite
3a	Mottled zone saprolite
5	Subcrop of bedrock

RELICT REGIMES

1	Lateritic residuum
1a	duricrust
1b	gravel

Gradational subdivision within Unit 2

DEPOSITIONAL REGIMES

7	Alluvium
7a	in minor tributaries
7b	in major tributaries
6	Colluvium as sheet wash

Traverse

Regolith cross sections from Anand et al (1989)

McCaffery and Weight Hill mine pits

Agnew-Leinster road

Fig. 5. Map showing the surface distribution of regolith units and vegetation for the Agnew-McCaffery area as an overlay to the colour air photograph (Photo 4/9544, 6.12.88). Bedrock lithologies are mafic and ultramafic. Airphotograph taken by Kevron Aerial Surveys, published with permission of Homestake Gold of Australia Limited.

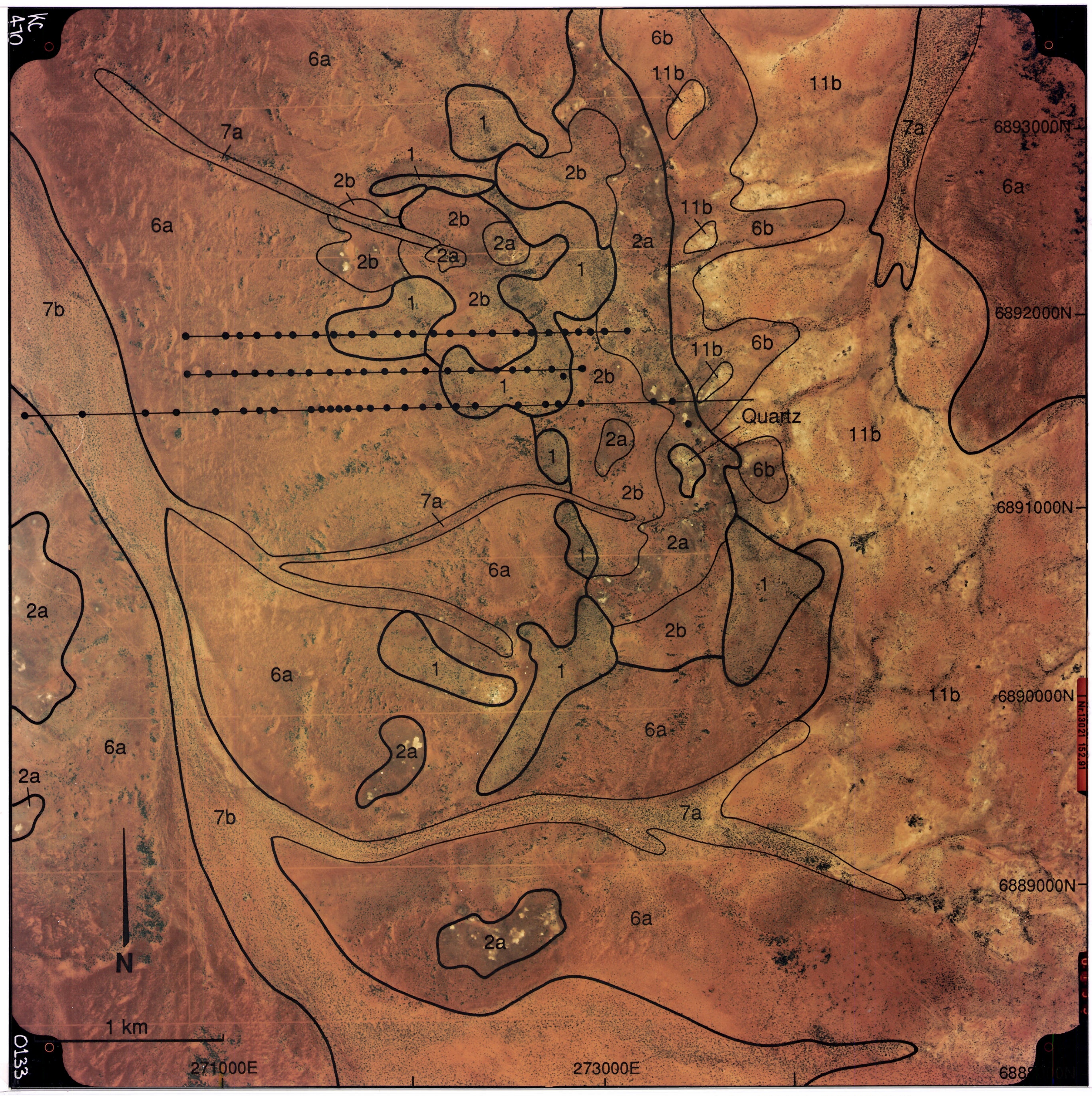

EROSIONAL REGIMES

Saprolite

2a	Sandy light clay soil, coarse black lag on saprolite, pedogenic calcrete
2b	Sandy clay loam soil, coarse lag on saprolite
11b	Granitic, felsic lithologies

RESIDUAL REGIME

Lateritic residuum

1	Sandy light clay loam soil, lateritic lag, lateritic residuum

DEPOSITIONAL REGIMES

Colluvium

6a	Sandy clay loam soil, fine mixed lag, colluvium sheet wash
6b	Sandy loam soil, on felsic saprolite

Alluvium

7a	Light clay soil, alluvium in minor tributaries
7b	Sandy clay loam soil, alluvium in major tributaries

•	Observations and/or sample sites

Fig.6. Map showing the surface distribution of regolith units and vegetation for the Meatoa area as an overlay to the colour airphotograph (Kevron Aerial Surveys: Run 6/0133, 4.1.89) published with permission of Homestake Gold of Australia Limited.

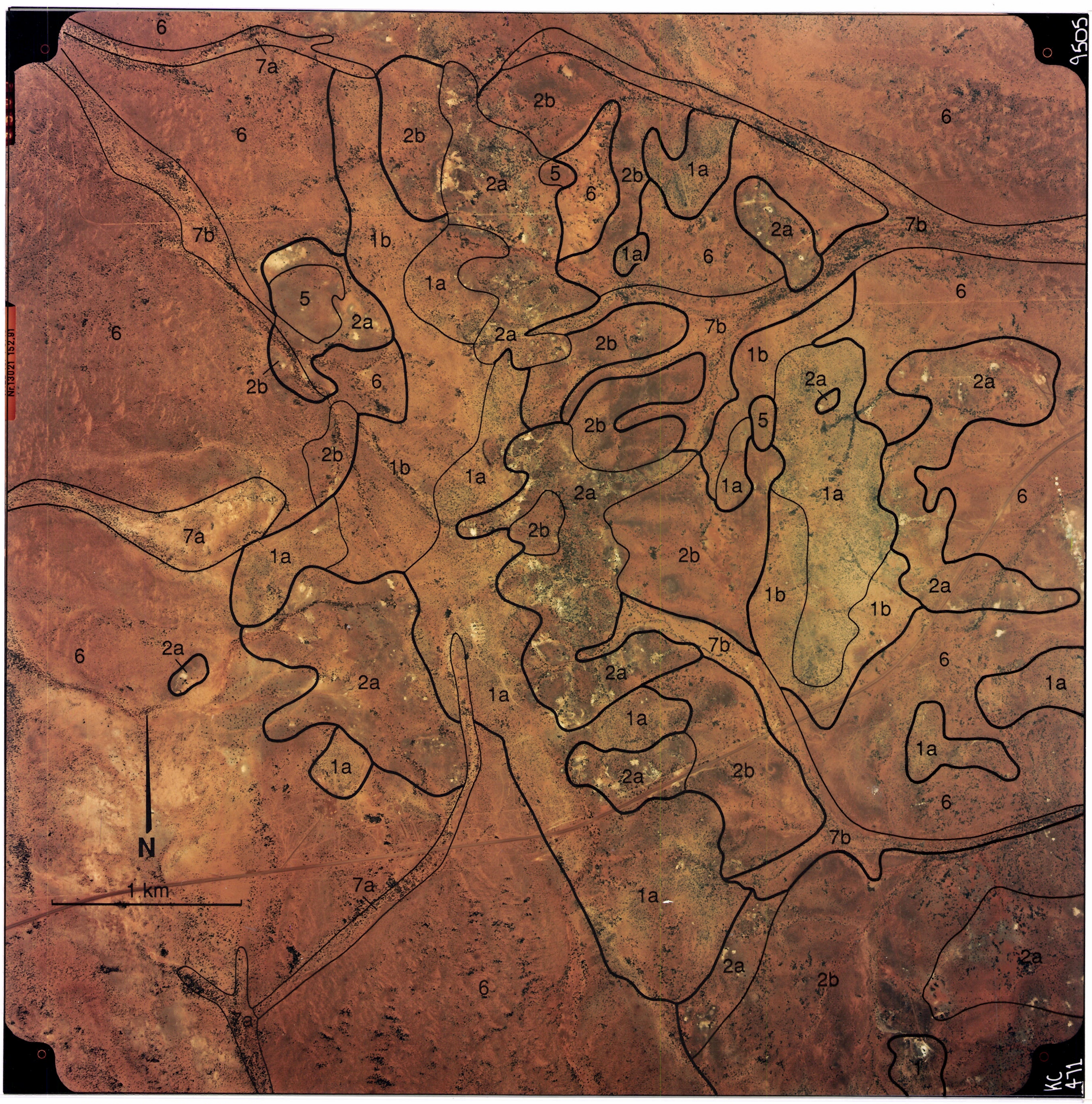

EROSIONAL REGIMES

Saprolite

2a	Sandy light clay soil,coarse black lag on saprolite, pedogenic calcrete
2b	Sandy clay loam soil, coarse lag on saprolite
5	Subcrop of bedrock

RESIDUAL REGIMES

Lateritic residuum

1a	Sandy clay loam soil, Fe-rich duricrust, coarse lateritic gravels
1b	Sandy clay loam soil, fine lateritic gravels

DEPOSITIONAL REGIMES

Colluvium

6	Sandy light clay soil, fine mixed lag, colluvium as sheet wash

Alluvium

7a	Light clay soil, alluvium in minor tributaries
7b	Light clay soil, alluvium in major tributaries

Fig.7. Map showing the surface distribution of regolith units and vegetation for the Brilliant area as an overlay to the colour airphotograph (Kevron Aerial Surveys: Run 3/9505, 6.12.88) published with permission of Homestake Gold of Australia Limited.

Table 1. Regolith Stratigraphy and Characteristics Of Regolith Units : Lawlers District

TYPE OF REGIME	EROSIONAL REGIMES						RESIDUAL REGIME	DEPOSITIONAL REGIMES					
REGOLITH UNIT AT SURFACE	2	3a	3b	5	11a	11b	1	6	7a	7b	7c	8	9
LANDFORM	Low hills	Breakaway and pediment slopes		Convex hills	Pediplain		Undulating upland (crests with back slopes)	Long very gentle slopes	Floors of minor tributaries	Broad wash features of major tributaries	Broad alluvial floors - braided drainage	Calcreted drainage lines	Local drainage sumps
VEGETATION	Mulga	Mulga		Mulga	Mulga		Mulga	Mulga, Eremophila shrubs	Mulga			Mulga, Eucalyptus	Mulga
LAG	Coarse lag of iron segregations vein quartz, ferruginous saprolite	Lag of ferruginous saprolite, iron segregations	Fine quartz, feldspar grit	Lags not common, rock outcrops	Lags not common, saprolite outcrops	Quartz, saprolite outcrops	Lateritic nodules, pisoliths, fragments of Fe-rich duricrust	Mixture of coarse and fine-grained lag Fine grained lag (<10mm) (Lag of mixed origins)	Medium ferruginous lag (30-50mm)	Medium - fine ferruginous lag (10-30mm)	Fine grained lag (<10mm)	Lags not common	Lags not common
SOILS	Red sandy light clays	Red sandy clay loam	Clayey sand	Stony clay loam	Red sandy clay	Clayey/loamy sand	Brown fine sandy loam to fine sandy light clays	Red fine sandy clay loam to fine sandy light clays	Red sandy clay loam to light clays			Calcarous red light clays	Red clay (Smectitic)
ALLUVIUM	-	——		-	——		-	Some at depth	Extensive alluvium Thickness not known			Extensive alluvium	Extensive alluvium
COLLUVIUM	Shallow stony clay loam (1-2m)	Shallow clay loam with abundant lateritic debris (0.5-4m)		Minor	——			Sands, white grey clays with lateritic debris (2-22m)	-	-	-	-	-
HARDPAN (developed in colluvium/alluvium)	-	Minor		-	——		-	Hardpan can be present at 0.5-10m	Hardpan can be present				-
CALCRETE	Pedogenic calcrete	——		-	——		-	-	-			Abundant calcrete	-
LATERITIC RESIDUUM	-	——		Some duricrust on crests	——		Lateritic pisoliths, nodules, nodular duricrust (1-8m). Duricrust can be Fe-rich	Commonly present beneath colluvium at 2-20m thickness 0.5-8m	May be present beneath alluvium			-	-
FERRUGINOUS SAPROLITE		Present	-	-	——		Present with iron segregations	Present with iron segregations (8-30m)	Present with iron segregations			-	-
SAPROLITE	Multicoloured clay rich saprolite with iron segregations, variable thickness		Granitic/felsic saprolite	-	Mafic saprolite	Felsic saprolite	Clay rich saprolite with iron segregations, variable thickness					?	?
BEDROCK	Mafic, ultramafics		Granitic/felsic Rocks	Mafic ultramafics	Mafic	Felsic	Mafic, ultramafics		Mafic, ultramafics				

Depositional Regimes

Depositional regimes include colluvial and alluvial outwash plains(Units 6 and 7). These form widespread regolith-landform units which account for about 70% of the mapped area. The origin of the sediments may range from local to distal and the thickness of which can reach tens of metres. These depositional units commonly conceal extensive areas of complete or nearly complete lateritic weathering profiles. A lag of mixed origin is common on the colluvial plains, comprising iron segregations, lateritic pisoliths, nodules, ferruginous saprolite and vein quartz. The lag is widely distributed on colluvial slopes and becomes finer downslope. The alluvial plains are also mantled by coarse to fine lag of mixed origin.

4.4 Regolith Stratigraphy

For the successful application of geochemical exploration programmes in deeply-weathered terrain, it is important to have an understanding of the distribution of regolith units and the regolith stratigraphy.

In the Lawlers district, exposures of the regolith stratigraphy have been provided by the open pit mining operations at McCaffery, Turrett, and Waroonga. Opportunities to examine subsurface regolith relationships are also provided by the spoil from the numerous regional exploration drill holes. Of particular importance was a series of some 100 holes drilled early in the programme by Forsayth specifically to establish the regolith stratigraphy beneath the colluvial and alluvial plains. This information, for example, has allowed us to construct a series of regolith cross sections for the North Pit and Meatoa areas and has enabled an understanding of regolith stratigraphy, evolution of weathering profile, and regolith facies relationships to be established.

The position of the designated mine pits and positions of observation points are shown in Fig. 8.

In general terms, the regolith stratigraphy of the Lawlers district is complex because of the cyclic history of erosion and deposition which has resulted in a diversity of material being present in any particular area.

4.4.1 REGOLITH STRATIGRAPHY - McCAFFERY-NORTH PIT

A detailed investigation was carried out over an area to the N of the McCaffery Pit, centred on a multi-element geochemical anomaly located by the GEOCHEMEX laterite sampling programme (Butler *et al.*, 1989). Regolith mapping of the North Pit location was carried out prior to mining which commenced in March 1991.

An area of 1000 x 800 m between mine coordinates 9400N to 10400N and 5000E to 5800E was mapped and data compiled at 1:2500 (Fig. 9).

The area is dominated by gravel-strewn colluvial out-wash plains (Unit 6) sloping eastward at about 1° towards a local drainage axis and truncated to the W by a NW trending line of breakaways. This line of breakaways affords exposure of the NE-dipping regolith units along pedimented slopes (Unit 3a), underlain by both ferruginous saprolite and saprolite.

Pulps from 92 drill holes in the North Pit area were logged in the field to discriminate between transported and residual regolith units. Logging of samples from selected holes in the laboratory confirmed the field logging. This work involved separate examination of the nodule and pebble-size fractions in addition to the matrix. From this data set, eight regolith cross-sections at 1:500 scale were completed along the following sections: 9500N; 9700N; 9800N; 9900N; 9950N; 10050N; 10150N; 10250N, (local mine grid).

The stratigraphic sequence of regolith units in the North Pit area is summarized in Table 2.

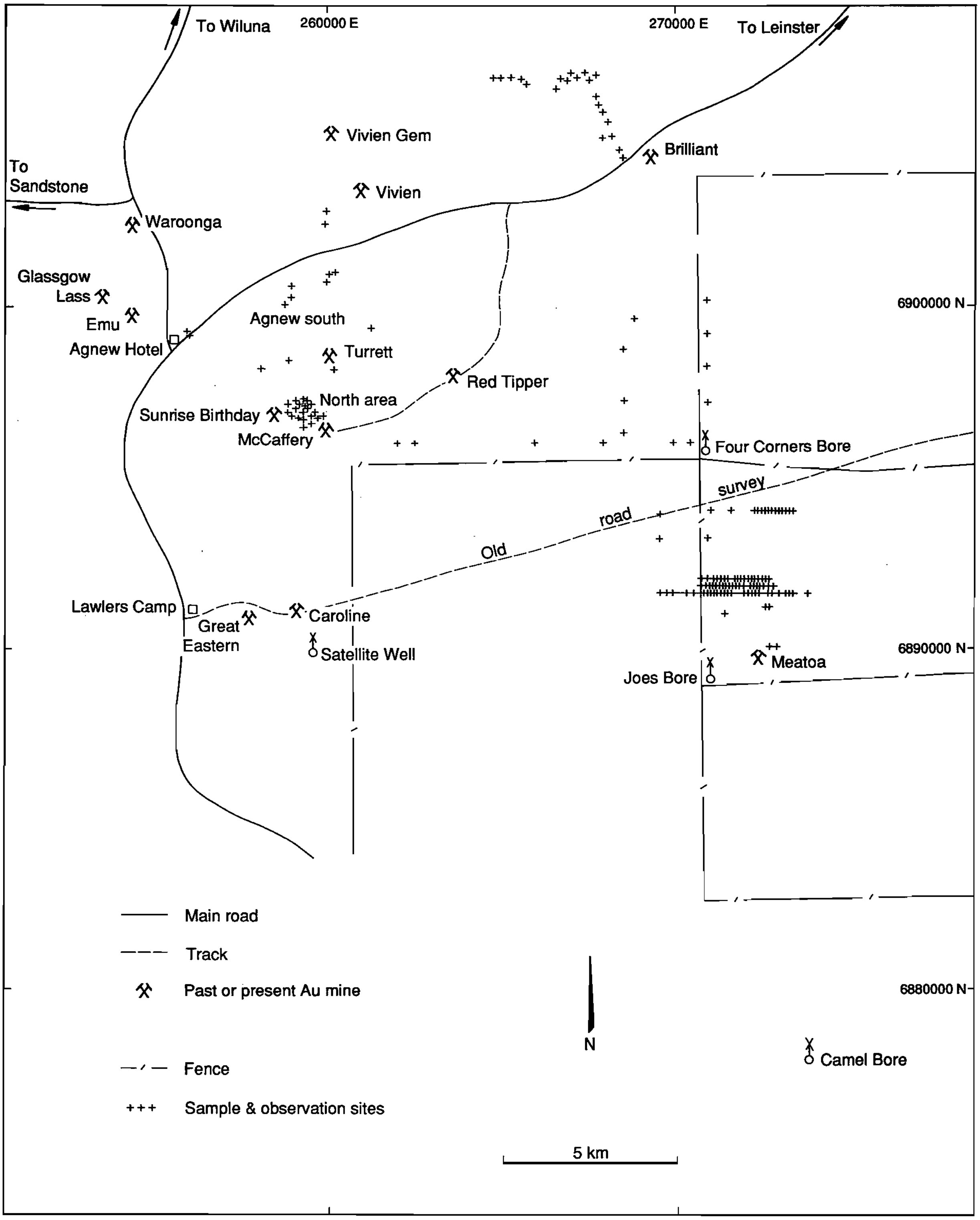

Fig.8. Map of Lawlers district showing the mine pits, observation and sample sites.

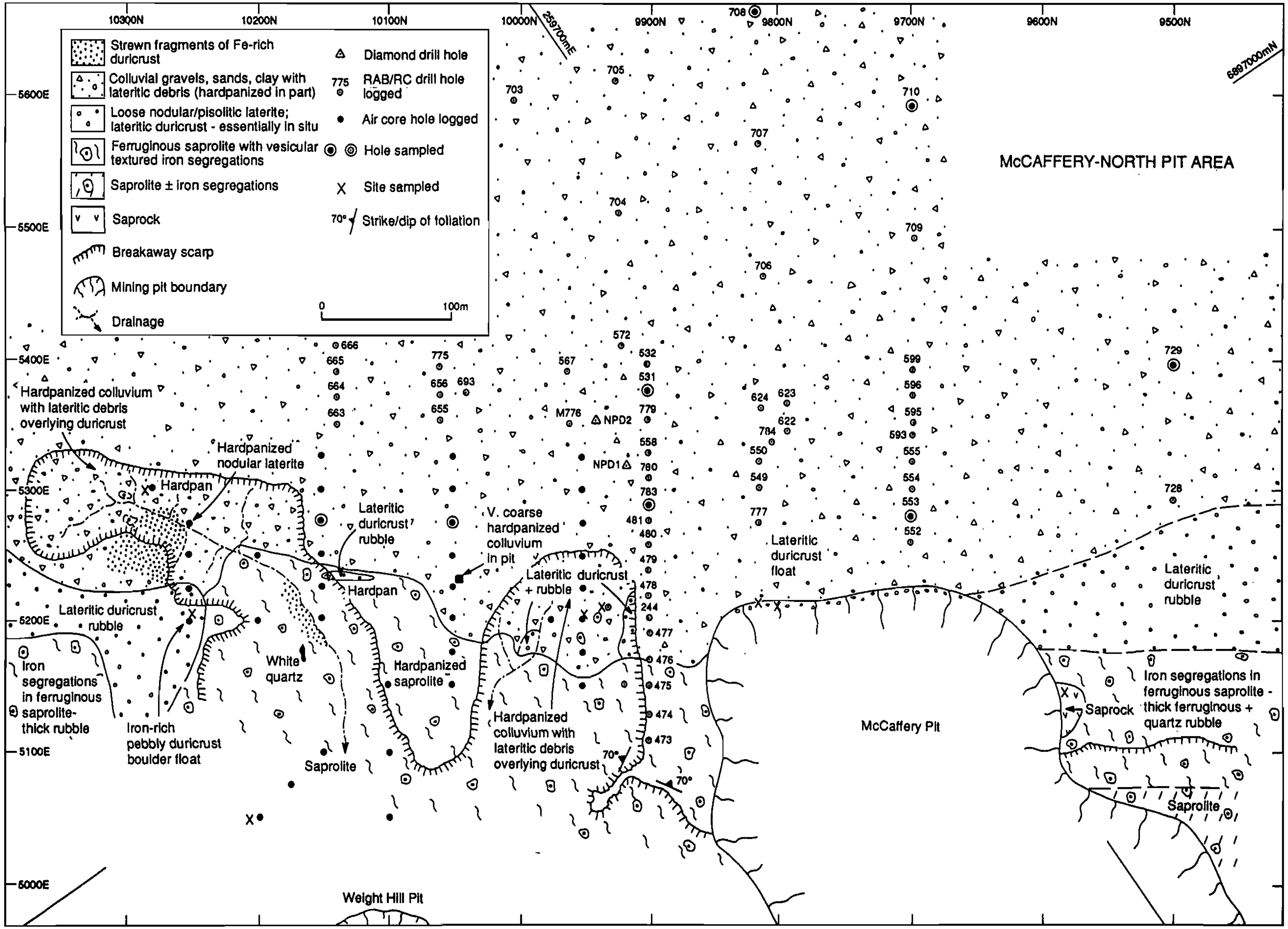

Fig.9. Map showing the surface distribution of regolith units for the McCaffery-North Pit area.

Table 2. Regolith stratigraphy and characteristics of units, North Pit area, Lawlers

TYPE OF REGIME	EROSIONAL	RESIDUAL REGIME	DEPOSITIONAL REGIME
REGOLITH UNIT AT SURFACE	3a	1	6
LANDFORM	Breakaway, pedimented slopes	Crest, back slopes	Long gentle slopes (colluvial outwash plains)
VEGETATION	Mulga	Mulga	Mulga
LAG	Coarse lag of Fe-rich duricrust, ferruginous saprolite	Lateritic gravel	Lateritic gravels, boulders of white vein quartz, lithic fragments
SOILS	Sandy clay	Sandy clay loam	Sandy clay loam
COLLUVIUM	Very thin polymictic gravels on pediments (10-30 cm thick). Coarse nodular lateritic debris (4-5 m thick)	—	Polymictic angular, unsorted gravels fining downwards to sands, white/grey clays with lateritic pisoliths. Maximum thickness 22m. Lenses of lateritic debris within colluvium, 2-8 m
HARDPAN (developed in colluvium)	Hardpan can be present	—	Hardpan can be present at 0.5-10 m
LATERITIC RESIDUUM	—	Fe-rich pebbly duricrust (0.5 m) Lateritic pisoliths, nodules Max thickness 10 m	Loose nodular, pisolitic unit. Max thickness 8 m. Unit may be absent. Nodular duricrust (4-8 m). Unit may be absent. Loose coarse pisoliths, nodules. Max thickness 4 m
FERRUGINOUS SAPROLITE	Yellow clay rich saprolite with vesicular textured iron segregations. Hardpan developed in upper part	Multicoloured saprolite with vesicular textured iron segregations	Bleached, yellow or yellowish-brown with iron segregations
SAPROLITE	Massive clay rich, abundant quartz veins and iron segregations	Yellow saprolite with iron segregations, white quartz veins	Multicoloured clay rich with iron segregations
BEDROCK	Fresh amphibolite, gabbro, serpentinized or silicified ultramafics at 50-70 m depth		

In the North Pit area, an extensive, but somewhat discontinuous, horizon of essentially-residual laterite is unconformably overlain by a varying thickness of colluvium, which itself has components derived by partial or complete stripping of lateritic residuum and ferruginous saprolite. Erosional and depositional regimes, corresponding to regolith-landform Unit 3a (breakaway and pedimented slopes) and Unit 6 (colluvial outwash plains), are separated by areas of lateritic residuum, typified by Unit 1 (lateritic crests above breakaways). These regolith-landform relationships are exemplified in the sections 9500N, 9900N and 10250N (Figs. 10, 11, 12). Examples of the typical detailed regolith stratigraphy in residual and depositional regimes are shown in Figs. 13 and 14.

Colluvial outwash plains, sloping at approximately 1°, extend eastwards from a breakaway scarp, towards a SE-draining braided fluvial system. The plains in the North Pit area, as elsewhere in the Lawlers tenements, have a loose surface veneer of mixed lithic and lateritic debris. This surface veneer typically overlies a layer (up to 4 m in thickness, but typically 0.5-2 m) of unconsolidated, coarse, polymictic gravels with very crude bedding in the few exposures and some imbrication of the larger flattened clasts. Clasts are angular, unsorted and range to 15 cm in maximum dimension. Lithologies are similar to those in the surface gravels, although the proportion of lateritic gravels generally decreases markedly with depth.

The coarse, near-surface deposits of polymictic gravels fine downwards into thick deposits of loams, sandy loams, and puggy grey-white and white clays interstratified with more gravel-rich intervals which may include one or two intervals of transported lateritic nodules and pisoliths. Drilling has established that the total colluvial sequence exceeds 10 m in thickness and may reach about 40 m in the vicinity of 5600E e.g., Fig. 10.

Interbeds of clays may be devoid of any gravel and can reach a thickness of 1.5 m but with little apparent continuity from section to section. Likewise, beds of transported lateritic debris appear as lenses at one or two horizons within the colluvium. The transported laterite may extend up and down dip for 50 to 200 m and along strike for distances of perhaps 500 m, but correlations are difficult in the thicker colluvium sections.

Authigenic *hardpanization* affects much of the colluvial profile and reaches a maximum development in the near-surface, more coarsely-clastic gravels. In places (e.g., 10050N: 5225E) hardpan development comes within 30-40 cm of the surface. The thickness of its development increases eastward to a maximum of 15 m (commonly 6-7 m), although it is possible that a thicker development exists in areas of a deeper colluvial profile. Generally, the hardpan is not developed in the thicker, loamy colluvium in the North Pit area.

Near surface, hardpan exhibits a sub-horizontal lamination or inter-clastic "pseudo-foliation" or parting and the colour is brownish changing to a characteristic brick-red with depth. The hardpan matrix is characteristically porous, and unctuous to the tongue. Deposits of glassy, botryoidal opal (hyalite variety), and films of black Mn oxide are sometimes present in pores or along cleats in the upper half of the hardpanized profile, although the Mn oxide films are not as common nor extensively developed in the North Pit area as in many other areas of hardpan development at Lawlers.

In detail, hardpanization is not stratigraphically controlled, but transgresses lithologic contacts and locally extends down through colluvium into the underlying residual loose nodular laterite. Westward and up-dip in the regolith profile, the thickness of hardpan steadily decreases to the breakaway scarp where it forms a drape-like effect over the breakaway embayment and has permeated downwards into the ferruginous saprolite in the erosional regime.

A *lateritic residuum*, comprising rubbly, nodular duricrust is exposed on ridge crests along 5200E in the vicinity of lines 9500N and 10250N (Fig. 9) and on the breakaway scarp. These surficial deposits show evidence of down-slope sheet wash, so it is probable that the upper part of the loose nodule/pisolith horizon in the residual laterite will have a small degree of transport involved. From outcrop, the laterite dips E at 12-14°, thickening to a maximum of about 15 m. On some sections, e.g. 10250N (Fig. 12), the residual laterite thins down-dip within less than 100 m of outcrop; in other sections, e.g. 9900N (Fig. 10) and 9800N (not shown), the laterite forms a continuous blanket for distances of at least 500 m eastward, reaching a probable maximum thickness in the vicinity of a palaeo-trough infilled with loamy colluvium in the vicinity of the 5400-5500E.

FIG. 10 : CROSS SECTION SHOWING THE REGOLITH STRATIGRAPHY FOR LINE 9500N NORTH PIT AREA

FIG. 11 : CROSS SECTION SHOWING THE REGOLITH STRATIGRAPHY FOR LINE 9900N NORTH PIT AREA

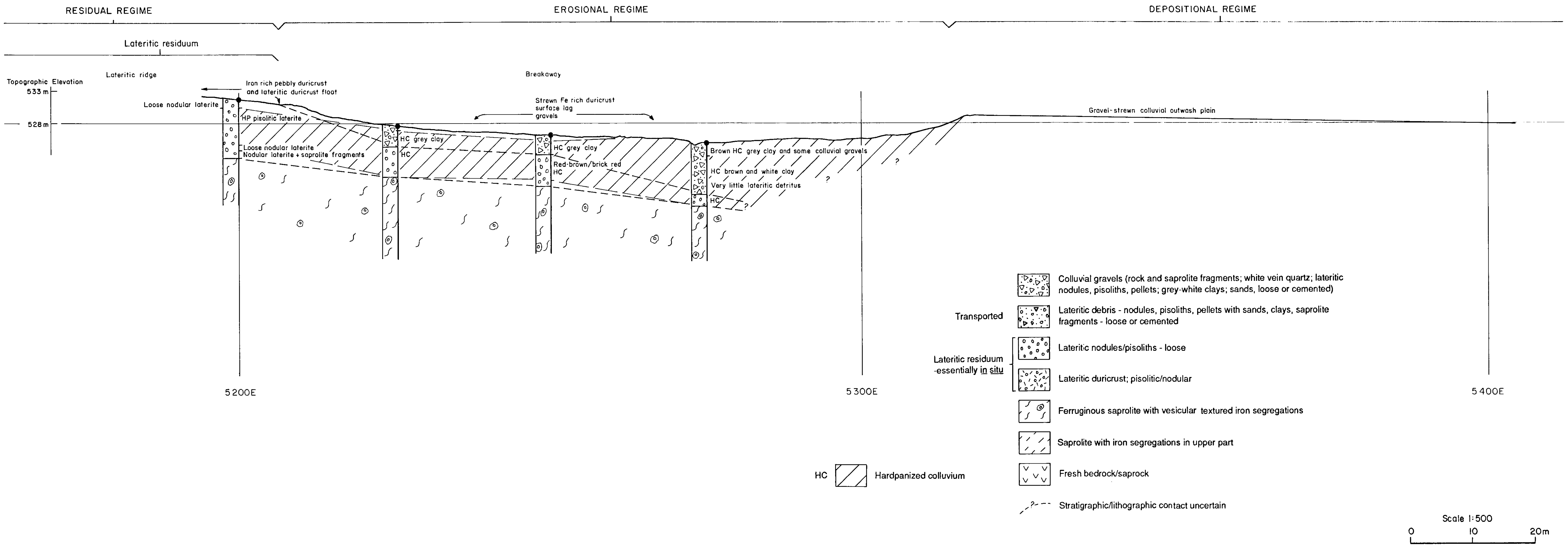

FIG. 12 : CROSS SECTION SHOWING THE REGOLITH STRATIGRAPHY FOR LINE 10250N NORTH PIT AREA

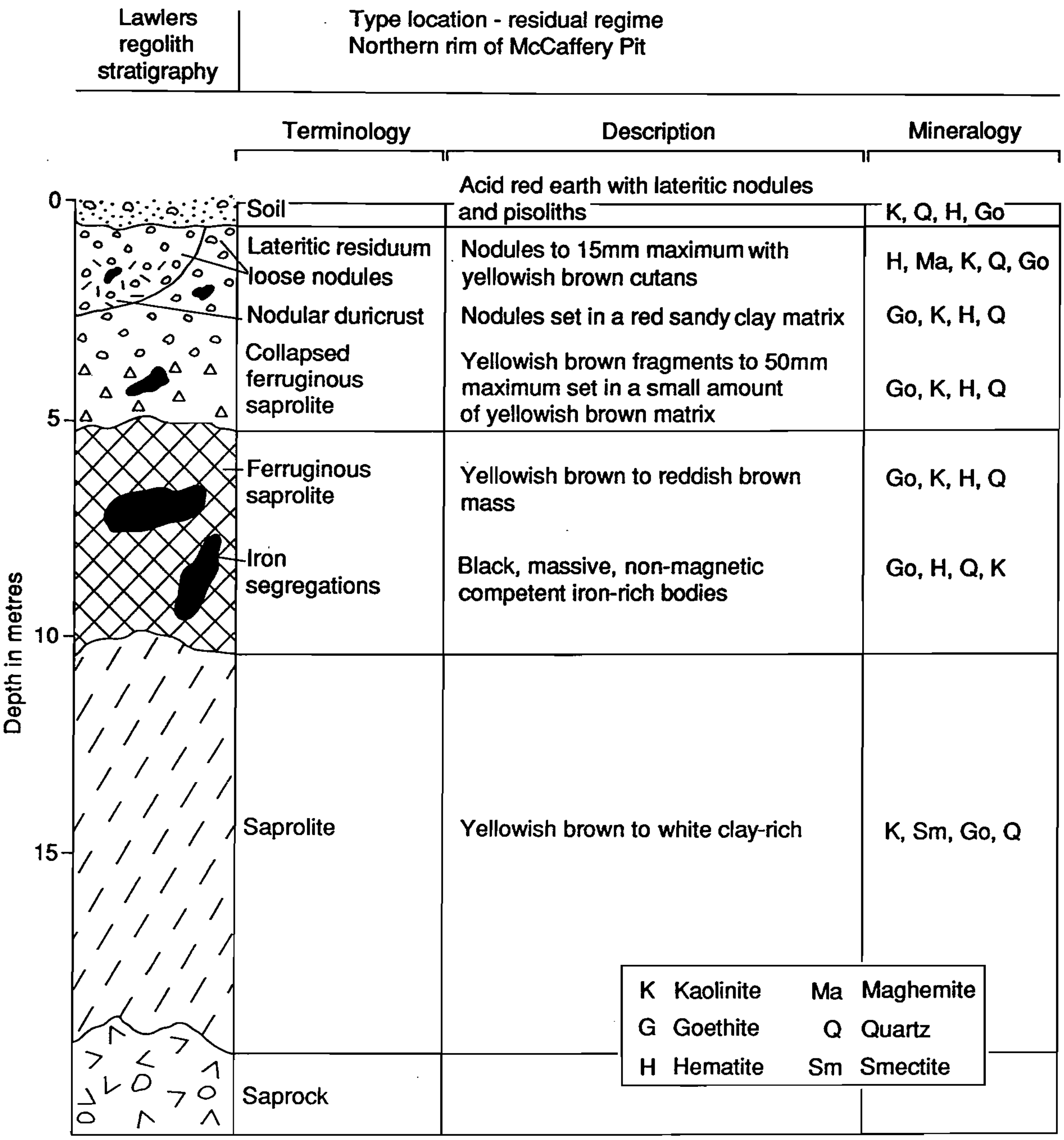

Fig.13. Vertical profile showing the regolith stratigraphy and mineralogy of the regolith units for the residual regime.

Lawlers regolith stratigraphy	Type location - depositional regime North Pit - hole 783, 5296E 9899N	
Terminology	**Description**	**Mineralogy**
Colluvium (transported)	Brown sandy loam with lateritic nodules, pisoliths, lithic and quartz fragments	H, K, Go, Q, Ma, R, Il
Hardpanized colluvium (transported)	Hardpanized red-brown sandy clay loam to clay with lateritic nodules, pisoliths and lithic fragments. Mn staining (⫽) in colluvium. Nodules to 15mm maximum without yellow cutans	K, H, Go, Q, Ma, R, Sm
Transported lateritic debris	Reddish brown silicified lateritic nodules without cutans	K, H, Ma, Go, R, Q
Lateritic residuum (residual)	Loose nodules, pisoliths and nodular-pisolitic duricrust. Nodules to 35mm maximum with yellowish brown or greenish cutans	K, H, Go, Gi, Ma, Q
Collapsed ferruginous saprolite	Yellow-brown fragments of ferruginous saprolite	Go, K, Q
Iron segregations	Black, non-magnetic, massive competent iron-rich bodies	
Ferruginous saprolite	Yellow-brown saprolite with black, non-magnetic iron segregations	Go, K, Q
Saprolite	Pale clay-rich	K, Sm, Go, Q

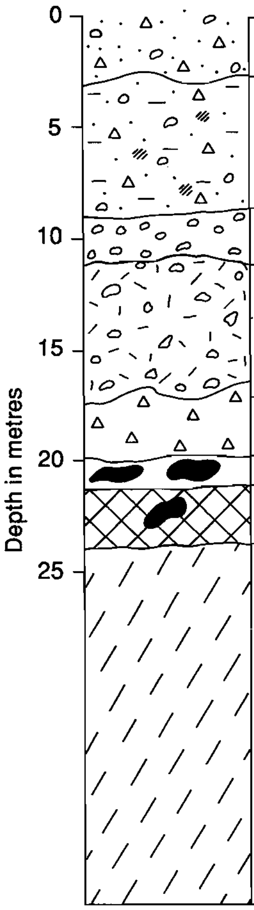

K	Kaolinite	Sm	Smectite
Go	Goethite	R	Rutile
H	Hematite	Il	Ilmenite
Ma	Maghemite	Gi	Gibbsite
Q	Quartz		

Fig.14. Vertical profile showing the regolith stratigraphy and mineralogy of the regolith units for the depositional regime.

The residual laterite profile generally comprises an upper and lower horizon of loose pisolitic/nodular laterite. Nodules/pisoliths with yellowish brown/olive green cutans are common. The upper horizon reaches 8-m thickness and the lower 4 m, although either may be absent. Where the lower unit is present, it is separated from the upper by a 2- to 6-m thickness of nodular lateritic duricrust and itself lies directly on ferruginous saprolite. Where the lower unit of loose nodules is not developed, duricrust lies directly on collapsed ferruginous saprolite (Fig. 15A).

A zone of *ferruginous saprolite* commonly underlies the residual laterite horizon in the North Pit area and consists of pale multi-hued saprolite derived from mafic or ultramafic rocks and having a weak relict metamorphic foliation. The zone is characterized by the presence of rounded to ovoid pods of massive, vesicular-textured *iron segregations* ranging up to 30 cm in diameter (Fig. 15B). Occasionally, the ferruginous saprolite may be thinly developed or absent, but it is normally 5-15 m thick and, in turn, overlies a saprolite zone devoid of mottling. The *saprolite* extends to around 70-m depth, passing into fresh mafic or serpentinized ultramafic rocks. The upper half of the saprolite is characterized by the presence of discrete iron segregation bodies or replacement bodies of Fe-enrichment ranging from a few centimetres to several metres in size, and localized by breccia matrices and structural surfaces such as joints, schistosity, and bedding. The lower half of the saprolite unit consists of pale yellow, brown, orange, and green weakly-foliated or massive clay-rich saprolite with no evidence of Fe-enrichment.

Lateritic crests above breakaways extend for a distance in excess of 1 km NW from the eastern rim of the McCaffery Pit and continue beyond the mapped North Pit area. They form the topographically higher parts of the environs, are transitional between erosional and depositional regimes and represent a lateritic residuum. Cappings and deflation residues of *black Fe-rich pebbly duricrust* (LT228) overlie an upper horizon of loose lateritic pisoliths and nodules (LT103 e.g. Section 10250N, 5250E). Mechanical disaggregation of the Fe-rich pebbly duricrust followed by sheet wash and down-slope movement of the fragments results in fields strewn with Fe-rich lag gravels (Fig. 9). Loose pisoliths/nodules and rubbly duricrust are exposed over maximum widths of 110 m on the laterite ridges. The sub-surface profile is similar to that described for the colluvial outwash plains (Fig. 14).

Breakaways and pediments are typically deeply incised through both the colluvial cover and the residual laterite into the lower portion of the saprolite zone. The mottled zone and the upper half of the saprolite zone with bodies of iron segregations are exposed on the pediment below the breakaway scarp. Some embayments in the breakaways are abundantly strewn with Fe-rich gravels overlying thin (<30-40 cm), quartz-rich, colluvial gravels which, in turn, cover both transported and residual nodular laterite. The thickness of *transported lateritic colluvium* in this situation may be up to 5 m. An example is the creek-bed exposure at 10210N: 5250E where the lateritic nodules are extensively hardpanized and large clasts of white quartz are interspersed with the lateritic debris.

Hardpanization does not follow the general westward up-dip projection of the contact between colluvium and laterite, but is draped over the breakaway scarp, and has permeated the exposed mottled zone and saprolite on the pediment slopes. Its distribution in saprolite is, at least in part, structurally controlled.

4.4.2 REGOLITH STRATIGRAPHY - TURRETT PIT

Turrett Pit, located in the depositional regime (Figure 4, Unit 6) 2 km N of McCaffery pit, provides an opportunity to compare its regolith stratigraphy with that of North Pit which is within the same depositional regime. Mining commenced at Turrett in September, 1990. In general terms, stratigraphic sequences observed in eastern and western walls of Turrett Pit are similar to those of North Pit. However, the colluvium is shallow and reaches a maximum thickness of only 4 m (holes T271A, T274, T327 and eastern/western wall of Turrett Pit) and bodies of *iron segregations* are relatively more abundant. In the W wall of Turrett Pit, gravelly colluvium (3 m) overlies the 6-7 m thick pisolitic lateritic residuum. At depth, lateritic residuum merges into yellowish-brown collapsed ferruginous saprolite. Large bodies of iron segregations are present within lateritic residuum and ferruginous saprolite (Fig. 16A). These iron segregations range from pods (10 to 40 cm across) to large slabs, 10 to 25 m across, which can occur at various depths, from 4 to 10 m. Bodies of iron segregations appear to have been modified by weathering processes and releasing nodules into the lateritic residuum.

Lateritic residuum (weakly indurated pisolitic-nodular duricrust)

Collapsed ferruginous saprolite

Fig.15A. Vertical profile showing weakly indurated nodular-pisolitic duricrust overlying collapsed ferruginous saprolite, location north east rim of McCaffery Pit.

Iron segregations

Fig.15B. Iron segregations in a pale yellow ferruginous saprolite, location north-east rim of McCaffery pit.

Fig.16A. Large black bodies of iron segregations several metres across in a yellowish-brown ferruginous saprolite, location western wall of Turrett Pit.

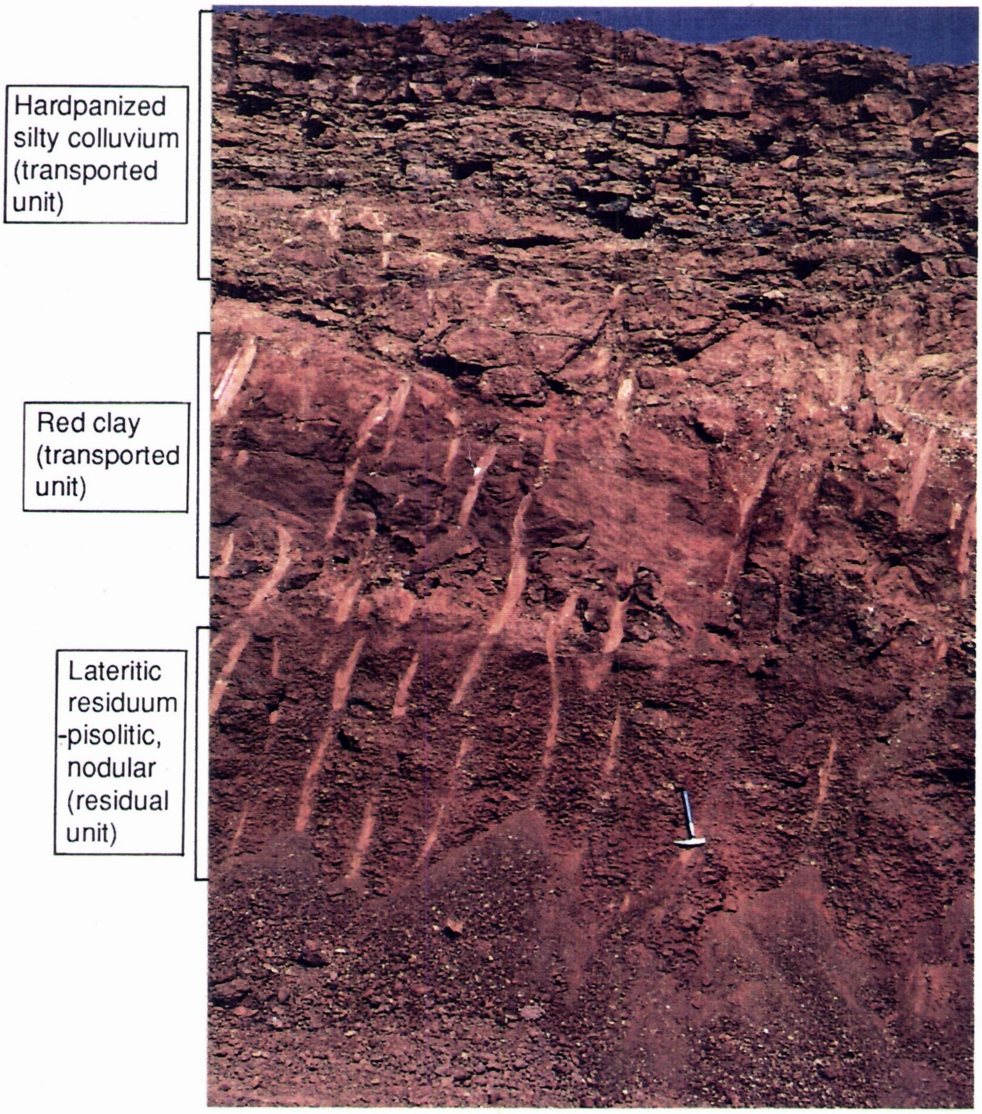

Fig.16B. Mine pit exposure of a hardpanized colluvium overlying lateritic residuum, location western wall of Waroonga Pit.

Hardpan is developed in both colluvium and lateritic residuum which is well expressed in the E wall of the pit.

4.4.3 REGOLITH STRATIGRAPHY - AGNEW AREA

The surface distribution of regolith units in the Agnew-McCaffery area is shown in Fig. 5 as an overlay to airphoto 4/9544. In order to compare the regolith and characteristics of an area characterized by lateritic residuum at surface with those from an area that has been modified by stripping processes, a traverse was selected for detailed study some 3.5 km ENE of Agnew, the location referred to in Section 3.3 immediately S of the Agnew-Leinster road (Fig. 17). The location comprises two parallel minor valleys. In the more northerly valley, smooth gentle slopes on either side of the valley extend down from a broadly-convex crest to a broadly-concave unchannelled floor. Southward, the smooth slopes rise to another broadly-convex crest forming the interfluve to the adjacent valley. This crest is flanked to the S by a low breakaway from which the pediments slope gently downwards to a flat valley floor.

A regolith-landform model for this area is shown in Fig. 17A. Changes in regolith stratigraphy and soil types along the traverse AB are shown in Fig. 17B. Details of the regolith at sample sites along the transect are given in Table 3. The dominant features of the regolith of the study area are related to the occurrence of lateritic gravels and duricrust (Unit 1) on broad crests and backslopes, subcropping saprolite (Unit 2) on the breakaway and upper pediments and colluvium/alluvium (Unit 7) dominating the valley floors. However, locally-derived colluvium also occurs in the valley floors. The regolith of the northern valley is characterized by gravelly sandy loam to sandy clay loam soils which overly lateritic residuum. For the purpose of discussion, this area can be referred to as a residual area. The regolith of the southern valley, by contrast, is characterized by gravelly sandy clay loam soil overlying saprolite. It is interpreted that lateritic residuum once covered most and possibly all of the area and the main regolith-landform features are due to partial truncation by erosional processes which continue today.

Nodular duricrust (LT204) and medium to coarse (4-12 mm) yellowish-brown lateritic pisoliths and nodules dominate the lags of the broad crests (Unit 1a), forming a divide between the valleys. Down the slopes of the more northern valley, gravels become finer and dominantly comprise lateritic pisoliths and nodules (Unit 1b). Nodules forming the lateritic gravels on the broad crests have black or reddish-brown hematite-rich cores, each having a goethite-rich yellowish-brown cutan. Downslope in the northern valley, the gravels with dark brown to brownish-black surfaces become increasingly more common. The pediments below the breakaway of the southern valley are mantled by a coarse lag containing yellowish-brown fragments of ferruginous saprolite similar to those at Meatoa (Unit 2). These lags also become finer downslope, they are a mixture of clasts with yellowish-brown goethite-rich surfaces and others that are black. Cutans are not present on these clasts.

The mineralogy of the lag samples along the traverse, on a semi-quantitative basis, is shown in Fig. 18. Hematite, goethite, maghemite, kaolinite, and quartz (not shown) are the dominant crystalline minerals in all lags. However, the relative abundances of these minerals vary widely between the lag types and particularly as a function of the regolith-landform unit. Hematite and maghemite are more abundant in lateritic lag gravels on the broad crest (Unit 1a) forming a divide between the valleys. This suite of minerals also dominates the backslope and valley floor of the northern valley (i.e. the residual regime). By contrast, goethite is the dominant mineral in lags of ferruginous saprolite of the southern valley, where stripping is suggested by the absence of lateritic residuum. Kaolinite is relatively more abundant in ferruginous saprolite than in lateritic lag gravels. The differences in mineralogy between the lateritic lag and fragments of ferruginous saprolite are due to differences in the degree of weathering. Fragments of ferruginous saprolite are derived from the breakdown of upper parts of saprolite, while lateritic nodules/pisoliths are the product of breakdown of nodular/pisolitic duricrust. Fragments of ferruginous saprolite have experienced a lesser degree of weathering compared with those of lateritic gravels as is shown by the large amounts of goethite and kaolinite in fragments of ferruginous saprolite.

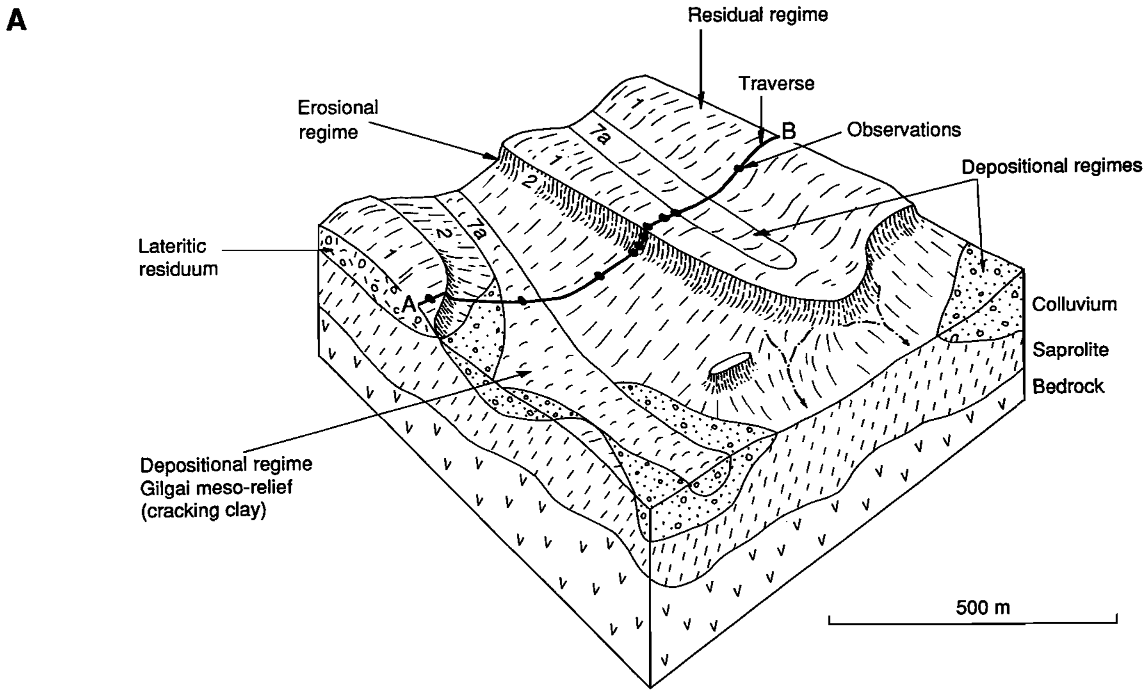

Fig.17A. Generalized regolith-landform model based upon the Agnew-McCaffery study area.

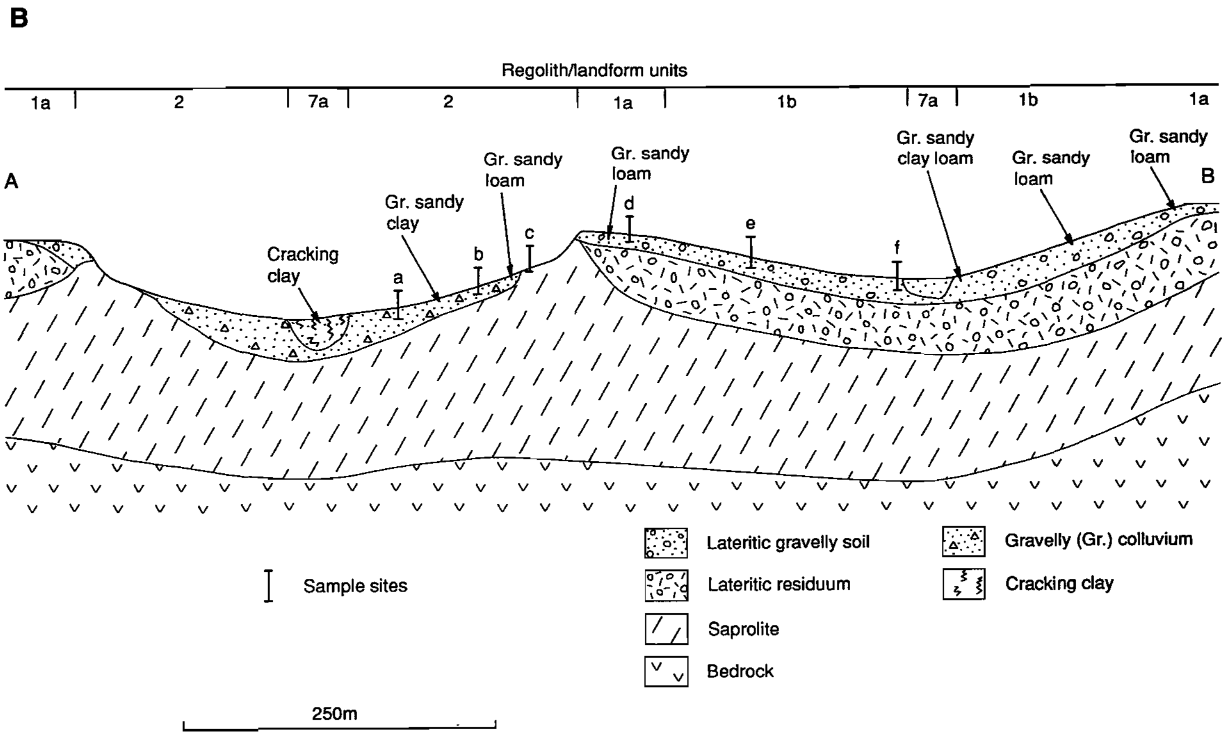

Fig.17B. Schematic regolith cross section showing trends in soil and regolith stratigraphy for the traverse shown in Fig.17A.

Table 3. Regolith stratigraphy and characteristics of units , Agnew Area

SAMPLE SITES (See Fig. 17A)	a	b	c	d	e	f
REGOLITH UNIT AT SURFACE	2	2	2	1a	1b	1b
TYPE OF REGIME	Erosional	Erosional	Erosional	Residual	Residual	Residual
LANDFORM	Valley floor	Upper pediment	Breakaway scarp	Broad smooth crest	Smooth gentle slopes "back slopes"	Valley floor
LAG	Lag of mixed origin (ferruginous pebbles/ granules, lateritic nodules)	Fragments of ferruginous saprolite	Fragments of ferruginous saprolite	Lateritic nodules, pisoliths	Lateritic nodules, pisoliths	Lateritic nodules, pisoliths
SOILS	Gravelly red fine sandy clay	Reddish-brown gravelly fine sandy loam	-	Gravelly reddish-brown fine sandy loam	Gravelly reddish-brown fine sandy loam	Gravelly brown fine sandy clay loam
COLLUVIUM	Gravelly colluvium	Gravelly colluvium		-	-	Gravelly colluvium
HARDPAN	Present within a metre of surface	Present within a metre of surface	-	-	Some	Some
LATERITIC RESIDUUM	-	-	-	Nodular duricrust	Nodular duricrust	Nodular duricrust
SAPROLITE	Ferruginous and clay-rich saprolite (?)	Ferruginous and clay-rich saprolite	Ferruginous and clay-rich saprolite	Ferruginous and clay-rich saprolite (?)	Ferruginous and clay-rich saprolite (?)	Ferruginous and clay-rich saprolite (?)

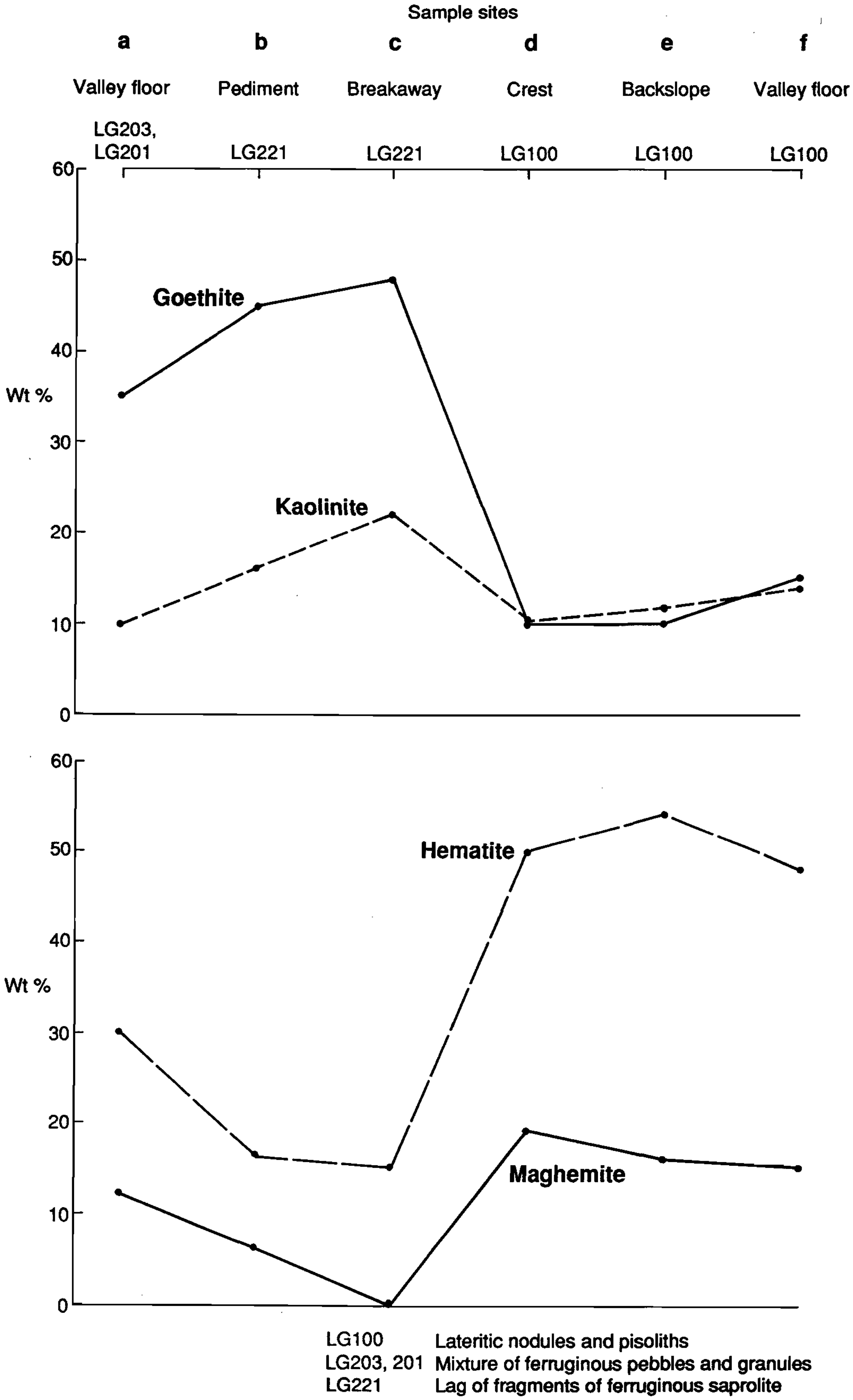

Fig.18. Distribution of goethite, kaolinite, hematite and maghemite in lag gravels for the sample sites shown in Fig.17B.

On the crests (Unit 1a) the soils are reddish brown (7.5-5YR 5/6, moist), friable fine sandy loams. Down the smooth slopes, there is a slight but perceptible increase in the clay fraction leading to fine sandy loams and fine sandy clay loams. On the upper pediments, the soils are red brown (5YR 5/6, moist) sandy loams, but merge downslope to red (5YR 4/6, moist) sandy light clays. Deep, cracking, self-mulching, red, smectite clays associated with gilgai mesorelief occur in the floor of the southern valley.

The clay mineralogy of the soils of the regolith units on various topographic positions is shown in Table 4. The clay fraction was sedimented onto a glass slide and saturated with Mg, with and without glycerol, to confirm the identity of smectites. XRD traces of these indicate that kaolinite is the dominant soil mineral of the crest and breakaway/pediments while smectite dominates soils on the floor of the southern valley. However, it is of interest to note, that small to moderate amounts of smectite are present in all the samples. Chlorite occurs in significant amounts in the floor of the southern valley. Small amounts of interstratified clays and illite are also present in a few samples.

Kaolinite is generally a product of weathering of well-drained highly-weathered soils. Its formation is not favoured in the current overall soil chemical environment for this arid area since the leaching conditions are not optimum. Kaolinite in these soils is thus related to more severe leaching conditions during the paleoweathering regime. It can then be concluded, that the soils under investigation on the crests and breakaways have developed on remnants of the old lateritic profile which were formed under a warm humid climate.

Soils on the floor of the southern valley are largely developed in colluvium/alluvium derived from the erosional areas. Smectite development in these soils is compatible with the truncated provenance areas being more labile. In addition, poor drainage conditions in the valley floor would further lead to the formation of smectite.

4.4.4 REGOLITH STRATIGRAPHY - MEATOA AREA

The dominant regolith features in the Meatoa area relate to the occurrence of lateritic residuum (Unit 1), to partial truncation of the deep weathering profile and exposure of saprolite (Units 2a, 2b and 11b) to the E, together with colluvial (6a) and alluvial deposition (7a, 7b) in the western part of the area (see Fig. 6). To the E, gentle slopes are mantled by depositional Unit 6b consisting of mafic detritus which overlies felsic bedrocks.

Except for the pedimented area of granitoids forming the eastern third of the Meatoa area, outcrop or subcrop of bedrock is generally poor, with some isolated areas having float of saprolitic lithologies amongst abundant ironstone rubble. Typically the ground surface is soil-covered and is strewn with lag, which is derived from various surficial regolith units.

The regolith stratigraphy for the Meatoa area (Table 5) was established by logging spoil from many of the exploration drill holes along lines 6 891 600N, 6 891 800N, and 6 892 000N. These lines typified the main Meatoa area. From these data, an EW cross section was constructed for line 6 891 600N, showing the regolith stratigraphy and regolith-landform relationships (Fig. 19). The eastern end of the cross-section is characterized by red sandy light clay and/or sandy clay loam soils overlying saprolite with sporadic outcrops of pedogenic calcrete. It is interpreted that lateritic residuum once covered this part of the section and has been removed by erosion to the level of saprolite. This eastern part of the area is thus designated as an *erosional regime*. *Erosional* (units 2a, 2b) and *depositional* (units 6a, 7) *regimes* are separated by the *residual regime* (Unit 1).

The dominant soils of Unit 1 vary from friable brown gravelly fine sandy loams to fine sandy clay loams with *lateritic residuum* at shallow (1 m) depth which in turn overlies *ferruginous saprolite* and/or *clay-rich saprolite*. Lateritic residuum reaches four metres in thickness in the area and consists of both lateritic duricrust and a unit comprised of loose lateritic nodules and pisoliths. Lenses of *iron-segregations* also occur within ferruginous saprolite and upper saprolite.

Table 4. The types of layer-silicate minerals present for the different regolith-landform situations along the studied traverse of Figs 17 A and B in the Agnew area.

	EROSIONAL REGIMES			RESIDUAL REGIMES	
REGOLITH/ LANDFORM UNIT:	7a	2	2 (in part)	1a	1b
LOCATION:	Cracking clay	a	c	d	f
LANDFORM SETTING:	Central drainage with gilgai meso-relief	Valley floor	Breakaway	Crest	Valley floor
KAOLINITE:	+	++	+++	+++	+++
SMECTITE:	+++	++	+	?+	++
CHLORITE:	++	++			
INTER-STRATIFIED:	+		++		
ILLITE:		+			

Codes for abundances:
Dominant +++
Sub-dominant ++
Minor +

Table 5. Regolith Stratigraphy and Characteristics of Regolith Units: Meatoa Area

TYPE OF REGIME	EROSIONAL REGIMES			RESIDUAL REGIME	DEPOSITIONAL REGIMES			
REGOLITH UNIT AT SURFACE	2a	2b	11b	1	6a	6b	7a	7b
LANDFORM	Low hills, local valleys	Pediments, breakaway scarps (amphitheatres)	Pediplain	Undulating upland (crests, with backslopes)	Long very gentle slopes	Long very gentle slopes	Floors of minor tributaries	Broad wash features of major tributaries
VEGETATION	Mulga shrubs	Mulga shrubs	-	Mulga shrubs	Eremophila shrubs Geranium herbs	Mulga shrubs	-	Eremophila shrubs
LAG	Coarse lag of iron segregations	Lag of fragments of ferruginous saprolite, iron segregations	Quartz	Fragments of Fe-rich duricrust, pisoliths and nodules, fragments of ferruginous saprolite	Fine lag of mixed origin (ferruginous granules, lateritic nodules, fragments of ferruginous saprolite)	Lag of iron segregations, lithic fragments, and vein quartz from mafic terrain	Lag not common	Lag not common
SOILS	Red sandy light clays	Red sandy clay loams	Loamy sand	Brown fine sandy loam to fine sandy light clays	Red fine sandy clay loam to fine sandy light clays	Reddish-brown sandy loams	Red light clays	Reddish-brown sandy clay loams to light clays
ALLUVIUM	-	-	-	-	Some at depth	-	Thickness not known	2 - 3 m
COLLUVIUM	-	1 - 2 m	-	-	Sands, white/grey clays (2-14 m)	1 - 2 m	-	-
HARDPAN (developed in colluvium/alluvium)	-	Minor	-	-	Hardpan can be present at 0.5-6 m	-	?	0.5 - 1.5 m
CALCRETE	Pedogenic calcrete	Pedogenic calcrete (minor)	-	-	-	-	?	-
LATERITIC RESIDUUM	-	-	-	Loose lateritic pisoliths/nodules, nodular duricrust (1-4 m) Duricrust can be Fe-rich	May be present beneath colluvium at 2.8 m. Thickness 0.5-3.5 m)	-	?	1 - 2 m
MOTTLED ZONE	-	Minor	-	Minor	-	-	-	-
SAPROLITE	Multicoloured clay rich/ferruginous saprolite		Granitic/felsic saprolite	Multicoloured clay rich/ferruginous saprolite, occasionally-mottled saprolite, variable thickness		Clay-rich felsic saprolite	Clay rich/ferruginous saprolite, variable thickness	
BEDROCK	Basalt, Gabbro, Dolerite, Ultramafics, etc.		Granitic/felsic rocks	Basalt, Gabbro, Dolerite, Ultramafics, etc.		Granite	Basalt, Gabbro, Ultramafics, etc.	

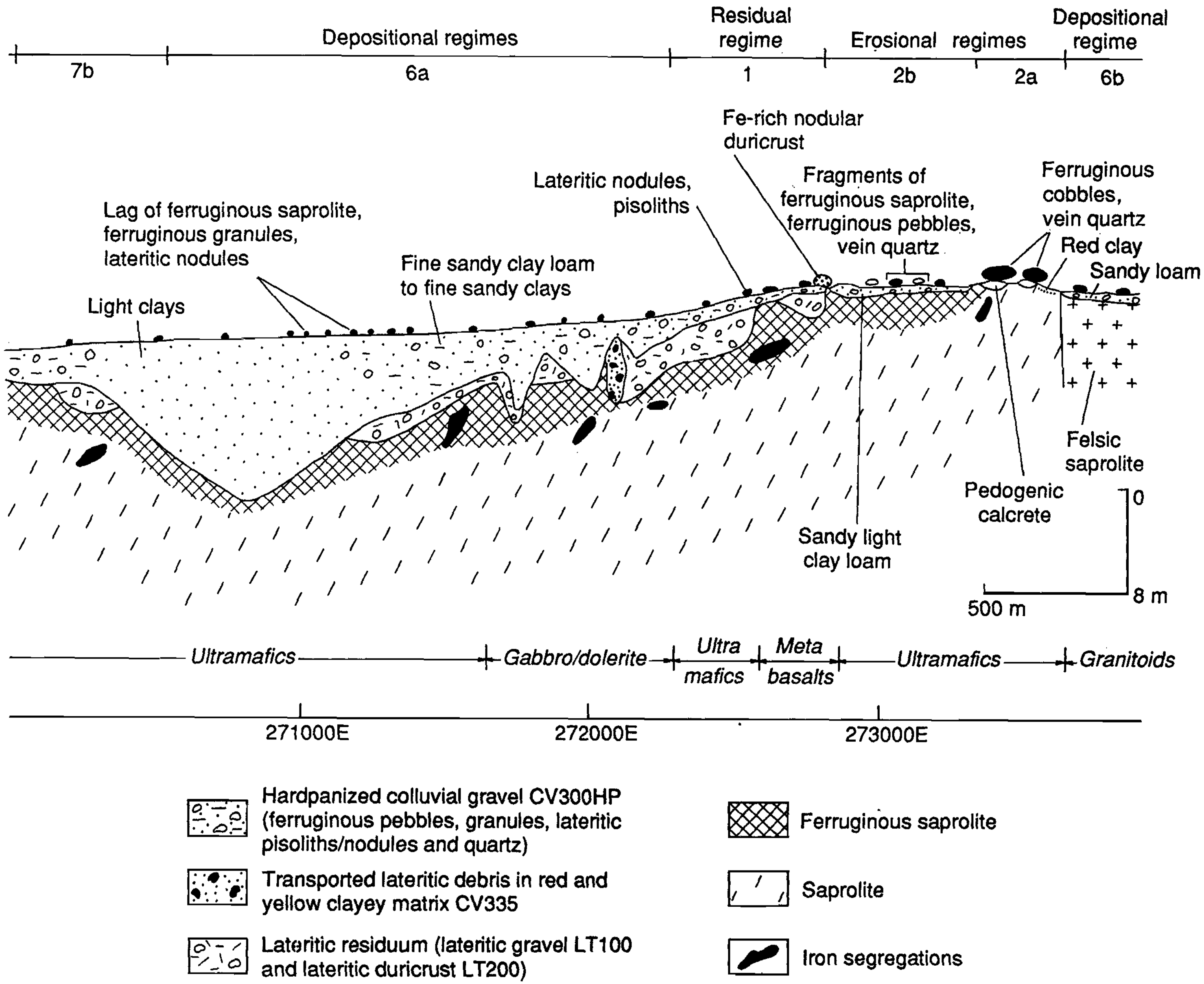

Fig.19. Cross section showing the regolith stratigraphy for line 6891600N, Meatoa area.

Extensive red gravelly sandy clay loam to fine sandy light clay soils dominate the depositional areas. These gravelly soils fine downwards and merge at depth with colluvium comprising sandy/silty clay/loam interstratified with more gravel-rich intervals. The colluvium reaches a thickness of 13 m in the Meatoa area. The colour of the matrix of the colluvium is generally red at the top, but becomes paler with depth. The lateritic residuum beneath the colluvium forms an almost continuous blanket for a distance of 1.5 km westwards from the broad crest at 272800E reaching a maximum thickness of 3.5 m. However, local truncation has been observed and regolith relationships can be complex. *Transported lateritic material* occurs as sporadic lenses of loose nodules/pisoliths within the colluvial unit. *Hardpanization* is widespread in much of the colluvial/alluvial unit, its development decreases westwards. Typically underlying the colluvium of residual lateritic horizon is multicoloured saprolite derived from mafic and ultramafic rocks. The *saprolite* extends to a depth of around 40 m passing into fresh mafic/ultramafic rock. A mottled zone is generally missing or is only very weakly developed.

The lags which occur on most ground surfaces at Meatoa contain a variety of clast types including fragments of ferruginous saprolite, ferruginous granules, pebbles and cobbles after iron segregation bodies, fragments of Fe-rich duricrust, lateritic nodules and pisoliths, and white vein quartz. The various clast types are mixed, but their distribution can be related to the source material, such as regolith substrate or upslope outcrops, and to landform position. Coarse black lags of iron segregations tend to dominate the erosional areas (regolith Units 2a, 2b) to the east, whereas fine lag of mixed origin dominates the regolith Unit 6. Fragments of Fe-rich duricrust dominate the lag on Unit 1. The increase in the abundance of fine lag in lower slopes is probably related to the colluvial sedimentation and fractionation of the lag as it passes downslope and away from the sources, whereas the large fragments of iron segregations and Fe-rich duricrusts show lesser dispersion. Fine lag is therefore allochthonous and does not relate to the immediate underlying lithology.

4.4.5 REGOLITH STRATIGRAPHY - BRILLIANT AREA

The Brilliant area, 14.5 km NE of Agnew, was chosen to be that covered by airphoto 3/9505 (6.12.88), occupying approximately 30 km^2 in the Lawlers district (see Fig.7). The regolith-landform model derived from the study area is depicted in Fig.20. The dominant features of the distribution of regolith units are the occurrence of erosional regimes (Units 2a,2b) on low stony hills in the central zone, and residual areas (Units 1a,b) on broad crests/backslopes and depositional regimes (Units 6,7) on colluvial/alluvial outwash plain areas in both the eastern and western sides of the figure. Drainage in the erosional regimes finds its way through gaps between residual and depositional regimes to the main regional drainages. The data show that regolith relationships in the Brilliant area are similar to those described for the Meatoa area in Section 4.4.4. These relationships therefore will not be described in detail here. However, the features that differ from those of Meatoa area are as follows:

- An erosional regime (Units 2a, 2b) occupies the central zone. It is flanked by residual Units 1a, 1b and depositional Units 6, 7 on either side of the study area. This relationship was not observed in the Meatoa area where the erosional regimes (Units 2a, 2b) are flanked by exposures of the felsic bedrock to the east and residual and depositional regimes to the west.

- The residual regime (Unit 1) has been subdivided largely on the basis of the nature and size of the lateritic materials and topographic characteristics. Unit 1 is mantled by Fe-rich duricrust and coarse lateritic gravels, whereas Unit 1b is dominated by fine lateritic gravels. Unit 1b generally merges downslope with Unit 6. In the Meatoa area, the differences in the clast-size of gravels were not apparent and therefore Unit 1 was not subdivided.

- Outcrops of mafic/ultramafic rocks forming low hills have been mapped as Unit 5 at Brilliant. These features were not prominent at Meatoa.

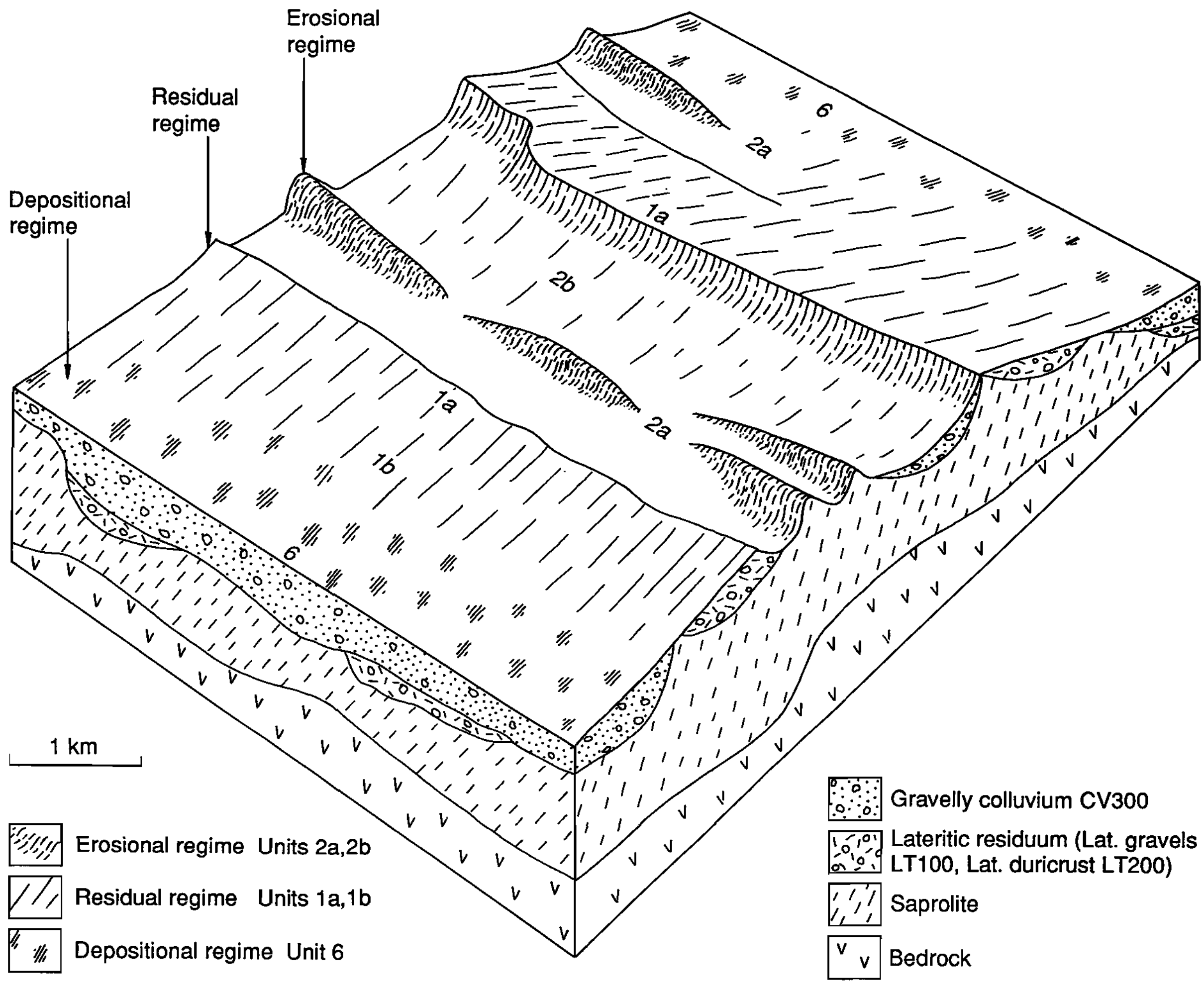

Fig.20. Generalized regolith/landform model based on the Brilliant study area.

4.4.6 REGOLITH STRATIGRAPHY - WAROONGA PIT

The Waroonga Pit, located on Fig. 8 and developed during late 1990, provides an excellent exposure to study the regolith stratigraphy in depositional regimes. The deposit is located within the Scotty Creek Sequence of metasedimentary rocks and thus contrasts with the dominantly mafic/ultramafic settings of the McCaffery, North Pit, Turrett, and Meatoa areas. The N and W walls expose a shallow 1-1.5 m thick weakly-indurated nodular duricrust which is overlain by 7-8 m thick transported regolith (Fig. 21). Loose pisolitic, nodular unit as seen overlying lateritic duricrust at the North Pit and Turrett areas is not present at Waroonga. *Transported regolith* comprises 1.5 m thick acid red clays overlying 4-6 m gravelly hardpanized co-alluvium which in turn overlies 1.5 m thick red clay (Fig. 16B). At depth, the lateritic duricrust merges into the mottled zone with the appearance of large grey to red mottles in a clayey mass. Iron segregation bodies were not observed within the lateritic residuum or mottled zone. This is in contrast to Turrett and North Pit areas where iron segregations commonly occurred in the upper part of the regolith.

Lateritic residuum comprises red matrix with abundant incipient reddish-brown nodules and pisoliths. The pisoliths ranged in size from 2 to 15 mm and are clearly defined from the matrix by yellowish-brown 1-mm cutans.

In Waroonga, weak development of lateritic residuum (in terms of thickness) and the lack of iron segregations may be related to the nature of the underlying lithology. The Waroonga Pit is sited within the Scotty Creek Sedimentary Sequence comprising feldspathic sandstone, chert, and conglomerate of mafic and ultramafic origin (Partington, 1986). In contrast, lateritic residuum over mafic and ultramafic rocks at North Pit and Turrett Pit is relatively much thicker. This suggests that lateritic residuum is well developed over the mafic and ultramafic lithologies of the Lawlers greenstone sequence being less developed over the Scotty Creek Sequence. This is probably due to the differences in the amount of Fe available during lateritic residuum formation.

Mottling has also developed in red alluvial clays just above the zone of lateritic residuum. Mottling in co-alluvium resemble the mottling of mottled zone underlying the lateritic duricrust. This mottling in alluvium is an example of lateritization of transported regolith, and has developed features in this case similar to those of a mottled zone developed during the deep weathering of underlying rocks during the Tertiary period. The material can easily be misidentified as being a residual mottled zone because of the abundance of the mottles. Such a misidentification is likely to jeopardize the success of a geochemical exploration programme.

The Waroonga Pit exemplifies the prominent development of hardpan in the Lawlers district. At Waroonga, hardpan occurs beneath the acid clays at a depth of about 1.5 m and is brittle, dull, porous, laminar, partly-silicified, and red-brown in colour. Accumulations of black Mn oxides are characteristic and can occur on subhorizontal partings and on vertical hardpan fracture-surfaces. The hardpan is developed within layers of gravelly co-alluvium which comprises ferruginous clasts, lithic fragments, and quartz.

4.5 Description of Regolith Units

4.5.1 EROSIONAL REGIMES

Unit 2 -Ferruginous cobbles of iron segregations, red clay soils, fragments of ferruginous saprolite and *calcrete pockets*

This unit represents areas of mafic and ultramafic bedrock from which lateritic duricrust or any laterally-equivalent regolith cap rock has essentially been removed by erosion. Unit 2 is widely distributed throughout the Lawlers district, it can be subdivided as is now described.

Unit 2a

Unit 2a has a consistently heterogeneous and almost ubiquitous association of black ferruginous cobbles and pebbles, cobble-sized fragments of vein quartz, some silicified saprolitic fragments after

Lawlers regolith stratigraphy	Type location - depositional regime western wall of Waroonga Pit	
	Terminology	**Description**

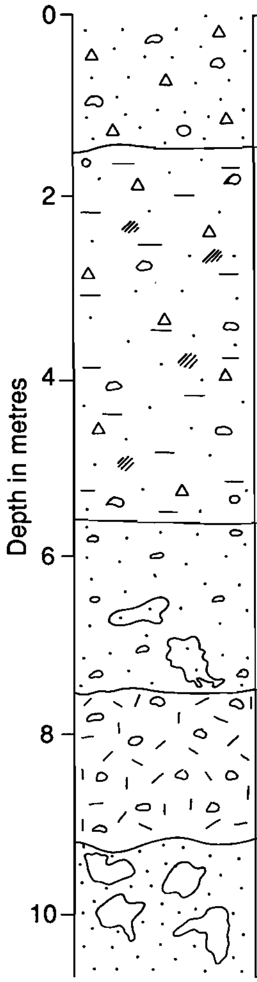

Terminology	Description
Colluvium (transported)	Red sandy clay loam with ferruginous clasts
Hardpanized colluvium (transported)	Hardpanized red-brown sandy clay loam to clay with lithic fragments, quartz and ferruginous clasts, Mn staining, (///) white fine silica along partings
Colluvial red clay (transported)	Red clay with few black ferruginous granules. Irregular pale mottles superimposed on a red matrix
Lateritic residuum (residual)	Nodular-pisolitic duricrust. Red-brown 5-10mm nodules and pisoliths with yellow-brown, 1mm cutan, set in a red matrix
Mottled zone	Pale to brown large mottles in a clay rich matrix

Fig.21. Vertical profile showing regolith stratigraphy at Waroonga, located within a depositional regime.

high Mg-basalts. These are associated with red friable sandy light clay soils and randomly-distributed isolated patches of pedogenic calcrete typically from 1 m to 5 m or more across which are commonly sites for goanna activity. The ground appearance of this unit is shown in Fig. 22A, B.

The *black lag* consists dominantly of rounded to subrounded fragments of iron segregations with a goethite-hematite mineralogy (Fig. 22C). Cobbles exceeding 10-cm in diameter are common. Some of the cobbles/pebbles show goethite pseudomorphs after sulphides and are thus gossan cobbles. The characteristics of these are described in detail in Section 6.0.

The *calcrete* is pinkish, massive and contains inclusions of iron segregations.

The *soils* are red (10 R 4/6, 2.5 YR 4/6, moist) gravelly light clays reaching 0.4-m in thickness and are acid except in the vicinity of the areas of pedogenic calcrete. Hardpan is generally absent. There soils show close association with weathered or subcropping mafic rocks and appear to result from *in situ* weathering of bedrock. Several soil samples from the Meatoa and North Pit areas were separated into their size fractions: gravel (>2 mm), sand (0.05 to 2 mm) and clay (<2μm).

The *gravel-sized fraction*, which represents 20-30% of the soil volume, largely consists of black ferruginous pebbles and ferruginous granules. The ferruginous pebbles are similar to the cobbles and pebbles of iron segregations which form the lag. Subordinate amongst the pebble-sized material are subangular to angular yellowish-brown (10 YR 5/8 to 10 YR 6/6, dry) fragments of ferruginous saprolite which are goethite- and kaolinite-rich. Some fragments of ferruginous saprolite show recognizable relict textures after amphiboles or pyroxenes.

The *sand-sized fraction* consists of fragments of ferruginous saprolite, grains of goethite pseudomorphs after primary minerals, earthy siliceous white fragments, ooliths, and quartz grains.

Goethitic pseudomorphs after amphibole form black (7.5 R 2.5/0, dry) millimetre grains. Surfaces of the pseudomorphs are heavily pitted which result in the formation of fragile shells or ghosts (Fig. 23) and largely consist of blade-shaped crystals of goethite. The semi-quantitative chemical analysis of such crystals shows them to consist of Fe with small amounts of Al, Ca, Ti, K, Si, and Cu. The traces of Ca probably represent the unweathered parts of amphiboles, whereas Ti, Si, Al, and Cu can substitute for Fe^{3+} in goethite, but the presence of K is not explained. Titanium and Al can also be present as discrete minerals.

The *clay fractions* of Units 2a are dominated by kaolinite. Other minerals present are illite, chlorite, smectite, and mixed-layer minerals as well as goethite and hematite. The clay minerals are the result of weathering of amphiboles and plagioclase feldspars. The presence of illite cannot be explained by the weathering of primary mineral grains of the bedrock, because mica is generally absent in mafic and ultramafic rocks as is K-feldspar. Mica is possibly aeolian in origin, apparently derived from the adjoining granitic terrain.

Unit 2b

Unit 2b is characterized by an association of the following regolith components: a coarse lag of fragments of ferruginous saprolite, iron segregations and vein quartz, a surface red (10 R 4/6, moist) sandy clay loam soil, and locally-derived colluvium of sandy clay loam and sandy light clays. The colluvium can be 1 m thick.

Regolith Unit 2b represents areas of Unit 2 where the locally-derived colluvium has accumulated, suppressing topographic variations. Authigenic hardpanization affects much of this colluvium. The hardpan matrix is characteristically porous and red to red-brown (2.5 R 2/4, 5/6, moist) with films of Mn oxides being present on surfaces. The lag is relatively finer (up to 50 mm) and less abundant on this unit in comparison with Unit 2a and mainly consists of yellowish-brown (10 YR 5/8, dry) kaolinite- and goethite-rich fragments of ferruginous saprolite with small amounts of black (2.5 YR 3/8, dry) hematite-goethite-rich ferruginous pebbles of iron segregations, and a few scattered pisoliths. The goanna mounds marking the presence of calcrete in Unit 2a are characteristically absent from Unit 2b.

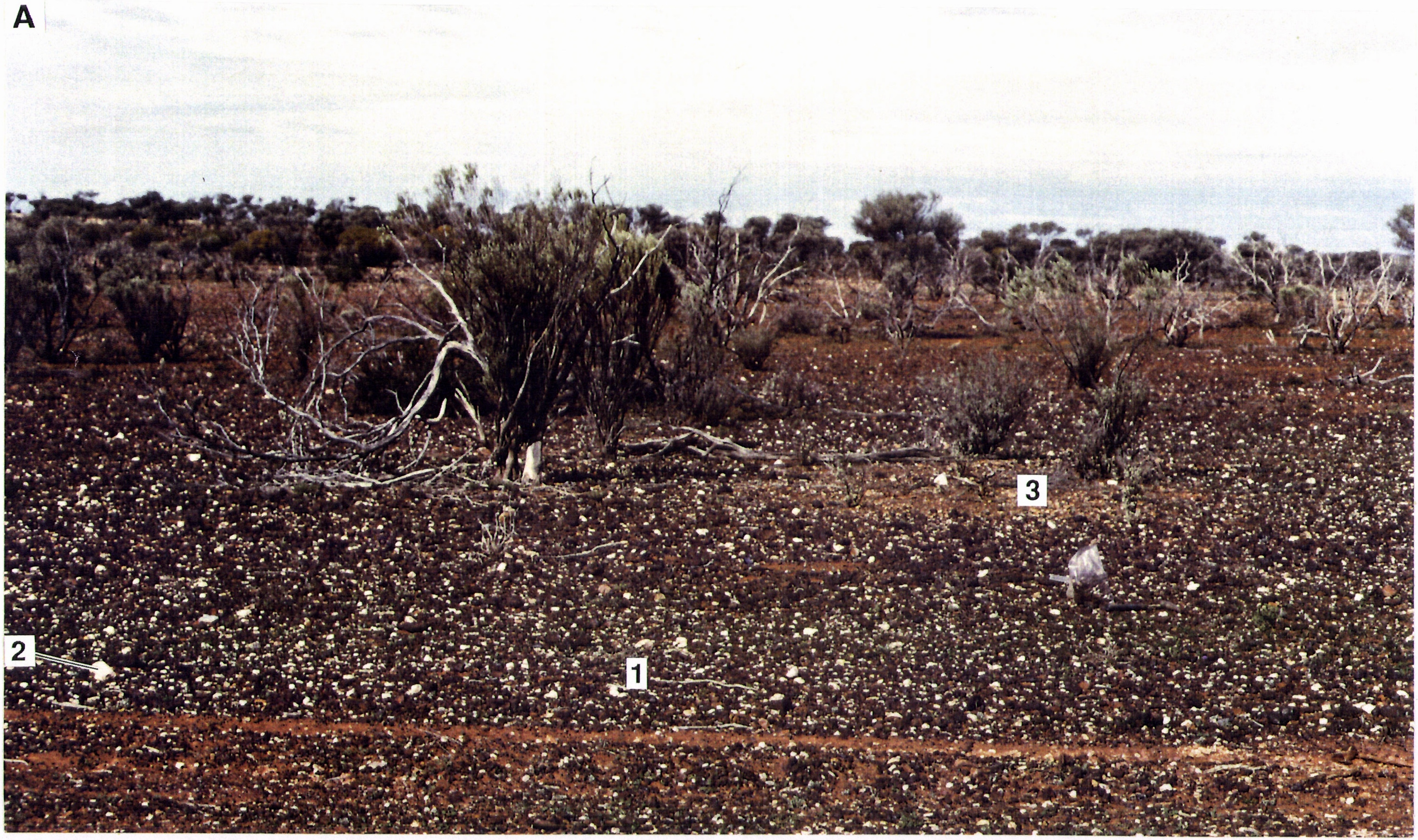

Fig.22A. Regolith Unit 2a: Abundant lag of cobbles and pebbles of iron segregations (1), vein quartz (2) and pockets of pedogenic calcrete (3) over sandy light clay soil, with degraded mulga shrubs, location 6891600N, 273350E, Meatoa area.

Fig.22B. Close up of ferruginous cobbles and vein quartz of Fig.22A.

Fig.22C. Hand specimen of cobbles and pebbles of iron segregations. Sample 07-1310, Meatoa area.

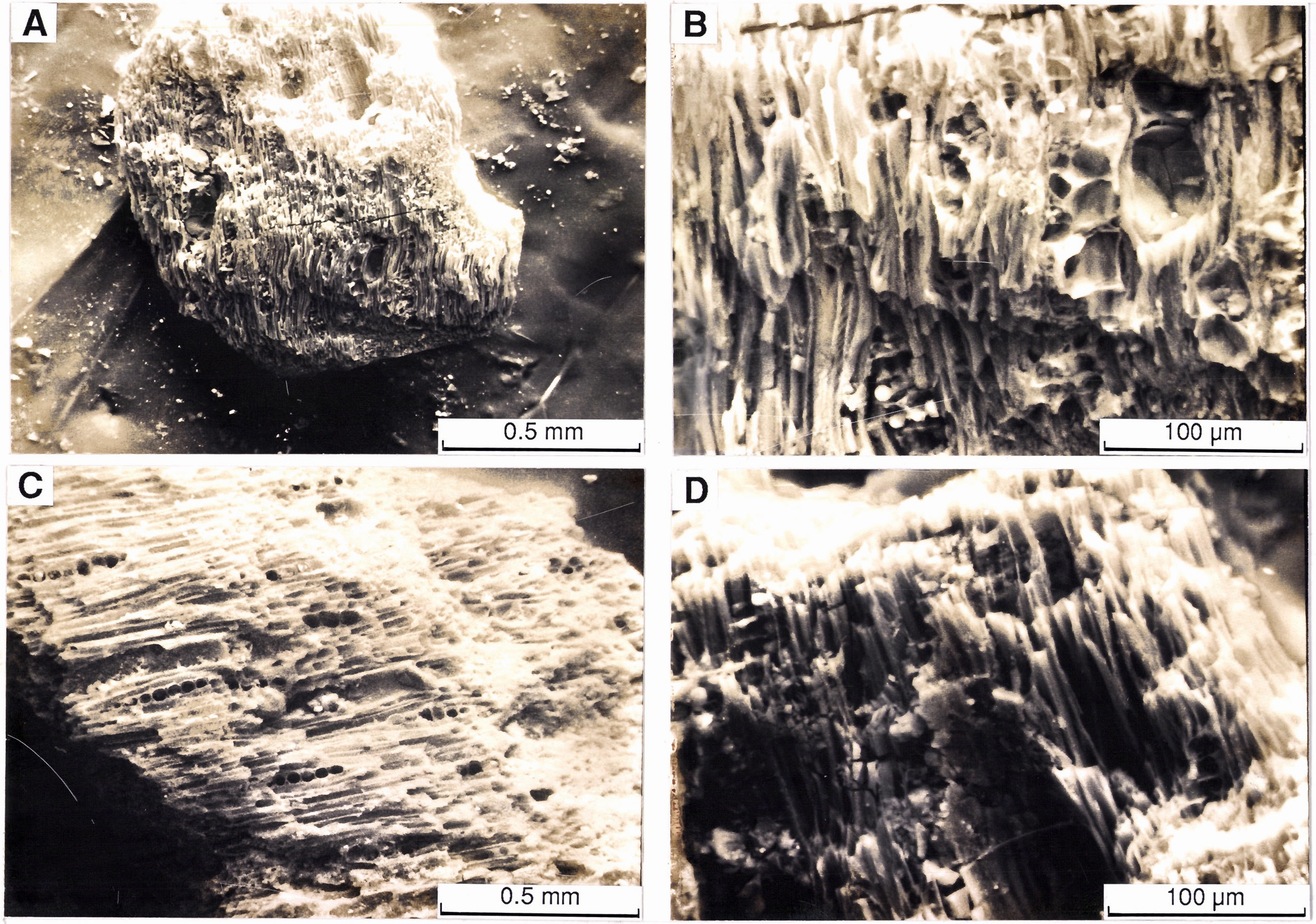

Fig.23. Low (A,C) and high (B,D) magnification scanning electron photomicrographs of grains of pseudomorphs after amphiboles separated from soils of regolith Unit 2a. These grains are replaced by blade-shaped crystals of goethite. Energy dispersive X-ray (EDX) spectra indicated the presence of Fe confirming the presence of goethite, location 6891600N, 273350E, Meatoa area.

Unit 3 - Lag of ferruginous saprolite, fragments of Fe-rich duricrust

Unit 3 has been subdivided into two subunits on the basis of the nature of their lithologies.

Unit 3a - mafic substrate

Unit 3a comprises breakaway and pediment slopes surface is dominated by outcrop of ferruginous saprolite and associated coarse lag. Lag derived from the breakdown of Fe-rich duricrust is also common. There may be a few pockets of bodies of iron segregations and associated black cobbles of iron segregations lag.

The dominant soils are red-brown sandy clay loam, hardpanization may affect much of these soils.

Unit 3b - granitic/felsic substrate

Unit 3b is characterized by paler clayey sand soils. Fine quartz with feldspar grit is common lag.

Unit 5 - mafic outcrops, shallow stony soils

Unit 5 is characterized by areas of rock outcrop. Ferruginous lag is not common. The soils are dominantly shallow stony clay loam and appear to have developed *in situ.*

Unit 11 - Saprolite

Unit 11 has been subdivided into two.

Unit 11a - mafic saprolite

Unit 11a represents areas of outcrops of mafic saprolite. The dominant soils are red sandy clay.

Unit 11b - felsic/granite saprolite

This unit represents areas of outcrops of granitic/felsic lithologies with a thin sandy soil cover. Quartz lag is common.

4.5.2 RESIDUAL REGIMES - LATERITIC RESIDUUM

Unit 1 represents areas where the complete lateritic weathering profile, including the lateritic residuum is essentially preserved. The unit is generally composed of the following regolith: friable brown (7.5 YR 4/4, moist) gravelly fine sandy loam to fine sandy clay loam soil, loose pisoliths/nodules, Fe-rich duricrust, and nodular/pisolitic duricrust. The lateritic residuum generally passes downwards into a thin zone of ferruginous saprolite. Ferruginous saprolite/saprolite outcrops where the duricrust is locally eroded. The residual regime (Unit 1) has been subdivided largely on the basis of surface expression, nature and size of lateritic materials, and topographic characteristics. These are now described.

Unit 1a - Fe-rich duricrust

Unit 1a is largely mantled by Fe-rich duricrust and may have nodular (LT224), pisolitic (LT222) or oolitic (LT221) structures. However duricrust low in Fe such as pisolitic (LT202), nodular (LT204) or vermiform (LT231) may also occur. The characteristics and origins of Fe-rich duricrusts are described in detail in Section 5.0.

Lag on Unit 1a is dominated by black (2.5 YR 3/0, dry) magnetic, hematite-rich coarse fragments (20-60-mm dia.) of Fe-rich duricrust and reddish brown (2.5 YR 4/4, dry) 5-10-mm pisoliths and nodules. Some saprolitic fragments may also occur, these are related to pockets of saprolite exposed in the unit. Saprolitic lag consists of yellowish-brown to reddish-brown subangular to angular, 2-30-mm kaolinite-rich fragments. Some fragments retain the primary rock fabric.

On the crest, the soils are reddish-brown (5 YR 5/6, dry), friable fine sandy loams and are slightly acidic.

Unit 1b - Lateritic pisoliths, nodules

Lag on Unit 1b is dominated by medium to fine (3-15-mm dia.) yellowish-brown lateritic pisoliths and nodules. Nodules and pisoliths have black or reddish brown cores with 1-2-mm thick yellowish brown cutans. There are no outcrops of duricrust. Surface expression of this Unit is shown in Fig. 24.

Soils in Unit 1b are brown (7.5 YR 5/4, moist), gravelly fine sandy loams to sandy clay loams which overlie lateritic residuum. Soils are generally residual on this unit, however on long gentle slopes there may be some local colluvium. Hardpan is weakly developed at a depth of 0.5 to 1 m. The dominant (25-40 vol%) gravel component of these soils consists of 2- to 15-mm-sized lateritic nodules and pisoliths. Occasionally, reddish-brown pseudomorphic grains are also present, but it is not clear whether these are after orthopyroxenes or amphiboles. The pseudomorphic grain shown in Fig. 25 is about 4 mm in size and is completely replaced by a mixture of laths and platy crystals of Fe oxides and kaolinite. Qualitative chemical analysis of this crystalline aggregate shows the presence mainly of Fe with small amounts of Al and Si. Aggregates of similar morphology have been shown to develop from chemical weathering of orthopyroxenes in ultramafic rocks under lateritic conditions by Nahon and Colin (1982). These authors considered that lath-shaped goethite is pseudomorphic after talc.

The *sand fraction* (25-35% vol%) largely consists of yellow to dark reddish brown ooliths, quartz, black ferruginous granules, and yellowish-brown fragments of ferruginous saprolite.

The *clay fraction* is largely dominated by kaolinite. Traces of chlorite, illite, and interstratified minerals are also present, smectite is typically absent.

The *lateritic residuum* includes both loose, nodular/pisolitic laterite and nodular/pisolitic duricrust. Loose or weakly-cemented lateritic pisoliths/nodules in a yellowish-brown sandy clay matrix form a widespread unit that can outcrop, or more commonly lies beneath soil or hardpanized colluvium. This unit may merge at depth with lateritic duricrust. The loose nodular/pisolitic unit is well developed at McCaffery, Turrett and Agnew-gravel Pits but was absent in Waroonga Pit. In the western wall of Waroonga Pit, nodular duricrust is overlain by alluvial red clay.

The cores of the nodules and pisoliths are dark reddish-brown (5 YR 3/3, dry), through black (2.5 YR 3/0, dry) to red with thin, usually <2-mm, yellowish brown/olive green cutans. Nodules and pisoliths are present, however nodules are generally dominant. Greatest development of pisoliths was seen in Agnew gravel Pit. They are spherical ranging in size from 3- to 5-mm with 1 mm thick yellowish-brown cutans. These pisoliths are comprised mainly of goethite and hematite with small amounts of kaolinite, gibbsite and anatase. The nodules are subrounded to irregular in shape with a size range of 2-15 mm and are indurated by hematite and goethite. Of the various size-categories, 3-6-mm nodules are most common. Generally both the magnetic and non-magnetic fractions are present. Magnetic nodules are hematite- and maghemite-rich with small amounts of kaolinite. The non-magnetic nodules contain large amounts of goethite and kaolinite, but maghemite was not detected. The nodules and pisoliths may contain inclusions of quartz and ilmenite grains (< 1 mm).

At Lawlers, the most characteristic feature of residual nodules and pisoliths is the presence of yellowish-brown/olive-green cutans on the outer surface. The cutans are generally less than 2-mm in thickness. Electron-microprobe analysis of olive-green cutans show them to consist of mixture of gibbsite and Fe-oxides (Table 6). The cores of nodules are Fe-oxide rich ($\approx$85% Fe_2O_3).

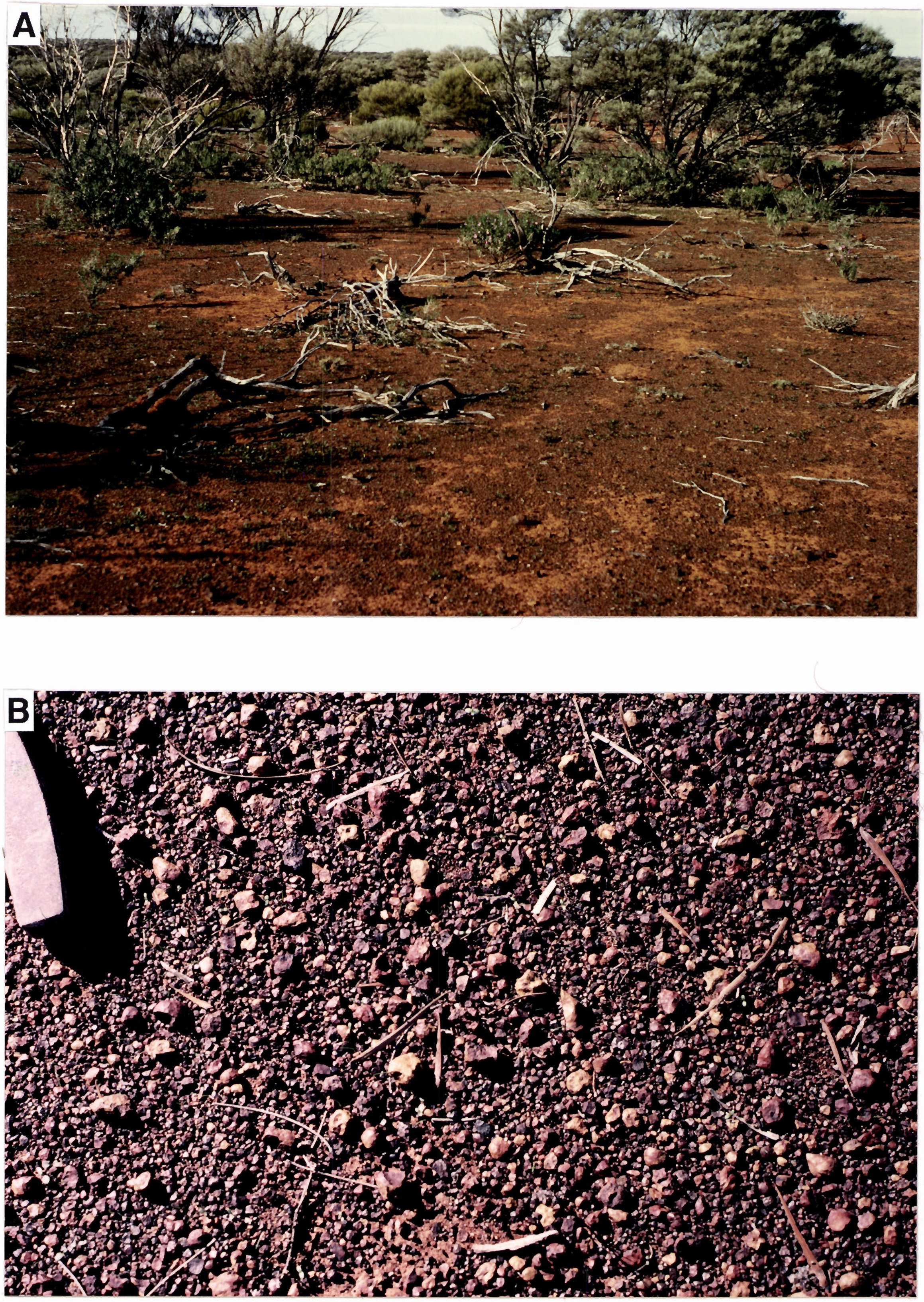

Fig.24A. Regolith unit 1b: Lateritic lag (nodules, pisoliths) and mulga shrubs on long gentle slopes (backslopes), Agnew area.

Fig.24B. Close up lateritic nodules and pisoliths with yellowish brown cutans.

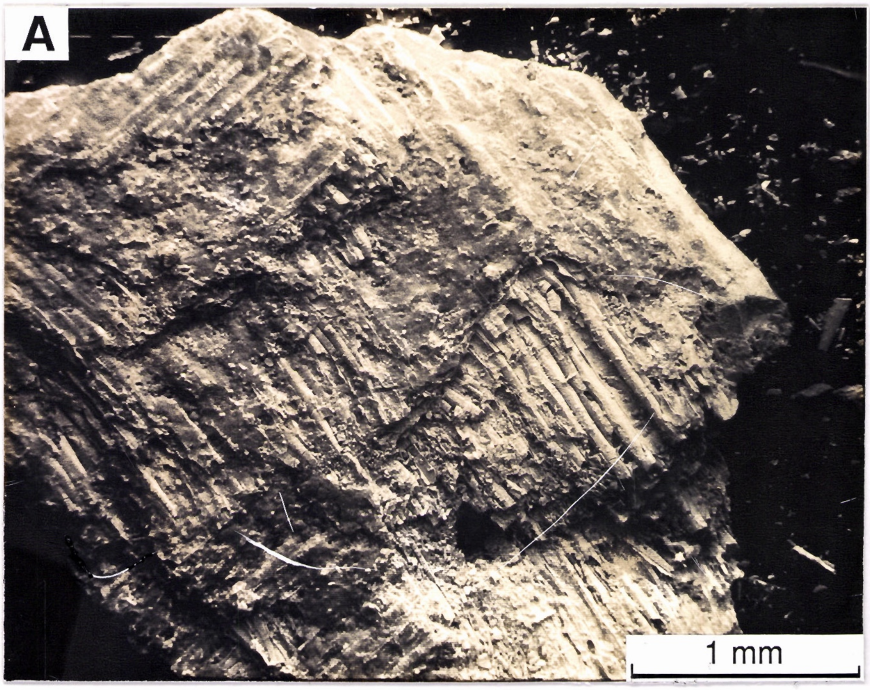

Fig.25A. Low magnification scanning electron photomicrograph of separated grain of a pseudomorph after orthopyroxenes (?) from soil of regolith Unit 1, location 6891600N, 272700E, Meatoa area.

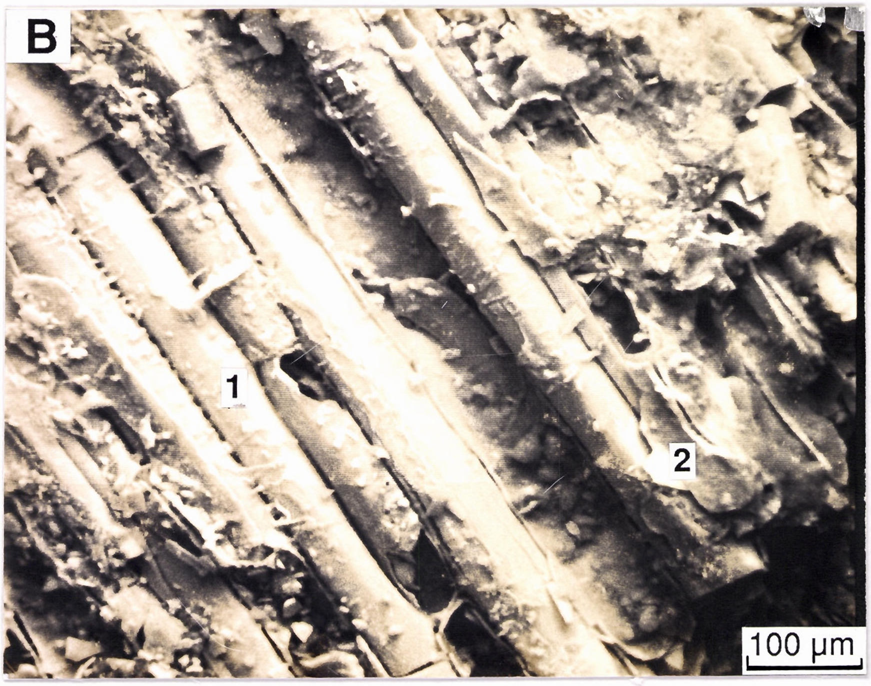

Fig.25B. High magnification scanning electron photomicrograph of part of grain of Fig.25A showing laths of goethite (1) and platy crystals of kaolinite (2).

Table 6. Microprobe analyses of cores and green cutans of nodules from residual laterite (Hole No. 729, Sample 07-0838, Depth 26-27 m), North Pit area.

	Hematite-rich Core		Gibbsite-rich Green Cutans	
wt%	1	2	1	2
SiO_2	1.34	1.39	7.21	1.55
TiO_2	0.70	0.68	0.87	0.12
Al_2O_3	9.13	10.2	50.44	40.00
Cr_2O_3	0.39	0.45	1.03	0.80
Fe_2O_3	85.03	83.62	34.02	57.08
MnO	<0.03	<0.03	<0.03	0.03
MgO	0.02	0.02	0.31	0.04
CaO	<0.01	<0.01	0.07	0.03
K_2O	<0.01	<0.01	0.05	<0.01
Na_2O	0.02	0.03	0.03	<0.01
TOTAL	96.64	96.40	94.04	99.65

Original rock fabrics are observed in some pisoliths and nodules. The cores of a few pisoliths contain goethite and kaolinite pseudomorphs after mica and amphiboles. Some nodules and pisoliths developed from ultramafics show the preservation of talc in their cores.

Cores of the nodules also show the development of oval voids, some of which have infill or coatings of kaolinite, goethite, and small quartz grains. These voids are reception-structures for the secondary accumulation of clays and Fe-oxides.

Some nodules are partly replaced or surrounded by secondary silica. Compound nodules enclosing small pisoliths and nodules are also present.

Lateritic duricrust

The distribution of duricrust is patchy at Lawlers; generally occurring beneath the loose pisolitic-nodular unit. When duricrust is absent, a loose pisolitic unit merges downwards with ferruginous/mottled saprolite. It is typically 1-2 m thick when exposed in pit faces. Introduction of silica cement has modified some duricrusts, resulting in a coarsely-laminated appearance, referred to as "hardpanized duricrust".

Pisolitic nodular duricrusts (LT203) are the most common type of duricrust (Fig. 26A). They are coherent weathering crusts composed of accumulations of ferruginous nodules and pisoliths cemented by Fe-oxides and clays. A sandy clay matrix (20-50%) is pale through yellowish-brown to dark red and is predominantly hematite, goethite, kaolinite, and quartz. Between the nodules a network of pale zones may occur consisting only of kaolinite and quartz. These result from removal of Fe from the matrix. Ellipsoidal to irregular voids (1-10 mm) also occur in the matrix and are generally less than 15% of each handspecimen. Voids may have an earthy infill of kaolinite, quartz, and goethite.

Nodules and pisoliths in the duricrust make up about 40-60% of handspecimens and are reddish-brown to black. Black nodules are dominant at McCaffery, North Pit, Turrett, and Meatoa areas. However, this was not the case at Waroonga where reddish-brown nodules are dominant while magnetic black nodules are typically absent (Fig. 26B). Black nodules tend to magnetic, whereas reddish-brown nodules are non-magnetic. As mentioned before, this probably relates to bedrock types.

The internal and external characteristics of nodules and pisoliths in duricrust are similar to those of nodules and pisoliths in the loose lateritic gravels described above.

Bodies of Iron Segregations

Iron segregations are present within lateritic residuum and ferruginous saprolite. They occur as pods, lenses, and large slabs and are black, non-magnetic and goethite-hematite rich. Many of the iron segregations show goethite pseudomorphs after pyrite and/or pyrrhotite. Such bodies of iron segregations are then referred to as gossans. These are described in detail in Section 6.0.

Ferruginous Saprolite

Ferruginous saprolite generally underlies lateritic residuum. These are massive to mottled hard masses and are dominated by goethite and kaolinite. The matrix may have irregular light brown to yellowish-brown mottles with abundant vesicular and vermiform voids. The matrix also show the relict rock textures. These are described in detail in Section 6.0.

4.5.3 DEPOSITIONAL REGIMES - COLLUVIUM, ALLUVIUM

Much of the Lawlers area is characterized by colluvium and alluvium, a significant part of which has been derived from erosion of lateritic weathering profiles in upland areas. There is a widespread occurrence of buried, complete laterite profiles beneath many of the colluvial and alluvial plains of Lawlers.

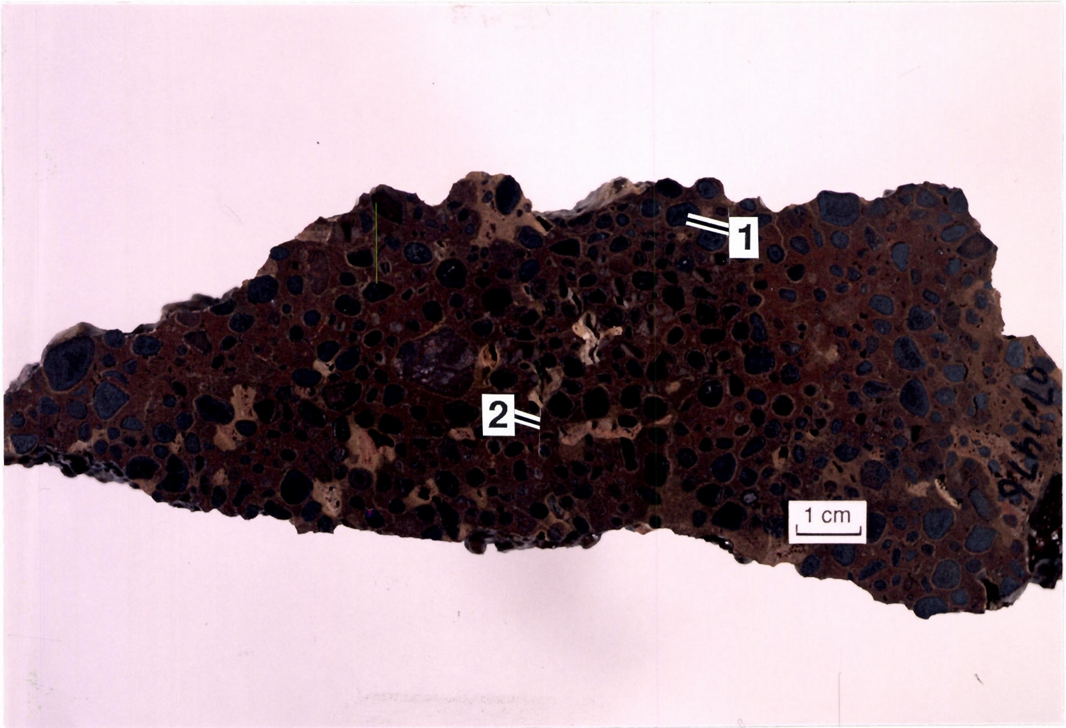

Fig.26A. Slice through pisolitic-nodular duricrust showing black pisoliths (1) set in a dark brown sandy clay matrix (2), location western wall of Turrett Pit, Sample No. 07-1476.

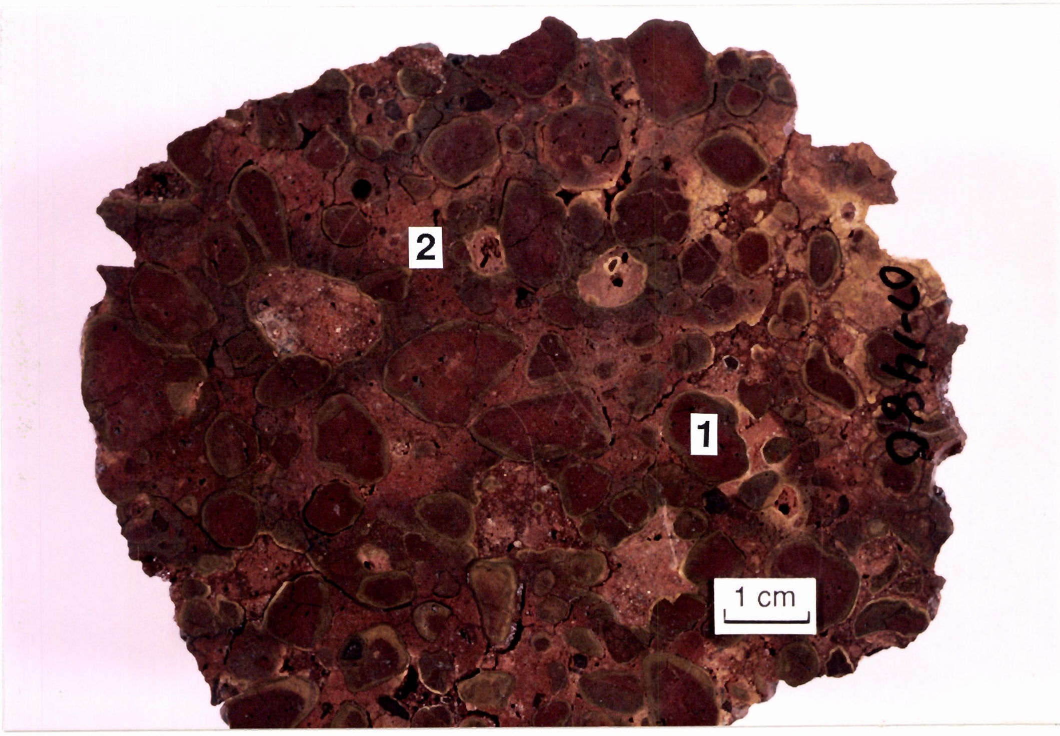

Fig.26B. Slice through weakly indurated pisolitic-nodular duricrust showing reddish brown nodules and pisoliths (1) set in a yellowish-brown sandy clay matrix (2), location western wall of Waroonga Pit, Sample No. 07-1480.

Unit 6 - Colluvium

Unit 6 is a sand-silt-gravel colluvial unit which is well represented throughout the Lawlers district, and is believed to represent sheet wash and braided wash sediments derived from dismantling of adjacent lateritic and saprolitic uplands. In the Lawlers district, Unit 6 reaches 25 m in thickness and has resulted in burial of the lateritic residuum and suppression of local relief of the partly-eroded lateritic surface. Hardpan due to cementation of the sandy clay/silty clay colluvial units is variable and reaches a maximum development within 2 m of surface. The maximum depth of hardpan noted was 10 m.

Unit 6 has a veneer of lag in the 2 to 30-mm size range. This lag is very heterogeneous containing fragments of various colours lateritic pisoliths, nodules, ferruginous granules, pebbles, and quartz fragments. The fragments derived from ferruginous saprolite are yellow, yellowish brown, reddish brown, greyish-brown or red, subrounded to angular, 2-15 mm in size and are generally non-magnetic. Outer surfaces of the lag have a varnished appearance and lack cutan development. Fabrics of some fragments preserve their mafic and ultramafic origin. The lateritic pisoliths/nodules are yellow to red, rounded to subrounded in shape, with a size range of 3-5 mm and they consist of black to reddish brown hematitic cores with greenish goethite-rich cutans. Nodules with black cores are generally magnetic because of the presence of maghemite. The variety of components in the lag indicate their diverse origins, much material being derived upslope from the breakdown of lateritic duricrust, large fragments of ferruginous saprolite, and from ferruginous cobbles. For example, pisoliths and nodules related to lateritic duricrust have hematite-rich black cores with yellow goethite-rich cutans. These pisoliths are commonly observed in lateritic residuum of regolith Unit 1. A few black subangular to angular granules without any cutans are related to bodies of iron segregations of regolith Unit 2. Yellow, reddish-brown, and red fragments are related to the large fragments of ferruginous saprolite in erosional areas. This lag typically overlies a gravelly red (10 R 4/6, moist) soil consisting of sandy clay loam to fine sandy light clay. The clay content generally increases with depth, and, in places, is mottled lower in the profile. The matrix is redder at the surface and generally becomes pale and has a puggy consistence in the subsurface. The surface appearance of this unit is shown by Fig. 27.

Varying amounts of the clasts occur in the colluvium. The upper horizons of the colluvium at the North Pit and Meatoa areas are dominated largely by coarse gravels, the unit becoming finer with depth. The lower horizons are mainly comprised of fine to medium (2-15 mm) lateritic gravels with small amounts of lithic fragments and quartz fragments. This material can easily be misidentified as being a residual laterite because of the abundance of lateritic pisoliths and nodules.

The gravel fractions of surface soils developed in colluvium consist of a variety of clasts including lithic and ferruginous pebbles, quartz fragments, and lateritic pisoliths and nodules. The clasts are subangular to angular, unsorted and reach 40 mm in diameter. The variety of clasts indicates their diverse origin, possibly from the breakdown of saprolite and lateritic duricrust.

The lateritic gravel fraction within colluvium generally consists of dark reddish-brown/black (5 YR 3/3, 5 YR 2/1, d) to dusky-red (2-5 YR 2/2, 10 R 3/3, d) nodules and pisoliths, averaging fine to medium size (2 to 15 mm) and are predominantly rounded. A variety of lateritic gravel was observed which differs from the other gravels in colour, presence or absence of concretionary cutans and/or lithorelics and in mineralogy. Within this gravel some nodules show concretionary cutans in a succession of layers (yellow-red-yellowish-brown) which are $<$1-mm thick. Others have only red cutans, which are also thinner. There is a sharp contact between the cores of nodules and the concretionary cutans. Single grains ($<$0.2 mm) of quartz or lenses of quartz grains are abundant in the cutans. Electron microprobe analyses of the yellowish-brown cutans showed them to mainly consist of clay minerals. Given that no gibbsite was detected by XRD in the laterite gravels from the colluvial units, the cutans with a composition of 44-48% SiO_2 and 35-36% Al_2O_3, can be interpreted as consisting mostly of kaolinite. Small amounts of Fe (approx. 5%) are present as Fe oxides. Some Fe is probably present in the structure of kaolinite. In contrast, red cutans are a mixture of Fe oxides and kaolinite. The laminar cutans around cores of nodules clearly represent a succession of depositional layers, and the commonly observed incorporation of single grains or lenses of grains of quartz between the layers suggests an accretionary origin of the cutans.

Fig.27A. Regolith Unit 6a: Fine lag of mixed origin and eremophila shrubs and geranium herbs on colluvial outwash plains, location 6891600N, 271300E, Meatoa area.

Fig.27B. Close up of fine lag of mixed origin of Fig.27A.

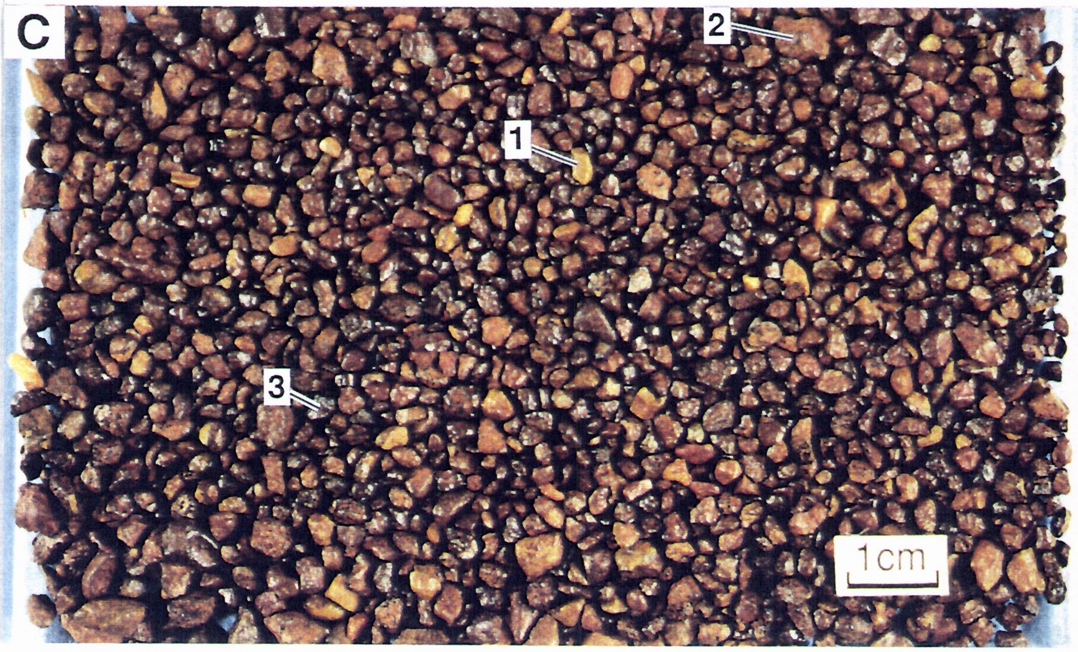

Fig.27C. Detail of fine lag of mixed origin showing fragments of ferruginous saprolite (1), lateritic pisoliths/nodules (2) and ferruginous granules (3). Sample 07-1330, Meatoa area.

The *sand-sized fraction* consists of rounded to subrounded shiny black and red ferruginous granules, black lateritic pisoliths, and grains of quartz. Both magnetic and non-magnetic granules are present. Many of the rounded ferruginous granules are transported.

The *clay-sized fraction* largely consists of kaolinite with small amounts of smectite and illite. Chlorite and mixed-layer minerals were not detected. Both goethite and hematite are present.

Loose Lateritic Gravels occur as lenses of loose nodules/pisoliths within the colluvium and represent transported lateritic detritus. These lenses are generally thinner than the fine-grained colluvial subunits. Their thickness does not exceed 5 m. The nodules are reddish-brown/black (5 YR 3/3, 5 YR 2/1, dry) to red (10 YR 3/3, dry), generally well rounded, and small (generally < 10 mm in diameter) with or without greenish/red/yellow cutans.

Several types of nodules were recognized based on their chemical compositions and mineralogies. Of particular interest is the composition of nodules which have core materials reflecting a variety of sources and concretionary cutans which record a complex history of development. For example, electron microprobe analyses of cores of nodules from transported laterite (Hole No. 729) show large differences in chromium contents (Table 7). Some nodules have chromium values up to 2.5%, whereas others reach only 0.5%.

At Meatoa, regolith Unit 6 was divided into Unit 6a and 6b. Unit 6b characterizes areas which have a felsic substrate, but which have a mantle of colluvium derived from the adjacent mafic/ultramafic terrain. The lags of iron segregations, fragments of ferruginous saprolite, and vein quartz derived from mafic terrain contrast with the quartzose and feldspar grits of areas of granitic rocks. Red friable fine sandy clay loams dominate the mafic detritus, while reddish-brown to brown gritty sandy loams are common soils on felsic detritus.

Unit 7 - Alluvium

Alluvium in the Lawlers area overlies lateritic duricrust or saprolite at depth and is in excess of 3-m thick. Alluvium accounts for about 30% of the mapped area at Lawlers. Unit 7 is divided into three subunits :

Unit 7a - alluvium in minor tributaries

Red (10 R 4/6, moist) friable light clays are dominant. Lags are not common.

Unit 7b - alluvium in major tributaries

The dominate surface soil is a reddish-brown (5 YR 3/3, moist), gravelly sandy clay loam varying to a light textured clay. Hardpan is developed at about 30 cm. There is very little lag on the surface.

Unit 7c - alluvium in braided-wash valleys

Light clays are dominant. Fine lag (< 10 mm) of lateritic nodules, iron segregations, ferruginous saprolite, and quartz fragments is common. Hardpan is developed.

4.6 Synthesis of Regolith Development - facies relationships

The development of the regolith of the Lawlers district can be related to processes of deep lateritic weathering, subsequent erosion, deposition and modification through leaching and cementation. The processes responsible for the formation of the regolith at Lawlers are described below.

Table 7. Microprobe analyses of cores of nodules from transported lateritic gravels (Hole No. 729, Sample 07-0835, Depth 9-10 m), North Pit area

	Hematite-rich Core		Hematite-rich Core	
wt%	1	2	1	2
SiO_2	6.56	10.94	5.96	7.33
TiO_2	0.06	0.07	0.25	0.60
Al_2O_3	6.36	4.29	6.73	10.35
Cr_2O_3	2.09	2.50	0.27	0.44
Fe_2O_3	81.31	77.59	80.67	75.68
MnO	<0.03	<0.03	<0.03	<0.03
MgO	<0.03	0.10	0.06	0.08
CaO	0.11	0.20	0.10	0.11
K_2O	0.09	0.10	0.05	0.05
Na_2O	0.09	0.06	0.03	0.07
TOTAL	96.67	95.85	94.12	94.72

4.6.1 LATERITIC RESIDUUM - FORMATION AND PARTIAL DISMANTLING

Figure 28 shows the facies relationships for the development of lateritic residuum in the Lawlers district. Arrows show the genetic link between the facies. Weathering of the mafic and ultramafic rocks has produced a thick, deeply-weathered mantle which shows vertical differentiation of the developed horizons. The successive arrangement of these horizons, follows this upward sequence: parent rock saprock saprolite ferruginous saprolite lateritic duricrust loose lateritic pisoliths/nodules. These horizons tend to merge one with another. Primary minerals (amphiboles, feldspars, pyroxenes) weather into secondary products which in turn are transformed, later and higher in the profiles, into new products, amongst which iron oxides and oxyhydroxides are the most abundant. It should be pointed out that ferruginous saprolite forms a blanket deposit up to several metres thick in many areas in the Lawlers district and is preferentially developed over mafic and ultramafic lithologies.

Weathering of amphiboles generates smectites in parts of the saprolite which further weather to kaolinite. Gibbsite is known to occur in highly-weathered, acid environments where its formation appears to be dependent on the intensity of leaching under conditions of free drainage (Hsu, 1979). Kaolinite and halloysite may be precursors of gibbsite in such environments. The presence of gibbsite in small amounts in the lateritic residuum at Lawlers does not account for the abundant kaolinite in the saprolite. It appears that kaolinite may have been replaced by hematite through the epigenetic reaction suggested by Didier (1983) and Cantinolle *et al.* (1983). This reaction is important since it involves the dissolution of kaolinite with the accompanying release of protons (lowering of pH) which may contribute to the dissolution and dispersion of Au (Ambrosi *et al.*, 1986; Colin *et al.*, 1989).

Two modes of formation of pisoliths and nodules in lateritic residuum have been identified at Lawlers; these are now described below.

Fragmentation

Development of many of the nodules and pisoliths is associated with fragmentation of ferruginous saprolite (Fig. 28A). This is well seen in the walls of the McCaffery Pit, Fig. 15A. Ferruginous saprolite is a yellowish-brown indurated mass which is produced by the infusion of Fe into clay-rich saprolite. Higher in the profile, ferruginous saprolite is then subjected to modification by weathering. A more important process in the modification is its fragmentation by the development of numerous irregular voids. Dissolution or dispersion of soft clay-rich masses leads to the development of voids which allow the separation of hard material into fragments. Voids weaken the whole mass which may eventually lead to the complete fragmentation (collapse) of ferruginous saprolite. Fragments are further broken down into small nodules which commonly have yellowish-brown olive-green outer cutans. As sphericity of nodules increases, up the profile, by dissolution of irregularly-shaped edges, some nodules develop into pisoliths. The cutans may form and become further rounded by concentric concentrations of Fe and Al around the nucleus.

This model indicates that fragmentation of bodies of iron segregations can yield nodules and pisoliths which become incorporated in the lateritic residuum.

Small-Scale Migration and Accumulation of Fe as Mottles

This represents the more classical model of pisoliths formation described in the literature (Fig.28B). Development of pisoliths is associated with the small-scale migration and accumulation of Fe. As weathering progresses higher in the profile, Fe is mobilized and concentrated as spots, blotches and streaks leading to the generation of mottles and incipient nodules (precursors of nodules), forming a mottled clay zone, where the major difference between the mottles and the surrounding matrix is the Fe content in the mottles. Incipient nodules have more or less diffuse outer rims and are partly indurated. The areas within the mottled zone from which the Fe is moved in solution, essentially as soluble Fe^{2+}, exhibit a progressively white or grey colour on deferruginization and essentially consist of kaolinite and quartz which is predominantly relict. These changes can be accompanied by a strong increase of microporosity, leading subsequently to the formation of voids such as tubules, etc.. The voids left by dissolution of the matrix are occupied by secondary accumulations of kaolinite, hematite, and fine grained quartz, and may become indurated masses.

With further mobilization and concentration of Fe, mottles and incipient nodules evolve into nodules. Hematite generally replaces some of the goethite in nodules. In the duricrust, the nodules become more indurated and their boundaries with the matrix becomes distinct.

Nodules commonly become increasingly abundant towards the top of the profile. As sphericity of nodules increases, generally by dissolution of irregularly-shaped edges, some nodules develop into pisoliths. Following this evolutionary trend, pisoliths are relatively more abundant in the upper portion of the lateritic residuum.

Partial Dismantling

Also shown schematically in Fig. 28A is the dismantling of the regolith (in particular lateritic residuum, ferruginous saprolite) by pluvial processes. Dismantling of lateritic residuum leads to the deposition of colluvial/alluvial units rich in lateritic nodules and pisoliths. In contrast colluvial/alluvial units derived from ferruginous saprolite, saprolite, and lateritic residuum are dominated by polymictic gravels. All of the colluvial/alluvial units can be further modified by cementation resulting in hardpan.

Erosion has affected some parts of the landscape, while other parts such as back slopes, remain relatively unchanged. Materials removed from the erosional areas have been deposited on lower slopes with consequent burial of deeply-weathered profiles and the reduction of relief. Field relationships and subsurface information provided by drilling indicate that the present colluvial slopes, for example, have had relatively-higher relief before erosion. The occurrence of saprolite in the low hill areas suggests that the land surface was truncated by some 10-m or more. Perhaps the low hills were topographically higher than the present crests which are now capped with Fe-rich duricrust, once hardened, the latter would be resistant to erosion. Inversion of relief may have eventually caused Fe-rich duricrust to be located on ridge crests. The origin of these Fe-rich duricrusts is discussed in detail in Section 5.0.

4.6.2 REGOLITH FACIES RELATIONSHIPS FOR EROSIONAL AREAS

Figure 29 depicts the effects of post-lateritic weathering upon areas where erosion has removed the lateritic residuum and ferruginous saprolite. Weathering of saprolite and bedrock continues. Erosional areas are covered by red clays and coarse lags derived from iron segregations. Red clays have a much more immature weathering status based upon the presence of recognizable pseudomorphs after amphiboles and fragments of ferruginous saprolite.

Origin of Friable Red Clays

One of the main characteristic features of the soils in the erosional areas at Lawlers is the occurrence of red clays, which from drilling, are seen to overlie mafic saprolite. It might be expected that the soils developed from mafic lithologies would be calcareous and have significant amounts of smectite-type clay minerals, but these red clays lack carbonates and smectite.

The non-calcareous nature and low level of smectite in these soils suggest that they have formed under generally mild to warm conditions, free drainage, and sub-humid to humid climates with alternating wet and dry periods. These are the conditions necessary for leaching of carbonates and bases and the formation of kaolinitic clays that are acid and unsaturated with bases. Some Fe released on weathering has been mobilized and segregated as granules presumably during brief periods of partial saturation following heavy or prolonged rains.

These observations do not support the general belief that red clay soils are the product of weathering of mafic lithologies during an arid climate in which they now occur. In arid climates, pedogenic processes, such as the leaching of carbonates, do not occur due to the lack of a leaching regime. However, the genesis of these red clays can be explained by the following: the red clay soils

LATERITIC RESIDUUM FORMATION AND DISMANTLING

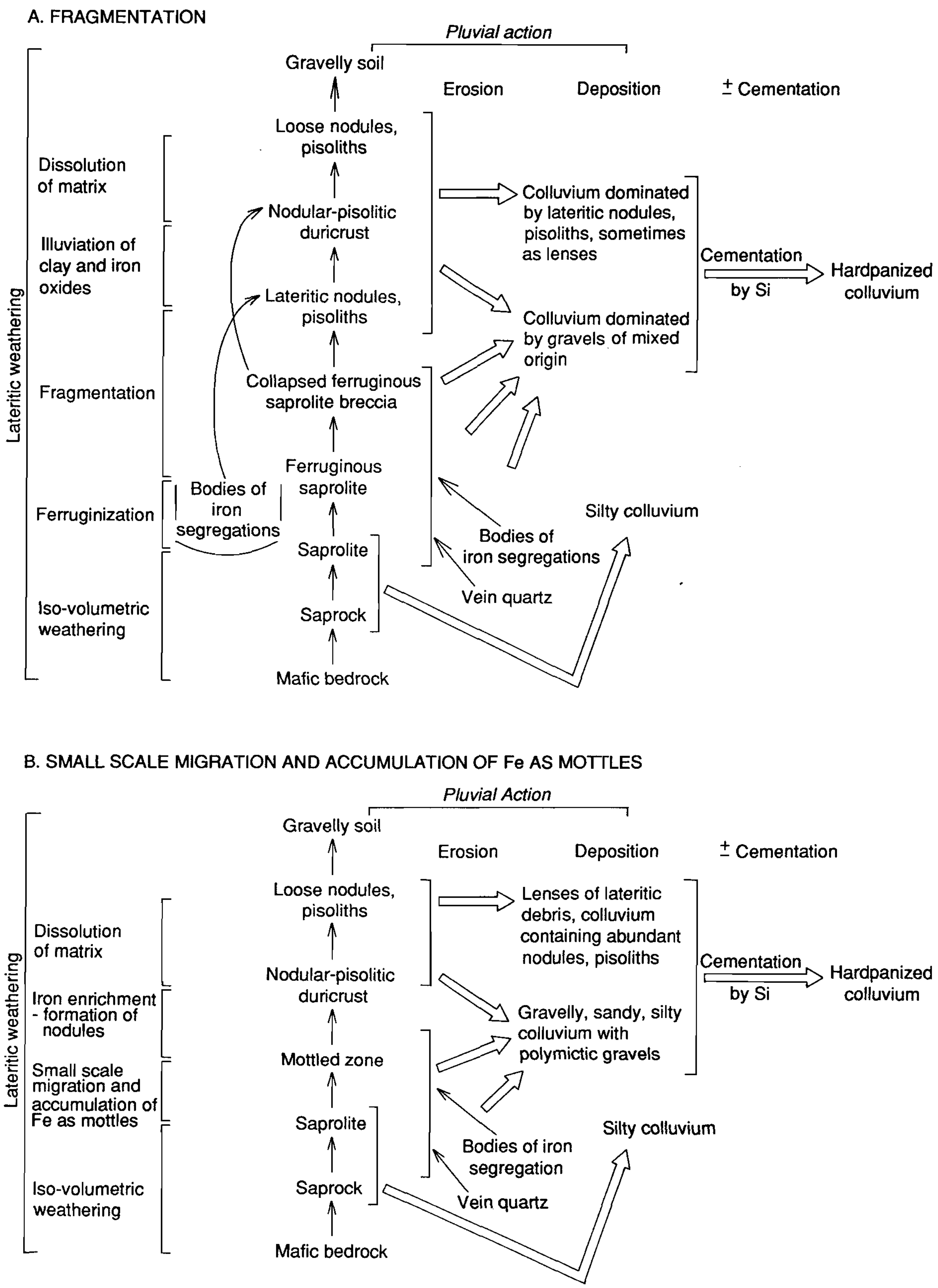

Fig.28. Schematic facies relationship diagram for the formation of lateritic residuum. (A) by fragmentation (B) by small scale migration and accumulation of Fe, and its subsequent dismantling.

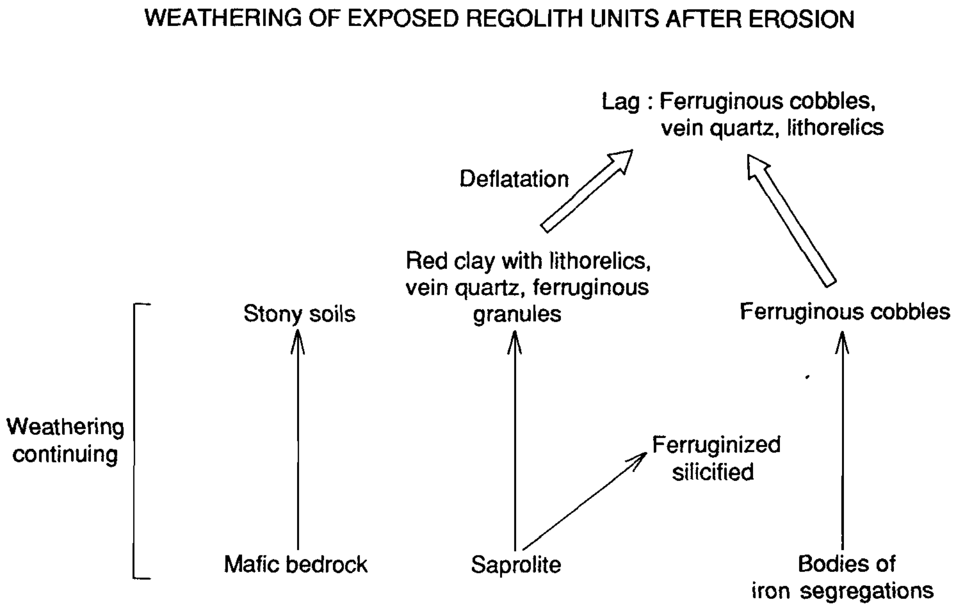

Fig.29. Schematic facies relationship diagram for the formation of regolith after erosion.

are recent residual soils formed in an arid climate from highly-leached kaolinitic mafic saprolite, the latter being a product of the earlier tropical weathering. Thus, kaolinization and leaching of bases and carbonates of mafic saprolite occurred in the earlier humid-tropical climates. Due to a general change to an arid climate during the mid-Tertiary, deep weathering ceased and vegetation changed, resulting in slope instability. Erosion removed the upper part of the weathering profile, including lateritic residuum, thereby exposing the leached saprolite. This leached saprolite then became the parent material of the red clays which formed during the arid conditions.

The red colour of these clays is due to the presence of hematite. Hematite formation is favoured by higher temperature, low moisture and low organic material. Such conditions occur in the Lawlers district.

4.6.3 HARDPAN AND PEDOGENIC CALCRETE

Both hardpan and calcrete are clearly much younger than the original lateritized surface. At Lawlers, hardpan has developed in both *in situ* regolith and detritus resulting from the erosional modification of the old surface. Cementation of these materials by silica to form the hardpan is a relatively recent process (but the actual ages are not known), because the hardpanization is affecting colluvial units and some soil units. Microscopic evidence indicates a complex development of cementation resulting in hardpan development. This appears to be related to alternating authigenic deposition of silica, clay minerals, and Fe-oxide phases. These findings contrast with some previous views that amorphous silica cementation is dominantly responsible for the distinctive properties of hardpan. Although amorphous silica undoubtedly occurs within the hardpans investigated, it is by no means the only cementing agent.

Calcrete in erosional areas is pedogenic in origin and has formed by the relative accumulation of carbonates due to the alteration of Ca-rich host materials, in this case from mafic rocks. Calcite is the dominant carbonate mineral present in calcrete.

4.6.4 ORIGIN OF LAGS

The general distribution of lag gravels can be understood in terms of regolith-landform relationships. In the erosional regimes, coarse black lags of iron segregations, or lags of fragments of ferruginous saprolite (where stripping is less extensive), appear to be largely the result of present-day *in situ* weathering of the landscape. In the same sense, lateritic lag comprising nodules and pisoliths is the *in situ* product of present-day weathering of lateritic duricrust. These lags may have been concentrated at the surface by a variety of processes including deflation, removal of matrix, burrowing action of termites, ants, and rabbits, etc.; these processes have been discussed in detail by Mabbutt (1977) and Carver *et al.* (1987). These *in situ* lags have been further subjected to physical and chemical weathering and dispersion processes. Lateral dispersion of these lags by the action of water has resulted in a layer of fine lag comprising a variety of clasts on the colluvial outwash plains. The increase in the proportion of fine lag in the lower slopes is probably related to the colluvial sedimentation and fractionation of the lag as it passes downslope and away from the source, whereas the large fragments of iron-segregations and nodular-duricrusts show lesser dispersion. Fine lag is therefore commonly allochthonous and does not relate to the immediately underlying-lithology.

4.6.5 GENERALIZED REGOLITH-LANDFORM MODEL

Figure 30 is a schematic cross section showing regolith-landform relationships for the Lawlers district. The generalized regolith-landform model summarizing the regolith stratigraphy for three dominant regimes derived from the Lawlers study is shown in Fig. 31. Both these figures are based upon the regolith-landform assessment throughout the Lawlers district coupled with the detailed study at McCaffery-North Pit, Turrett Pit, Waroonga Pit, and Meatoa areas. The dominant features are a residual lateritic weathering profile that undulates over the landscape, erosion partly dismantling the lateritic residuum and ferruginous saprolite, cutting into the saprolite, and the resulting debris being deposited as colluvium and alluvium in areas of low relief. From this study, together with the application work of Geochemex (Butler *et al.*, 1989), it is now well established

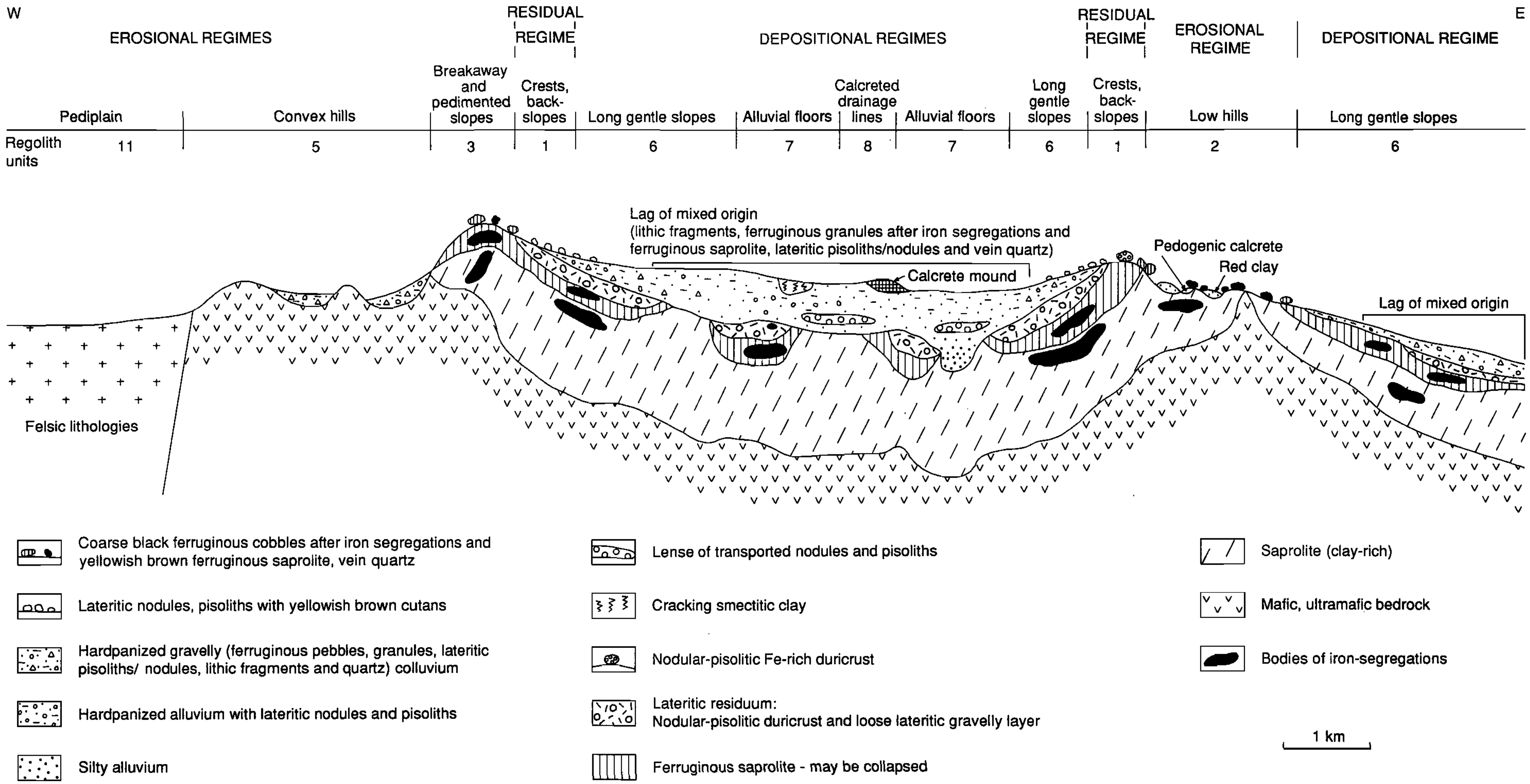

Fig 30. Schematic cross section for the Lawlers district showing regolith stratigraphy and landforms.

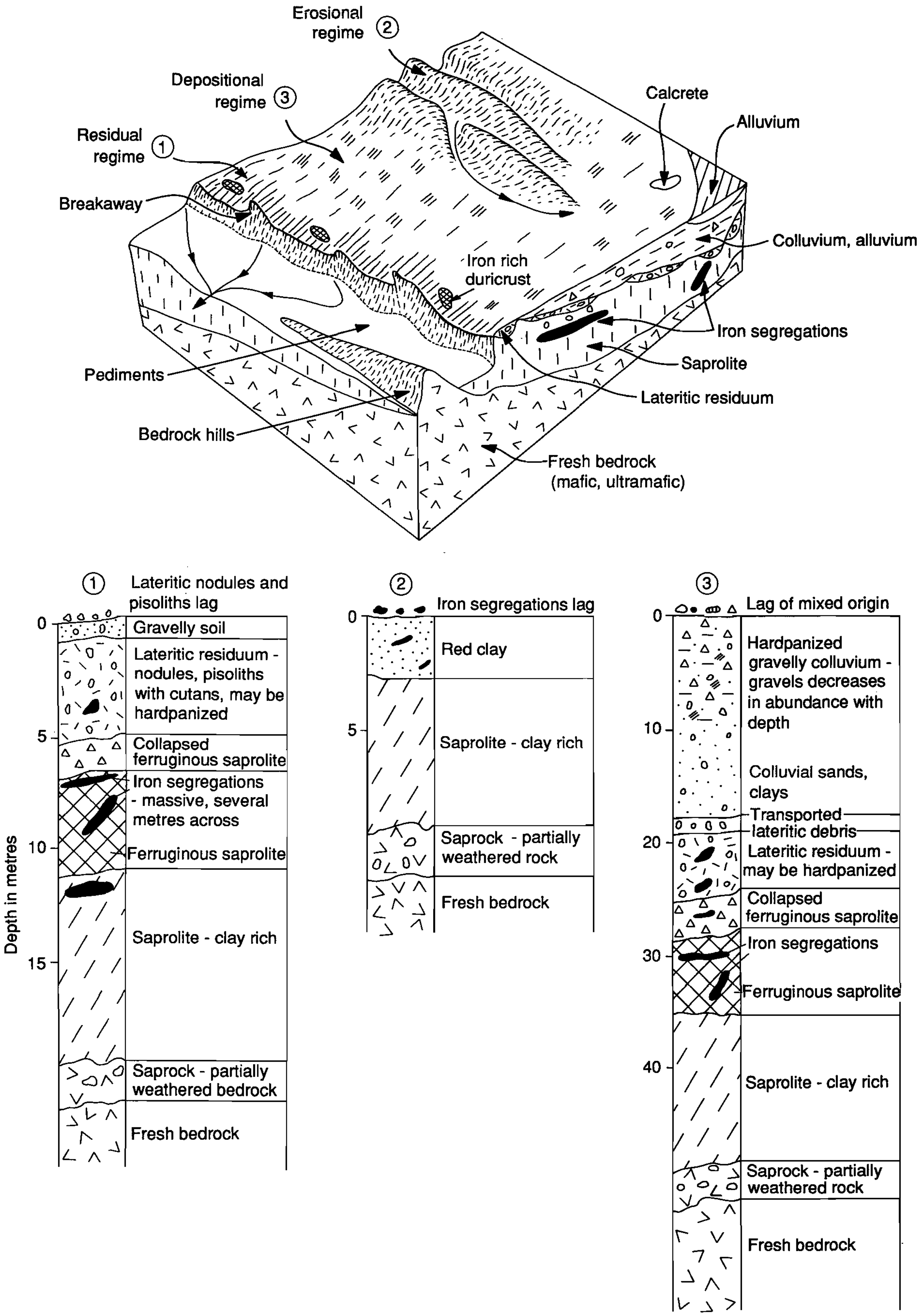

Fig.31. Generalized regolith-landform facies model for the Lawlers district.

that buried residual laterite profiles are widespread beneath the colluvium and alluvium. Their distribution is however, erratic and difficult to predict because of the partial stripping of the old surface.

4.7 Implications for Geochemical Exploration

Knowledge of regolith relationships at Lawlers provides a framework of understanding for geochemical exploration programmes. Besides application specifically in the Lawlers district, the results of the research have application to other parts of the Yilgarn. The research has shown, for example, that buried laterite profiles can be widespread despite extreme stripping of exposed uplands. The implications to exploration are then obvious - explore such areas by widespaced drilling for buried multi-element geochemical haloes in laterite. The feasibility of this approach has been proven by the discovery by Geochemex and Forsayth of the Turrett and Waroonga deposits using these concepts.

An understanding of regolith stratigraphy and recognition of sample media and their characteristics are important to avoid collection of inappropriate material for geochemical analysis. In the residual regime (Unit 1), where the lateritic residuum (either duricrust or loose lateritic nodules) occur at or near the surface, sampling of lateritic nodules should be adequate to detect geochemical expressions of mineral deposits. By contrast, in the erosional regime (Unit 2a) different sample media (e.g. soil, red clay or saprolite) have to be employed because the lateritic residuum has been removed by erosion. Here in the erosional areas, saprolite is the parent material of red clays and the geochemical patterns in the red clays will closely resemble those of the original saprolite, modified by later processes, for example, leaching or calcrete formation. Hence soil geochemistry using BLEG techniques is effective, for example, within Unit 2a.

In the depositional regimes (Units 6, 7), where the lateritic residuum can be present at depth, it can be effective to drill for *in situ* samples, the nature of which will depend upon the degree of truncation of the profile before deposition. In drilling designed to detect buried laterite geochemical haloes, it is important to distinguish colluvial/alluvial units containing an abundance of lateritic pisoliths and nodules from lateritic residuum. The criteria for distinguishing between residual and transported laterite are discussed in detail in Section 7.0.

The combined effects of deep weathering and differential erosional/depositional processes lead to a great variety of materials exposed at the surface. The understanding of regolith relationships at Lawlers has also provided a framework within which lag types can be understood. The research on lag gravels highlights the importance of understanding their origin, particularly in terms of their regolith-landform history, when planning, executing, and interpreting an exploration geochemical survey in this style of deeply-weathered terrain.

5.0 THE IRON-RICH DURICRUSTS

5.1 Introduction

Iron-rich duricrust is the nomenclature used in this report in the sense of Anand *et al.* (1989) for dense, black duricrusts with greater than 70% Fe_2O_3. In the Lawlers district, they characteristically have a nodular, nodular-pisolitic, or oolitic fabric being categories LT 224, LT 223, and LT 221 respectively. They are sporadically distributed throughout the Lawlers district and commonly occur on topographically-elevated areas (Fig. 32). The objective of the present study is to understand the possible relationships of Fe-rich duricrust with the underlying lithology, nodular/pisolitic duricrust (low in Fe), and the period of lateritic weathering. Bedrock can profoundly influence the nature of the lateritic duricrust. However, present knowledge of the distribution of bedrock types for the non-outcropping, regolith-covered parts of the Lawlers district is apparently scarce and is inadequate for a definitive study of the genesis of the Fe-rich duricrusts. The following progress has been made within these limitations.

Samples of Fe-rich duricrust collected in the vicinity of Meatoa, Brilliant, North pit, and the Agnew gravel pit were investigated for petrological, mineralogical, and geochemical characteristics which are described below.

5.2 Meso and Microscopic Characteristics

The Fe-rich duricrusts are coherent weathering crusts comprised of accumulations of ferruginous nodules/pisoliths/ooliths cemented by Fe oxides. Three broad categories were identified on the basis of their fabric and microstructure: nodular duricrust, pisolitic nodular duricrust, and oolitic duricrust. Nodular duricrust is the most common type. The outer surfaces of all three types of duricrusts may have a pebbly appearance.

Nodular duricrust (LT224) consists of abundant subrounded to irregular, 2-15-mm dark reddish-brown/reddish black (5R 2.5/1, dry) hematite-rich nodules set in a fine-grained, uniform weak red (5R 4/3, dry) hematite-goethite-rich matrix (Fig. 33A). Nodules up to 35 mm in size may also occur. A few pisoliths are also commonly present in the nodular duricrusts. Matrix generally occurs in small amounts. The ratio of nodules to matrix ranges from 60:40 to 80:20; most samples having a ratio close to 80:20. The boundary between nodules and matrix is not well defined and nodules do not show the development of cutans. Nodules are generally magnetic because of the presence of maghemite which may occur around the margins or within cores of nodules. There is commonly more than one form of Fe-oxide present (hematite, goethite, maghemite) in nodules and, in some samples, several generations of Fe oxides (e.g. goethite) can be recognized.

Pockets of nodules having weak red colour appear to have been further enriched with Fe to give a rim of reddish-black colour (Fig. 33A-1). This enrichment began at the borders of the grain or along cracks and proceeded inwards to give reddish-black grains containing isolated weak red areas (Fig. 33A-2) and finally nodules of reddish-black colour consisting of hematite and maghemite (Fig. 33A-3). Red colouration is provided by hematite. The cores of nodules can have oval voids and cracks, some of which have infilling of goethite and small quartz grains. The cracks may have developed during the dehydration of goethite to hematite.

Weathered ilmenite grains consisting of pseudorutile and anatase are included in the cores of nodules. These grains are subrounded, 10-40 μm in size and are randomly oriented. They were identified using a scanning electron microscope. Dark areas of back scattered-electron images of ilmenite grains are Ti-rich whereas light areas are Fe-rich.

The matrix has consistent characteristics with numerous cavities showing dissolution to the stage where only nodules are left with no matrix. Cavities generally contain small quartz grains. The fabric and mineralogy of the matrix is very similar to the weak red areas of nodules. Occasionally, Ti- and Fe-rich ooliths (2-40 μm) were seen concentrated in the matrix, apparently having crystallized from solution. The dark cores of the ooliths are Ti-rich and the light areas are Fe-rich.

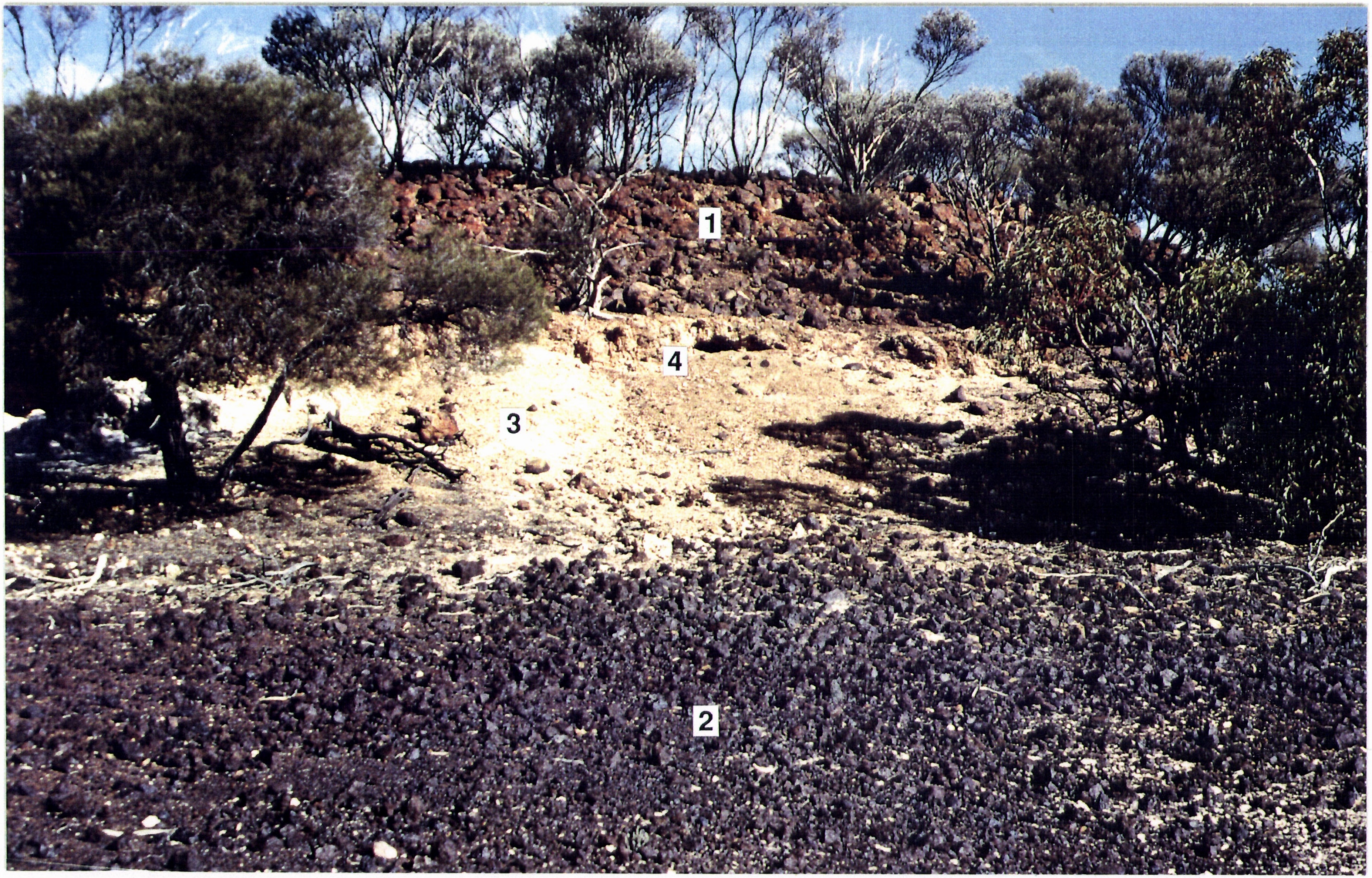

Fig.32. Iron-rich duricrust on crest and low breakaway face (1). On the pediment occur coarse lag of fragments of Fe-rich duricrust (2), local pockets of pedogenic calcrete (3) and saprolite (4), location 4.7 km SE of Brilliant.

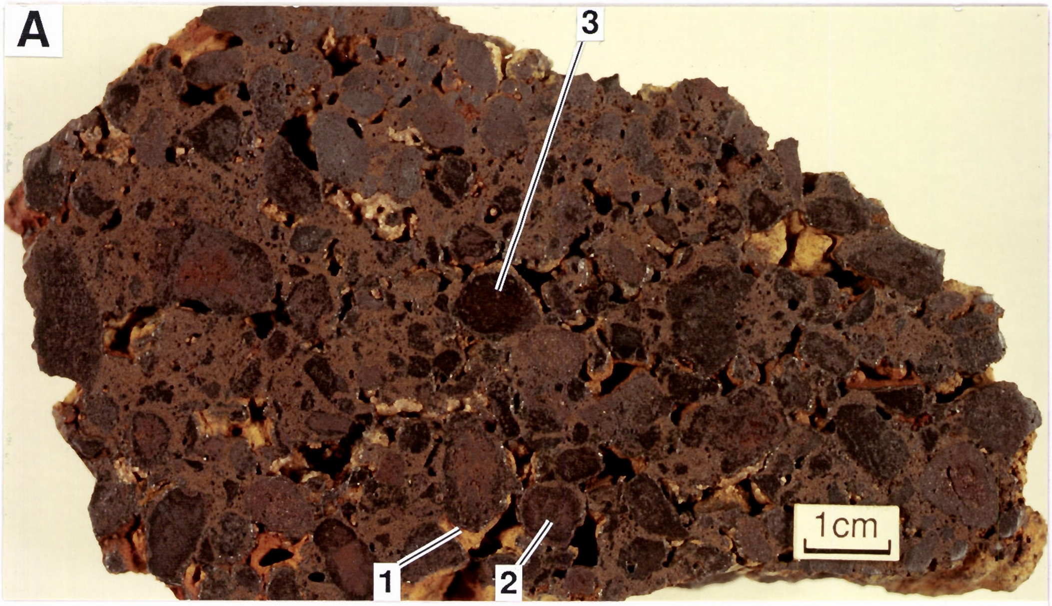

Fig. 33A. Slice through an Fe-rich nodular duricrust showing various stages of fabric development. Weak red areas enriched with Fe to give a reddish black rim (1), reddish black grains with isolated weak red areas (2) and finally reddish black grains (3). Sample 07-1314, Meatoa area.

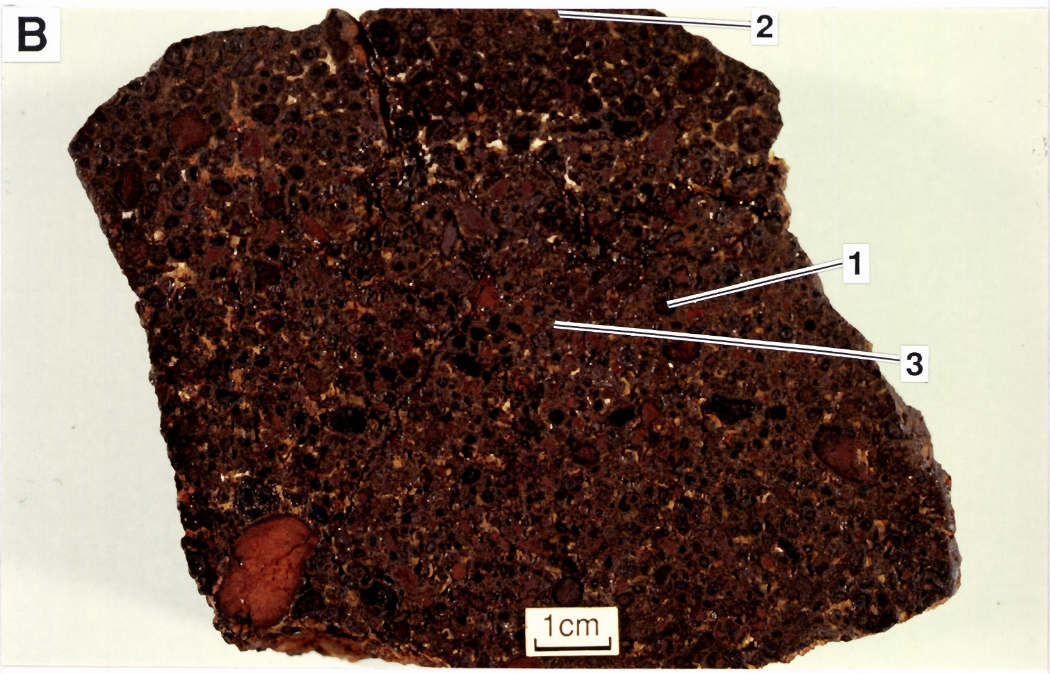

Fig. 33B. Slice through an Fe-rich oolitic duricrust showing ooliths (1) and lithic fragments (2) set in a sandy clay matrix (3). Sample 07-1390, 4.7 km SE of Brilliant.

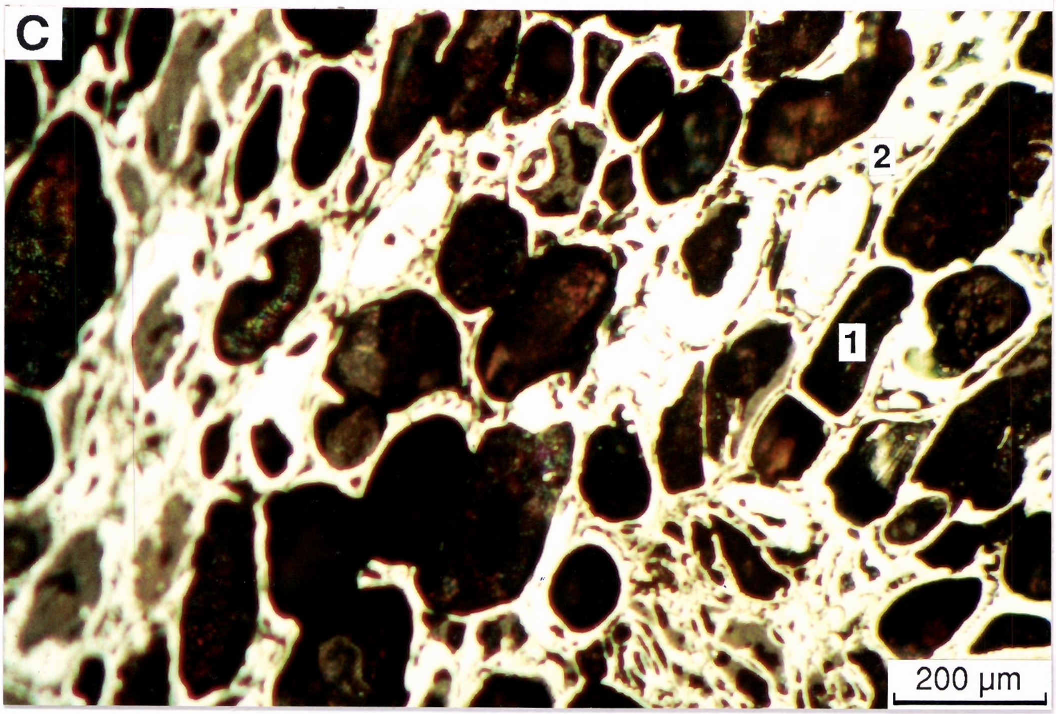

Fig. 33C. Polished section of part of an oolith in the Fe-rich nodular duricrust (shown above) showing slightly ferruginized charcoal fragments (1) within a goethite-rich core (2). Sample 07-1390.

Oolitic duricrusts (LT221) shown in Fig. 33B have abundant hematite-goethite rich reddish black (5 R 2.5/1, dry) magnetic ooliths separated by a very small amount of weak red (5 R 4/3, dry) matrix. A few pisoliths up to 5 mm in diameter are also present. Several irregular to angular lithic fragments of variable degrees of ferruginization occur in the matrix. In polished sections, *pseudomorphed wood fragments* are conspicuous and occur in a finely crystalline matrix of hematite and goethite (Fig. 33C). In the ooliths, many pieces of wood are replaced by Fe oxides so completely, that in sections the cell structures can readily be seen.

The cores of ooliths are weak red which are further ferruginized to give rims of reddish-black colours. A similar process of Fe enrichment was seen in nodular duricrust and is described above. Ooliths have multiple thin light grey/dark grey cutans, which are a series of depositional layers usually of goethite. Cutans show at least three generations of goethite.

Goethite which has in-filled irregularly-shaped voids is common and there are rare small (0.5 mm) quartz grains.

The most characteristic features of Fe-rich duricrusts are:

- The boundaries between nodules/ooliths and matrix are not well defined in sliced surfaces, despite the pebbly appearance of weathered surfaces
- The matrix and nodule compositions are not significantly different and both are Fe-rich.
- The volume of matrix between the nodules is small.
- Nodules generally lack cutans.
- Microscopic examination and XRD suggest the absence of clay minerals and gibbsite.
- Weathered ilmenite grains and slightly-ferruginized charcoal fragments commonly occur within the ooliths.

5.3 Fabric Development

Based upon their fabrics, possible processes involved in the formation of the Fe-rich duricrusts may be explained by two alternative scenarios:

(i) The duricrust had originally a weak red/dusky red uniform matrix which has been modified by enrichment of Fe under appropriate conditions to give rise to reddish black nodules. Enrichment of Fe evolved into three discrete facies: pale weak red, weak red/dusky red or reddish black. The enrichment of weak red areas began along cracks or at the borders and proceeded inwards to give reddish-black grains containing isolated weak red areas and finally reddish-black nodules.

(ii) The duricrust originally had reddish-black nodules which have been weathered/leached out to give a matrix of pale red/weak red colours. Reddish-black nodules are disaggregated by leaching into a weak red matrix retaining the same fabric. The latter are thus residues of the original reddish-black nodules. Leaching necessitates dissolution of Fe-oxides. Voids developed by leaching serve as secondary "reception" structures for highly-crystalline goethite.

5.4 Mineralogy and Aluminium Substitution in Fe-Oxides

The mineralogical compositions of Fe-rich duricrusts and Al substitution of their Fe-oxides are given in Tables 8 and 9. Hematite, goethite, and maghemite are the major minerals and are present in all the samples. Rutile and anatase, weathering products of ilmenite, are present in all samples and range from 1 to 9%. However, pseudorutile identified petrographically was not detected by XRD.

Table 8. Semi-quantitative mineralogy (wt.%) of Fe-rich duricrusts

Sample No.	Type	Hematite	Goethite	Maghemite	Kaolinite	Quartz	Rutile	Anatase	Talc	Gibbsite	Hm/(Hm+Gt)
07-0825	Nodular LT 224	53	21	10	Tr	1	7	2	0	Tr	0.72
07-0828	Nodular LT 224	32	38	12	Tr	5	0	0	0	Tr	0.46
07-0921	Nodular LT 224	35	30	12	Tr	2	4	2	0	Tr	0.54
07-0922	Nodular LT 224	70	13	Tr	Tr	3	6	4	0	Tr	0.84
07-1314	Nodular LT 224	44	20	18	0	4	1	2	0	3	0.69
07-1344	Nodular LT 224	56	22	8	0	5	2	4	0	0	0.72
07-1378	Nodular LT 224	52	20	17	0	2	1	5	<1	0	0.72
07-1390	Oolitic LT 221	24	45	15	0	5	0	1	<2	0	0.35

0 = below detection limit
Tr = trace
Hm = hematite
Gt = goethite

Table 9. Al substitution in goethite, hematite, and maghemite for some Fe-rich lateritic duricrusts

Sample No.	Type	Goethite (mole % Al)	Hematite (mole % Al)	Maghemite (mole % Al)
07-0825	Nodular LT 224	4	4	2
07-0828	Nodular LT 224	3	4	3
07-0921	Nodular LT 224	9	6	4
07-0922	Nodular LT 224	10	5	3
07-1314	Nodular LT 224	9	6	4
07-1344	Nodular LT 224	6	5	4
07-1378	Nodular LT 224	9	6	0
07-1390	Oolitic LT 221	4	0	0

Kaolinite and gibbsite are either absent or present in trace amounts. Talc was recorded in two samples. Quartz occurs in small amounts.

A range in the ratio of hematite/hematite + goethite (0.35-0.84) indicates variable amounts of hematite and goethite in samples. Hematite is dominant in nodular duricrusts and goethite in oolitic duricrust. This difference may reflect conditions during Fe-oxide formation. The relative concentrations of goethite and hematite in pedogenic environments are strongly influenced by the initial oxidation state of the Fe, the concentration of Fe in solution, and factors such as temperature, moisture activity, pH, Eh, presence of organic matter, and the ionic environment - including the activity of Al and other ions in soil solution (Schwertmann, 1985). Hematite may form the internal dehydration of ferrihydrite. High temperature and low moisture content are more influential in the transformation of ferrihydrite to hematite. Low temperature, high water activity, and high amounts of organic matter favour goethite formation. Bushfires commonly convert goethite to hematite by locally heating exposed soils or duricrust at temperatures up to 600-800°C. In the intimate presence of organic matter under such conditions, goethite may transform to highly magnetic Fe-oxide — maghemite (Schwertmann, 1985, Anand and Gilkes, 1987). Alternatively, hematite may form from goethite by dissolution and reprecipitation under appropriate conditions (Schwertmann, 1985).

X-ray diffraction studies of Fe-rich duricrusts show that the goethite generally has a low degree of Al substitution (3-10 mole%) and that Al-substitution is even lower in hematite and maghemite. By contrast, goethite in duricrusts and loose pisoliths and nodules low in Fe from the North Pit and Meatoa areas contain much higher levels of Al substitution (19-26 mole%). Fitzpatrick and Schwertmann (1982) reported that goethites formed by absolute accumulation of Fe contain low Al substitution (<10 mole %). They further concluded from their study of goethites from different environments, that low Al substitution in goethite is characteristic of hydromorphic environments, while substitution above 15 mole % is typically of highly-weathered, non-hydromorphic environments. These results suggest that goethites in Fe-rich duricrusts are formed by absolute accumulation of Fe.

5.5 Geochemistry

The chemical composition of bulk samples of Fe-rich duricrust is given in Table 10 These are characterized by high concentrations of Fe_2O_3 and low concentrations of SiO_2 and Al_2O_3. Electron microprobe analysis of nodules and matrix shows that both are Fe-rich and that the composition of internodular matrix is not significantly different from that of the nodules (Table 11). Small concentrations of Al, both in the matrix and nodules of Fe-rich duricrusts, further confirm the low degree of Al substitution in Fe oxides. Similar results were obtained from XRD data.

Analysis of a weathered ilmenite grain within a nodule shows the presence of Ti-rich minerals. One spot analysis of a mixture of hematite and goethite shows high values of Ti (6.9% TiO_2) which probably occurs as coatings or substitutes for Fe^{3+} in Fe oxides.

Iron-rich duricrusts show large ranges in values of Mn, Cr, V, Zn, Ni, Co, As, Sb, and Ga. This distribution may be controlled by the nature of bedrock; however, as mentioned above, bedrock knowledge is presently inadequate for enabling this interpretation. High values of Cr are accompanied by moderate values of Ni and Co suggesting an ultramafic origin for some samples. Arsenic and Sb values reach 340 and 72 ppm respectively. Gold values, however, are low, in the ppb range. Copper, Pb, Bi, Sn, and Ge occur in small amounts.

5.6 Genesis

Genesis of Fe-rich duricrust in the Lawlers district may be explained by two alternate scenarios. Lateritic processes have produced the Fe-rich duricrust by the *in situ* deep weathering of mafic and ultramafic rocks, resulting in a relative accumulation of Fe. Alternatively, the Fe-rich duricrusts may have been produced by the absolute accumulation of Fe in ancient valley floors, in this manner receiving a considerable contribution of Fe in solution from upland areas of that time. The occurrence of Fe-rich duricrust on present topographically-high areas may be explained by the process of relief inversion. These two hypotheses are now discussed.

Table 10. Chemical analyses of some Fe-rich duricrusts

Sample	07-0825	07-828	07-0921	07-0922	07-1314	07-1344	07-1378	07-1390
Type	Nodular	Nodular	Nodular	Nodular	Nodular	Nodular	Nodular	Oolitic
Element/ Oxide								
Wt %								
SiO_2	5.7	7.2	7.8	4.7	4.5	6.5	2.0	5.7
Al_2O_3	3.99	6.03	9.11	4.21	7.10	4.91	4.97	4.67
Fe_2O_3	78.90	75.90	69.40	78.10	76.20	76.92	82.42	79.03
MgO	0.064	0.142	0.135	0.080	0.056	0.042	0.029	0.056
CaO	0.030	0.036	0.047	0.122	0.032	0.088	0.046	0.040
Na_2O	<0.007	<0.007	0.013	0.017	0.013	0.013	0.013	0.014
K_2O	<0.06	<0.06	<0.06	<0.06	<0.06	<0.06	<0.06	<0.06
TiO_2	8.040	1.012	5.621	9.541	2.519	5.688	4.421	1.020
ppm								
Mn	218	1265	253	326	1432	255	493	479
Cr	1031	16700	7701	3550	12600	917	10100	2849
V	3884	410	1823	3498	1486	2326	1758	760
Cu	13	14	22	26	17	25	15	11
Pb	9	18	6	16	10	<2	<2	11
Zn	15	50	5	3	55	44	60	20
Ni	<4	1820	94	44	330	42	190	590
Co	10	135	24	14	78	20	50	210
As	66	74	340	340	68	16	<2	11
Sb	11	<2	64	72	2	<2	<2	<2
Bi	<2	<2	4	<2	>2	3	2	>2
Mo	9	7	7	9	3	9	5	3
Ag	<0.1	0.6	<0.1	0.5	0.6	<0.1	<0.1	<0.1
Sn	6	<2	3	6	<2	6	7	4
Ge	<4	<4	4	<4	<2	<2	<2	<2
Ga	155	30	96	100	90	135	100	18
W	54	6	22	10	<4	14	<4	4
Ba	837	272	1277	71	142	766	56	672
Zr	108	38	97	73	68	68	26	21
Nb	34	11	26	34	9	19	18	<2
Au	0.009	0.004	0.013	0.130	<0.001	<0.001	<0.001	<0.001

Table 11. Electron-microprobe analysis of components within some selected Fe-rich duricrusts

Sample No.	Components	wt %						TOTAL
		SiO_2	Al_2O_3	Fe_2O_3	TiO_2	MgO	CaO	
07-1314	reddish-	2.05	1.64	88.26	0.15	0.03	0.01	92.14
	black core	2.09	1.60	88.86	0.37	0.06	0.01	92.99
	weak red	1.00	2.97	83.04	1.35	0.01	0.02	88.39
	matrix	1.41	2.43	80.95	1.08	0.03	0.01	85.91
		1.05	1.85	80.16	6.89	0.05	0.01	90.01
07-921	reddish-	1.76	1.23	87.89	1.41	0.03	0.01	92.33
	black core	1.35	1.11	89.34	1.63	0.05	0.01	93.49
	weak red	2.10	1.61	82.56	1.21	0.03	0.01	87.52
	matrix	2.08	1.50	84.36	0.89	0.06	0.03	88.92

Hypothesis 1:
If the Fe-rich duricrust is residuum, it might be expected that part of its gross chemistry would relate to that of the parent rock. Experience has shown that concentrations of Cr, Co, and Ni can sometimes be used to discriminate the duricrusts derived from mafic and ultramafic rocks. Our data suggest that these Fe-rich duricrusts do have a geochemical affinity with mafic and ultramafic Fe-rich bedrocks. Those rich in Cr, Ni, and Co are likely to be derived from the weathering of ultramafic rocks, whereas those containing relatively-low levels of these elements are likely to have a mafic origin. Ilmenite and weathered ilmenite grains in the nodules are probably inherited from Ti-rich parent materials which further suggest their origin from Ti-rich bedrock such as gabbros. However, Ti also appears to be fairly mobile as indicated by the presence of Ti coatings around nodules and Ti-rich ooliths in the matrix, this may indicate its introduction from external sources.

The modification/weathering of bodies of iron segregations may result in Fe-rich duricrust. However, there are significant differences in mineralogical and chemical composition particularly in maghemite, Ti, Mn and Zn concentrations (see Section 6.0) between the iron segregations and Fe-rich duricrusts which may suggest that they are not related to each other.

Hypothesis 2:
The fabric and Al substitution of goethite in Fe-rich duricrust do not fully support its origin as a residuum. The goethites show little Al substitution, so that they must have grown in an environment almost free of dissolved Al. This is supported by the observation that neither kaolinite nor gibbsite was detected in appreciable amounts. By contrast, the goethites from loose pisoliths and from nodular duricrust (low in Fe) from the North Pit area, Agnew gravel Pit, and the Meatoa areas have higher Al substitution (17-26 mole%) (Anand *et al.*, 1989; and this report). Fitzpatrick (1988) interpreted from his study that the degree of Al substitution in goethite structure can be used to differentiate between the older "iron segregations" formed by the relative accumulation of Fe (> 15 mole% AlOOH in goethite) and relatively-younger "iron segregations" formed primarily by absolute accumulation of Fe (< 10 mole% AlOOH in goethite). This suggests that Fe-rich duricrusts in the Lawlers district are formed by absolute accumulation of Fe. Iron segregations formed by absolute accumulation of Fe in ancient lowland positions were reported from South Australia by Maud (1972) and Milnes *et al.* (1985) and contain goethite of low Al substitution (<10 mole%). Iron-rich duricrusts in the Lawlers district occur on ridge crests so that their formation is a paradox and may be explained by the following. Ridge crest duricrusts are remnants of what was once an ancient valley or depression, into which sediments accumulated. The valleys became favoured sites for the precipitation of Fe oxides from groundwater. In this regard, ridge crests and their Fe-rich duricrusts could be an expression of a complex series of erosional, aggradational, and weathering events. Relief inversion in the Lawlers district may have occurred and duricrust-covered valleys may have become ridges (Fig. 34). Many examples of relief inversion have been provided in the literature, some including laterites which occur as long sinuous ridges and may have formed as valley laterites (Maignien, 1966; Goudie, 1973; Ollier *et al.*, 1988). Iron may have been derived by weathering processes from ancient upland positions and transported laterally to valley floors. The dissolved ferrous iron is subsequently precipitated and oxidized or oxidized and precipitated. In general, goethite and hematite form where oxidation precedes hydrolysis, when hydrolysis and precipitation occur before oxidation lepidocrocite and maghemite may occur (Taylor and Schwertmann, 1974). These possible processes could result in the formation of Fe-rich duricrust. The valley floors capped with Fe-rich duricrust are the most indurated, and as they are then resistant to erosion, softer upland and valley side materials are eroded, leaving the former valleys as the ridges.

On the available evidence, either of the two mechanisms described above could have been responsible for the formation of Fe-rich duricrusts. The lack of knowledge on bedrock under the duricrusts does not allow us to make conclusions at this stage about its influence on the genesis of Fe-rich duricrusts. The geochemistry of duricrusts suggests that their component materials were derived from both the mafic and ultramafic rocks. However, it is the high amounts of Fe, charcoal wood fragments in nodules, and the factors which affect the Al substitution in pedogenic environments which provide a basis for the interpretation of conditions under which Fe-rich duricrusts are formed. Low Al substitution in goethites suggests that Fe-rich duricrusts are formed by absolute accumulation of Fe. Iron impregnated the soils/sediments in ancient valleys or drainage depressions which now occur as crests in the present landscape because of inversion of relief.

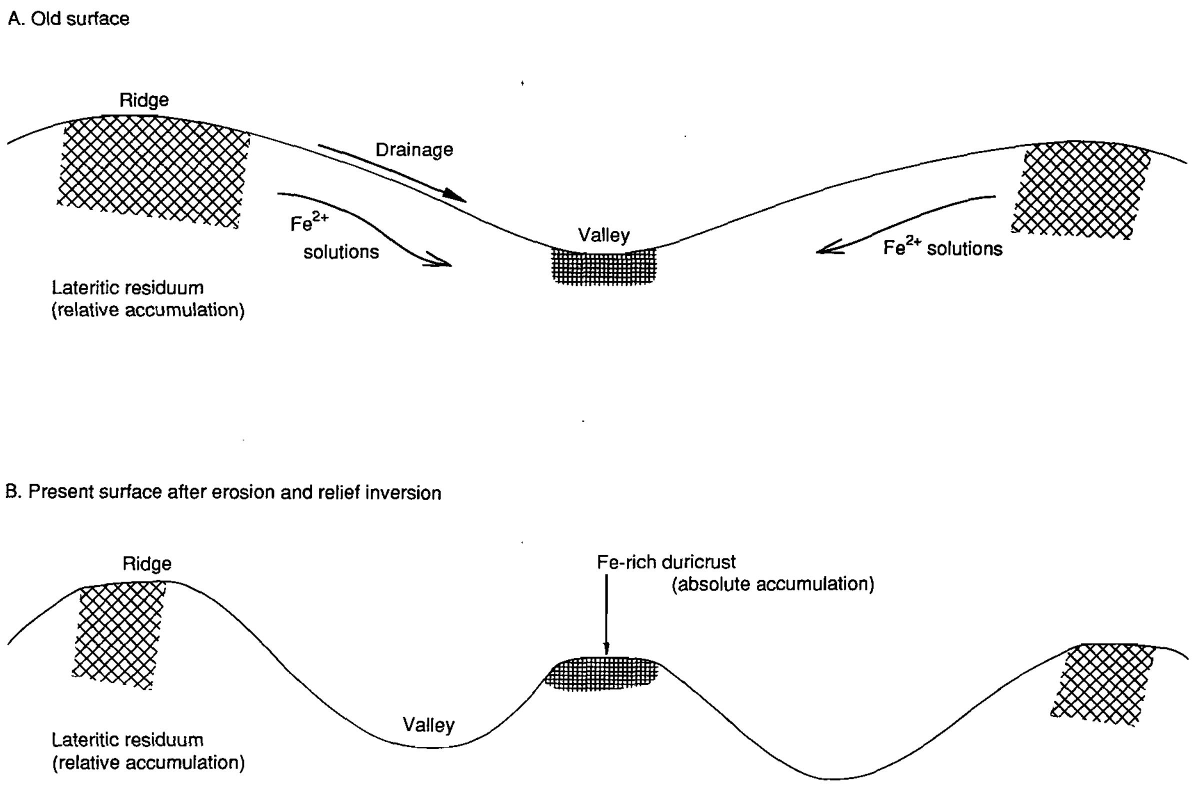

Fig.34. The development of Fe-rich duricrust by absolute accumulation of Fe and relief inversion.

6.0 MORPHOLOGICAL, MINERALOGICAL AND GEOCHEMICAL CHARACTERISTICS OF SAMPLE MEDIA

6.1 Introduction

The combined effects of deep, lateritic weathering and differential erosion processes lead to a great variety of materials exposed at the landsurface. Units of the lateritic weathering profile may occur as a patchwork of different facies, so that a mineralogical and geochemical characteristics of surface samples will differ as function of the facies sampled. Materials may be similar in appearance in handspecimens, but they may have a different origin and geochemical characteristics. This section addresses the objectives of gaining an understanding of such variations in the mineralogical and geochemical characteristics of various sample types. This includes the distribution of minerals and chemical elements in the different sample types and the way in which elements concentrate in these sample types and reflect the mineralization, and parent rock from which they were developed. Four sample media are also evaluated in terms of their effectiveness as geochemical sampling media.

6.2 Sampling Parameters and Analytical Procedures

6.2.1 SAMPLE COLLECTION

One hundred and eighty-one samples consisting of colluvium, lateritic residuum, ferruginous saprolite, and iron segregations were collected (Fig. 35) from McCaffery-North Pit and Turrett areas. Field Sheets record whether the samples were taken from the natural ground surface, from mining pit faces, or from drill spoil. Samples of specific units within vertical profiles generally consisted of a 1.5-kg grab sample. The samples of lag were taken at 20- to 100-m intervals, depending upon the type of lag and the mapped regolith-landform units. At each sample site, about 1.5 kg of the loose surface material was swept from an area of 0.25-1 m^2 using a plastic dustpan and brush. Coarse lag, such as fragments of iron segregations, were collected by hand. Vein quartz in the pebble and cobble-size range was discarded.

6.2.2 LABORATORY METHODS

A small, representative portion of each sample was selected for future reference, slicing and petrographic examination, the remainder was crushed and ground using non-metallic methods described by Smith (1987). Oversize materials, particularly coarse lags, were reduced to minus 8 mm by crushing between zirconia plates in an automated hydraulic press with the undersize then being processed through an epoxy-resin-lined disc grinder with alumina plates and reduced to minus 1 mm. Final milling was done in a motorized agate mill.

6.2.3 ANALYTICAL METHODS

Chemical methods

A combination of chemical analytical methods including inductively coupled plasma spectroscopy (ICP), X-ray fluorescence (XRF) and atomic absorption spectrophotometry (AAS) were used to analyse 32 elements. Table 12 shows the elements analysed, method used, and lower limits of detection.

Petrography

Samples were sliced for petrographic study of the colour and major fabric under a binocular microscope. Polished sections of selected samples were prepared and examined using a reflected light petrographic microscope in order to provide information on mineralogy and internal fabrics.

X-ray Diffraction

XRD patterns on pulps of 128 representative samples were obtained using Cu Kα radiation with a Philips vertical diffractometer and graphite diffracted beam monochromator. The diffraction peaks

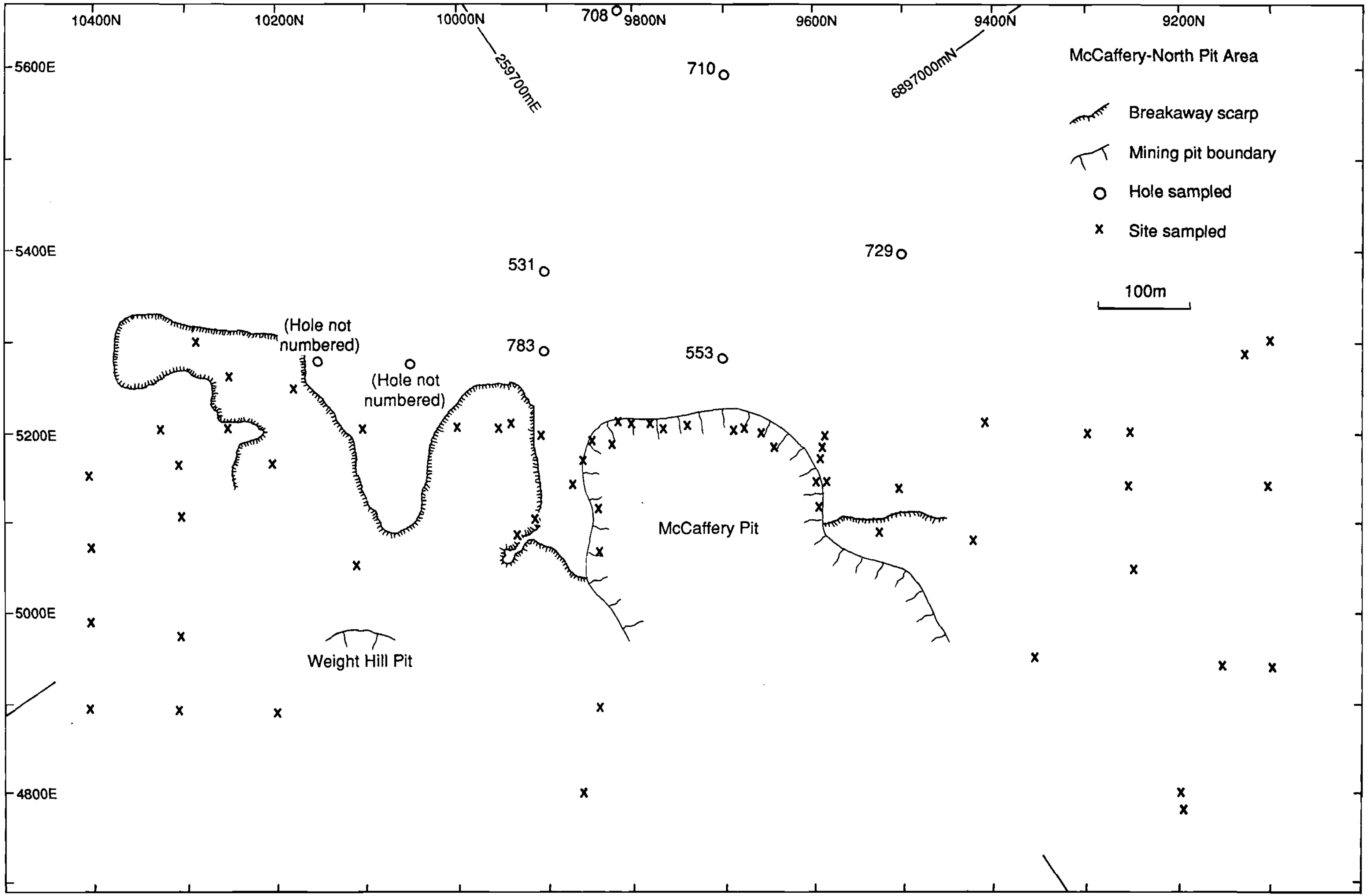

Fig 35. Map showing the location of sites/holes sampled.

Table 12. Analytical methods and lower limits of detection

Element	Reported as	Method	Detection Limit
SiO_2	wt%	ICP	0.2
Al_2O_3	wt%	ICP	0.04
Fe_2O_3	wt%	ICP	0.03
MgO	wt%	ICP	0.004
CaO	wt%	ICP	0.007
Na_2O	wt%	ICP	0.007
K_2O	wt%	ICP	0.06
TiO_2	wt%	ICP	0.003
Mn	ppm	ICP	15
Cr	ppm	ICP	20
V	ppm	ICP	5
Cu	ppm	AAS	2
Pb	ppm	XRF	2
Zn	ppm	AAS	2
Ni	ppm	AAS	4
Co	ppm	AAS	4
As	ppm	XRF	2
Sb	ppm	XRF	2
Bi	ppm	XRF	2
Mo	ppm	XRF	1
Ag	ppm	AAS	0.1
Sn	ppm	XRF	2
Ga	ppm	XRF	4
W	ppm	XRF	4
Ba	ppm	ICP	5
Zr	ppm	ICP	5
Nb	ppm	XRF	2
Se	ppm	XRF	2
Be	ppm	ICP	1
Au	ppm	Graphite furnace AAS Aq req.	0.001

ICP = inductively coupled plasma optical spectroscopy, Si, Al, Fe, Ti, Cr, V after an alkali fusion, others after $HCl/HClO_4/HF$ digestion.

XRF = X-ray fluorescence

AAS = Atomic absorption spectrophotometry, after $HCl/HClO_4/HF$ digestion were recorded over the 2Θ range of 3-65° and data collected at 0.02° 2Θ intervals. The semi-quantitative abundance of minerals in each sample was estimated using a combination of XRD and chemical analyses of bulk samples. The relative proportions of constituent minerals were estimated from peak intensities of selected characteristic lines on XRD traces. This approach provides a reconnaissance assessment of relative mineral abundance. The following diffraction lines were used - 111 and 110 lines of goethite, 012 and 202 lines of hematite, 313 and 220 lines of maghemite, 001 of kaolinite, 101 of anatase, 110 of rutile the Al from and 101 of quartz.

Aluminium substitution in Fe-oxides

The type, crystallinity, and Al substitution of Fe-oxides are influenced by pedogenic environments (Fitzpatrick and Schwertmann, 1982; Schwertmann, 1985). Because of its identical valency and its similar size (r = 0.51 Å for Al^{+3} and 0.64 Å for Fe^{3+}) the Al ion can replace Fe^{3+} in its octahedral position in Fe (III) oxides. An important characteristic of Al substituted Fe (III) oxides is their smaller unit cell size (shift in XRD peaks) caused by the slightly smaller size of Al. In all samples, the concentrations of goethite and hematite were high enough to be easily detected by XRD without any pre-treatment. For Al substitution measurements, a NaCl or quartz internal standard was added. Measurement errors in the position of peaks were estimated and the positions of diffraction lines corrected. Aluminium substitution in goethite was determined from the 111 reflection using the relationship of mole % Al = 2086-850.7d 111 as established by Schulze (1984). Aluminium substitution in hematite was calculated from the a dimension of the hematite unit cell as obtained from the d110 line using the relationship mole% Al = 3109-617.1a (Schwertmann *et al.*, 1979). Aluminium substitution in maghemite was determined from the spacings of the 220 reflection and a calibration curve given by Schwertmann and Fechter (1984).

Scanning electron microscopy

The micromorphology and qualitative energy dispersive x-ray analysis of materials in polished sections of hand picked clasts from the gravels were carried out using a JEOL Geo SEM 2.

Microprobe analysis

Geochemical analysis of each bulk sample provided the average chemical composition of that sample type. However a variety of clast types generally occurs within each sample type. The chemical composition of individual grains however, can be determined by microprobe analysis which also provides information on the association of elements within particular mineral species. Selected mineral grains in polished sections were thus analysed using a Cameca SX-50 microprobe (specimen current 100 nA, accelerating voltage 25 kV). A suite of major and minor elements including Si, Al, Fe, Ti, Mg, Ca, Na, K, As, Cr, Cu, Mn, Ni, V, and Zn were determined.

6.3 Classification of Sample Media

The 181 samples were separated into four broad groups based mainly upon their morphological characteristics and regolith-landform framework. These include materials both from surface (lag) and sub-surface units of the weathering profile. Figure 36 shows the field relationships for several categories of lateritic materials and iron segregations for McCaffery Pit. Each group is described briefly below in terms of its morphological characteristics. Detailed descriptions of their characteristics are given in Section 4.5 and are summarized in Table 13.

Colluvium: Surficial zones, consisting of varying proportions of lateritic pisoliths and nodules, lithic, and quartz fragments set in a sandy, loamy matrix. The particle size is very heterogeneous, and the materials coarser than 2 mm often exceeds 50%. Hardpan is commonly developed in the colluvial units. These materials are transported and are not related to the underlying lithology. The gravels-fraction in colluvium may display morphological features that are indicative of an inherited, transported origin. These features include: roundness of clasts, different particle-size distributions of sand and silt grains in adjacent clasts, incomplete broken surface cutans on some of the clasts, and diverse lithologies of adjacent clasts.

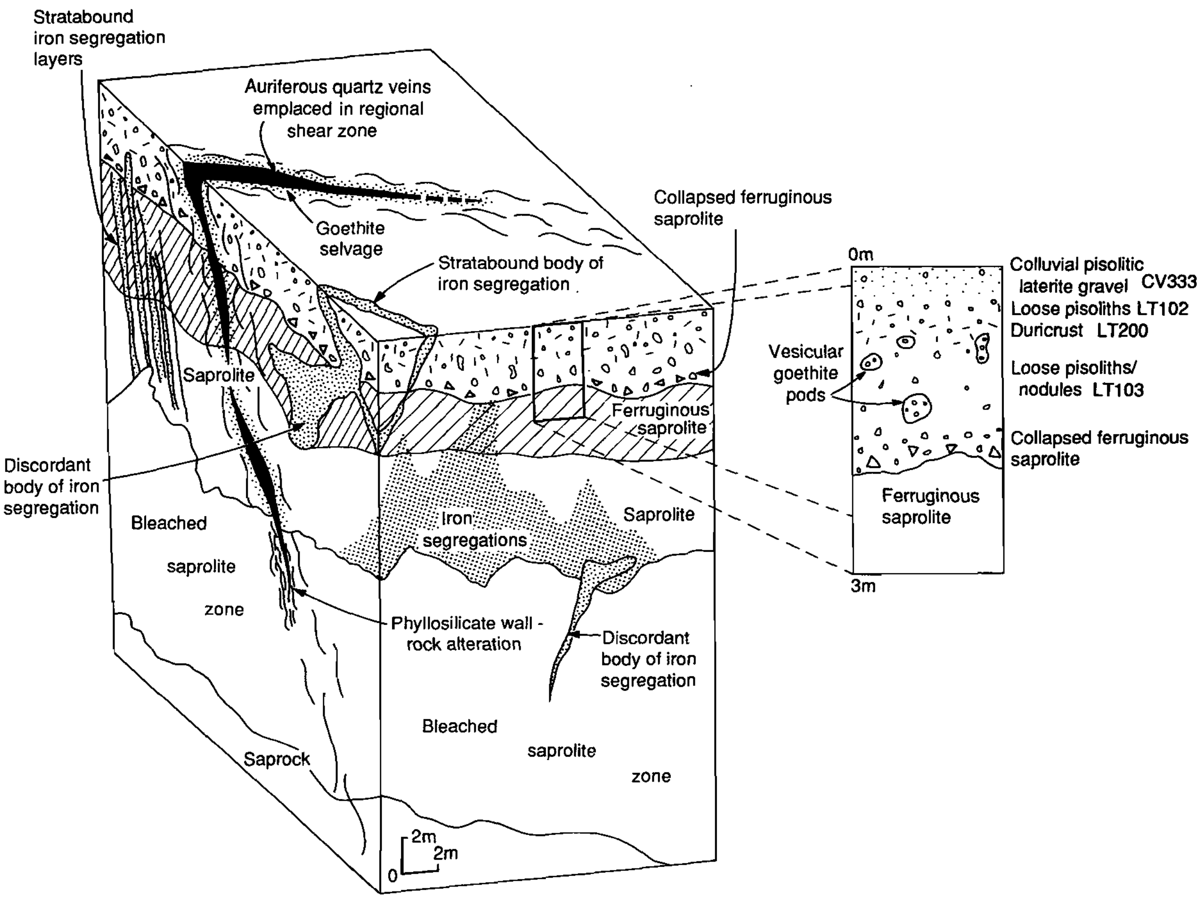

Fig.36. Detailed block diagram showing field relationships for several categories of lateritic materials and iron segregations.

Table 13. Morphological Characteristics of Four Sampling Media

Lateritic Residuum	Ferruginous Saprolite	Iron Segregations	Gravel Fraction From Colluvium
Rounded to subrounded, magnetic and non-magnetic, 5-20 mm, nodules/pisoliths, typically have 1-2 mm thick yellowish-brown cutans; may preserve relics of primary minerals	Irregular, yellow-brown non-magnetic fragments, 10-50 mm, may be mottled with incipient nodular structure, preservation of relics of primary minerals	Irregular, black, non-magnetic, 30-300 mm fragments, preservation of pseudomorphic texture after pyrite and/or pyrrhotite	Rounded clast, absence of yellowish-brown cutans, diverse lithologies of some adjacent gravels

Lateritic residuum: includes loose pisolitic, nodular laterite, nodular duricrust and lateritic lag. This sample type commonly forms a blanket deposit, whether loose or cemented, up to a few metres in thickness.

Loose pisoliths and nodules have dark reddish-brown to black cores, are subrounded to irregular in shape, with a common size range of 2-15 mm (Fig. 37A). Both magnetic and non-magnetic fractions occur. Nodules and pisoliths with black cores are generally magnetic because of the presence of maghemite. Cores of nodules show the development of oval voids, which have yellowish-brown/greenish (< 1 mm) cutans of kaolinite, gibbsite, and goethite. The occurrence of cutans with greenish outer surfaces is typical of residual nodules/pisoliths of the Lawlers district.

Nodular-pisolitic duricrusts are coherent weathering crusts composed of accumulations of nodules and pisoliths cemented by Fe-oxides and clays. Nodules and pisoliths in duricrust make up about 40-60% of hand specimens, are reddish-brown to black, and commonly have greenish cutans.

Lateritic lag, comprising nodules and pisoliths occurs on regolith Unit 1, where the complete or nearly complete lateritic profile is preserved. This lag is mainly derived from the breakdown of pisolitic-nodular duricrust.

Fragments of ferruginous saprolite: A ferruginous saprolite zone underlies the residual lateritic horizon and is yellowish to reddish-brown in colour. It commonly yields 10-50-mm size fragments (Fig. 37B). Ferruginous saprolite differs from the iron segregations (described below) in its yellow-brown colour, has less Fe and may have a mottling with small incipient nodular structures. Interior surfaces display a variety of colours including yellow, reddish-brown, and dusky-red indicating a range of hematite contents. Numerous irregular and mamillated to regular and subrounded voids are lined, and in places filled, with yellow fine-grained material. Some fragments also show the development of incipient yellowish-brown nodules/pisoliths which are goethite- and kaolinite-rich.

Iron segregations and cobbly ferruginous lag: includes black, Fe-rich massive discrete bodies which occur within the upper part of the weathering profile. Ferruginous cobbles which largely occur within erosional regimes, particularly Unit 2, appear to have been derived from the breakdown of iron segregation bodies. Preliminary data interpretation indicated that the mineralogical and geochemical characteristics of ferruginous cobbles are similar to iron-segregation bodies and were therefore grouped together. The external appearance of fragments of iron segregations is generally black and subrounded to subangular, and commonly ranges in size from 20 to 200 mm (Fig. 37C). Fragments of iron segregations exceeding 100 mm are common. These iron segregations are typically non-magnetic. It is significant that the iron segregations do not show any development of cutans. Sliced surfaces show the interiors to be reddish-black to reddish-brown mixtures of goethite and hematite. Dissolution cavities are filled with brownish-yellow secondary goethite and traces of kaolinite. Some cavities are lined with chalcedonic silica.

Petrographic examination of many of the iron segregations shows goethite pseudomorphs after pyrite and pyrrhotite (Fig. 38) and therefore these iron segregations may be classified as gossans. The spaces originally occupied by sulphides are filled to varying degrees by goethite, and where sulphides have diagnostic crystal shapes, as is commonly the case for pyrite and pyrrhotite, pseudomorphic textures are retained. Such boxwork textures in the gossans have already been described by several workers (Blain and Andrew, 1977; Andrew, 1980).

6.4 Mineralogy and Petrology

Mineralogical data on individual samples are given in Appendix 1. The relative abundances of kaolinite, goethite, hematite, maghemite, and quartz in the four categories of samples are shown in Fig. 39. Kaolinite, goethite, hematite, and quartz are the major constituents and are present in all the materials. However, the relative abundances of these minerals vary widely between the categories and particularly as a function of origin. Iron segregations are dominated by oxides, mainly goethite, that have been formed during development of gossans. Hematite is also present in iron segregations, although greatly subordinate to goethite. These Fe-oxides have developed ***in situ***, as the pseudomorphic replacement of pyrite/pyrrhotite (Fig. 38B,C.) or they may be deposited in solution

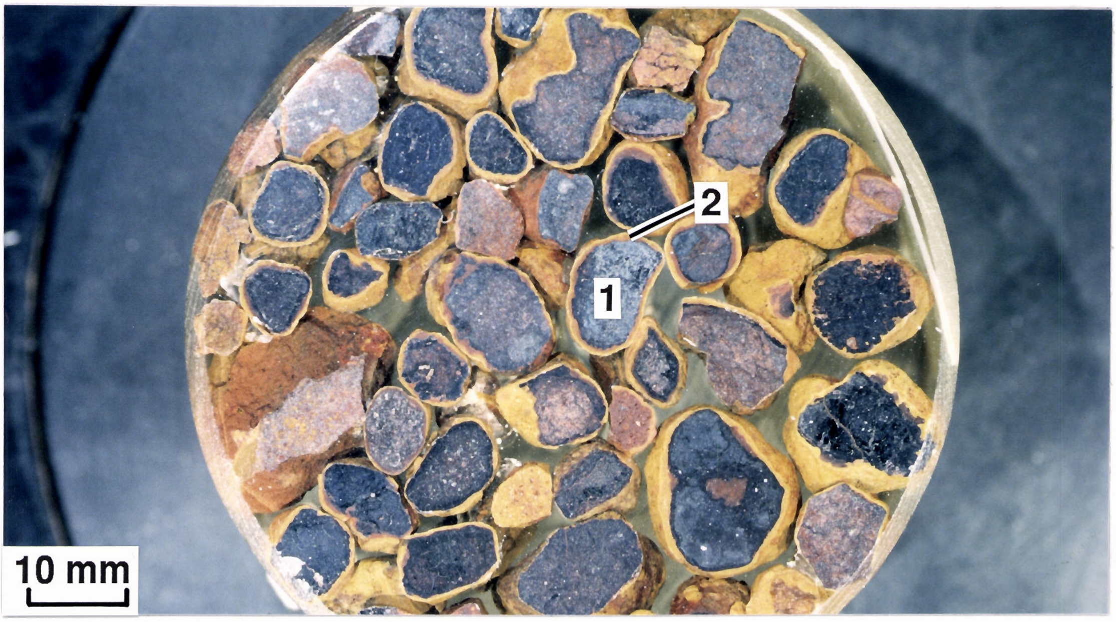

Fig.37A. Loose lateritic pisoliths showing black hematite-rich core (1) and yellowish-brown gibbsite-goethite-rich cutan (2), Sample No. 07-0814, McCaffery Pit.

Fig.37B. Fragments of ferruginous saprolite showing reddish-brown to dark brown internal surfaces, Sample No. 07-1175, McCaffery Pit.

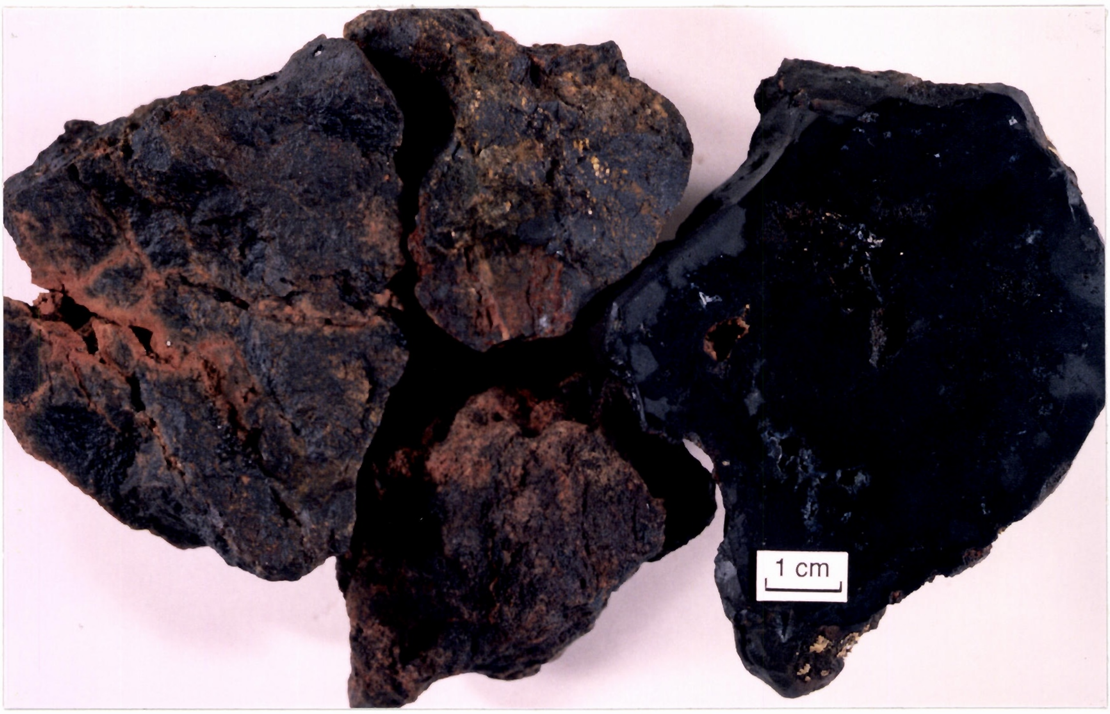

Fig.37C. Ferruginous cobbles of iron segregations, Sample No. 07-1221, 259744E, 6896694N.

Fig.38A. Iron segregations showing box work texture after sulphides, Sample No. 07-1181, McCaffery Pit.

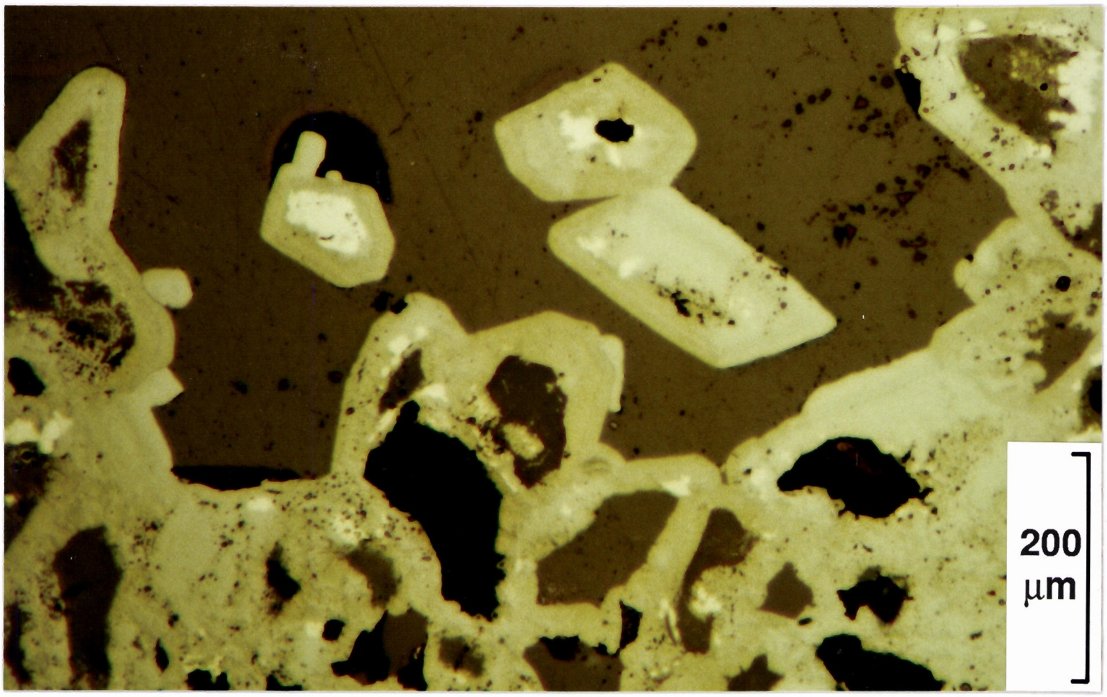

Fig.38B. Photomicrograph of polished section of iron segregation (shown above) showing goethite pseudomorph after pyrite in a silicified matrix, Sample No. 07-1181.

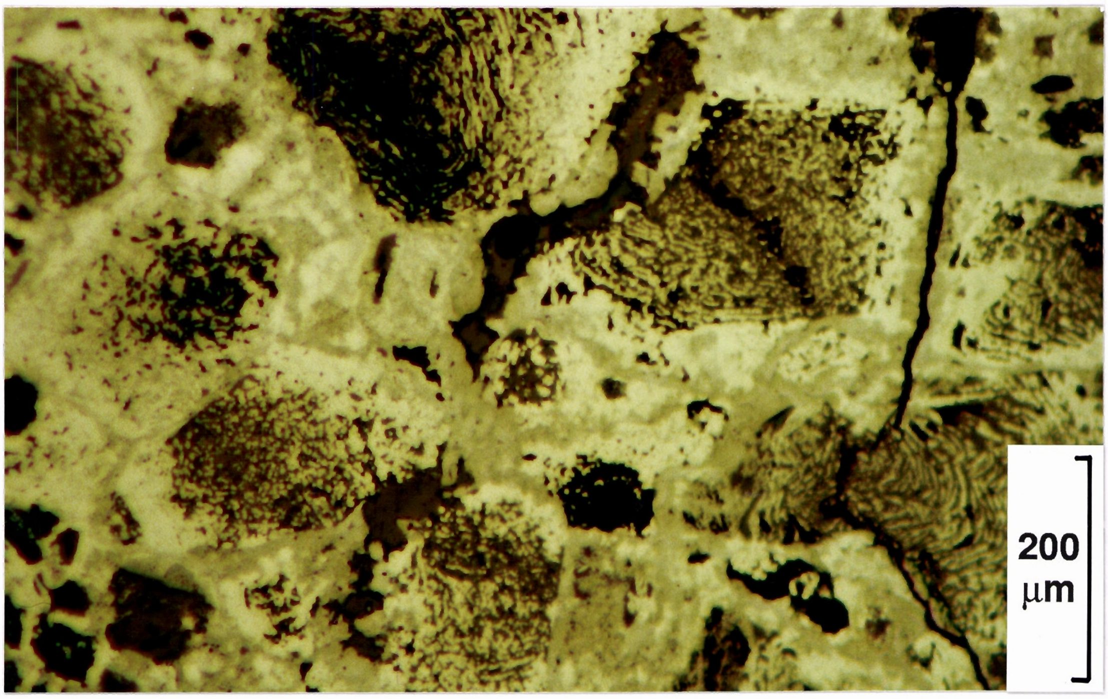

Fig.38C. Photomicrograph of polished section of iron segregation showing goethite pseudomorph after pyrrhotite, Sample No. 07-1193, McCaffery Pit.

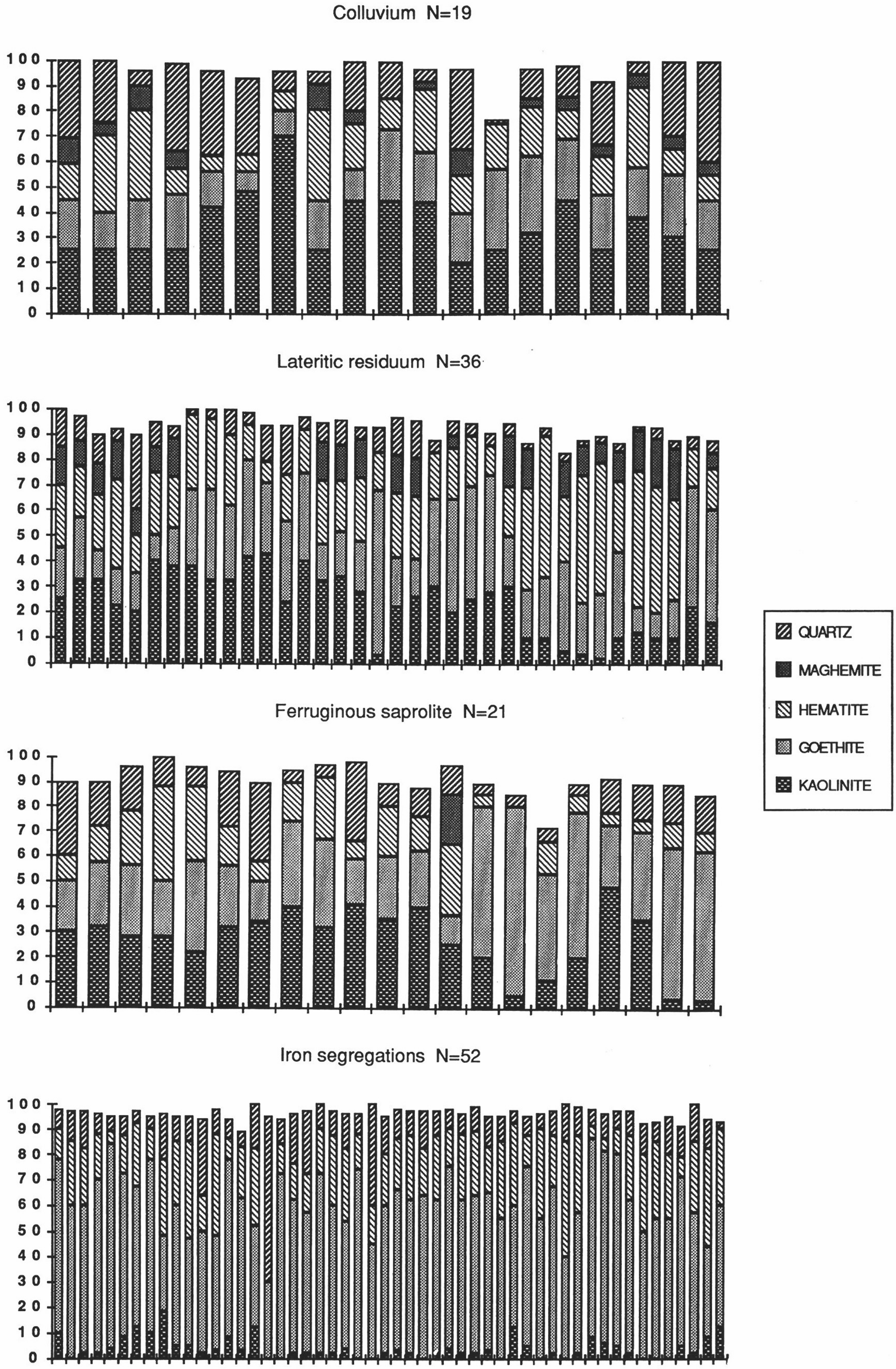

Fig.39. Bar chart showing mineral abundances of individual samples in four sample media.

cavities formed by the dissolution of former sulphides. A delicate boxwork texture may also result when pyrite dissolution is accompanied or followed by silicification. On average, hematite is relatively more abundant in the lateritic residuum at Lawlers while goethite is more abundant in the ferruginous saprolite. Colluvium contained almost equal proportions of goethite and hematite. It is interesting to note that maghemite is absent in iron segregations and ferruginous saprolite, but occurs in the magnetic gravel-fraction in lateritic residuum and colluvium. This is compatible with a bushfire origin for the maghemite: forest being inferred during the Tertiary lateritization whereas the present-day erosional regimes, exposing ferruginous saprolite and iron segregations, lack a forest cover because of the arid environment. Maghemite formation requires the heating of Fe-oxides and oxyhydroxides to $\approx$230°C in a reducing environment. Such an environment occurs during bushfires when the forest ground cover contains fallen trees, thereby providing high temperatures and localized oxygen - deficient conditions in contact with the surface soil. This environment, however, does not occur in the present-day arid environment because of the lack of forest cover.

Goethite (goethite + hematite) ratios are shown in Fig. 40 and indicate that there is an upward increase in hematite in lateritic residuum in lateritic profiles, which suggests that goethite dehydrates to hematite in the course of time however, not all the hematite occurring in lateritic residuum is a dehydration product of goethite. Hematite can also form directly by internal dehydration of ferrihydrite.

Kaolinite is either absent or present in very small amounts in the iron segregations. In contrast, colluvium, ferruginous saprolite, and lateritic residuum contain significant amounts of kaolinite. Kaolinite may occur as accordian-like structures (Fig. 41A).

Quartz is present in small amounts in all the sample types. However, some samples of iron segregations and colluvium contain large amounts. Quartz is largely residual, although there is a minor amount of secondary quartz.

Evidence for a few other minerals is seen on X-ray charts of the samples studied. Anatase and rutile are present in appreciable amounts in lateritic residuum and are seen in the thin section to be products of ilmenite weathering. Relict talc, up to 20%, was recorded in some samples of lateritic residuum and ferruginous saprolite, this was taken as an indication of materials developed from ultramafic bedrock or lithology. It occurs as lath-shaped crystals in the cores of lateritic pisoliths (Fig. 41B). Traces of gibbsite occurred in a few samples of lateritic residuum. Smectite was observed in a few samples of colluvium and ferruginous saprolite, but only in small amounts.

The differences in mineralogy between the groups of materials are due to the differences in their origin and the degree of weathering. Goethite in iron segregations is derived mainly from Fe released into solution by the weathering of sulphides, although there may also be contributions from other Fe-bearing minerals. Goethite has been reported to be the dominant mineral in gossans by several workers (e.g. Nickel, 1984). The differences in abundances of minerals between ferruginous saprolite and lateritic residuum are due to differences in the degree of weathering. Ferruginous saprolite has experienced a lesser degree of weathering compared with that of lateritic residuum as is shown by the large amounts of goethite and kaolinite in ferruginous saprolite. Colluvium derived from erosion of lateritic residuum and ferruginous saprolite showed a mixed mineralogy.

6.5 Al Substitution in Fe-Oxides

The levels of Al substitution in goethite for the four sample groups are shown in histograms (Fig. 42). Values for individual samples are given in Appendix 1.

The Al substitution of goethite in samples studied ranges from 0 to 28 mole %. Goethites in the iron segregations show the lowest Al substitution (median value less than 5 mole %). In contrast, goethites in lateritic residuum and ferruginous saprolite contain moderately-high levels (18 mole %) of Al substitution. Goethite in colluviums contain low levels (10 mole %) of Al substitution. However, a wide range of Al substitution occurs for goethite in colluvium, lateritic residuum, and ferruginous saprolite.

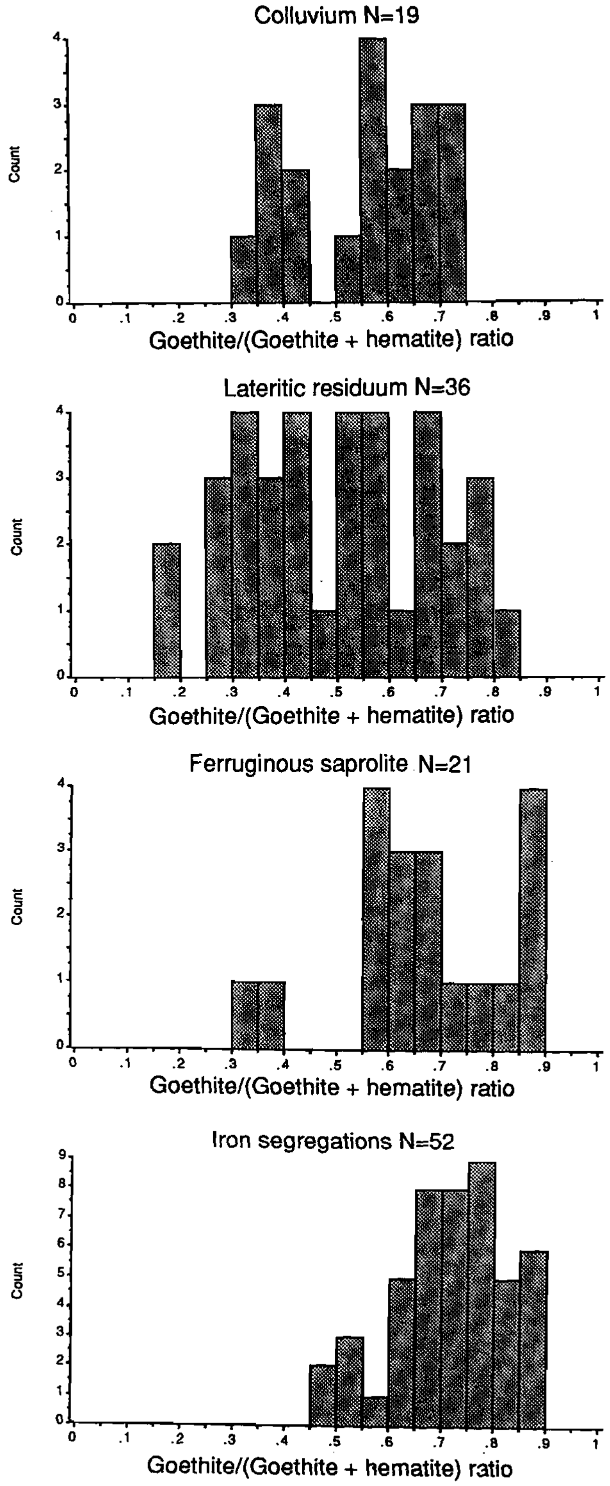

Fig.40. Histograms of goethite/(goethite + hematite) ratio for four categories of sample media.

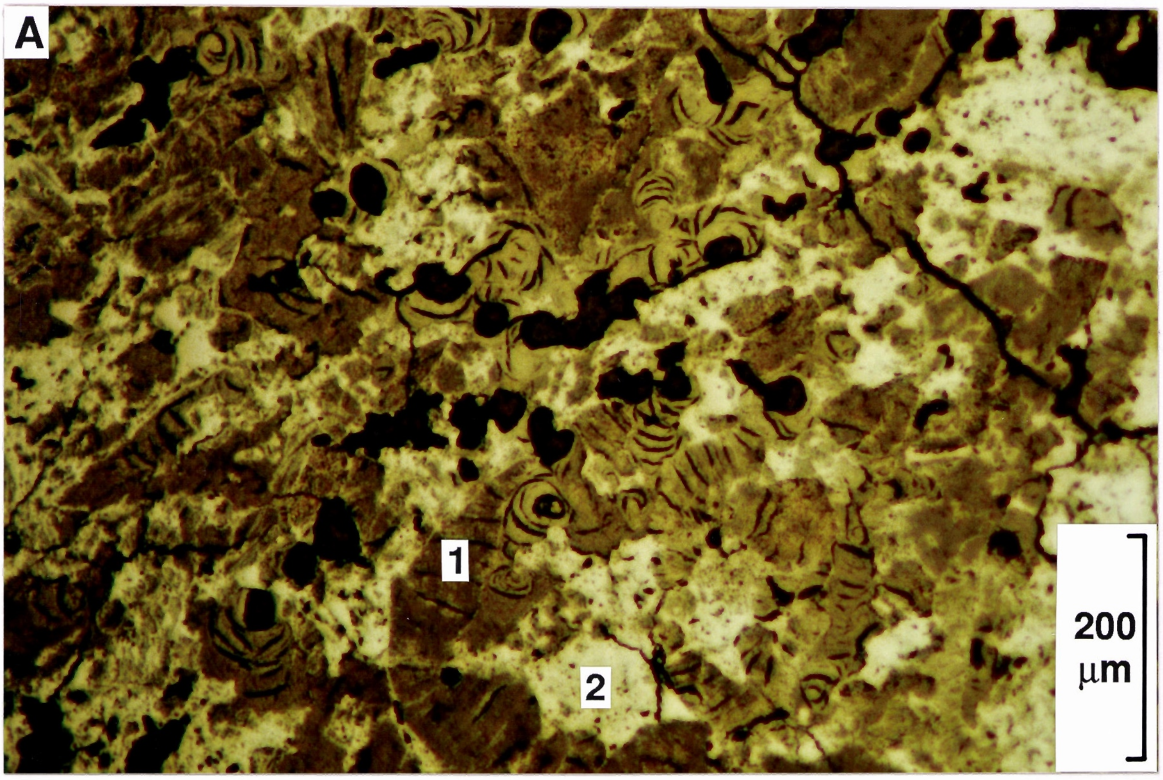

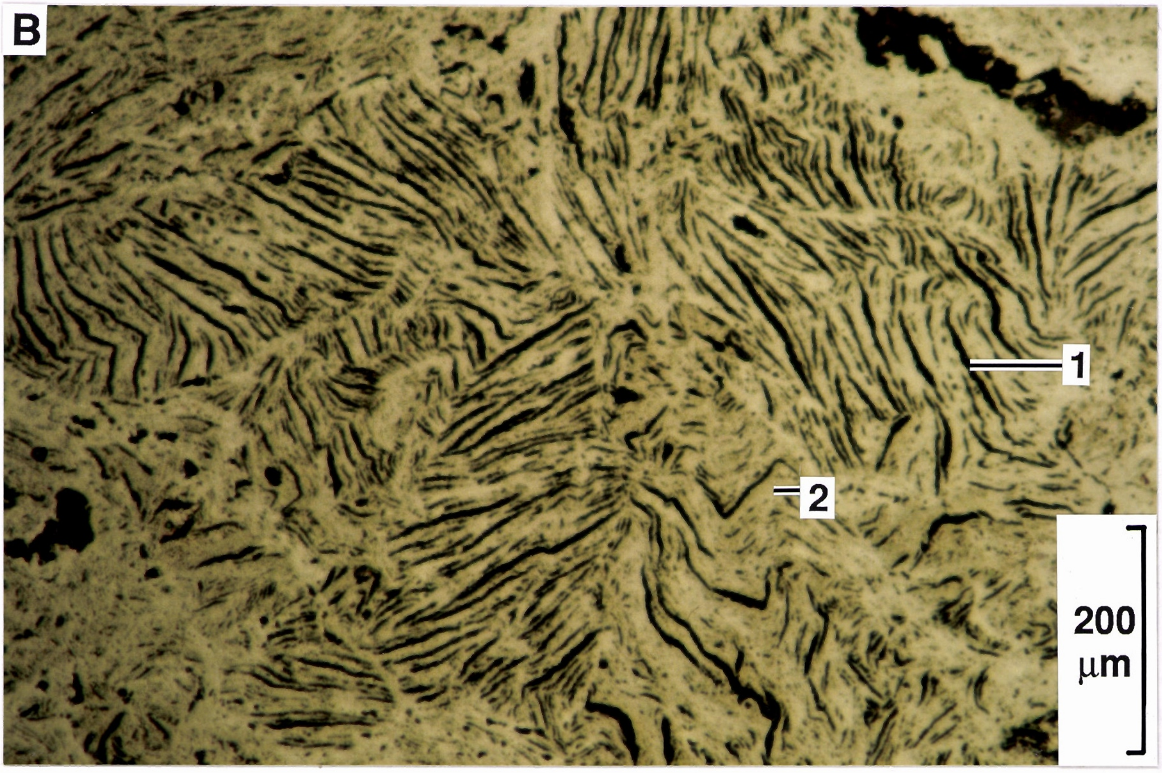

Fig.41A. Photomicrograph of polished section of a lateritic nodule showing accordian-like structure of kaolinite (1) set in a goethite-rich matrix (2), Sample No. 07-0874, North Pit area.

Fig.41B. Photomicrograph of polished section of a lateritic nodule showing relict talc (1) in a goethite-rich matrix (2), Sample No. 07-0851, North Pit area.

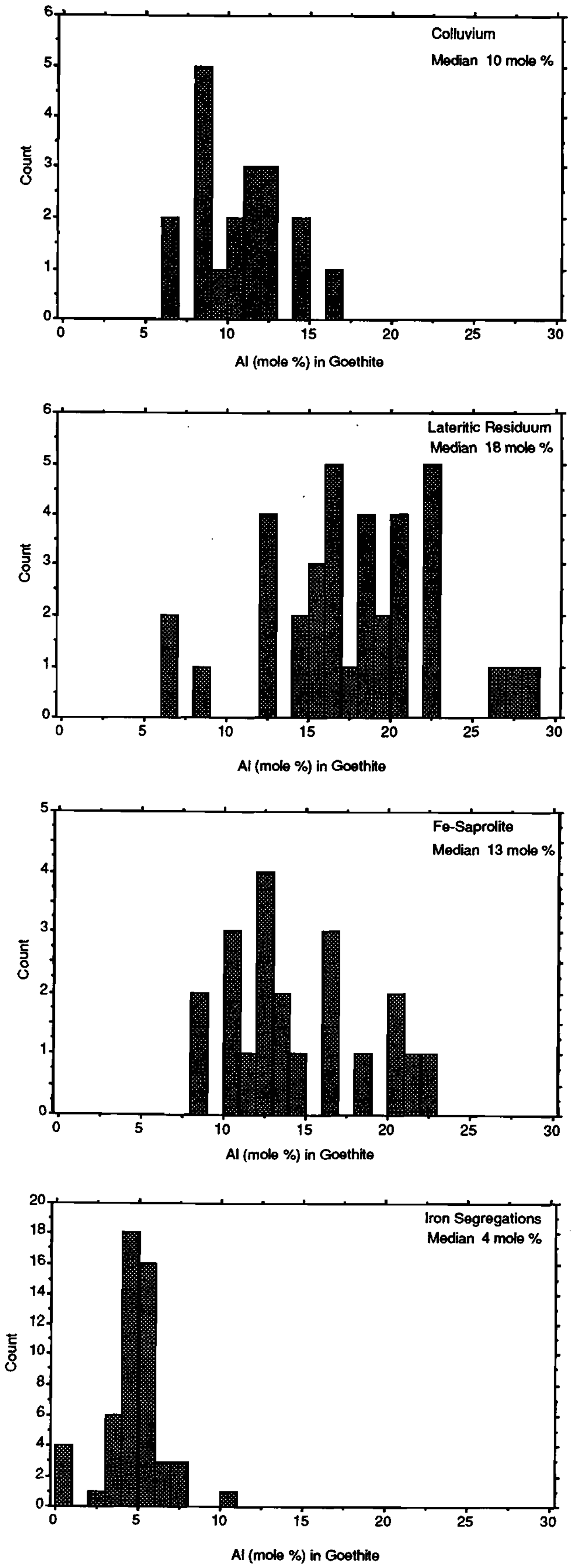

Fig.42. Histograms of the values of mole % Al in goethite for four categories of sample media.

These different levels of Al substitution in goethite between the sample types suggests different environments and/or mechanism for their formation. Very low Al substitution in the goethite of the iron segregations indicates that they must have grown in an environment almost free of accessible Al. On the other hand, goethite in lateritic residuum has formed in an Al-rich environment as indicated by the presence of kaolinite.

Iron segregations, comprising mixtures of goethite and hematite occur as discrete bodies at several levels within the saprolite horizon of laterite profiles in the Lawlers district. Iron segregations are well exposed in the walls of the McCaffery Pit and Turrett Pit and these two locations were chosen for a systematic study of the characteristics and genesis of the bodies. This research shows that the goethites in iron segregations at McCaffery and elsewhere in the Lawlers district are characterized by a very low level of Al substitution, possibly due to an absolute accumulation of Fe under hydromorphic conditions in an environment almost free from available Al. This follows the conclusions of Fitzpatrick and Schwertmann (1982) and Schwertmann and Latham (1986) that goethites formed by absolute accumulation of Fe contain low (< 10 mole %) amounts of Al substitution. It therefore seems likely, that many of the iron segregations in the Lawlers district formed under the influence of at least some hydromorphic concentration of Fe within the saprolite horizon in the past, although they now occur on areas which are freely drained today. The lower substitution of Al in Fe-oxides may also be due to the lower availability of Al.

At Lawlers, Al substitution in hematite (10 mole %- mean) and maghemite (6 mole %-mean) is generally lower than in goethite in the same sample which is in keeping with the findings of other researchers (e.g. Schwertmann and Latham, 1986; Anand and Gilkes, 1987). These authors conclude that since both minerals are assumed to have crystallized in the soils, this difference is probably a consequence of the lower capacity of hematite to accommodate Al.

6.6 Geochemistry

6.6.1 GENERAL

The compositions of the four sample media in terms of the three major components of Fe_2O_3, Al_2O_3, and SiO_2 are plotted in the triangular diagrams in Fig. 43. Silica and Al_2O_3 are present in higher amounts in colluvium and ferruginous saprolite, whereas Fe_2O_3 dominates in the iron segregations. With the increase in Fe_2O_3, there is a concomitant decrease in SiO_2 and Al_2O_3. Silica and Al_2O_3 occur in the form of kaolinite, some Al occurs in goethite, and Si in quartz.

Analytical data on individual samples are given in Appendix 2. The statistical distribution of elements within the four sampling media is characterized by five parameters (Table 13). The median value is used for estimating the central value of distribution, while the two extreme percentiles (5% and 95%) effectively indicate the limit of the variation. Prior to this stage, all censored values (less than lower limit of determination) were assigned one third of the detection limit as the default minimum value for the statistical analyses.

An immediate obvious feature of the results shown in Table 14 is the marked spread of values found in all categories. However, a comparison of median values for the four categories suggests a marked difference in average composition for many elements despite their overlap. The major and minor element chemistry of the iron segregations is quite different from that of lateritic residuum and ferruginous saprolite (iron segregations have higher Fe_2O_3, Mn, Zn, Co, Ba, and lower Al_2O_3, TiO_2, Cr, V, Ga, Zr, Au than lateritic residuum and ferruginous saprolite). Although Fe_2O_3 and Al_2O_3 contents of lateritic residuum are comparable with ferruginous saprolite, there is a strong geochemical distinction between these two media. Lateritic residuum shows high median values of Cr, V, Pb, Ni, As, and Ga and relatively low levels of Cu, Zn, Co, Bi, and Au compared with the median values of ferruginous saprolite. Colluvium is enriched in SiO_2, Al_2O_3, TiO_2, Ga, Zr, and Nb relative to the other categories.

Histograms of the elements for the four categories are shown in Figs. 44, 45, 46, 47, 48 and Appendix 3. Above each histogram is a box and whisker plot that shows the median, left hinge (25th percentile), right hinge (75th percentile), and range (minimum and maximum values in a numerical

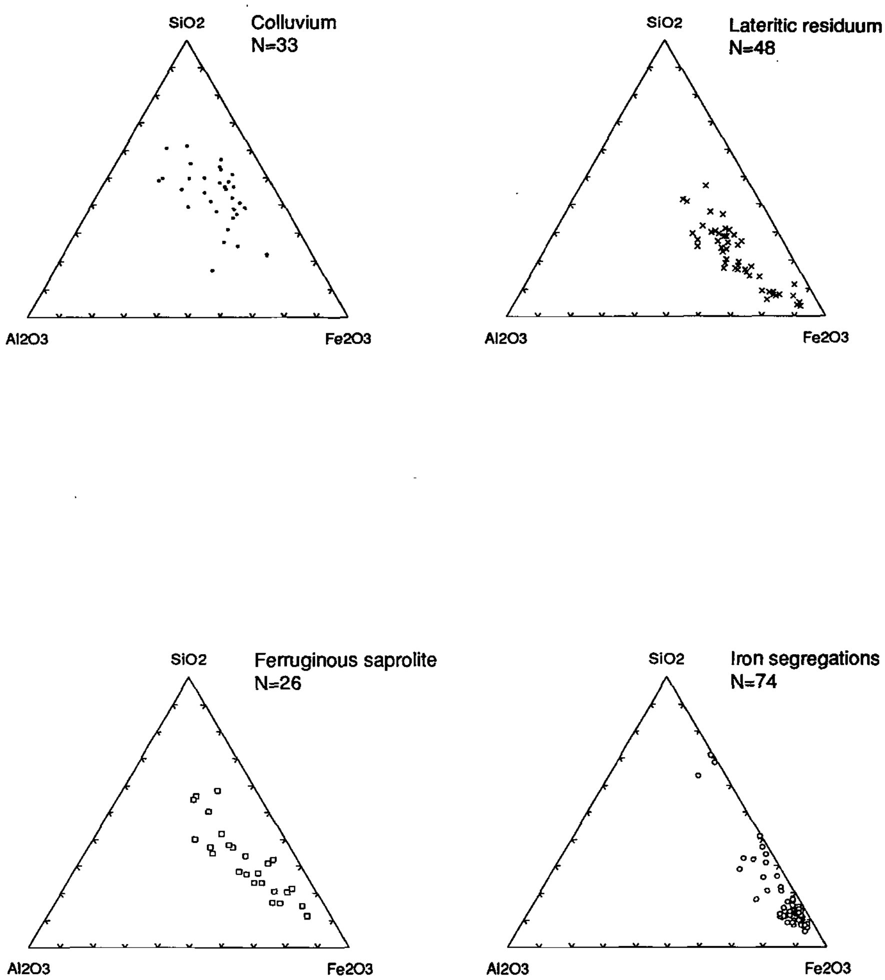

Fig.43. Triangular diagrams showing compositions of four categories of sample media, in terms of weight percent of SiO_2, Al_2O_3, and Fe_2O_3.

Table 14. Some summary statistics on element levels in four sample categories: 5th percentile, median (50th), and 95th percentile.

Sample Type	Colluvium n = 33			Lateritic Residuum n = 48			Ferruginous Saprolite n = 26			Iron Segregations n = 74		
Percentile	5th pct	Median	95th pct	5th pct	Median	95th pct	5th pct	Median	95th pct	5th pct	Median	95th pct
wt.%												
SiO2	18.69	40.00	53.88	4.01	18.80	35.66	9.68	25.10	51.58	7.01	11.60	43.78
Al2O3	10.35	16.70	29.05	5.09	14.93	23.86	6.00	14.16	23.05	1.28	3.10	8.33
Fe2O3	12.95	34.31	58.07	32.11	52.20	77.53	20.74	47.12	67.85	44.04	73.67	78.89
MgO	0.105	0.265	0.936	0.027	0.154	0.952	0.034	0.137	3.405	0.028	0.081	0.305
CaO	0.042	0.214	1.023	0.033	0.089	0.349	0.051	0.113	0.399	0.033	0.095	0.368
Na2O	0.008	0.046	0.251	0.005	0.017	0.172	0.013	0.034	0.376	0.002	0.014	0.035
K2O	0.020	0.102	0.521	0.020	0.020	0.207	0.020	0.020	0.093	0.020	0.020	0.038
TiO2	0.856	1.343	2.804	0.246	1.128	5.054	0.091	1.125	1.929	0.056	0.236	0.985
Mn ppm	99	288	1730	78	205	1928	93	238	1038	40	2820	4328
Cr	306	554	8287	200	5640	23720	85	238	13730	7	47	1850
V	444	814	1687	233	847	2485	236	502	19679	83	236	1076
Cu	38.2	60.0	93.2	14.0	70.0	388.5	58.9	195.0	978.5	64.8	130.0	372.5
Pb	3.4	14.0	28.6	1.3	14.0	41.1	0.7	0.7	22.2	0.7	3.0	16.0
Zn	2.3	22.0	100.9	5.4	35.0	106.5	28.8	57.0	344.5	34.3	320.0	695.0
Ni	37	62	840	20	210	2249	10	68	5305	27	69	218
Co	8.8	20.0	52.4	3.4	28.0	109.2	5.4	35.0	241.0	8.0	84.0	137.5
As	9.8	46.0	374.0	13.6	127.5	1746.0	7.7	55.5	2165.0	4.5	33.0	545.0
Sb	0.7	4.0	12.8	1.3	5.0	41.1	1.5	6.5	31.3	0.7	4.0	12.3
Bi	0.7	0.7	5.1	0.7	0.7	17.1	0.7	6.5	143.3	0.7	0.7	14.0
Mo	0.3	2.0	3.0	0.3	3.0	9.0	0.3	2.0	9.3	0.3	2.5	5.0
Ag	0.03	0.20	1.29	0.03	0.20	1.06	0.03	0.10	0.30	0.03	0.10	0.43
Sn	0.7	2.0	6.3	0.7	2.0	7.0	0.7	2.0	8.0	0.7	0.7	5.0
Ge	0.7	1.3	4.0	0.7	1.3	4.0	0.7	2.5	6.0	0.7	1.3	7.3
Ga	21.4	44.0	64.6	12.0	45.0	121.5	1.3	17.5	45.9	1.3	4.0	24.5
W	1.3	8.0	53.2	1.3	10.0	89.3	1.3	4.5	17.0	1.3	1.3	26.0
Ba	19	105	774	11	38	618	2	72	490	13	147	2416
Zr	76	110	159	37	100	150	12	74	142	7	20	66
Nb	6.7	10.0	13.3	0.7	7.0	21.8	0.7	3.5	7.7	0.7	2.0	6.0
Se	0.7	0.7	4.0	0.7	2.0	7.6	0.7	0.7	2.7	0.7	0.7	3.3
Be	0.8	1.0	2.0	0.3	1.0	2.0	0.3	1.0	1.7	0.3	1.0	2.0
Au ppb	4	64	859	0	110	11700	5	365	4995	1	17	745

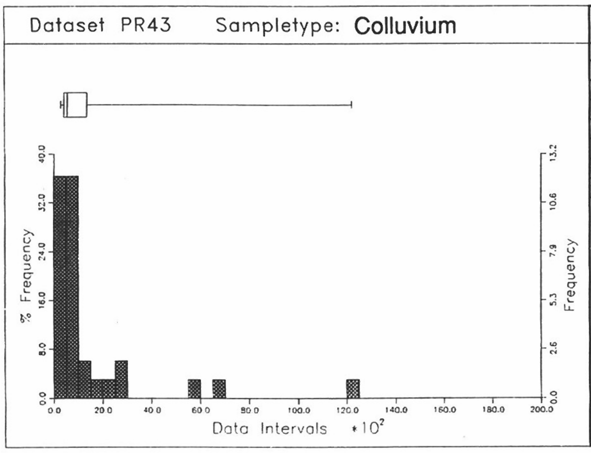

Cr	
Samples	33.
Mean	1471.52
Std. Dev.	2425.79
Max	12200.00
Min	302.00
Median	554.00
L Hinge	425.00
R Hinge	1367.00

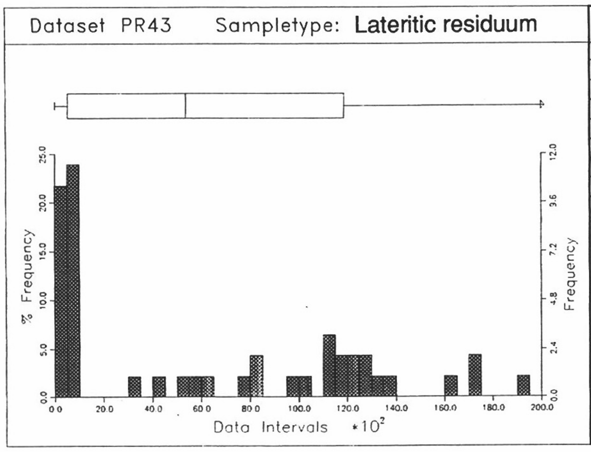

Cr	
Samples	48.
Mean	7257.25
Std. Dev.	8251.90
Max	40200.00
Min	38.00
Median	5378.00
L Hinge	539.00
R Hinge	11900.00

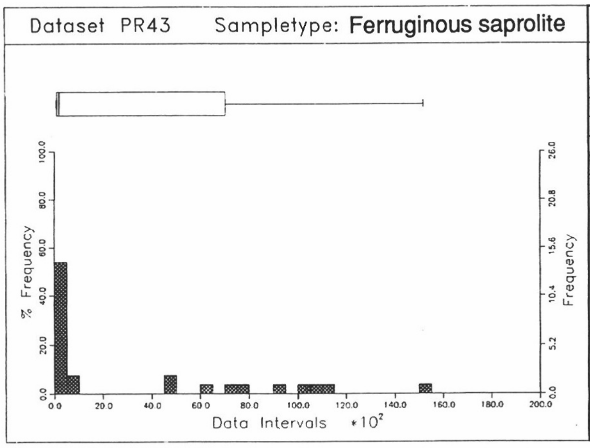

Cr	
Samples	26.
Mean	3460.38
Std. Dev.	4645.95
Max	15200.00
Min	83.00
Median	210.00
L Hinge	115.00
R Hinge	7060.00

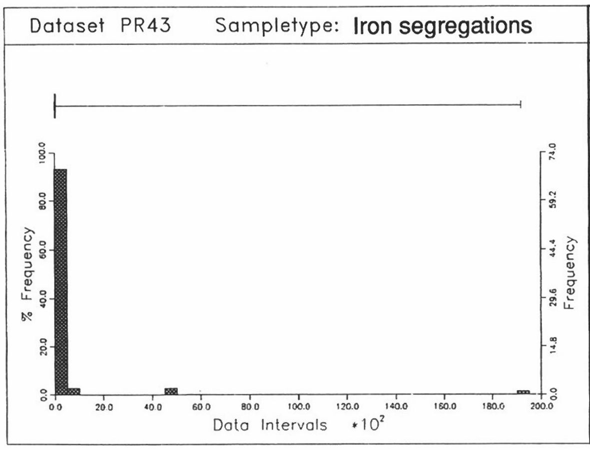

Cr	
Samples	74.
Mean	460.46
Std. Dev.	2331.64
Max	19200.00
Min	6.67
Median	47.00
L Hinge	31.00
R Hinge	72.00

Fig.44. Histograms of the values of Cr for four categories of sample media.

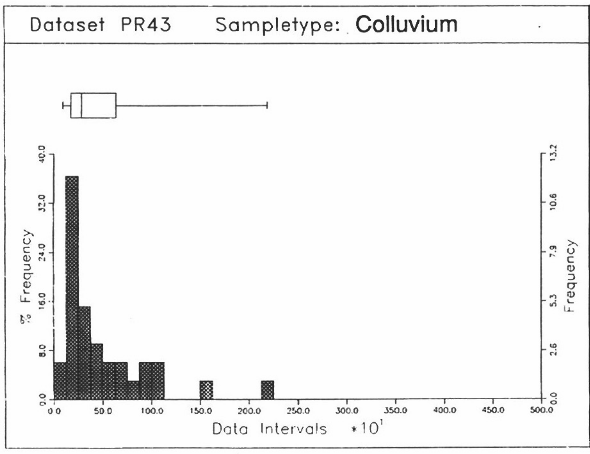

Mn	
Samples	33.
Mean	492.15
Std. Dev.	460.40
Max	2188.00
Min	95.00
Median	288.00
L Hinge	180.00
R Hinge	642.00

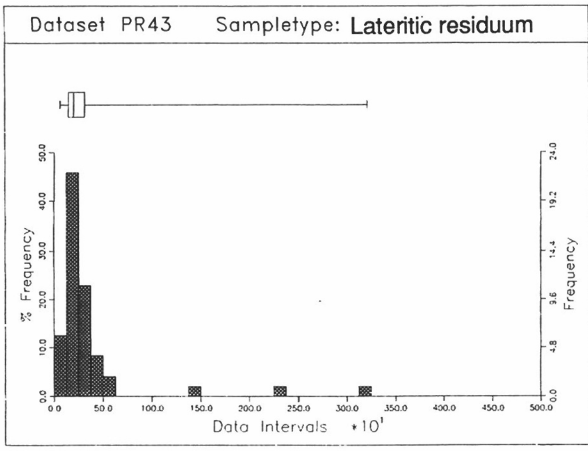

Mn	
Samples	48.
Mean	353.27
Std. Dev.	555.71
Max	3210.00
Min	64.00
Median	204.00
L Hinge	149.00
R Hinge	316.00

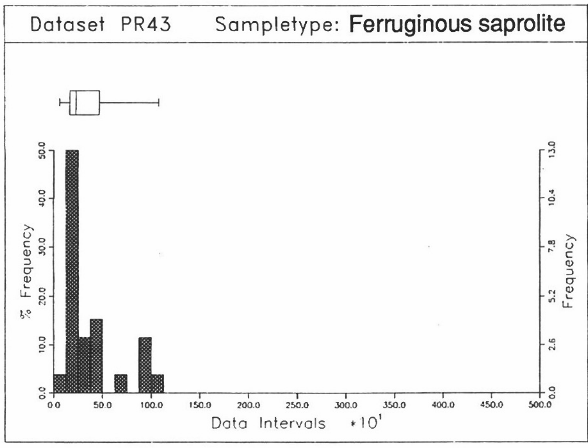

Mn	
Samples	25.
Mean	370.92
Std. Dev.	293.92
Max	1080.00
Min	66.00
Median	229.00
L Hinge	159.00
R Hinge	469.00

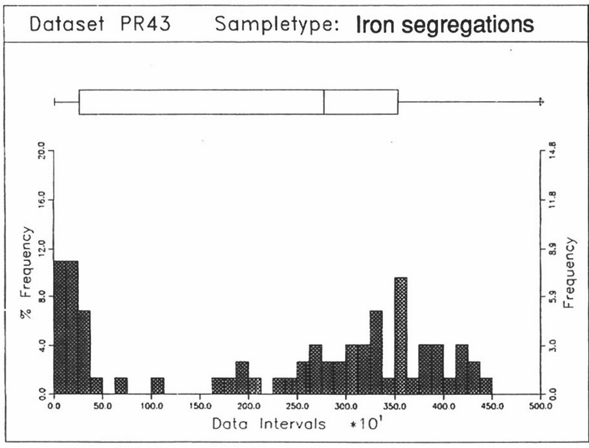

Mn	
Samples	74.
Mean	2300.20
Std. Dev.	1568.66
Max	5250.00
Min	15.00
Median	2780.00
L Hinge	271.00
R Hinge	3540.00

Fig.45. Histograms of the values of Mn for four categories of sample media.

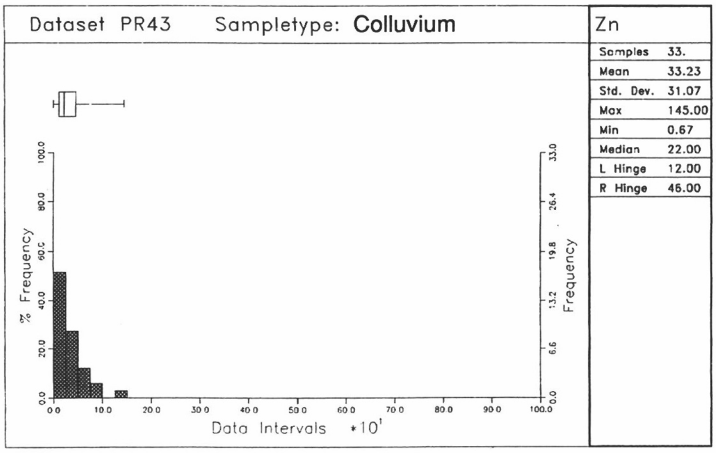

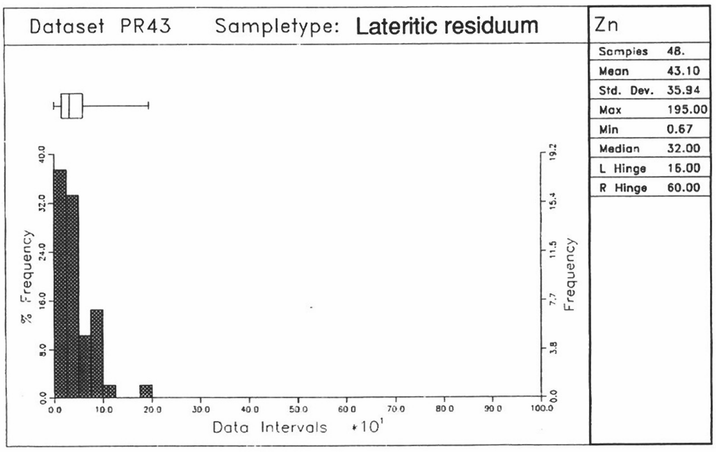

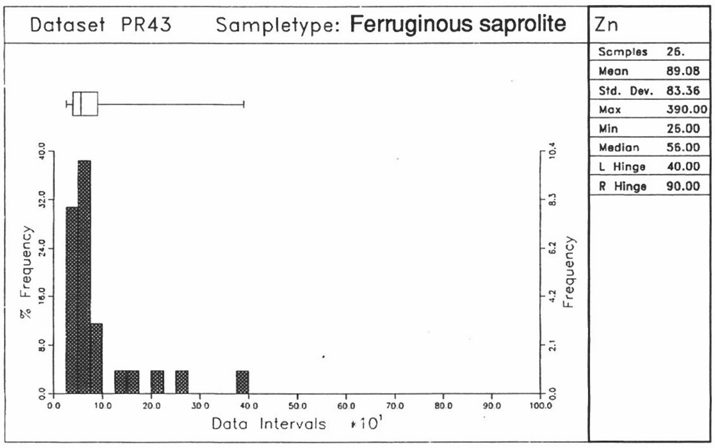

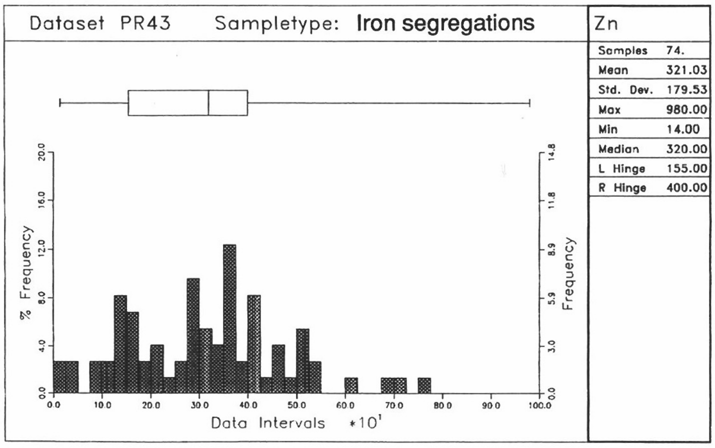

Fig.46. Histograms of the values of Zn for four categories of sample media.

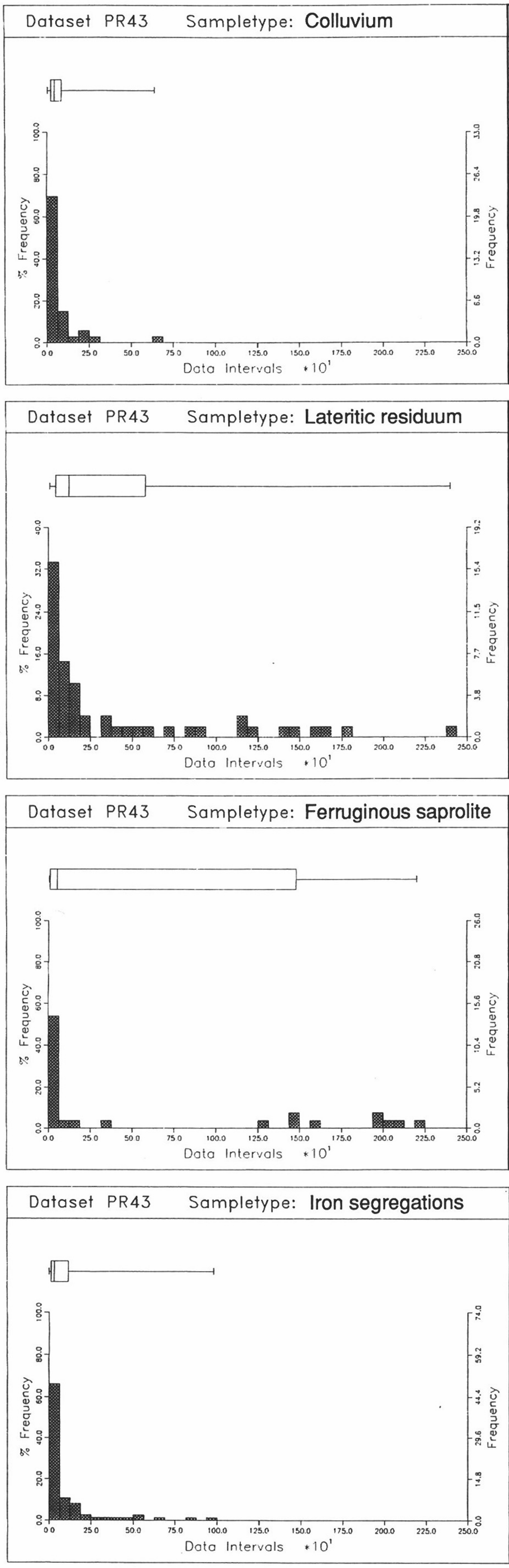

As (Colluvium)	
Samples	33.
Mean	81.82
Std. Dev.	116.12
Max	640.00
Min	7.00
Median	45.00
L Hinge	25.00
R Hinge	85.00

As (Lateritic residuum)	
Samples	48.
Mean	442.90
Std. Dev.	598.30
Max	2400.00
Min	10.00
Median	125.00
L Hinge	45.00
R Hinge	580.00

As (Ferruginous saprolite)	
Samples	26.
Mean	654.31
Std. Dev.	863.37
Max	2200.00
Min	7.00
Median	55.00
L Hinge	13.00
R Hinge	1480.00

As (Iron segregations)	
Samples	74.
Mean	110.14
Std. Dev.	189.13
Max	980.00
Min	0.67
Median	32.00
L Hinge	14.00
R Hinge	115.00

Fig.47. Histograms of the values of As for four categories of sample media.

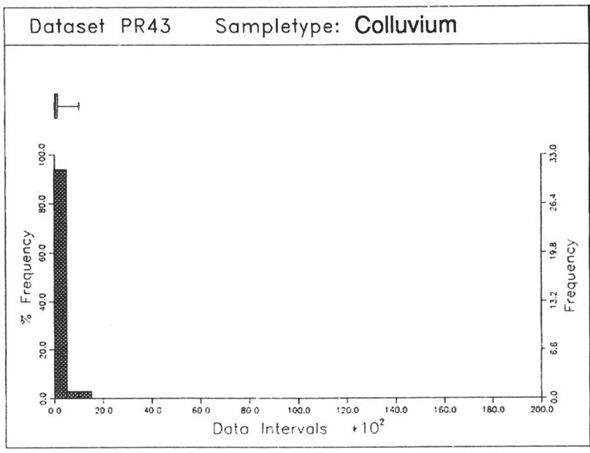

Au	
Samples	33.
Mean	124.85
Std. Dev.	214.13
Max	1020.00
Min	0.11
Median	64.00
L Hinge	24.00
R Hinge	140.00

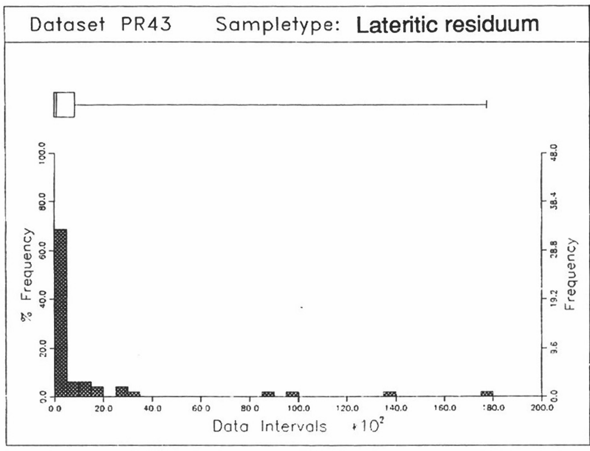

Au	
Samples	48.
Mean	1463.65
Std. Dev.	3575.72
Max	17750.00
Min	0.33
Median	110.00
L Hinge	6.00
R Hinge	840.00

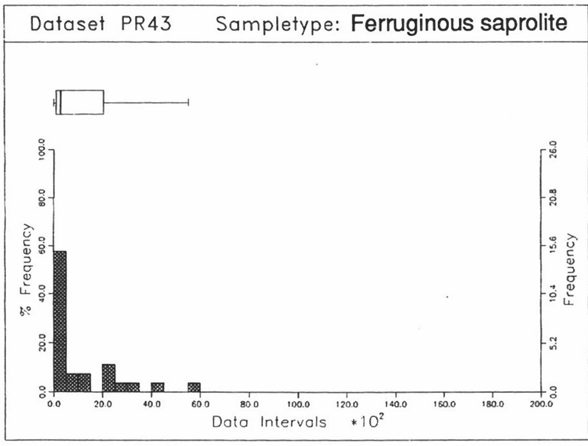

Au	
Samples	26.
Mean	1096.19
Std. Dev.	1467.55
Max	5520.00
Min	4.00
Median	270.00
L Hinge	100.00
R Hinge	2050.00

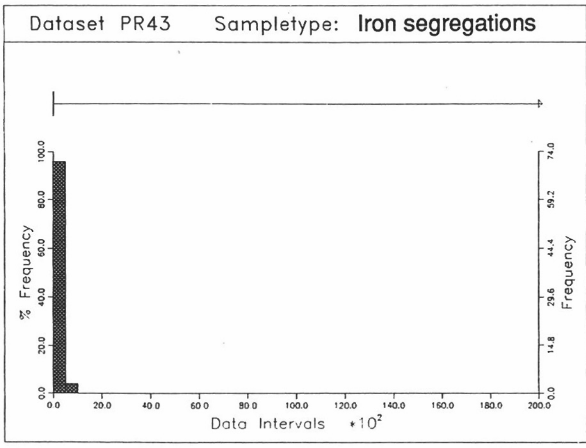

Au	
Samples	74.
Mean	901.78
Std. Dev.	7213.45
Max	62100.00
Min	0.33
Median	16.00
L Hinge	4.00
R Hinge	37.00

Fig.48. Histograms of the values of Au for four categories of sample media.

form at the right hand side of the figure). Inspection of the histogram for each element for the four categories shows that there is an overlap in values for many elements. Some elements display bimodal or polymodal distributions. This occurs with elements that reflect underlying lithologies and mineralization. Elements that exhibit these characteristics are TiO_2, Cr, Ni, As, Sb, Zr in lateritic residuum and ferruginous saprolite and Mn in iron segregations. Elements such as Cr, Ni, Ti reflects the differences in underlying lithologies (mafic vs. ultramafic) whereas As and Sb may be associated with mineralization. It is almost certain that high Cr lateritic residuum and ferruginous saprolite are derived from the weathering of ultramafic rocks. Drilling shows that both mafic and ultramafic rocks are present.

6.6.2 BIVARIATE ANALYSIS

A more direct assessment of the geochemical and mineralogical differentiation between the four groups is obtained by comparing the intra-group parameters with the global distribution parameters. A differentiation index, Di, was calculated as the percentage difference between intra-group and global median values relative to the global variation range of the element considered (Roquin *et al.*, 1990):

$$Di = 100 \times [\text{median (group i) - median}]/(\text{Pct95/Pct 5})$$

or

$$Di = 100 \times \text{Delta (Median)/Range}$$

This index clearly displays the geochemical contrasts between the four sampling media (Fig. 49). According to their mode of differentiation four groups of elements and minerals can be distinguished.

(i) Elements and minerals of group (i) (SiO_2, MgO, TiO_2, Zr, Nb, quartz) are distinguished by higher contents in gravelly colluvium than in iron segregations. The strongest contrast is observed for quartz which is even more concentrated in colluvium than in lateritic residuum. This association is characteristic of heavy minerals (zircon, rutile, ilmenite) accumulated with quartz in colluvial outwash plain areas.

(ii) Elements and minerals of group (ii) (Fe_2O_3, Mn, Zn, Co, Ba, goethite) are higher in iron segregations and lower in colluvium, lateritic residuum, and ferruginous saprolite. This suite of elements is diagnostic of gossans (Andrew, 1980). Manganese and Zn are highly variable within and between Lawlers McCaffery gossans (Table 15). Electron microprobe analysis of Fe-oxides pseudomorphs after sulphides showed that Mn and Zn ranges from 1720 to 36142 ppm and 326 to 2250 ppm respectively. Iron is the dominant constituent of the pseudomorphs. Some residual sulphides occur which are indicated by the small concentrations of SO_3 (up to 0.29%). Apart from the fundamental association of trace metals with Fe-oxides in gossans, hydrous Mn-oxides also compete for trace metal ions amenable to adsorption. Indeed, strong correlations occur between Mn, Zn, and Co.

(iii) Elements and minerals of group (iii) (Cr, V, Ni, As, Mo, Pb, Ga, hematite, maghemite) are distinguished by higher concentrations in lateritic residuum than in iron segregations. The strongest contrasts are observed for Ni, As, Pb, and hematite which are even more concentrated in lateritic residuum than in ferruginous saprolite and colluvium.

(iv) Elements and minerals of group (iv) (Cu, Sb, Bi, Au, kaolinite) are highly concentrated in ferruginous saprolite.

6.6.3 MULTIVARIATE ANALYSIS

The observed overlap in values required a multivariate technique that could unambiguously distinguish sample types on the basis of combinations of elements. Discriminant analysis appeared to be ideally suited to this task because the technique establishes the optimum combination of

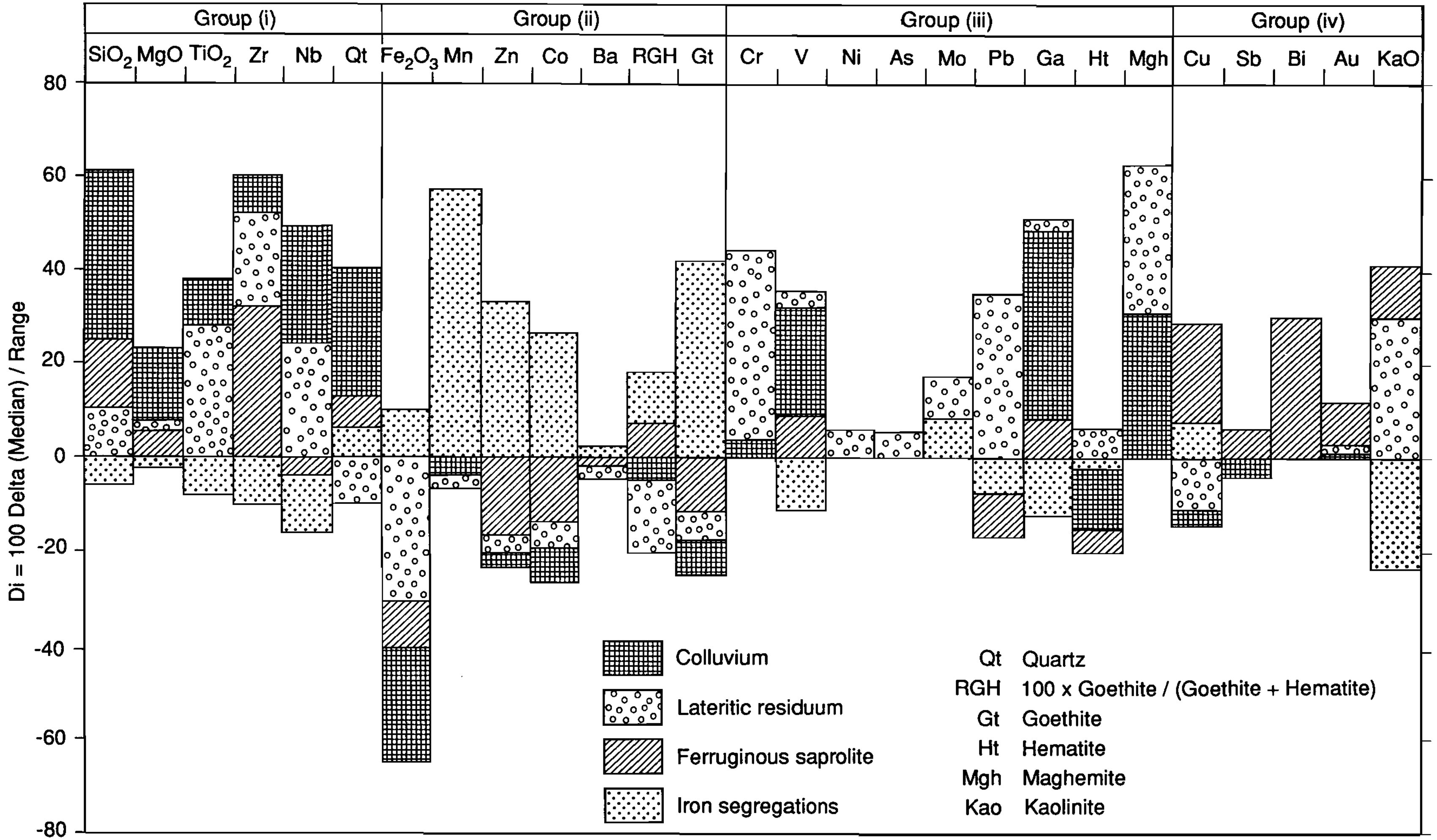

Fig.49. Classification of elements and secondary minerals according to their differentiation index between four categories of sample media.

Table 15. Electron-microprobe analysis of Fe-oxide pseudomorph after pyrite within selected iron segregation sample (07-1181)

	SiO_2 wt%	Al_2O_3 wt%	Fe_2O_3 wt%	SO_3 wt%	Mn ppm	Zn ppm
Range	0-24.7	0-1.2	71.3-96.3	0.08-0.24	1720-36142	326-2250

variables to differentiate one group from another by assigning different weightings to the variables. Specific applications of the methods in exploration include classification of gossans (Taylor and Scott, 1982; Smith *et al.*, 1984), classification of panned heavy-mineral concentrates (Clausen and Harpoth, 1983) and identification of diagnostic geochemical alteration patterns around base metal deposits (Amor and Nichol, 1983).

In canonical variate analysis, linear combinations of the elements are chosen to maximize the ratio of the between-groups to within-groups sums of squares for the resulting scores, with successive linear combinations being uncorrelated both within and between groups. The coefficients defining the linear combinations give the components of the canonical vectors, while the ratios of sums of squares give the canonical roots. The components of each of the canonical vectors are usually scaled so that the pooled within groups standard deviation of the resulting canonical variate scores is unit.

Data Analysis and Statistical Testing of the Reference Groups

The samples were initially subdivided into four reference groups based on morphology and field relationships; colluvium, (N=33), lateritic residuum, (N=48), iron segregations, (N=74), and ferruginous saprolite, (N=26). It was thought that the differences between these groups should be reflected by differences in their geochemistry.

These groups were subjected to analysis by the use of:

a) Q-Q (Quantile-Quantile plots),
b) Power Transformations,
c) Chi-square Plots,
d) All Possible Subset Combinations
e) Multiple Analysis of Variance
f) Canonical Variate Analysis

The analysis of the data was carried out in the following sequence:

1) For each element of each reference group, the data were initially examined by plotting histograms, box and whisker plots, and Q-Q plots. Examination of these plots enabled the identification of atypical observations (outliers) that distort the statistical characteristics of the reference groups. Elements with values less than the detection limit were set to one third of the detection limit.

Several obvious outliers were eliminated from the reference groups. However, because the samples represent weathered materials from at least two underlying lithologies, it was difficult to identify all outliers. During the initial investigation, each reference group was further subdivided into groups that reflected underlying lithologies; however, this resulted in reference groups with fewer observations than variables. Furthermore, the distinction between the groups was not enhanced by the additional subdivision and this approach was abandoned.

2) Many of the elements are not normally distributed. Since statistical procedures are based on the assumption that the sample populations are normally distributed, the data were subjected to a procedure that transformed them as closely as possible to normality. The procedure used is outlined in Howarth and Earle (1979) which transforms the data using power transformations.

3) Histograms, box and whisker plots, and Q-Q plots were plotted for the transformed data. The remaining outliers were eliminated by inspection of these diagrams.

4) The transformed data of the four reference groups were then tested for the combination of elements that maximized the distinction between the groups. The All Possible Subsets procedure (Campbell, 1980) was used to determine which suite of elements best separated the groups from each other. The data were tested using four combinations of elements, all 23 elements, seven chalcophile elements, seven lithophile elements, and a combination of 14 chalcophile and lithophile elements.

5) The 14 element combination (power transformed) was subjected to a multiple analysis of variance (MANOVA) which provides a measure of similarity of covariance, and F-ratio scores for each element. If the covariances between the reference groups are significantly different, then it may be difficult to interpret the results of canonical variate analysis. The F-ratio of the elements indicates which elements are the most significant between the groups (already determined in the all possible subsets). The ordered F-ratios represent the ordered significance of the elements.

6) Canonical variate analysis was carried out on the 14 element subset of the reference groups. Canonical variate analysis maximizes the differences between the groups and provides coefficients of linear discriminant functions that separate the groups. The roots of the analysis indicate the significance of each linear discriminant function. Generally, the first canonical root is the most significant and accounts for maximum group separation. This was the case for the four reference groups used here.

Results

Figure 50 presents a plot illustrating the effect on group separation as the elements are added into the discriminate analysis. This figure shows the results of three separate analyses involving the different suites of elements. For each suite of elements, the all possible subsets program lists the elements which are most effective in separating the groups. The all possible subsets procedures indicated that while all 23 elements gave maximum separation of the groups, the combination of 14 chalcophile and lithophile elements gave almost as good a group separation. The seven chalcophile and seven lithophile element groups did not provide as good a measure of group separation. As can be judged by the progressive flattening of the 14 element curves, the first eleven elements effect much of the separation. The addition of Sn, W, and Ni has little affect. It should be pointed out that several other combinations of elements give similar group separation and it is impractical to list all the possibilities.

Table 16 shows the canonical variate analysis which includes discriminant function co-efficients, the relative relationships of variables and significance of variables given by communality. Figures 51 and 52 show histograms of canonical scores of variable (CV1) and variable (CV2) based on 14 elements. The right hand side of each histogram lists the mean, standard deviation, minimum, maximum, median, and left and right hinge. The histograms for lateritic residuum, ferruginous saprolite, and iron-segregation are well separated. The histograms of CV2 improve the separation between lateritic residuum and colluvium.

The separation of the four groups can be best presented in terms of a two dimensional plot of the first two canonical variables (Fig. 53). The X-axis is the first canonical variable representing the linear combination of significant elements that account for most of the variance between the groups. The Y-axis or second canonical variable in the next best linear combination and is orthogonal (at right angles) to the first one. The canonical variables are evaluated at the group means by analysis of variance (Dixon, 1985). The procedure is analogous to the extraction of the first two principal component axes in factor analysis. Canonical variate analysis is performed as the final step in the discriminate procedure to produce a two dimensional representation of sample relationships. Figure 53 shows that the residual materials (lateritic residuum, ferruginous saprolite, iron segregations), are well separated whereas the transported group (colluvium) shows overlap with lateritic residuum. Zinc Cr, Zr, Nb, and Fe are the most significant contributors to canonical variate 1. Ferruginous saprolite is even better separated from the lateritic residuum by the third canonical variate (Fig. 54). The elements which contribute most to the separation of lateritic residuum from ferruginous saprolite are Bi, Sb, and Pb. These elements are associated with mineralization.

The results of stepwise discriminant analysis are satisfactory. It is not surprising however to see some overlap between lateritic residuum, colluvium, and ferruginous saprolite. Overlap may be attributed to several factors, such as degree of weathering, weathering processes, and mineralization. For example, the overlap observed between lateritic residuum and colluvium is consistent with field relationships and morphological classification suggesting that colluvium is mainly derived from the erosion of lateritic residuum. Indeed, colluvium consists of lateritic pisoliths/nodules which look very similar to those of lateritic residuum. Therefore, a sample containing abundant lateritic debris will have a high probability of falling within the lateritic residuum or vice versa.

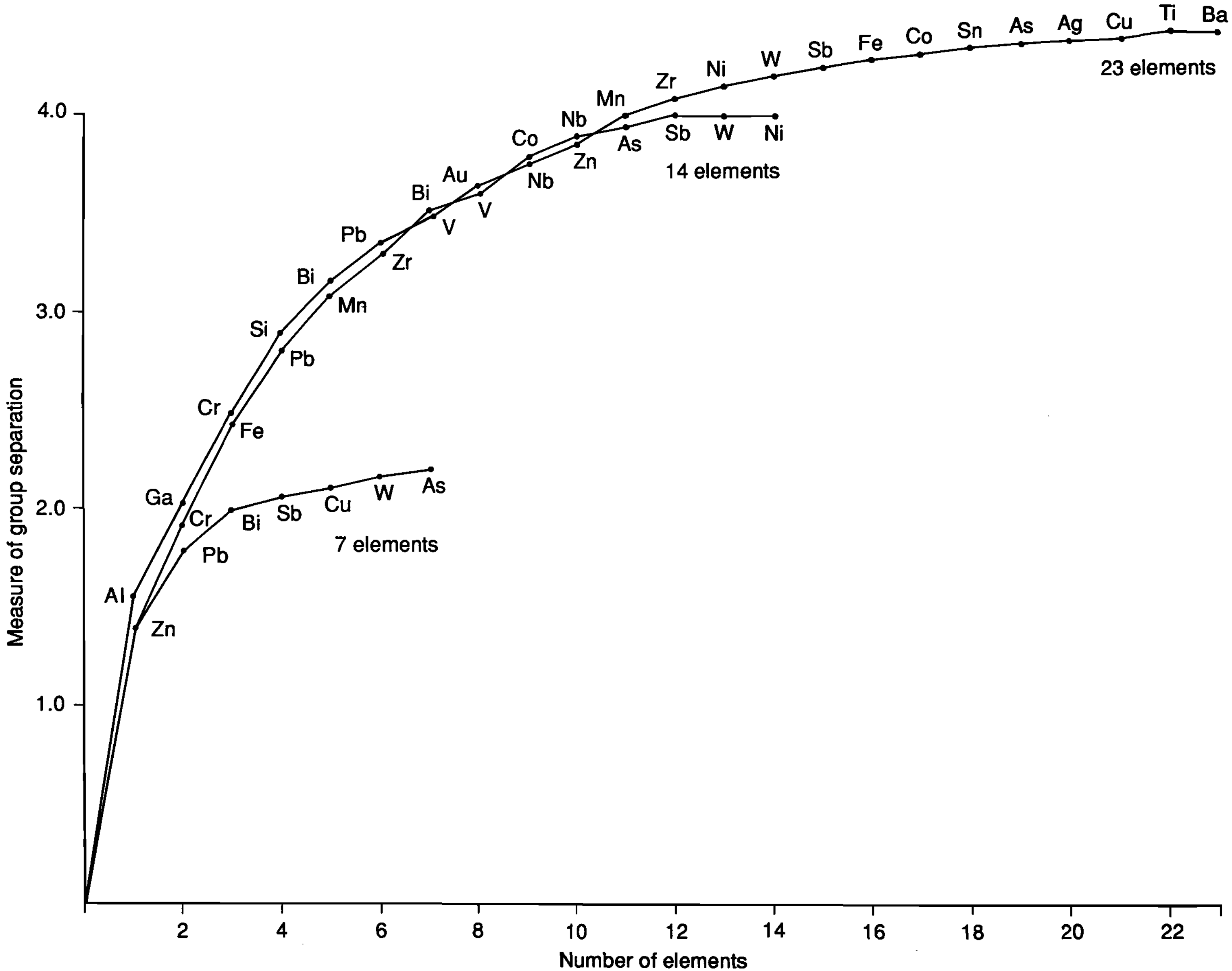

Fig.50. Plots from the all possible subsets calculations. The vertical axis shows the degree of separation of four groups. Three sets of results are shown.

Table 16. Multiple Group Discriminant Analysis

Lawlers Groups Colluvium, Iron Segregations, Lateritic Residuum, Ferruginous Saprolite [14 elements]

Wilks lambda=.0177
generalized correlation ratio, Eta square=.9823
F-ratio for h2 (overall discrimination)= 15.16
ndf1= 80 and ndf2= 419

Chi-square tests with successive roots removed

Roots Removed	Canonical r	R squared	Eigenvalue	Square	n.d.f.	Lambda	Chi % Trace
0	0.971	0.942	16.314	597.	42	0.0177	90.98
1	0.696	0.484	0.937	175.	26	0.3071	5.23
2	0.637	0.405	0.681	77.	12	0.5948	3.80

	Discriminant Function Coefficients			Factor pattern for disciminant functions			Communalities for 3 Discriminant factors	
	DF1	DF2	DF3	1	2	3		
Fe3	0.0140	0.0418	0.0070	0.768	0.458	0.009	0.7992	
Mn	-0.1106	-0.2638	0.2482		0.096	-0.238	0.224	0.1160
Cr	-0.1053	0.0969	-0.2121	-0.719	0.249	-0.230	0.6321	
V	-0.0351	-0.7779	0.4897	-0.685	-0.285	0.153	0.5743	
Pb	-0.0668	0.1653	0.3542	-0.586	0.391	0.395	0.6524	
Zn	0.0636	0.0013	-0.0424		0.883	-0.010	0.075	0.7848
Ni	-0.0220	0.2451	0.2226	-0.198	0.252	-0.150	0.1255	
Co	-0.1208	0.1891	-0.0070		0.512	0.010	0.067	0.2668
As	-0.0244	0.0935	-0.1195	-0.215	0.264	-0.225	0.1668	
Sb	0.0261	-0.0071	-0.3339	-0.183	0.099	-0.543	0.3381	
Bi	-0.0235	-0.1860	-0.3949		0.069	-0.128	-0.687	0.4935
W	-0.0122	0.1984	0.0931	-0.389	0.256	0.117	0.2307	
Zr	-0.0461	0.1348	-0.1004	-0.868	0.118	-0.003	0.7667	
Nb	-0.0544	-0.0935	0.1602	-0.783	0.035	0.270	0.6866	

Percentage of trace of r accounted for by each root

1	32.9363
2	5.7368
3	8.7104

Centroids for groups in 3 dimensional discriminant space

Group 1	-1.1552	2	-0.6740	3	0.7943
Group 2	-0.7925	2	1.0275	3	-0.2722
Group 3	1.1189	2	0.0468	3	0.2261
Group 4	-0.1625	2	-0.9347	3	-1.2729

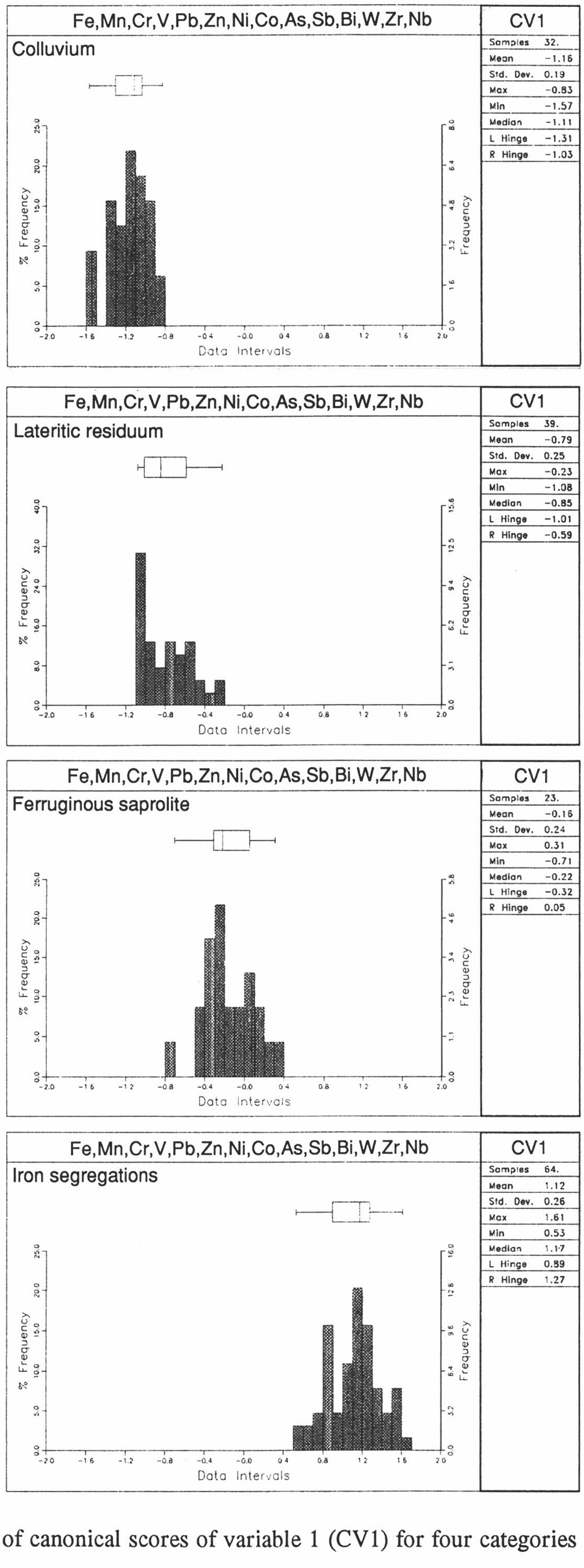

Fig.51. Histograms of canonical scores of variable 1 (CV1) for four categories of sample media.

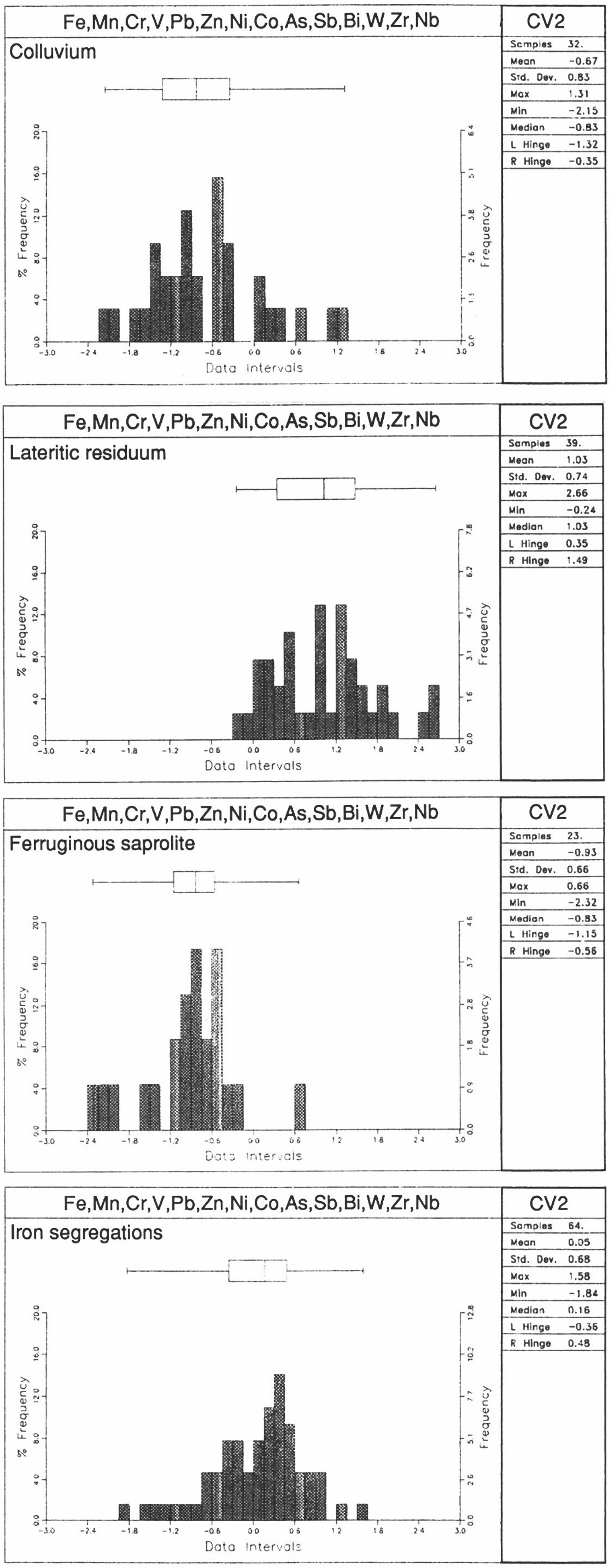

Fig.52. Histograms of canonical scores of variable 2 (CV2) for four categories of sample media.

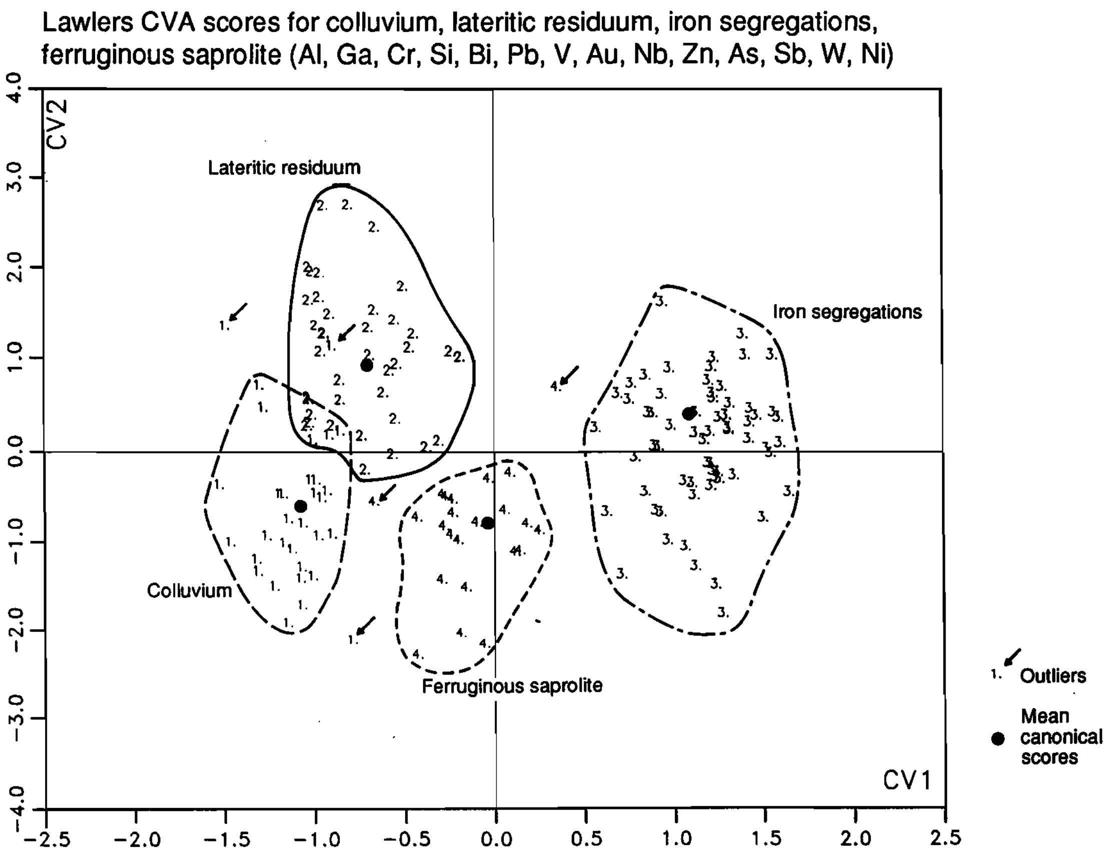

Fig.53. Plot showing CVA scores (CV1 vs CV2) for colluvium, lateritic residuum, iron segregations and ferruginous saprolite.

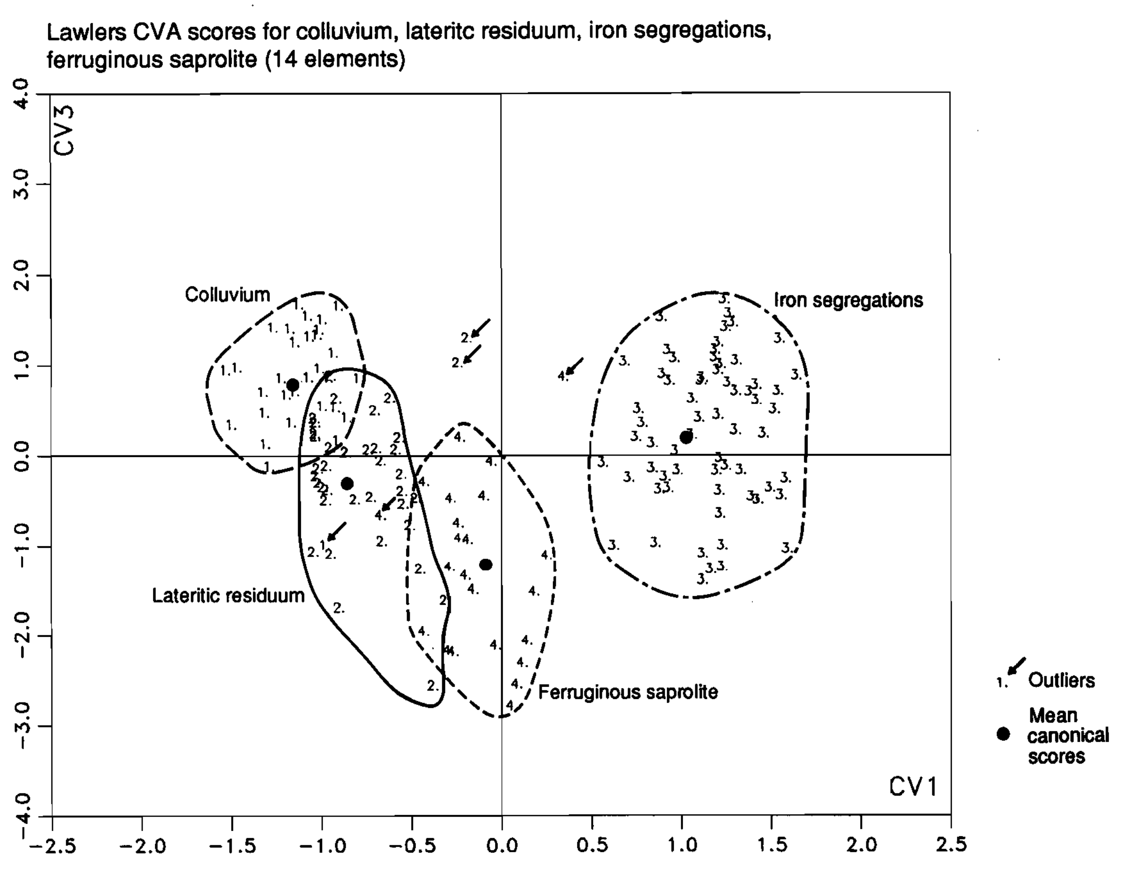

Fig.54. Plot showing CVA scores (CV1 vs CV3) for colluvium, lateritic residuum, iron segregations and ferruginous saprolite.

6.7 Discussions and Conclusions

6.7.1 MORPHOLOGY

Morphological characteristics and regolith-landform framework allowed separation of the four sample types described above: lateritic residuum, ferruginous saprolite, iron segregations, and colluvium. These four types are shown to have different morphological, mineralogical and geochemical characteristics.

Iron segregations can be recognized by their irregular, black, non-magnetic and pitted surface properties. These are larger in size (30-300 mm) compared with the gravel fraction of lateritic residuum, and fragments of ferruginous saprolite. Internal fabric of iron segregations may show goethite and hematite pseudomorphs after sulphides. Lateritic pisoliths/nodules of lateritic residuum typically have 1-2-mm thick yellowish-brown/greenish cutans around black/red nuclei. Pisoliths are rounded to sub-rounded and are 5-20 mm in diameter. The presence of cutans may be used to recognize nodules derived from the breakdown of lateritic residuum. Internal surfaces may preserve relics of resistant primary minerals (e.g. talc, chromite) allowing one to predict the underlying lithology. These features may, however, be destroyed by extensive weathering and ferruginization. Fragments of ferruginous saprolite differ from lateritic residuum in having a yellow-brown colour, irregular shape, and are non-magnetic with incipient nodular structure. The gravel fraction from colluvium displays features that are indicative of an inherited, transported origin. These features include: roundness of gravels, absence of cutans, different particle-size distributions of the sand and silt grains inside and outside the gravels and diverse lithologies of some adjacent gravels.

6.7.2 MINERALOGY

Optical microscopy, X-ray diffraction, scanning electron microscopy, and electron microprobe have been used to determine the mineralogy of the four sample groups. Semi-quantitative mineralogical determination of common occurring minerals quartz, hematite, goethite, maghemite and kaolinite is most effectively used by X-ray powder diffractometry. Specific identification of secondary minerals of Cr and Ba is more difficult, particularly if these minerals present form less than 1% of the total volume. The distribution of elements between mineral phases can be achieved by using electron microprobe or SEM fitted with energy dispersive X-ray detectors.

X-ray powder diffractometry is of most use in the mineralogical characterization of ferruginous materials to delineate the composition of iron segregations and to distinguish lateritic residuum from ferruginous saprolite. Mineralogy may also give valuable information concerning which part of the weathering profile is exposed at the surface. For example, iron segregations differ from lateritic residuum by having abundant goethite and less hematite and kaolinite. Maghemite is typically absent in iron segregations. Lateritic residuum can be distinguished from ferruginous saprolite by having abundant hematite and less kaolinite. Colluvium differs from other groups in having abundant quartz, kaolinite, and some heavy minerals. These four groups also show differences in the degree of Al substitution in goethite which appear to be related to the maturity of regolith, level of truncation, and may also reflect the environments in which the particular regolith unit has formed. Evaluation and identification of various sample media by the degree of Al substitution in goethite can be of great value. Iron segregations, for example, may be recognized by their low degree of Al substitution in goethite. This is in contrast to lateritic residuum which is characterized by a high degree of Al substitution in goethite.

6.7.3 GEOCHEMISTRY

In the present study, a major distinction is clearly evident between the iron segregations (gossans) and other facies of the weathering profile. Iron segregations are dominated by Fe_2O_3, Mn, Zn, Co, Ba, and goethite and these elements can be used as indicator elements in order to discriminate iron segregations from lateritic residuum, ferruginous saprolite, and colluvium. Many of the chalcophile elements and Au exhibit lower levels of abundance to those in lateritic residuum and ferruginous saprolite. However, the prominent regional distribution of iron segregations, often as scree on pediment surfaces in partly stripped profiles, offers potential for use as a geochemical sampling medium.

Although the lateritic residuum is derived from the fragmentation of ferruginous saprolite as described in Section 4.6, there are significant differences in the chemical composition of the two groups. Whilst the Fe_2O_3 contents of the ferruginous saprolite are comparable with those of the lateritic residuum, there are strong geochemical distinctions between the two types. The samples of lateritic residuum studied here are depleted in Cu, Sb, Bi, and Au relative to the mean values for the ferruginous saprolite. Conversely, the lateritic residuum carried significantly higher levels of As and Pb. The progressive modification of the geochemical signature of primary mineralization with the degree of evolution of the weathering facies has also been described in many studies of dispersion haloes of elements in the succession horizons of a laterite profile (e.g. Zeegers *et al.*, 1981; Davy and El Ansory, 1986). These differences may be due to the degree of weathering and mechanisms of accumulation of the secondary weathering products.

Ferruginous saprolite is relatively less weathered and most representative of mineralization. Ferruginous saprolite, or lag derived from it, could be used for exploration geochemical sampling. At this stage, however, studies at Lawlers have not established the geometry of dispersion pattern in ferruginous saprolite.

The gravelly colluvium is derived from erosion of lateritic residuum. These materials have often been laterally transported several hundred metres from their source. As a consequence of this process, they are enriched in quartz by the washing out of fine particles and the mineralization features are thus strongly depleted. Therefore, this sampling medium appears to be diluted in all the elements except Ti, Zr, Nb, and Mg which are probably located in resistant heavy minerals such as rutile and zircon.

The group separation using canonical variate analysis and all possible-subset calculations has indicated that effective separation of the four sampling medium may be made. A combination of 14 (lithophile and chalcophile) elements would seem to be most useful for separation of the groups.

7.0 DISCUSSION: DISTINGUISHING RESIDUAL REGOLITH FROM TRANSPORTED REGOLITH

Transported regolith embraces materials of redistributed origin such as alluvium, colluvium, sheetwash gravels, and aeolian clay that blanket fresh or weathered bedrock. Areas of alluvial/colluvial outwash plains are widespread in the Yilgarn Block and are common in the Lawlers district. In these landform situations, seeking geochemical haloes in buried residual laterite can be of great advantage in exploration. This requires accurate, sub-surface sampling of the lateritic materials and knowledge of the regolith stratigraphy. However, the colluvial/alluvial units may include materials, such as lateritic gravels (nodules, pisoliths) and clays derived from erosion of lateritic profiles. These may be misidentified as residual lateritic materials. Pisoliths, developed *in situ* in transported regolith, may have different geochemical and mineralogical characteristics from those in a lateritic residuum. Thus, the transported regolith may have been lateritized — hence its identification can pose problems. Lateritic gravels which have been transported long distances may not be a suitable medium for geochemical sampling at the prospect scale. In sampling for exploration geochemistry, it is therefore important to distinguish between transported nodules and pisoliths in alluvial/colluvial units and those of a buried residual laterite profile.

7.1 Criteria for Identification of Regolith Units in Drill Spoil or in Exploration Pits

The following criteria, taken conjointly, are believed sufficient to establish the characteristics of residual and transported regolith in a field situation, although ambiguous situations arise.

Hardpanized colluvium/alluvium

- Red-brown, non-hardpanized colluvium may have variable colours.
- Hard, brittle, irregular dull fracture faces, very fine porosity.
- Abundant Mn staining.
- Glassy, botryoidal opal in pores or along partings.
- Soft carbonates along partings.
- Exhibit coarse subhorizontal lamination.
- Presence of large amounts of sandy/gritty clays and/or exotic lithorelics.
- Presence of polymictic gravels - exotic lithorelics, lateritic gravels, quartz.

Lateritic residuum

- At Lawlers, the presence of nodules and pisoliths with yellowish brown/olive green cutans are believed to be confined to residual laterites or those with minimal transport (less than say 50 m).
- Presence of small fragments of lateritic duricrust in drill spoil.

Transported lateritic gravels

- Large proportion of nodules/pisoliths which are fractured or the abundance of chipped cutans would be indicative of transport. Conversely, the presence of coherent (not disaggregated) clusters of nodules and pisoliths in drill hole pulps indicates residual material.
- Layers of well-sorted and well-rounded lateritic gravel may indicate transported laterite.
- Presence in a profile of cyclic bands of packed lateritic debris alternating with layers of colluvial/alluvial clays/loams indicates a transported regolith.

8.0 PRELIMINARY INVESTIGATIONS OF THE SITING AND BONDING OF ELEMENTS AND DISPERSION PROCESSES

8.1 Introduction

The objectives of this section of the research are to establish (a) the morphology of Au; (b) the siting and bonding of Au and the ore associated elements within selected samples from within laterite geochemical anomalies in order to establish any relationships of these elements to Fe-oxides, clay minerals, or carbonates; and (c) to complement petrographic studies on the types of nodules in lateritic environments. This research should lead to an improvement of geochemical exploration sampling methods, a better understanding of the mobility and behaviour of Au and chalcophile elements in weathering profiles, provide information on whether anomalies may exist from which Au is leached, but chalcophile elements remain; and aid the understanding of the genesis of nodules and the accompanying dispersion processes.

Preliminary investigations on the above topics were made on geochemically-anomalous laterite samples collected from the North Pit and Turret areas.

8.2 North Pit Area

Gold-rich lateritic material was examined from drill hole 783 which occurs on line 9900N (local grid). The local regolith setting together with cross-sections through the regolith units are given in Section 4.4.1 The lateritic weathering profile at this location is about 40 m thick and distinct horizons from drill spoil have been recognized. At the base of the profile, the mafic lithologies are altered to kaolinite, smectite, and goethite to produce the saprolite. The saprolite grades into ferruginous saprolite comprising goethite, kaolinite, and quartz. The residual laterite horizon is about 6 m thick and consists of loose nodules and nodular duricrust, overlying ferruginous saprolite. The duricrust comprises of kaolinite, hematite, goethite, gibbsite, maghemite, and quartz. The residual laterite profile is overlain by a thin layer of transported loose lateritic nodules (2 m thick) and hardpanized colluvium of variable mineralogy.

8.2.1 MORPHOLOGY AND COMPOSITION OF GOLD

The lateritic nodules examined are 10-20 mm in size, subrounded and consist of multicoloured cores ranging from yellowish brown to reddish brown. These nodules have thin greenish-yellow goethite-rich cutans. Kaolinite, hematite, and goethite are the main minerals; gibbsite, maghemite, and quartz are less abundant. Cores of the nodules studied have compositions ranging from 56.0-82.4% Fe_2O_3, 2.5-26.0% SiO_2, and 3.1-26.2% Al_2O_3. Iron is mainly present as goethite and hematite, whereas Al and Si are present as kaolinite. The bulk sample from which these nodules were taken contains 17 ppm Au.

The Au observed in the nodules occurs as irregular subhedral to anhedral crystals, and as delicate wire forms in voids or cracks, which are either filled with kaolinite and goethite or are empty. Gold crystals also commonly occur on the surfaces of residual or colloform goethite and range in size from 15 to 80 μm (Fig. 55). Under higher magnification some of these Au crystals show dissolution features and surface pitting. Both small (5-10 μm) and large voids (50-100 μm) are observed in the cores of nodules and in the gold crystals. Occasionally, these voids may be connected to each other, creating bigger voids which are filled with Au or highly-crystalline kaolinite and goethite. Energy dispersive microprobe analysis shows that Ag in the Au grains is below the detection limit of the technique ($\approx$1%). Such a low Ag content is compatible with other observations on secondary Au and leached primary Au (Freyssinet and Butt, 1988a, b).

The close association of Au and Fe-oxides, morphology, and geochemistry (low Ag) of Au indicates that the Au analysed is dominantly secondary, having been remobilized and precipitated (Mann, 1984). During weathering, both the crystal morphology and composition will change as primary Au is dissolved and reprecipitated as secondary crystals. The physico-chemical conditions required for the dissolution of Au have been studied intensively (Boyle, 1979). The most common ionic species are Au^+ and Au^{3+}. Ions in these oxidation states are unstable in solution. To remain

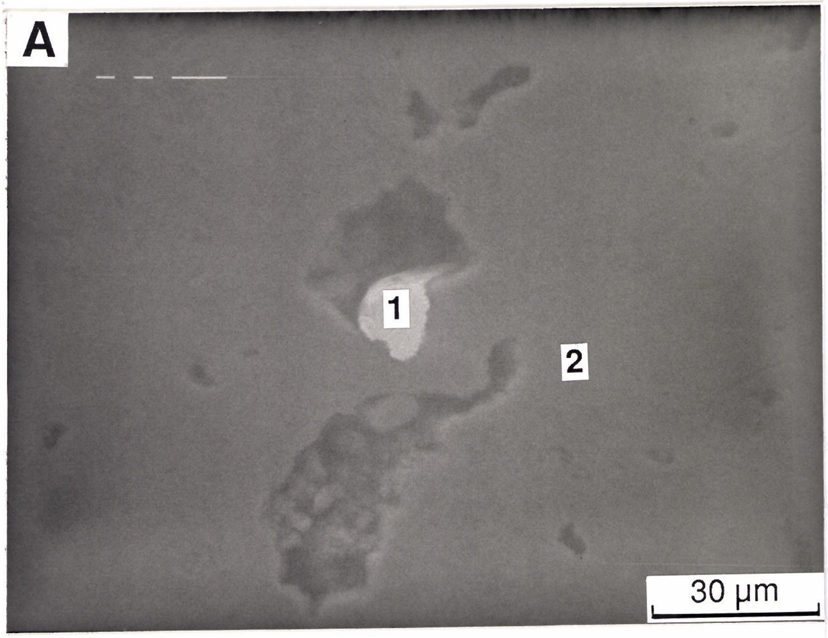

Fig. 55A. Scanning electron photomicrograph of part of a lateritic nodule showing a subhedral crystal of Au (1) in a void. Matrix of the nodule is Fe-rich which is a mixture of hematite and goethite (2). Location 9899N, 5296E North Pit Sample 07-0878.

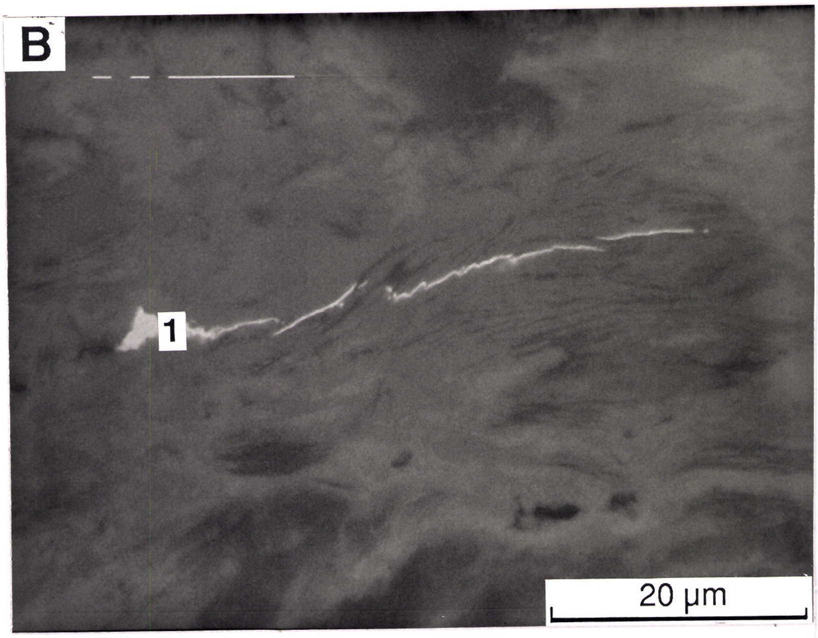

Fig. 55B. Scanning electron photomicrograph of part of a lateritic nodule showing wire shaped crystals of Au (1) attached to the goethite-rich surface, location 9899N, 5296E North Pit. Sample 07-0878.

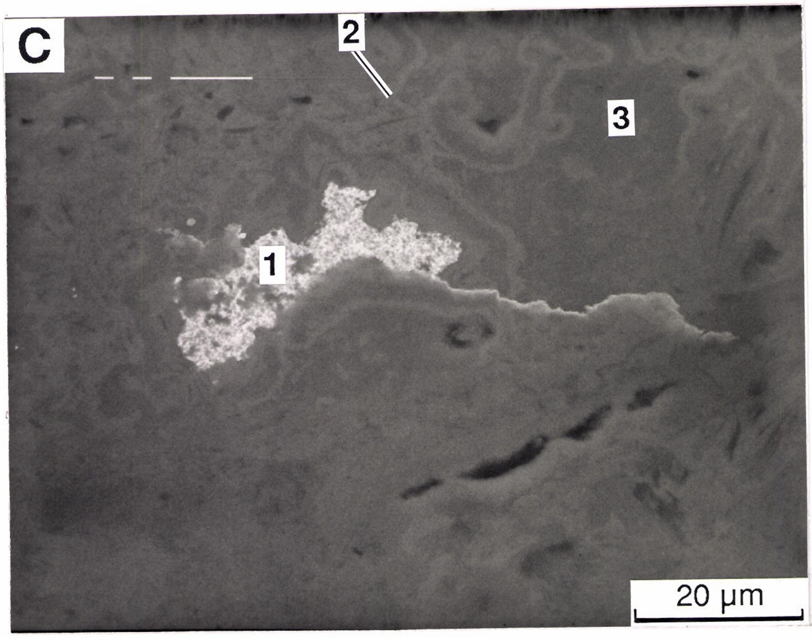

Fig. 55C. Scanning electron photomicrograph of part of a nodule showing dendritic form of Au (1) attached to the goethite-rich surface. The Au crystal shows dissolution features. Light areas of matrix are Fe-rich (2), dark areas are Al-Si rich (3), location 9899N 5296E North Pit. Sample 07-0878.

in solution, the ions need appropriate ligands as well as suitable pH and Eh conditions. Possible ligand donor ions are OH^-, I^-, Br^-, Cl^-, SO_3^{2-}, $S_2O_3^{2-}$, and SO_4^{2-} (Boyle, 1979), but few of these anions occur in percolating solutions under semi-arid conditions. In the semi-arid environment of Western Australia, Au is thought to have been remobilized and precipitated during saline groundwater conditions and reprecipitated by supergene processes (Mann, 1984; Gray, 1988). Processes operating during the formation of the lateritic nodules could also have contributed to the dissolution of Au particles. For example, the epigenetic replacement of kaolinite by hematite in the ferruginous zone involves the dissolution of kaolinite and the release of protons which may contribute to the dissolution of Au particles (Colin *et al.*, 1989).

8.2.2 OTHER ELEMENTS

Arsenic was found to range from 900 to 4400 ppm in lateritic nodules and was strongly associated with goethite/hematite. Kaolinite-rich areas of nodules generally contained only small amounts of As (50-120 ppm). The distribution of Cu (100 to 1500 ppm) within nodules was erratic and tends to be present in the kaolinite-rich areas. The surface adsorption of Cu by kaolinites has been observed by McBride (1978) and McLaren and Crawford (1973). They give 120 ppm for kaolinite as the maximum Cu adsorption calculated with Langmuir equations at pH 5.5. The much higher values found in Lawlers kaolinites permit us to assume that Cu is mainly in the kaolinite lattice and not adsorbed on its surface. This means that the metal is not likely to be released by partial or weak extraction techniques. Bismuth and Sb were below the detection limit ($\approx$40 ppm) of the microprobe techniques used.

8.3 Turrett Pit

The morphology of Au and siting and bonding of elements were also investigated on laterite samples from the Turrett area. The residual laterite in three holes (T271A, T274, T327) generally passes downwards into ferruginous-saprolite/collapsed saprolite. The pisoliths/nodules are dark reddish brown/black to red, rounded to subrounded, with a size-range of 3-15 mm. The cutans are greenish and are less than 1 mm thick. The saprolite and lateritic residuum are dominated by goethite and talc. Kaolinite and hematite are either absent or present in very small amounts. These samples contain high concentrations of Cr (to 1.4%), Ni (to 6900 ppm), and Mg (to 10%). The mineralogy and geochemistry indicate that these three weathering profiles are ultramafic in origin.

8.3.1 MORPHOLOGY AND COMPOSITION OF GOLD

Gold ranges in values from 0.005 to 8.0 ppm for whole samples studied, however, visible Au was not detected under SEM and optical microscopy.

8.3.2 OTHER ELEMENTS

Preliminary results on lateritic pisoliths show Ba occurring as laths of barite in their cutans (Fig. 56). The dark areas of cutans shown in Fig. 56 are Al and Si rich, whereas the light areas are Fe rich. The cores of pisoliths are Fe-rich with some Cr and Mn. One possible explanation is that Ba occurs as secondary barite formed by the precipitation of evaporite-derived sulphate in groundwaters.

Investigation of a barite-containing pisolith shows that Cr mainly occurs as chromite in the Fe-rich core (Fig. 56). The core of this pisolith apparently formed from saprolite preserving a primary chromite grain which provides an indication of ultramafic lithology underneath. Arsenic, V, and Mn appear to be strongly associated with goethite and do not occur as discrete mineral species.

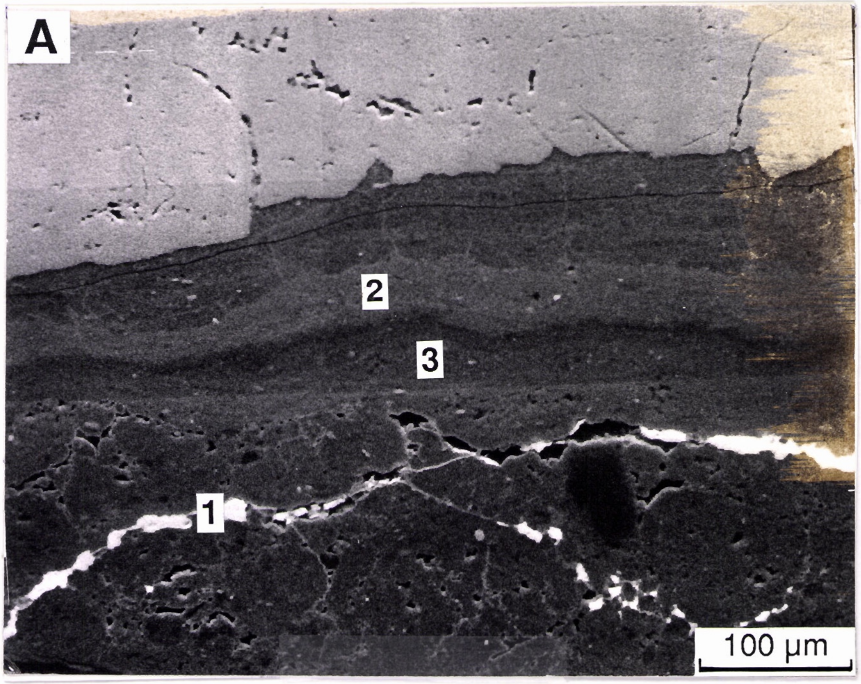

Fig. 56A. Scanning electron photomicrograph of part of a lateritic pisolith showing barite grains (1) in cracks of cutans. Alternative light (2) and dark areas (3) in cutans are caused by variation in Fe, Al/Si contents. Light areas are Fe-rich, dark areas are Al-Si rich. Location Turret area, hole No. T271A. Sample 07-1295.

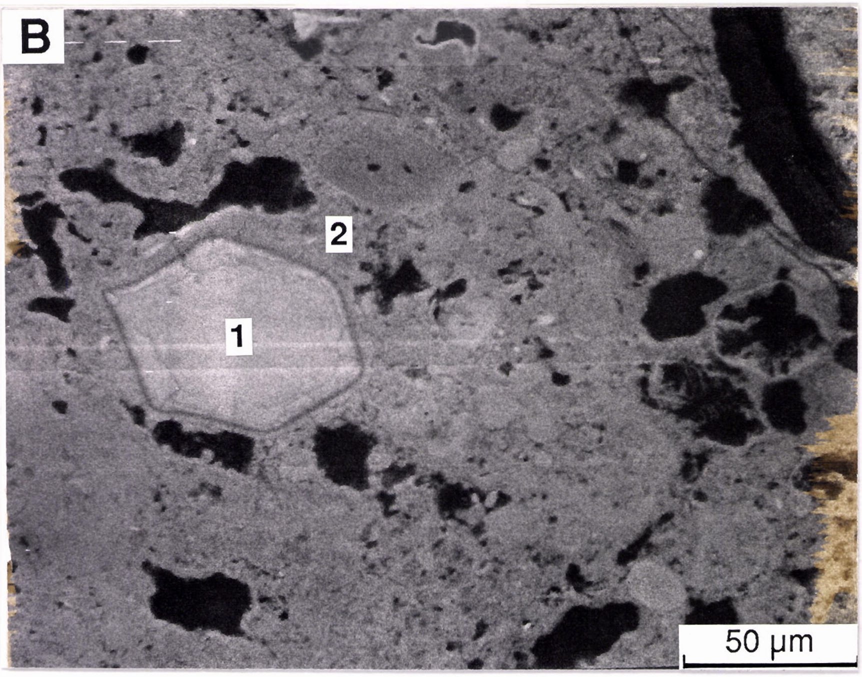

Fig. 56B. Scanning electron photomicrograph of part of a lateritic pisolith showing a hexagonal chromite grain (1) in an Fe-rich core (2). Black areas are voids, location Turret area, hole No. T271A. Sample 07-1295.

9.0 OUTLOOK

Research into exploration methods for concealed mineral deposits in the Lawlers district is likely to continue for some time because of the attributes of the district and the research knowledge base established to date during the course of the Laterite Geochemistry Project, P240. Some of the research underway is part of P240 or its extension P240A.

The following lists research that is either current or about to commence:

- Laterite geochemistry in the Lawlers district: systematically collected surface samples over the district; and orientation geochemistry about the McCaffery deposit. Research is collaborative with Forsayth and Geochemex and will be reported as part of project P240.

- Use of remote sensing for regolith mapping at Lawlers. This research is the result of collaboration with the CSIRO WA Remote Sensing Group. A report, when written, will be issued to P240 and P243.

- Research into the merging of data sets, involving collaboration between the CSIRO Division of Mathematics and Statistics, WA Remote Sensing and the Laterite Geochemistry Group, will be underway during late 1991. That research will be reported to sponsors of P240A.

- Research into geophysical methods for delineating regolith stratigraphy, particularly in areas of buried, partly complete, partly truncated laterite profiles is underway with Mr V.C. Wilson of Curtin University. During 1991 Mr Greg Cant is carrying out his Honours thesis on this topic at Lawlers, in part focussing on the colluvial plains W of the Turrett deposit. This research is neither part of P240 nor P240A.

10.0 CONCLUSIONS

- The regolith and landforms of the Lawlers district are related to the complex geomorphic history, including deep lateritic weathering and subsequent erosion and deposition. In such lateritic terrain, it is useful to consider the regolith-landform relationships of the surficial geology in terms of residual, erosional, and depositional regimes.

- At Lawlers, dismantling of the upper part of weathering profile, including lateritic residuum and ferruginous saprolite from the upland areas, has resulted in the burial of partly-truncated and/or complete laterite profiles in the lower slope areas. It is established that extensive areas in depositional regimes are underlain by complete or near complete lateritic weathering profiles.

- Four categories of sample media, namely lateritic residuum, ferruginous saprolite, iron segregations and colluvium, are shown to have different petrological, mineralogical, and geochemical characteristics. In the present study, a major distinction is clearly evident between the iron segregations and the three other horizons of the weathering profile. Iron, Mn, Zn, Co, Ba, and goethite can be used as indicator elements in order to discriminate iron segregations from lateritic residuum, ferruginous saprolite, and colluvium.

- Elevated levels of Au, As, Cu, Sb, and Bi characterize the geochemical anomalies in the lateritic residuum and ferruginous saprolite at North and Turrett Pits. Of the two sample media, the ferruginous saprolite is the less weathered and most representative of the mineralization. However, the geometry of dispersion patterns has not yet been established. In contrast, gravelly colluvium is less interesting because of its lateral transport far from the source and the high dilution of Fe-oxides by quartz. The iron segregations and the lag derived therefrom have considerable potential as sample media in partly-truncated areas of the Lawlers district in lieu of lateritic residuum and ferruginous saprolite.

- The application of canonical variate analysis and all possible subset investigations has indicated that effective separation of the four sample categories (lateritic residuum, ferruginous saprolite, iron segregations, and colluvium) exists. A combination of 14 elements (Fe, Mn, Cr, V, Pb, Zn, Ni, Co, As, Sb, Bi, W, Zr, Nb) would seem to be most useful for separation of the groups.

- At Lawlers, development of many of the lateritic nodules is associated with fragmentation of ferruginous saprolite. Ferruginous saprolite appears to form a blanket deposit in the upper saprolite over mafic and ultramafic lithologies and is typically absent over felsic or sedimentary sequences.

- Criteria have been summarized that allow residual regolith to be distinguished from transported regolith, applicable to drill hole logging.

- The nature and origin of lag gravels and soils are related to regolith substrate and processes of erosion and deposition.

- Existing evidence suggests that the Fe-rich duricrusts from various locations in the Lawlers district are probably formed by absolute accumulation of Fe originally impregnating the soils/sediments in previously low lying areas. Their present high landscape position could result from inversion of relief.

- The degree of Al substitution in goethite can be used to predict the weathering status of regolith materials and the environments in which they have formed. Aluminium substitution appears to be a parameter that can allow identification/characterization of sample type.

- Idealized regolith-landform models for the Lawlers area have been established to predict regolith relationships in comparable areas elsewhere.

- Hardpan has developed in both *in situ* regolith and depositional units which have resulted from the erosional modification of the old surface.

- Establishing knowledge of regolith relationships within the Lawlers district has provided a framework of understanding for geochemical sampling at Lawlers and in other districts of similar types of terrain.

- Preliminary investigation of the morphology of Au from anomalous laterite samples in the North Pit area suggests that it is mainly secondary, having been mobilized and precipitated during weathering. Arsenic appears to be strongly associated with goethite and Cu with kaolinite.

11.0 ACKNOWLEDGEMENTS

We wish to thank the Management and Staff of Forsayth (Lawlers) and Geochemex Australia for their co-operation and collaboration, as well as the hospitality provided by Forsayth in the field. This research has been carried out under the Lawlers collaborative research agreement between CSIRO and Geochemex, sponsored by Forsayth NL as an adjunct to research activities of the CSIRO/AMIRA Laterite Geochemistry Project P240.

Sample preparation was carried out by Ms Angela Janes under supervision by Mr John Crabb. The XRD analyses were performed by Mr M.K.W. Hart. Polished sections were prepared by Mr A.G. Bowyer. Assistance on the SEM and Cameca microprobe was given by Mr B.W. Robinson and G. Burkhalter.

Mr John Perdrix and Mr J Wildman assisted with checking the final document. Typing to the tight deadline was admirably carried out by Ms Jenny Porter. Diagrams were drafted by Mr Colin Steel and Mr Angelo Vartesi. Thanks also go to Dr Bob Gilkes and Mr Bob Gozzard who provided critical comment on the manuscript

12.0 REFERENCES

Ambrosi, J.P., Nahon, D. and Herbillon, A.J., 1986. A study of the epigenetic replacement of kaolinite by hematite in laterite-petrographical evidences and discussion on the mechanism involved. *Geoderma*, **37**, 283-294.

Amor, S.D. and Nichol, I., 1983. Identification of diagnostic geochemical alteration in the Wall-rocks of Archean volcanic-exhalative massive deposits. *J. Geochem. Explor.*, **19**, 543-562.

Anand, R.R. and Gilkes, R.J., 1987. Variations in the properties of iron oxides within individual specimens of lateritic duricrust. *Aust. J. Soil Res.*, **25**, 287-302.

Anand, R.R., Innes, J. and Smith, R.E., April 1989. Research into laterite geochemistry Lawlers District, Western Australia. Progress report to Geochemex Australia and Forsayth Mining Ltd. CSIRO Division of Exploration Geoscience Restricted Report 22R, 42pp.

Anand, R.R., Smith, R.E., Innes, J., Churchward, H.M., Perdrix, J.L. and Grunsky, E.C., August 1989. Laterite types and associated ferruginous materials, Yilgarn Block, W.A. *Terminology, Classification and Atlas*. CSIRO Division of Exploration Geoscience Restricted Report 60R (unpaginated).

Andrew, R.L., 1984. The geochemistry of selected base-metal gossans, Southern Africa. *J. Geochem. Explor.*, **22**, 161-192.

Andrew, R.L., 1980. Supergene alteration and gossan textures of base-metal ores in Southern Africa. *Miner. Sci. Eng.*, **12**, 193-215.

Blain, C.F. and Andrew, R.L., 1977. Sulphide weathering and the evaluation of gossans in mineral exploration. *Miner. Sci. Eng.* **9**, 119-150.

Boyle, R.W., 1979. The geochemistry of gold and its deposits. *Geol. Surv. Can. Bull.* **280**, 584pp.

Butler, I.K., Ewers, A., Birrell, R. and Smith, R.E., 1989. *Results of a landform survey and geochemical exploration programme, Lawlers Area, Western Australia.* Progress report of Geochemex Australia to Forsayth Mining Ltd, February 1989, 66pp.

Campbell, N.A., 1980. Robust procedures in multivariate analysis. 1: Robust covariance estimation. *Appl. Statist.*, **29**, 5-14.

Cantinolle, P., Didier, P., Meunier, J.D., Parron, C., Geundon, J.L., Bocquier, G. and Nahon, D., 1983. Kaolinites ferrifères et oxy-hydroxides de fer et d'alumine dans les bauxites des Canonnettes, S.E. de la France. *Clay Min.*, **19**, 125-135.

Carver, R.N., Chenworth, L.M., Mazzucchelli, R.M., Oates, C.J. and Robins, T.W., 1987. Lag-A geochemical sampling medium for arid regions. *J. Geochem. Explor.*, **28**, 183-189.

Churchward, H.M., 1976. *Landforms, regoliths and soils of the sandstone - Mt. Keith Area, Western Australia*. CSIRO, Division of Land Resources Management, Land Resources Management Series No.2, 22pp.

Clausen, F.L. and Harpoth, O., 1983. On the use of discriminant analysis techniques for classifying chemical data from panned heavy mineral concentrates - Central East Greenland. *J. Geochem. Explor.*, **18**, 1-24.

Colin, R., Lecomte, P. and Boulanges, B., 1989. Dissolution features of gold particles in a lateritic profile at Dondo Mobi, Gabon. *Geoderma*, **45**, 241-250.

Davy, R. and El-Ansary, M., 1986. Geochemical patterns in the laterite profile at the Boddington gold deposit, Western Australia. *J. Geochem. Explor.*, **26**, 119-144.

Didier, P., 1983. Activity of water as a chemical controlling factor in ferricretes. A thermodynamic model in the system: Kaolinite Fe-Al-oxyhydroxides. *Proc. Int. Colloq. Petrol. Weathering Soils,* 1983, pp.35-44.

Dixon, W.J., 1985. *BMDP statistical software manual.* 1985 printing. University of California Press, Berkeley, CA, 734pp.

Eisenlohr, B., 1989. *The structural development and control on mineralization of the northern sector of the Norseman-Wiluna Belt, Western Australia.* MERIWA Report No.47, pp.189.

Fitzpatrick, R.W., 1988. Iron compounds as indicators of pedogenic processes: Examples from the Southern Hemisphere. In: J.W. Stucki, B.A. Goodman and U. Schwertmann (Eds.), *Iron in Soils and Clay Minerals*, D. Reidel Publishing Company, pp.351-396.

Fitzpatrick, R.W. and Schwertmann, U., 1982. Al-substituted goethite - an indicator of pedogenic and other weathering environments in South Africa. *Geoderma*, **27**, 335-47.

Freyssinet, Ph. and Butt, C.R.M., 1988a. *Morphology and geochemistry of gold in a lateritic profile Beasley Creek, Laverton, Western Australia.* Report to Western Mining Corporation. CSIRO Division of Exploration Geoscience Report MG60R.

Freyssinet, Ph. and Butt, C.R.M., 1988b. *Morphology and geochemistry of gold in a lateritic profile Bardoc Mine, Western Australia.* Report to Aberfoyle Resources Ltd. CSIRO Division of Exploration Geoscience Report MG59R.

Gentilli, J., 1971. *Australian climatic patterns.* Nelson, Melbourne.

Goudie, A., 1973. *Duricrust in tropical and sub-tropical landscapes.* Oxford Research Studies in Geography, Oxford University Press, London, 174pp.

Gray, D.G., 1988. *The aqueous chemistry of gold in the weathering environment.* CSIRO Division of Exploration Geoscience Restricted Report EG4R, 65pp.

Howarth, R.J. and Earle, S.A.M., 1979. Application of a generalized power transformation to geochemical data, *Math. Geol.*, **11**, 45-62.

Hsu, P.D., 1979. Aluminium hydroxides and oxyhydroxides. In: J.B. Dixon and S.B. Weed (Eds.), *Minerals in Soil Environments.* Soil Sci. Soc. Am., Madison, Wisc. 2nd Ed., pp.99-143.

Jutson, J.T., 1950. The physiography (geomorphology) of Western Australia. *Geol. Surv. West. Aust. Bull.*, **95**, (3rd Ed.), 366pp.

Mabbutt, J.A., 1977. *Desert Landforms*, Vol.2, Australian Nat. Uni. Press, Canberra, 340pp.

Maignien, R., 1966. *Review of research on laterites*, UNESCO Natural Resources Research Sc., IV., Paris, 148pp.

Mann, A.W., 1984. Mobility of gold and silver in lateritic weathering profile: some observations from Western Australia. *Econ. Geol.*, **79**, 38-49.

Maud, R.R., 1972. *Geology, geomorphology and soils of central country Hindmarsh (Mount Compass-Milang) South Australia.* Soil publication No.29, CSIRO, Melbourne, Australia, 85pp.

McBride, M.B., 1978. Copper (II) interaction with kaolinite: factors controlling adsorption. *Clays Clay Miner.*, **26**, 101-106.

McLaren, R.B. and Crawford, D.W., 1973. Studies on soil copper. II. The specific adsorption of copper by soils, *J. Soil Sci.*, **24**, 352-443.

Milnes, A.R., Bourman, R.P. and Northcote, K.M., 1985. Field relationships of ferricretes and weathered zones in southern South Australia: A contribution to "laterite" studies in Australia. Aust. *J. Soil Res.*, **23**, 441-465.

Nahon, D.B. and Colin, R., 1982. Chemical weathering of orthopyroxenes under a lateritic condition. *Amer. J. Sci.*, **282**, 1232-1243.

Nesbitt, R.W., 1971. Skeletal crystal forms in the ultramafic rocks of the Yilgarn Block, Western Australia: evidence for an Archaean Ultramafic liquid. In: J.E. Glover (Ed.), *Symposium on Archaean rocks held at Perth*. Geol. Soc. Aust. Spec. Publ, 3, 331-347.

Nickel, E.H., 1984. The mineralogy and geochemistry of the weathering profile of the Teutonic Bore Cu-Pb-Zn-Ag sulphide deposit. *J. Geochem. Explor.*, **22**, 239-264.

Ollier, C.D., Chan, R.A., Craig, M.A. and Gibson, D.L., 1988. Aspects of landscape history and regolith in the Kalgoorlie region, Western Australia. *BMR J. Aust. Geol. and Geophys.*, 10, 309-321.

Partington, G.A., 1986. *The geological and structural relationships of the gold deposits in the Lawlers District, Western Australia.* Report to Forsayth, 28pp.

Platt, J.P., Allchurch, P.D. and Rutland, R.W.R. 1978. Archaean tectonics in the Agnew supracrustal belt, Western Australia. *Precambrian Res.*, **7**, 3-30

Roquin, C., Freyssinet, Ph., Zeegers, H. and Tardy, Y., 1990. Element distribution patterns in laterites of southern Mali: consequence for geochemical prospecting and mineral exploration. *Applied Geochem.*, **5**, 303-315.

Schulze, D.G., 1984. The influence of aluminium on iron oxides. VIII. Unit cell dimensions of Al-substituted goethites and estimation of Al from them. *Clays Clay Miner.*, **32**, 36-44.

Schwertmann, U., 1985. The effect of pedogenic environments on iron oxide minerals. In: B.A. Stewart (Ed.), *Advances in Soil Science*, Vol.1, Springer-Verlag, New York, NY, pp.172-196.

Schwertmann, U. and Fechter, H., 1984. The influence of aluminium on iron oxides. XI Aluminium-substituted maghemite in soils and its formation. *Soil Sci. Soc. Am. J.*, **48**, 1462-1463.

Schwertmann, U. and Latham, M., 1986. Properties of iron oxides in some new Caledonian oxisols. *Geoderma*, **39**, 105-123.

Schwertmann, U., Fitzpatrick, R.W., Taylor, R.M. and Lewis, D.G., 1979. The influence of aluminium on iron oxides. Part II. Preparation and properties of Al-substituted hematites. *Clays Clay Miner.*, **27**, 105-112.

Smith, R.E., 1987. *Patterns in laterite geochemistry Mt. Gibson, Western Australia.* Progress report of Geochemex Australia to Forsayth NL, December, 37pp.

Smith, R.E., Campbell, N.A. and Litchfield, R., 1984. Multivariate statistical techniques applied to pisolitic laterite geochemistry at Golden Grove, Western Australia. *J. Geochem. Explor.*, **22**, 193-216.

Taylor, R.M. and Schwertmann, U., 1974. Maghemite in soils and its origins. I. Properties and observations in soil maghemites. *Clay Miner.*, **10**, 289-98.

Taylor, G.F. and Scott, K.M., 1982. Evaluation of gossans in relation to lead-zinc mineralisation in the Mount Isa Inlier, Queensland. *BMR J. Aust. Geol. Geophys.*, **7**, 159-180.

Zeegers, H., Goni, J. and Wilhelm, E., 1981. Geochemistry of lateritic profiles over a disseminated Cu-Mo mineralization in Upper Volta (West Africa) - preliminary results. In: M.K. Roychowdhury, B.P., Radhakrishna, R. Vaidyanadhan, P.K. Banerjee and K. Ranganathan (Eds), *Lateritisation Processes*, A.A. Balkema, Rotterdam, pp.359-368.

Appendix I

Mineral Composition of Lawlers Samples.

Sample Number	Sample Type	Box field	Map Reference	AMG Coordinates Easting	AMG Coordinates Northing	Kaolinite	Goethite	Hematite	Goethite / Goethite + Hematite	Maghemite	Total Iron Oxides	Quartz	Mole % Al in Goethite
07-0813	CV305	CV	SH-51-01	259619	6896850	25	20	14	0.59	10	44	32	14
07-0833	CV305	CV	SH-51-01	259942	6896837	25	15	30	0.33	5	50	25	14
07-0835	CV333	CV	SH-51-01	259942	6896837	25	20	35	0.36	10	65	6	12
07-0847	CV305HP	CV	SH-51-01	259895	6897118	25	22	10	0.69	7	39	40	8
07-0854	CV305	CV	SH-51-01	259840	6897244	25	20	10	0.67	5	35	40	12
07-0856	CV101HP	CV	SH-51-01	259840	6897244	42	14	6	0.70	0	20	34	11
07-0857	CV101HP	CV	SH-51-01	259840	6897244	48	8	7	0.53	0	15	30	8
07-0858	CV101	CV	SH-51-01	259840	6897244	70	10	8	0.56	0	18	8	8
07-0863	CV305	CV	SH-51-01	259561	6896988	25	20	36	0.36	10	66	5	16
07-0867	CV334HP	CV	SH-51-01	259561	6896988	45	12	18	0.40	5	35	20	10
07-0871	CV334HP	CV	SH-51-01	259561	6896988	45	28	12	0.70	0	40	15	6
07-0873	CV333	CV	SH-51-01	259561	6896988	44	20	25	0.44	3	48	5	11
07-0888	CV305	CV	SH-51-01	259605	6897055	20	20	15	0.57	10	45	32	12
07-0891	CV104HP	CV	SH-51-01	259605	6897055	25	32	18	0.64	0	50	2	10
07-0898	CV334HP	CV	SH-51-01	259425	6897058	32	30	20	0.60	3	53	12	9
07-0905	CV334HP	CV	SH-51-01	259343	6897115	45	24	12	0.67	5	41	12	8
07-1284	CV334	CV	SH-51-01	258300	6898825	25	22	15	0.59	5	42	25	6
07-1285	CV333	CV	SH-51-01	258300	6898825	38	20	32	0.38	5	57	5	8
07-1293	CV334	CV	SH-51-01	258312	6898850	30	25	10	0.71	5	40	30	11

Appendix I **Mineral Composition of Lawlers Samples.**

Sample Number	Sample Type	Box field	Map Reference	AMG Coordinates Easting	AMG Coordinates Northing	Kaolinite	Goethite	Hematite	Goethite / Goethite + Hematite	Maghemite	Total Iron Oxides	Quartz	Mole % Al in Goethite
07-0816	LT102	LT	SH-51-01	259619	6896850	25	20	25	0.44	15	60	15	20
07-0818	LT104	LT	SH-51-01	259619	6896850	32	25	20	0.56	10	55	10	18
07-0844	LT102	LT	SH-51-01	259715	6896861	32	12	22	0.35	12	46	12	22
07-0851	LT104	LT	SH-51-01	259895	6897118	22	15	35	0.3	15	65	5	16
07-0859	LT104	LT	SH-51-01	259840	6897244	20	15	15	0.5	10	40	30	12
07-0874	LT102	LT	SH-51-01	259561	6896988	40	10	25	0.29	10	45	10	15
07-0875	LT102	LT	SH-51-01	259561	6896988	38	15	20	0.43	15	50	5	18
07-0877	LT204	LT	SH-51-01	259561	6896988	38	30	30	0.5	0	60	2	16
07-0878	LT204	LT	SH-51-01	259561	6896988	32	36	28	0.56	0	64	5	20
07-0879	LT204	LT	SH-51-01	259561	6896988	32	30	28	0.52	0	58	10	22
07-0880	LT204	LT	SH-51-01	259561	6896988	42	38	14	0.73	0	52	5	15
07-0881	LT104	LT	SH-51-01	259561	6896988	43	28	8	0.78	0	36	15	18
07-0882	LT104	LT	SH-51-01	259561	6896988	24	32	18	0.64	0	50	20	20
07-0899	LT104	LT	SH-51-01	259425	6897058	40	35	17	0.67	0	52	5	12
07-0919	LT204	LT	SH-51-01	256100	6899200	32	15	25	0.38	15	55	8	22
07-0920	LT102	LT	SH-51-01	256100	6899150	34	18	20	0.47	14	52	10	26
07-0924	LT204	LT	SH-51-01	256100	6899100	28	20	25	0.44	15	60	5	18
07-1176	LT104	LT	SH-51-01	259551	6896872	3	65	15	0.81	0	80	10	14
07-1271	LT204	LT	SH-51-01	259619	6896839	22	20	25	0.44	15	60	15	19
07-1272	LT204HP	LT	SH-51-01	259619	6896839	26	15	25	0.38	15	55	15	14
07-1275	LT102	LT	SH-51-01	258310	6898800	30	35	18	0.66	0	53	5	19
07-1277	LT204	LT	SH-51-01	258310	6898800	20	45	20	0.69	5	70	6	22
07-1287	LT102	LT	SH-51-01	258300	6898825	25	45	20	0.69	0	65	5	16
07-1288	LT204	LT	SH-51-01	258300	6898825	28	46	12	0.79	0	58	5	20
07-1295	LT102	LT	SH-51-01	258312	6898850	30	20	20	0.5	20	60	5	16
07-1315	LG100	LT	SH-51-01	272700	6891600	10	19	40	0.32	16	75	2	12
07-1345	LG100	LT	SH-51-01	273000	6892000	10	24	56	0.3	0	80	3	6
07-1357	LG100	LT	SH-51-01	271600	6892000	5	35	26	0.57	14	75	3	12
07-1363	LG100	LT	SH-51-01	272850	6891800	4	20	50	0.29	12	82	2	6
07-1364	LG100	LT	SH-51-01	272750	6891800	2	25	52	0.32	8	85	3	8
07-1392	LT204	LT	SH-51-01	260200	6900970	10	34	28	0.55	12	74	3	22
07-1394	LG100	LT	SH-51-01	260100	6900950	12	10	54	0.16	16	80	2	28
07-1395	LG100	LT	SH-51-01	260000	6900700	10	10	50	0.17	19	79	4	27
07-1396	LG100	LT	SH-51-01	259000	6900600	10	15	40	0.27	20	75	3	15
07-1397	LG100	LT	SH-51-01	258950	6900200	22	48	15	0.76	0	63	5	17
07-1398	LG100	LT	SH-51-01	258800	6900000	16	45	16	0.74	6	67	5	16

Appendix I **Mineral Composition of Lawlers Samples.**

Sample Number	Sample Type	Box field	Map Reference	AMG Coordinates Easting	AMG Coordinates Northing	Kaolinite	Goethite	Hematite	Goethite / Goethite + Hematite	Maghemite	Total Iron Oxides	Quartz	Mole % Al in Goethite
07-0817	IS101	IS	SH-51-01	259619	6896850	10	68	12	0.85	0	80	8	2
07-0820	IS100-gos	IS	SH-51-01	259619	6896850	0	60	25	0.71	0	85	12	4
07-0821	LG206	IS	SH-51-01	259619	6896850	2	58	22	0.73	0	80	15	4
07-0823	IS100-gos	IS	SH-51-01	259153	6897157	2	68	18	0.79	0	86	8	3
07-0923	IS100	IS	SH-51-01	256000	6899300	4	80	5	0.94	0	85	6	4
07-1164	IS102-gos	IS	SH-51-01	259528	6896853	8	64	15	0.81	0	79	8	7
07-1173	IS103	IS	SH-51-01	259508	6896810	12	55	25	0.69	0	80	5	10
07-1177	IS101-gos	IS	SH-51-01	259551	6896872	10	68	12	0.85	0	80	5	7
07-1178	IS100	IS	SH-51-01	259551	6896872	18	30	30	0.50	0	60	18	6
07-1179	IS100-gos	IS	SH-51-01	259700	6896775	5	55	25	0.69	0	80	10	4
07-1181	IS100-gos	IS	SH-51-01	259706	6896679	5	42	38	0.53	0	80	10	4
07-1182	IS100-gos	IS	SH-51-01	259706	6896679	2	48	14	0.77	0	62	30	5
07-1188	IS201-gos	IS	SH-51-01	259492	6896763	3	45	40	0.53	0	85	10	4
07-1189	IS201-gos	IS	SH-51-01	259500	6896769	8	70	8	0.90	0	78	8	7
07-1193	IS102-gos	IS	SH-51-01	259577	6896818	3	60	20	0.75	0	80	6	5
07-1196	IS102-gos	IS	SH-51-01	260128	6896452	12	40	30	0.57	0	70	18	5
07-1205	IS100	IS	SH-51-01	259584	6896849	0	30	0	1.00	0	30	65	0
07-1207	IS100	IS	SH-51-01	264628	6886971	0	72	12	0.86	0	84	10	3
07-1208	IS201	IS	SH-51-01	259926	6896640	2	60	14	0.81	0	74	20	5
07-1209	LG206	IS	SH-51-01	259996	6896566	2	55	15	0.79	0	70	25	5
07-1210	IS201	IS	SH-51-01	260008	6896496	2	70	18	0.80	0	88	10	6
07-1211	LG206	IS	SH-51-01	259951	6896415	2	58	27	0.68	0	85	10	3
07-1212	LG206	IS	SH-51-01	259812	6896390	4	50	28	0.64	0	78	14	4
07-1213	LG206	IS	SH-51-01	259849	6896181	0	74	14	0.84	0	88	8	5
07-1214	LG206	IS	SH-51-01	260046	6896036	0	45	15	0.75	0	60	40	3
07-1215	LG206	IS	SH-51-01	260016	6896247	2	58	20	0.74	0	78	15	4
07-1216	LG206	IS	SH-51-01	260131	6896410	3	63	20	0.76	0	83	12	0
07-1217	LG206	IS	SH-51-01	260007	6902420	2	60	25	0.71	0	85	10	5
07-1218	IS201	IS	SH-51-01	264628	6886971	0	64	18	0.78	0	82	15	4
07-1219	LG206	IS	SH-51-01	259767	6896727	2	60	25	0.71	0	85	10	0
07-1220	LG206	IS	SH-51-01	259755	6896710	4	71	15	0.83	0	86	8	4
07-1221	LG206	IS	SH-51-01	259744	6896694	2	60	26	0.70	0	86	8	5
07-1222	LG206	IS	SH-51-01	259798	6896632	2	62	25	0.71	0	87	10	4
07-1223	LG206	IS	SH-51-01	259775	6896599	3	62	18	0.78	0	80	12	5
07-1224	LG206	IS	SH-51-01	259829	6896537	0	55	30	0.65	0	85	10	4
07-1225	IS201	IS	SH-51-01	260217	6896533	12	48	32	0.60	0	80	5	5
07-1227	IS101	IS	SH-51-01	260189	6896528	5	70	12	0.85	0	82	8	3
07-1228	LG206	IS	SH-51-01	264628	6886971	0	55	35	0.61	0	90	6	3
07-1229	IS201	IS	SH-51-01	260053	6902693	2	65	20	0.76	0	85	10	5
07-1230	LG206	IS	SH-51-01	259316	6896554	0	40	45	0.47	0	85	15	5

Appendix I **Mineral Composition of Lawlers Samples.**

Sample Number	Sample Type	Box field	Map Reference	AMG Coordinates Easting	AMG Coordinates Northing	Kaolinite	Goethite	Hematite	Goethite / Goethite + Hematite	Maghemite	Total Iron Oxides	Quartz	Mole % Al in Goethite
07-1231	LG206	IS	SH-51-01	259398	6896619	2	55	30	0.65	0	85	12	4
07-1232	IS201	IS	SH-51-01	259447	6896829	8	78	5	0.94	0	83	7	6
07-1233	IS101	IS	SH-51-01	259505	6896910	6	75	5	0.94	0	80	10	5
07-1234	IS111	IS	SH-51-01	259417	6896820	5	75	10	0.88	0	85	7	4
07-1235	LG206	IS	SH-51-01	259423	6896968	2	60	25	0.71	0	85	10	4
07-1236	LG206	IS	SH-51-01	259341	6897025	0	50	30	0.63	0	80	12	0
07-1242	LG206	IS	SH-51-01	259067	6897156	0	55	30	0.65	0	85	8	4
07-1244	LG206	IS	SH-51-01	258912	6896935	0	55	25	0.69	0	80	15	5
07-1259	IS101	IS	SH-51-01	256100	6899050	5	66	8	0.89	0	74	12	4
07-1265	IS100-gos	IS	SH-51-01	259708	6896787	2	55	28	0.66	0	83	15	5
07-1310	LG206	IS	SH-51-01	273300	6891600	8	36	38	0.49	0	74	12	4
07-1343	LG206	IS	SH-51-01	273050	6892000	12	48	30	0.62	0	78	3	5

Appendix I

Mineral Composition of Lawlers Samples.

Sample Number	Sample Type	Box field	Map Reference	AMG Coordinates Easting	AMG Coordinates Northing	Kaolinite	Goethite	Hematite	Goethite / Goethite + Hematite	Maghemite	Total Iron Oxides	Quartz	Mole % Al in Goethite
07-1166	sap-f	Fe-sap	SH-51-01	259528	6896853	30	20	10	0.67	0	30	30	12
07-1170	sap-f	Fe-sap	SH-51-01	259511	6896824	32	25	15	0.63	0	40	18	11
07-1174	sap-f	Fe-sap	SH-51-01	259508	6896810	28	28	22	0.56	0	50	18	14
07-1175	sap-f	Fe-sap	SH-51-01	259551	6896872	28	22	38	0.37	0	60	12	12
07-1183	sap-f	Fe-sap	SH-51-01	259511	6896824	22	36	30	0.55	0	66	8	13
07-1195	sap-f	Fe-sap	SH-51-01	260128	6896452	32	24	16	0.60	0	40	22	8
07-1202	sap-f	Fe-sap	SH-51-01	259714	6896740	34	16	8	0.67	0	24	32	10
07-1203	sap-f	Fe-sap	SH-51-01	259643	6896811	40	34	16	0.68	0	50	5	12
07-1204	sap-f	Fe-sap	SH-51-01	259584	6896849	32	35	25	0.58	0	60	5	8
07-1266	sap-f	Fe-sap	SH-51-01	259708	6896751	41	18	7	0.72	0	25	32	13
07-1268	sap-f	Fe-sap	SH-51-01	259619	6896839	35	25	20	0.56	0	45	10	10
07-1269	sap-f	Fe-sap	SH-51-01	259619	6896839	40	22	14	0.61	0	36	12	21
07-1270	sap-f	Fe-sap	SH-51-01	259619	6896839	25	12	28	0.30	20	60	12	22
07-1279	sap-f	Fe-sap	SH-51-01	258310	6898800	20	60	5	0.92	0	65	5	16
07-1281	sap-f	Fe-sap	SH-51-01	258310	6898800	5	75	0	1.00	0	75	5	12
07-1282	sap-f	Fe-sap	SH-51-01	258310	6898800	11	42	13	0.76	0	55	6	10
07-1289	sap-f	Fe-sap	SH-51-01	258300	6898825	20	58	7	0.89	0	65	5	20
07-1296	sap-f	Fe-sap	SH-51-01	258312	6898850	48	25	5	0.83	0	30	14	18
07-1297	sap-f	Fe-sap	SH-51-01	258312	6898850	35	35	5	0.88	0	40	15	20
07-1298	sap-f	Fe-sap	SH-51-01	258312	6898850	4	60	10	0.86	0	70	16	16
07-1299	sap-f	Fe-sap	SH-51-01	258312	6898850	3	59	8	0.88	0	67	15	16

Note: Lower case terms in the Sample Type column are interim terms, i.e. not formal classification terms in Anand et al.(August 1989)

Appendix II **Chemical Composition of Lawlers Samples.**

Sample Number	Sample Type	Box field	Map Reference	AMG Coordinates Easting	AMG Coordinates Northing	SiO2 wt %	Al2O3 wt %	Fe2O3 wt %	MgO wt %	CaO wt %	Na2O wt %	K2O wt %	TiO2 wt %
07-0813	CV305	CV	SH-51-01	259619	6896850	44.60	12.00	34.75	0.118	0.107	0.094	0.47	1.176
07-0833	CV305	CV	SH-51-01	259942	6896837	37.90	12.40	42.61	0.126	0.043	0.010	0.35	1.561
07-0834	CV305HP	CV	SH-51-01	259942	6896837	35.10	15.00	40.46	0.365	0.221	0.033	0.07	1.364
07-0835	CV333	CV	SH-51-01	259942	6896837	20.70	13.50	58.47	0.151	0.118	0.016	<0.06	1.785
07-0837	CV104	CV	SH-51-01	259942	6896837	34.20	26.00	26.00	0.305	0.265	0.058	<0.06	3.236
07-0842	CV305	CV	SH-51-01	259715	6896861	41.90	13.70	35.31	0.181	0.145	0.050	0.39	1.396
07-0847	CV305HP	CV	SH-51-01	259895	6897118	49.30	12.10	31.02	0.181	0.120	0.046	0.56	1.141
07-0848	CV305HP	CV	SH-51-01	259895	6897118	44.70	17.80	26.60	0.753	1.020	0.301	0.15	1.284
07-0850	CV104	CV	SH-51-01	259895	6897118	42.40	28.20	14.58	0.266	0.207	0.045	<0.06	2.619
07-0854	CV305	CV	SH-51-01	259840	6897244	50.10	12.20	30.00	0.262	0.171	0.124	0.51	1.233
07-0856	CV101HP	CV	SH-51-01	259840	6897244	55.00	17.30	16.58	1.330	0.716	0.079	0.19	1.349
07-0857	CV101HP	CV	SH-51-01	259840	6897244	53.40	23.00	11.14	0.714	0.393	0.063	<0.06	1.935
07-0858	CV101	CV	SH-51-01	259840	6897244	41.80	29.40	13.73	0.420	0.284	0.050	<0.06	2.502
07-0863	CV305	CV	SH-51-01	259561	6896988	21.10	13.00	57.90	0.145	0.041	<0.007	0.10	1.868
07-0864	CV334HP	CV	SH-51-01	259561	6896988	33.60	15.30	42.46	0.199	0.152	0.017	0.18	1.851
07-0867	CV334HP	CV	SH-51-01	259561	6896988	39.80	20.20	29.17	0.415	0.392	0.040	0.07	2.435
07-0869	CV334HP	CV	SH-51-01	259561	6896988	43.90	21.50	22.02	0.492	0.197	0.045	0.10	1.718
07-0871	CV334HP	CV	SH-51-01	259561	6896988	37.00	20.00	32.45	0.290	0.351	0.043	0.14	1.146
07-0872	CV333	CV	SH-51-01	259561	6896988	28.40	19.90	41.75	0.264	0.357	0.043	0.07	1.156
07-0873	CV333	CV	SH-51-01	259561	6896988	23.85	22.50	41.89	0.326	0.347	0.049	0.06	1.163
07-0888	CV305	CV	SH-51-01	259605	6897055	43.20	11.40	37.46	0.137	0.067	0.026	0.47	1.258
07-0889	CV101HP	CV	SH-51-01	259605	6897055	49.50	19.00	20.44	0.652	0.421	0.098	0.08	1.643
07-0890	CV104HP	CV	SH-51-01	259605	6897055	40.00	25.20	21.87	0.265	0.220	0.041	<0.06	2.319
07-0891	CV104HP	CV	SH-51-01	259605	6897055	14.00	28.90	41.18	0.082	0.071	0.040	<0.06	1.608
07-0896	CV305	CV	SH-51-01	259425	6897058	36.00	11.70	44.46	0.118	0.066	0.037	0.39	1.314
07-0897	CV334HP	CV	SH-51-01	259425	6897058	39.30	13.80	38.89	0.290	0.238	0.068	0.20	1.343
07-0898	CV334HP	CV	SH-51-01	259425	6897058	31.70	16.70	41.03	0.203	0.249	0.077	0.07	1.194
07-0903	CV334HP	CV	SH-51-01	259343	6897115	46.30	9.56	34.31	0.767	1.030	0.229	0.20	1.186
07-0905	CV334HP	CV	SH-51-01	259343	6897115	33.90	20.30	35.74	0.223	0.237	0.061	<0.06	1.123
07-1273	CV334	CV	SH-51-01	258310	6898800	52.20	10.69	29.24	0.115	0.044	0.029	0.41	0.996
07-1284	CV334	CV	SH-51-01	258300	6898825	42.20	13.74	34.29	0.322	0.131	0.049	0.37	0.873
07-1285	CV333	CV	SH-51-01	258300	6898825	22.40	19.43	46.58	0.206	0.119	0.037	0.07	0.857
07-1293	CV334	CV	SH-51-01	258312	6898850	43.20	14.36	32.32	0.270	0.214	0.190	0.40	0.854

Appendix II **Chemical Composition of Lawlers Samples.**

Sample Number	Sample Type	Mn ppm	Cr ppm	V ppm	Cu ppm	Pb ppm	Zn ppm	Ni ppm	Co ppm	As ppm	Sb ppm	Bi ppm	Mo ppm	Ag ppm	Sn ppm	Ge ppm	Ga ppm	W ppm	Ba ppm	Zr ppm	Nb ppm	Se ppm	Be ppm	Au ppb
07-0813	CV305	270	433	775	64	14	30	30	12	26	2	<2	<1	<0.1	2	<4	32	16	323	128	10	2	2	790
07-0833	CV305	918	685	1047	50	28	42	54	28	36	4	<2	2	1.2	<2	<4	42	8	128	128	13	4	2	90
07-0834	CV305HP	642	407	1202	76	17	44	92	34	18	2	<2	2	0.5	3	<4	44	4	329	102	8	<2	2	31
07-0835	CV333	348	1367	1783	48	17	28	84	26	62	<2	<2	3	1.5	2	<4	64	<4	58	144	9	<2	2	24
07-0837	CV104	167	2367	1019	34	12	14	175	26	62	5	<2	2	0.2	4	<4	66	<4	21	93	13	<2	1	7
07-0842	CV305	756	530	968	72	19	32	44	18	52	5	<2	3	<0.1	3	<4	40	<4	336	115	10	2	1	140
07-0847	CV305HP	1534	554	754	60	19	44	54	26	28	3	<2	2	0.3	3	4	32	14	459	118	12	3	1	140
07-0848	CV305HP	474	302	814	92	4	28	58	22	13	7	<2	<1	0.2	<2	4	38	4	96	72	10	<2	1	140
07-0850	CV104	189	1516	531	40	9	6	390	24	24	5	<2	2	<0.1	3	<4	48	8	22	82	13	<2	1	12
07-0854	CV305	911	572	728	60	19	66	66	32	26	7	2	2	0.5	<2	<4	32	6	385	123	11	<2	1	62
07-0856	CV101HP	238	331	562	60	2	20	90	20	11	<2	<2	<1	0.1	3	<4	42	4	105	99	11	3	1	21
07-0857	CV101HP	173	412	417	52	7	15	110	18	7	4	<2	3	<0.1	6	<4	44	<4	31	85	14	<2	1	28
07-0858	CV101	100	2610	456	44	7	7	910	50	30	3	<2	1	0.5	5	<4	42	12	23	77	13	<2	1	18
07-0863	CV305	1103	635	1646	84	24	46	56	26	44	5	2	3	0.8	<2	<4	54	8	95	125	11	4	2	160
07-0864	CV334HP	595	558	1565	60	28	22	62	18	34	7	<2	2	<0.1	<2	<4	52	6	894	120	9	4	2	107
07-0867	CV334HP	226	426	1024	56	10	16	58	18	40	<2	<2	1	<0.1	<2	<4	52	16	71	101	12	<2	1	90
07-0869	CV334HP	173	356	697	46	4	12	40	10	52	<2	<2	1	<0.1	3	<4	44	16	66	95	10	<2	1	55
07-0871	CV334HP	288	454	730	74	11	20	56	14	110	6	<2	1	<0.1	<2	<4	42	22	110	108	9	3	1	44
07-0872	CV333	180	475	834	52	12	12	46	10	155	4	<2	<1	<0.1	2	<4	52	32	105	122	8	<2	1	150
07-0873	CV333	167	509	826	66	13	15	52	6	200	6	<2	<1	0.6	<2	<4	48	40	136	124	9	<2	2	150
07-0888	CV305	635	819	936	62	30	60	130	20	86	2	<2	3	0.1	4	<4	30	6	168	114	8	2	2	66
07-0889	CV101HP	204	308	781	50	4	5	62	18	20	3	<2	<1	1.0	<2	4	44	12	90	102	12	<2	1	99
07-0890	CV104HP	211	480	749	48	10	3	82	16	52	5	2	3	0.2	3	<4	50	14	41	93	10	<2	1	33
07-0891	CV104HP	189	1361	747	40	17	3	120	20	260	4	<2	2	0.7	6	<4	50	52	13	162	8	<2	<1	0
07-0896	CV305	530	717	1165	74	19	64	46	24	78	<2	<2	2	0.9	<2	<4	30	8	180	128	11	<2	1	24
07-0897	CV334HP	384	559	1333	50	17	18	54	30	48	6	<2	2	0.8	<2	<4	44	14	194	109	12	<2	1	1020
07-0898	CV334HP	162	535	954	96	10	3	44	14	640	5	<2	2	0.5	<2	<4	52	56	75	157	9	<2	1	47
07-0903	CV334HP	2188	349	934	72	12	42	78	58	28	6	<2	<1	0.5	2	<4	32	8	723	85	9	2	2	68
07-0905	CV334HP	96	513	1113	80	12	<2	40	16	98	4	<2	1	0.5	<2	<4	50	12	43	110	8	<2	1	340
07-1273	CV334	370	2660	573	64	16	82	94	15	46	4	10	1	<0.1	7	<2	20	4	140	106	6	<2	1	5
07-1284	CV334	1090	6610	586	62	26	145	410	38	78	10	3	0	<0.1	<2	3	22	4	337	125	11	<2	1	64
07-1285	CV333	253	12200	643	65	20	80	810	50	190	17	<2	3	<0.1	<2	<2	36	10	93	79	7	2	1	72
07-1293	CV334	477	5950	537	52	22	72	290	24	46	11	<2	2	0.2	3	2	24	4	494	139	9	<2	1	23

Appendix II

Chemical Composition of Lawlers Samples.

Sample Number	Sample Type	Box field	Map Reference	AMG Coordinates		SiO2	Al2O3	Fe2O3	MgO	CaO	Na2O	K2O	TiO2
				Easting	Northing	wt %	wt %	wt %	wt %	wt %	wt %	wt %	wt %
07-0814	LT102	LT	SH-51-01	259619	6896850	23.50	13.70	54.60	0.072	0.040	0.020	0.21	1.449
07-0815	LT204	LT	SH-51-01	259619	6896850	28.40	14.20	47.89	0.127	0.105	0.017	0.09	0.972
07-0816	LT102	LT	SH-51-01	259619	6896850	26.50	12.90	52.04	0.115	0.124	0.128	0.25	1.131
07-0818	LT104	LT	SH-51-01	259619	6896850	25.50	15.50	48.04	0.127	0.089	0.014	0.07	1.184
07-0839	LT204	LT	SH-51-01	259942	6896837	4.50	5.04	79.40	0.190	0.053	<0.007	<0.06	3.770
07-0843	LT102	LT	SH-51-01	259715	6896861	34.30	15.90	41.46	0.183	0.150	0.024	0.20	1.570
07-0844	LT102	LT	SH-51-01	259715	6896861	29.00	20.40	40.89	0.204	0.203	0.023	<0.06	1.124
07-0851	LT104	LT	SH-51-01	259895	6897118	15.50	12.80	59.76	0.294	0.109	<0.007	<0.06	1.498
07-0859	LT104	LT	SH-51-01	259840	6897244	39.90	11.90	33.45	0.530	0.186	0.009	<0.06	1.381
07-0874	LT102	LT	SH-51-01	259561	6896988	25.90	23.90	38.46	0.257	0.309	0.041	0.10	1.183
07-0875	LT102	LT	SH-51-01	259561	6896988	22.30	24.50	42.03	0.184	0.265	0.016	0.07	1.234
07-0876	LT102	LT	SH-51-01	259561	6896988	24.10	23.80	41.03	0.141	0.213	0.029	0.08	0.967
07-0877	LT204	LT	SH-51-01	259561	6896988	21.50	17.40	51.04	0.132	0.133	0.020	<0.06	0.661
07-0878	LT204	LT	SH-51-01	259561	6896988	17.30	15.60	55.90	0.128	0.080	0.016	0.15	0.804
07-0879	LT204	LT	SH-51-01	259561	6896988	23.35	15.40	49.61	0.120	0.082	0.015	0.09	0.936
07-0880	LT204	LT	SH-51-01	259561	6896988	26.10	18.10	42.46	0.152	0.124	0.009	<0.06	1.159
07-0881	LT104	LT	SH-51-01	259561	6896988	35.25	19.80	31.02	0.700	0.518	0.015	0.07	1.061
07-0882	LT104	LT	SH-51-01	259561	6896988	32.45	12.60	44.61	0.493	0.381	0.010	<0.06	0.227
07-0892	LT104	LT	SH-51-01	259605	6897055	5.17	13.60	68.50	0.100	0.047	0.018	<0.06	4.871
07-0899	LT104	LT	SH-51-01	259425	6897058	23.50	18.00	46.61	0.175	0.165	0.054	<0.06	1.168
07-0907	LT204	LT	SH-51-01	259343	6897115	36.00	20.50	29.88	0.168	0.176	0.066	<0.06	1.636
07-0918	LT104	LT	SH-51-01	256000	6899250	15.30	20.40	51.90	0.245	0.089	0.043	0.06	2.802
07-0919	LT204	LT	SH-51-01	256100	6899200	20.70	18.50	49.90	0.280	0.119	0.041	0.09	2.485
07-0920	LT102	LT	SH-51-01	256100	6899150	26.00	16.20	45.46	0.146	0.063	0.019	0.21	3.286
07-0924	LT204	LT	SH-51-01	256100	6899100	13.90	15.90	53.47	0.253	0.038	0.013	<0.06	0.429
07-1176	LT104	LT	SH-51-01	259551	6896872	9.80	3.76	72.98	0.059	0.033	0.011	<0.06	0.215
07-1271	LT204	LT	SH-51-01	259619	6896839	24.70	11.87	55.57	0.068	0.129	0.017	<0.06	1.122
07-1272	LT204HP	LT	SH-51-01	259619	6896839	28.20	13.68	49.63	0.088	0.129	0.024	0.11	1.102
07-1274	LT102	LT	SH-51-01	258310	6898800	25.50	16.31	41.67	3.416	0.169	0.034	0.09	0.941
07-1275	LT102	LT	SH-51-01	258310	6898800	20.30	16.91	45.48	1.158	0.089	0.023	<0.06	0.626
07-1276	LT102	LT	SH-51-01	258310	6898800	12.30	11.71	62.01	0.624	0.075	0.016	<0.06	1.486
07-1277	LT204	LT	SH-51-01	258310	6898800	14.20	14.34	56.14	0.572	0.073	0.017	<0.06	1.363
07-1286	LT102	LT	SH-51-01	258300	6898825	17.20	17.83	49.60	0.230	0.105	0.026	<0.06	0.967
07-1287	LT102	LT	SH-51-01	258300	6898825	13.50	13.91	56.42	0.271	0.091	0.023	<0.06	0.394
07-1288	LT204	LT	SH-51-01	258300	6898825	15.00	15.27	52.35	0.308	0.085	0.025	<0.06	0.270
07-1294	LT102	LT	SH-51-01	258312	6898850	25.70	15.34	49.09	0.215	0.252	0.296	0.13	0.931
07-1295	LT102	LT	SH-51-01	258312	6898850	17.10	19.31	52.36	0.155	0.220	0.208	<0.06	1.118
07-1315	LG100	LT	SH-51-01	272700	6891600	6.90	9.33	70.97	0.690	0.055	0.014	<0.06	3.003
07-1345	LG100	LT	SH-51-01	273000	6892000	6.40	5.67	75.23	0.027	0.049	0.014	<0.06	5.204
07-1357	LG100	LT	SH-51-01	271600	6892000	6.40	10.30	69.86	0.045	0.041	0.015	<0.06	4.137

Appendix II **Chemical Composition of Lawlers Samples.**

Sample Number	Sample Type	Mn ppm	Cr ppm	V ppm	Cu ppm	Pb ppm	Zn ppm	Ni ppm	Co ppm	As ppm	Sb ppm	Bi ppm	Mo ppm	Ag ppm	Sn ppm	Ge ppm	Ga ppm	W ppm	Ba ppm	Zr ppm	Nb ppm	Se ppm	Be ppm	Au ppb
07-0814	LT102	2342	688	1415	74	34	30	36	24	46	3	<2	3	<0.1	<2	<4	44	14	177	171	9	8	2	340
07-0815	LT204	128	435	968	125	9	22	38	14	36	2	2	2	0.7	<2	<4	38	20	5861	135	6	2	2	1800
07-0816	LT102	200	553	1081	70	20	22	40	10	40	4	<2	2	0.4	<2	<4	44	38	92	157	10	3	2	840
07-0818	LT104	174	419	1073	120	10	26	38	14	38	5	<2	2	0.4	4	<4	54	32	735	142	7	<2	2	3065
07-0839	LT204	365	5901	1724	14	3	15	710	60	400	15	<2	4	0.3	7	8	88	6	8	70	17	3	2	26
07-0843	LT102	547	543	1288	80	28	30	58	22	62	4	<2	1	0.2	2	<4	54	4	158	127	9	3	2	210
07-0844	LT102	122	594	1182	100	20	19	50	20	68	5	3	1	<0.1	<2	<4	54	8	31	136	7	4	1	400
07-0851	LT104	302	27500	535	14	14	46	650	54	110	8	<2	5	0.9	<2	4	52	16	81	59	14	<2	2	11
07-0859	LT104	113	40200	519	22	12	96	760	74	320	16	<2	3	<0.1	5	<4	40	8	55	49	12	<2	1	13
07-0874	LT102	168	529	816	68	12	15	50	12	210	3	<2	<1	0.9	2	<4	50	18	101	141	7	3	1	1150
07-0875	LT102	165	560	818	62	18	11	46	8	360	5	<2	<1	<0.1	2	<4	54	30	78	142	8	2	2	1090
07-0876	LT102	142	656	658	64	12	10	48	10	580	5	<2	<1	0.7	2	<4	46	44	65	138	6	<2	1	2700
07-0877	LT204	65	662	544	82	16	8	28	<4	1180	7	<2	<1	0.9	<2	<4	30	44	32	135	4	<2	1	13500
07-0878	LT204	163	539	519	125	15	20	22	6	1680	4	<2	<1	<0.1	3	<4	34	110	37	137	7	6	2	17750
07-0879	LT204	228	330	467	130	10	20	18	6	910	<2	<2	<1	0.3	<2	<4	24	64	31	105	7	<2	1	9500
07-0880	LT204	185	412	632	160	11	15	22	<4	1220	3	<2	1	<0.1	<2	<4	34	46	23	120	6	<2	1	1100
07-0881	LT104	149	289	446	115	5	18	22	12	870	4	<2	<1	0.3	4	<4	24	28	25	94	5	3	1	110
07-0882	LT104	93	127	174	115	38	38	22	16	700	3	8	1	0.7	<2	<4	12	50	36	35	3	<2	1	580
07-0892	LT104	264	4204	1411	12	7	7	250	74	520	5	2	5	1.0	3	<4	105	130	12	136	24	<2	<1	415
07-0899	LT104	155	305	639	160	14	16	28	14	470	7	<2	1	0.7	2	<4	48	36	39	133	9	<2	1	51
07-0907	LT204	64	290	994	155	2	<2	16	10	50	5	<2	<1	0.6	2	4	46	<4	48	91	8	<2	1	110
07-0918	LT104	203	8016	1261	30	9	8	270	58	150	46	<2	3	0.5	6	4	86	8	152	119	15	<2	1	20
07-0919	LT204	223	8043	1312	48	9	4	260	48	155	42	4	3	0.4	3	<4	78	12	398	130	13	4	1	18
07-0920	LT102	3210	6032	1199	40	40	14	150	52	145	40	<2	3	0.4	2	4	84	10	476	125	17	3	2	27
07-0924	LT204	1422	19100	305	260	14	115	1500	210	58	30	<2	<1	0.8	<2	4	22	<4	276	52	4	5	2	40
07-1176	LT104	110	38	132	190	2	195	46	25	18	14	<2	<1	0.1	<2	4	12	<4	140	19	<2	<2	1	6
07-1271	LT204	132	668	1313	70	22	46	24	10	62	6	5	3	0.2	<2	<2	42	20	269	129	4	4	<1	1750
07-1272	LT204HP	147	694	1251	70	22	46	34	10	74	7	<2	3	<0.1	2	<2	50	22	350	137	3	2	1	200
07-1274	LT102	299	10100	649	58	30	88	540	38	130	12	18	7	<0.1	3	<2	30	8	59	89	6	2	1	52
07-1275	LT102	285	7530	330	94	42	84	1880	62	1460	25	8	14	0.1	2	<2	14	<4	20	57	6	3	1	170
07-1276	LT102	206	11100	688	74	10	74	960	46	1580	35	<2	9	<0.1	5	<2	34	5	18	65	7	<2	<1	290
07-1277	LT204	149	13000	872	56	18	40	550	30	1160	34	<2	6	<0.1	3	<2	42	10	12	66	6	<2	1	490
07-1286	LT102	441	11000	455	350	5	66	1800	76	1800	28	9	7	<0.1	7	<2	24	<4	32	67	7	<2	1	650
07-1287	LT102	531	9860	386	420	<2	60	2900	120	2400	25	16	9	0.1	<2	<2	16	10	24	44	4	<2	1	2810
07-1288	LT204	343	11900	667	450	<2	78	2550	96	1420	32	18	9	<0.1	<2	<2	10	25	27	41	<2	<2	<1	8900
07-1294	LT102	204	12200	793	52	20	80	350	20	84	15	<2	2	0.1	<2	<2	38	8	154	137	8	<2	1	26
07-1295	LT102	137	13900	865	44	20	38	460	26	80	22	<2	<1	<0.1	4	<2	42	<4	71	83	9	<2	1	35
07-1315	LG100	316	12500	1569	34	16	70	820	74	195	5	3	3	<0.1	2	<2	88	5	11	79	10	2	1	<1
07-1345	LG100	411	342	2272	74	8	90	50	28	10	<2	2	3	<0.1	2	<2	80	14	34	87	18	5	1	<1
07-1357	LG100	259	5378	1176	32	18	55	210	48	18	2	5	6	0.2	6	<2	78	6	31	53	15	<2	2	2

Appendix II

Chemical Composition of Lawlers Samples.

Sample Number	Sample Type	Box field	Map Reference	AMG Coordinates Easting	AMG Coordinates Northing	SiO2 wt %	Al2O3 wt %	Fe2O3 wt %	MgO wt %	CaO wt %	Na2O wt %	K2O wt %	TiO2 wt %
07-1363	LG100	LT	SH-51-01	272850	6891800	3.20	5.14	77.63	0.037	0.048	0.017	<0.06	8.291
07-1364	LG100	LT	SH-51-01	272750	6891800	3.60	6.20	77.40	0.117	0.053	0.015	<0.06	4.704
07-1392	LT204	LT	SH-51-01	260200	6900970	7.40	10.69	69.08	0.021	0.040	0.012	<0.06	3.303
07-1394	LG100	LT	SH-51-01	260100	6900950	7.20	11.77	74.07	0.027	0.033	0.011	<0.06	1.061
07-1395	LG100	LT	SH-51-01	260000	6900700	7.90	12.75	72.63	0.030	0.035	0.012	<0.06	1.041
07-1396	LG100	LT	SH-51-01	259000	6900600	8.20	14.28	69.31	0.030	0.031	0.012	<0.06	1.123
07-1397	LG100	LT	SH-51-01	258950	6900200	14.80	16.70	54.03	0.034	0.034	0.009	<0.06	0.603
07-1398	LG100	LT	SH-51-01	258800	6900000	12.50	14.59	60.06	0.039	0.036	0.010	<0.06	0.733

Appendix II **Chemical Composition of Lawlers Samples.**

Sample Number	Sample Type	Mn ppm	Cr ppm	V ppm	Cu ppm	Pb ppm	Zn ppm	Ni ppm	Co ppm	As ppm	Sb ppm	Bi ppm	Mo ppm	Ag ppm	Sn ppm	Ge ppm	Ga ppm	W ppm	Ba ppm	Zr ppm	Nb ppm	Se ppm	Be ppm	Au ppb
07-1363	LG100	299	3211	3365	17	35	40	80	28	35	4	<2	8	0.7	12	<2	195	18	18	40	28	5	1	3
07-1364	LG100	419	12600	2659	22	125	75	240	48	125	6	<2	4	0.2	7	<2	135	<4	30	91	19	<2	1	<1
07-1392	LT204	208	11500	1139	34	14	32	210	38	18	2	<2	6	1.1	5	<2	70	12	92	76	13	7	1	<1
07-1394	LG100	361	16400	984	25	35	30	340	26	70	5	5	4	1.0	4	<2	56	<4	22	138	4	3	1	<1
07-1395	LG100	378	17300	960	25	26	40	390	34	68	6	3	4	1.2	3	<2	50	6	23	141	6	4	1	<1
07-1396	LG100	152	17200	829	24	20	32	410	34	40	4	3	5	0.4	2	<2	54	8	13	125	8	8	1	3
07-1397	LG100	254	11000	587	180	7	46	500	44	10	2	<2	<1	<0.1	<2	<2	24	<4	56	80	<2	4	1	<1
07-1398	LG100	204	12000	658	145	8	38	500	44	24	4	2	<1	<0.1	<2	<2	26	<4	28	76	<2	<2	1	<1

Appendix II **Chemical Composition of Lawlers Samples.**

Sample Number	Sample Type	Box field	Map Reference	AMG Coordinates Easting	AMG Coordinates Northing	SiO2 wt %	Al2O3 wt %	Fe2O3 wt %	MgO wt %	CaO wt %	Na2O wt %	K2O wt %	TiO2 wt %
07-0817	IS101	IS	SH-51-01	259619	6896850	10.20	5.84	71.80	0.129	0.046	0.000	<0.06	0.520
07-0820	IS100-gos	IS	SH-51-01	259619	6896850	12.50	1.43	77.20	0.185	0.271	0.009	<0.06	0.102
07-0821	LG206	IS	SH-51-01	259619	6896850	15.10	2.49	72.90	0.172	0.197	0.012	<0.06	0.150
07-0823	IS100-gos	IS	SH-51-01	259153	6897157	8.94	2.80	76.20	0.078	0.070	<0.007	<0.06	0.180
07-0826	LG206	IS	SH-51-01	259247	6897152	16.50	12.40	63.76	0.083	0.058	<0.007	<0.06	2.002
07-0829	LG206	IS	SH-51-01	271150	6895700	59.60	8.26	25.88	0.099	0.042	0.020	0.39	0.661
07-0923	IS100	IS	SH-51-01	256000	6899300	6.74	3.21	77.60	0.108	0.047	<0.007	<0.06	0.150
07-1163	IS102	IS	SH-51-01	259528	6896853	19.20	7.48	64.45	0.042	0.132	0.026	<0.06	0.672
07-1164	IS102-gos	IS	SH-51-01	259528	6896853	10.00	6.75	70.18	0.041	0.076	0.017	<0.06	0.553
07-1173	IS103	IS	SH-51-01	259508	6896810	9.90	7.61	71.47	0.039	0.047	0.015	<0.06	0.448
07-1177	IS101-gos	IS	SH-51-01	259551	6896872	9.90	6.92	69.91	0.083	0.042	0.016	<0.06	0.570
07-1178	IS100	IS	SH-51-01	259551	6896872	26.20	11.92	52.63	0.087	0.121	0.029	0.10	0.960
07-1179	IS100-gos	IS	SH-51-01	259700	6896775	10.20	4.69	74.49	0.059	0.068	0.016	<0.06	0.258
07-1181	IS100-gos	IS	SH-51-01	259706	6896679	12.60	3.21	74.20	0.072	0.056	0.027	<0.06	0.292
07-1182	IS100-gos	IS	SH-51-01	259706	6896679	28.10	3.46	58.36	0.081	0.073	0.019	<0.06	0.345
07-1185	IS103	IS	SH-51-01	259485	6896783	69.80	0.93	27.05	0.011	0.020	0.012	<0.06	0.020
07-1186	IS111-gos	IS	SH-51-01	259456	6896780	5.10	3.68	77.96	0.026	0.059	0.012	0.09	0.297
07-1187	IS111-gos	IS	SH-51-01	259492	6896763	28.70	8.41	49.01	0.346	0.197	0.060	<0.06	1.060
07-1188	IS201-gos	IS	SH-51-01	259492	6896763	10.10	2.99	77.70	0.122	0.108	0.032	<0.06	0.285
07-1189	IS201-gos	IS	SH-51-01	259500	6896769	11.50	5.67	69.24	0.144	0.133	0.040	<0.06	0.541
07-1193	IS102-gos	IS	SH-51-01	259577	6896818	8.70	4.74	75.31	0.053	0.064	0.015	<0.06	0.330
07-1196	IS102-gos	IS	SH-51-01	260128	6896452	23.60	6.33	60.75	0.070	0.065	0.016	<0.06	0.403
07-1201	IS101-gos	IS	SH-51-01	259714	6896740	16.20	1.93	71.95	0.210	0.137	0.029	<0.06	0.105
07-1205	IS100	IS	SH-51-01	259584	6896849	66.00	1.02	29.13	0.020	0.027	0.008	<0.06	0.034
07-1206	IS102	IS	SH-51-01	259549	6896850	9.90	8.30	69.33	0.064	0.057	0.014	<0.06	0.874
07-1207	IS100	IS	SH-51-01	264628	6886971	9.70	2.49	76.29	0.046	0.115	0.015	<0.06	0.145
07-1208	IS201	IS	SH-51-01	259926	6896640	20.00	2.87	66.20	0.053	0.095	0.018	<0.06	0.152
07-1209	LG206	IS	SH-51-01	259996	6896566	23.50	2.25	63.90	0.087	0.076	0.017	<0.06	0.076
07-1210	IS201	IS	SH-51-01	260008	6896496	8.80	2.70	79.06	0.111	0.103	0.014	<0.06	0.200
07-1211	LG206	IS	SH-51-01	259951	6896415	9.40	2.44	78.10	0.068	0.159	0.016	<0.06	0.188
07-1212	LG206	IS	SH-51-01	259812	6896390	13.50	3.14	73.60	0.098	0.182	0.016	<0.06	0.384
07-1213	LG206	IS	SH-51-01	259849	6896181	7.80	1.78	78.77	0.240	0.371	0.016	<0.06	0.091
07-1214	LG206	IS	SH-51-01	260046	6896036	38.50	0.72	53.90	0.072	0.109	0.015	<0.06	0.025
07-1215	LG206	IS	SH-51-01	260016	6896247	15.80	1.67	70.80	0.305	0.402	0.021	<0.06	0.179
07-1216	LG206	IS	SH-51-01	260131	6896410	11.70	2.44	73.94	0.081	0.093	0.016	<0.06	0.174
07-1217	LG206	IS	SH-51-01	260007	6902420	10.20	2.10	76.99	0.159	0.195	0.020	<0.06	0.125
07-1218	IS201	IS	SH-51-01	264628	6886971	13.70	1.36	75.76	0.092	0.156	0.015	<0.06	0.098
07-1219	LG206	IS	SH-51-01	259767	6896727	10.20	2.93	73.86	0.037	0.081	0.014	<0.06	0.242
07-1220	LG206	IS	SH-51-01	259755	6896710	8.00	3.31	76.67	0.050	0.091	0.013	<0.06	0.213
07-1221	LG206	IS	SH-51-01	259744	6896694	8.20	3.61	76.29	0.037	0.104	0.013	<0.06	0.251

Appendix II **Chemical Composition of Lawlers Samples.**

Sample Number	Sample Type	Mn ppm	Cr ppm	V ppm	Cu ppm	Pb ppm	Zn ppm	Ni ppm	Co ppm	As ppm	Sb ppm	Bi ppm	Mo ppm	Ag ppm	Sn ppm	Ge ppm	Ga ppm	W ppm	Ba ppm	Zr ppm	Nb ppm	Se ppm	Be ppm	Au ppb
07-0817	IS101	267	83	279	260	3	155	62	34	24	4	<2	3	<0.1	7	<4	16	6	124	42	5	2	2	330
07-0820	IS100-gos	4249	<50	127	76	3	380	58	110	650	11	<2	2	<0.1	<2	<4	12	<4	127	7	4	<2	2	7
07-0821	LG206	3537	<50	203	70	8	380	76	130	160	2	<2	1	<0.1	2	<4	12	<4	1020	6	3	4	2	3
07-0823	IS100-gos	2718	<50	102	240	5	350	58	84	510	<2	<2	2	<0.1	<2	<4	12	<4	223	8	3	<2	2	20
07-0826	LG206	364	613	2909	66	8	18	32	16	48	8	<2	3	<0.1	5	4	66	10	67	120	8	2	2	30
07-0829	LG206	230	4635	382	34	4	32	420	32	28	4	<2	2	<0.1	<2	<4	22	<4	112	86	8	2	1	2
07-0923	IS100	324	97	64	260	7	280	105	46	40	11	2	2	0.6	<2	<4	14	10	150	5	6	<2	1	22
07-1163	IS102	88	72	444	66	5	92	150	12	13	3	6	2	0.3	<2	8	12	8	108	59	2	<2	1	77
07-1164	IS102-gos	202	42	144	135	12	270	110	28	17	3	<2	1	0.3	<2	4	6	15	21	45	2	<2	1	45
07-1173	IS103	40	50	179	170	16	95	24	8	32	<2	2	3	<0.1	2	5	<4	<4	66	46	<2	<2	1	25
07-1177	IS101-gos	226	143	246	310	<2	140	66	24	35	7	<2	2	0.2	<2	6	10	<4	199	49	<2	<2	1	860
07-1178	IS100	147	429	866	90	15	35	36	8	32	4	4	3	0.3	2	<2	32	16	971	128	6	<2	1	730
07-1179	IS100-gos	3960	97	427	150	<2	400	92	135	10	4	<2	1	0.1	2	<2	<4	<4	73	31	<2	<2	1	100
07-1181	IS100-gos	3735	40	158	98	6	450	34	72	10	3	<2	3	<0.1	4	3	<4	<4	190	19	4	<2	<1	25
07-1182	IS100-gos	2510	48	413	145	<2	400	90	62	14	<2	<2	3	0.3	<2	4	<4	<4	3336	20	<2	<2	<1	11
07-1185	IS103	15	<20	546	90	10	14	4	<4	130	4	250	1	0.1	<2	4	<4	10	23	8	<2	11	<1	62100
07-1186	IS111-gos	122	40	1370	230	3	140	48	16	190	5	<2	7	0.1	3	<2	6	260	163	15	3	<2	1	790
07-1187	IS111-gos	739	71	347	135	7	430	80	52	32	6	20	2	0.5	2	<2	10	<4	28	57	6	<2	1	36
07-1188	IS201-gos	2860	40	224	75	3	480	70	115	95	3	<2	2	0.2	<2	7	12	12	86	18	<2	<2	<1	8
07-1189	IS201-gos	1880	66	347	130	16	470	105	115	50	9	3	4	<0.1	<2	2	12	<4	16	33	2	<2	<1	45
07-1193	IS102-gos	69	26	104	125	5	200	58	15	48	22	<2	5	0.1	5	3	<4	<4	17	27	3	3	1	16
07-1196	IS102-gos	3410	51	290	185	<2	610	110	145	26	5	<2	4	0.1	6	8	12	4	59	22	<2	2	<1	29
07-1201	IS101-gos	3970	33	694	60	<2	310	42	78	17	<2	<2	4	0.1	4	4	<4	<4	243	10	<2	<2	<1	4
07-1205	IS100	39	<20	47	66	<2	115	18	8	13	5	<2	1	0.2	2	<2	6	<4	13	13	2	<2	<1	2
07-1206	IS102	40	119	377	320	<2	120	45	10	28	<2	<2	<1	0.1	<2	8	20	32	10	58	4	<2	<1	1
07-1207	IS100	4190	32	212	105	<2	400	42	85	6	2	<2	1	<0.1	<2	2	<4	<4	149	14	2	<2	1	13
07-1208	IS201	3610	45	169	96	4	360	80	100	<2	5	<2	3	0.2	<2	<2	<4	<4	2060	16	<2	<2	1	31
07-1209	LG206	3330	<20	87	145	<2	400	74	105	5	<2	<2	1	0.1	<2	<2	<4	<4	2110	7	<2	<2	1	16
07-1210	IS201	3370	25	157	76	<2	340	66	94	12	5	3	<1	0.2	2	5	<4	<4	79	18	5	<2	1	10
07-1211	LG206	3280	34	140	94	<2	500	98	130	13	5	6	4	0.2	4	<2	15	<4	127	15	<2	<2	1	2
07-1212	LG206	1870	97	403	220	<2	280	56	65	42	5	5	2	0.3	<2	<2	<4	10	157	24	2	<2	1	37
07-1213	LG206	2300	20	180	130	<2	220	72	78	14	2	<2	<1	0.3	<2	<2	5	4	292	15	<2	<2	1	3
07-1214	LG206	1100	<20	271	420	9	150	28	72	105	3	3	1	0.3	<2	4	<4	4	33	8	<2	2	<1	10
07-1215	LG206	5250	29	1220	105	8	360	56	66	510	8	<2	3	0.1	4	<2	8	<4	95	13	<2	<2	<1	3
07-1216	LG206	2890	24	75	75	<2	410	64	88	7	2	<2	3	0.1	<2	<2	<4	4	153	16	5	<2	1	11
07-1217	LG206	3600	42	283	115	7	540	78	105	48	6	4	4	0.1	<2	<2	4	<4	55	29	<2	<2	<1	<1
07-1218	IS201	3110	32	170	95	<2	370	80	88	980	5	<2	3	0.1	<2	4	6	<4	128	9	2	<2	<1	9
07-1219	LG206	3530	46	229	220	5	980	115	120	18	7	<2	3	0.1	4	2	<4	<4	286	22	5	<2	1	120
07-1220	LG206	3870	48	312	165	17	710	80	84	18	7	<2	2	0.1	2	<2	6	8	526	20	2	<2	1	100
07-1221	LG206	3810	46	240	190	<2	760	130	100	14	<2	<2	3	0.1	<2	<2	<4	<4	532	21	<2	<2	1	41

Appendix II **Chemical Composition of Lawlers Samples.**

Sample Number	Sample Type	Box field	Map Reference	AMG Coordinates Easting	AMG Coordinates Northing	SiO2 wt %	Al2O3 wt %	Fe2O3 wt %	MgO wt %	CaO wt %	Na2O wt %	K2O wt %	TiO2 wt %
07-1222	LG206	IS	SH-51-01	259798	6896632	10.40	2.63	75.29	0.046	0.109	0.015	<0.06	0.163
07-1223	LG206	IS	SH-51-01	259775	6896599	12.10	4.01	71.81	0.057	0.094	0.013	<0.06	0.489
07-1224	LG206	IS	SH-51-01	259829	6896537	9.80	2.59	77.20	0.061	0.103	0.017	<0.06	0.150
07-1225	IS201	IS	SH-51-01	260217	6896533	11.40	7.82	72.10	0.279	0.077	0.011	<0.06	0.203
07-1227	IS101	IS	SH-51-01	260189	6896528	8.70	3.99	74.14	0.072	0.037	0.010	<0.06	0.212
07-1228	LG206	IS	SH-51-01	264628	6886971	6.60	2.25	81.43	0.072	0.069	0.011	<0.06	0.124
07-1229	IS201	IS	SH-51-01	260053	6902693	10.50	1.85	78.64	0.055	0.056	0.013	<0.06	0.080
07-1230	LG206	IS	SH-51-01	259316	6896554	13.80	2.74	75.78	0.090	0.141	0.016	<0.06	0.238
07-1231	LG206	IS	SH-51-01	259398	6896619	11.70	3.08	78.40	0.072	0.162	0.014	<0.06	0.261
07-1232	IS201	IS	SH-51-01	259447	6896829	7.20	5.44	73.74	0.033	0.044	0.010	<0.06	0.454
07-1233	IS101	IS	SH-51-01	259505	6896910	10.50	4.91	71.95	0.081	0.039	0.011	<0.06	0.408
07-1234	IS111	IS	SH-51-01	259417	6896820	7.10	3.63	76.94	0.053	0.073	0.012	<0.06	0.219
07-1235	LG206	IS	SH-51-01	259423	6896968	9.00	3.42	76.85	0.070	0.082	0.013	<0.06	0.273
07-1236	LG206	IS	SH-51-01	259341	6897025	12.70	2.06	74.96	0.108	0.073	0.010	<0.06	0.063
07-1237	LG206	IS	SH-51-01	259255	6896902	34.00	1.58	55.97	0.119	0.171	0.019	<0.06	0.115
07-1238	LG206	IS	SH-51-01	259040	6896943	13.20	3.12	71.01	0.215	0.216	0.013	<0.06	0.276
07-1239	LG206	IS	SH-51-01	258996	6896882	31.50	1.77	57.72	0.128	0.185	0.013	<0.06	0.091
07-1240	LG206	IS	SH-51-01	259120	6897058	11.10	2.85	73.77	0.058	0.609	0.012	<0.06	0.252
07-1241	IS201	IS	SH-51-01	259149	6897099	7.60	1.63	79.55	0.033	0.119	0.010	<0.06	0.064
07-1242	LG206	IS	SH-51-01	259067	6897156	7.40	2.53	78.83	0.029	0.066	0.011	<0.06	0.126
07-1243	IS100	IS	SH-51-01	258969	6897017	10.70	2.12	76.42	0.146	0.319	0.050	<0.06	0.115
07-1244	LG206	IS	SH-51-01	258912	6896935	13.40	2.85	71.65	0.193	0.266	0.014	<0.06	0.248
07-1245	IS201	IS	SH-51-01	259139	6896911	11.80	2.82	75.34	0.088	0.196	0.016	<0.06	0.252
07-1246	LG206	IS	SH-51-01	259173	6896960	12.10	2.53	74.59	0.306	0.367	0.012	<0.06	0.143
07-1247	LG206	IS	SH-51-01	259230	6897042	12.70	1.80	75.86	0.038	0.083	0.012	<0.06	0.089
07-1248	LG206	IS	SH-51-01	259304	6897112	11.80	2.51	77.06	0.086	0.107	0.012	<0.06	0.177
07-1253	IS201	IS	SH-51-01	259508	6896780	11.50	4.52	71.91	0.095	0.093	0.023	<0.06	0.440
07-1259	IS101	IS	SH-51-01	256100	6899050	12.50	5.59	68.77	0.055	0.129	0.013	<0.06	0.512
07-1262	IS101	IS	SH-51-01	261273	6899329	7.70	5.50	73.01	0.140	0.016	0.010	<0.06	0.566
07-1265	IS100-gos	IS	SH-51-01	259708	6896787	15.40	3.25	71.76	0.084	0.099	0.023	<0.06	0.234
07-1267	IS100-gos	IS	SH-51-01	259725	6896696	18.80	3.85	67.54	0.058	0.079	0.018	<0.06	0.286
07-1292	IS100	IS	SH-51-01	258312	6898850	27.00	5.69	49.56	4.095	0.218	0.033	<0.06	0.128
07-1310	LG206	IS	SH-51-01	273300	6891600	15.50	3.85	71.77	0.165	0.146	0.014	<0.06	0.615
07-1343	LG206	IS	SH-51-01	273050	6892000	8.10	7.12	72.89	0.030	0.035	0.013	<0.06	1.718

Appendix II **Chemical Composition of Lawlers Samples.**

Sample Number	Sample Type	Mn	Cr	V	Cu	Pb	Zn	Ni	Co	As	Sb	Bi	Mo	Ag	Sn	Ge	Ga	W	Ba	Zr	Nb	Se	Be	Au
		ppm	*ppm*	*ppm*	*ppm*	*ppm*	*ppm*	*ppm*	*ppm*	*ppm*	*ppm*	*ppm*	*ppm*	*ppm*	*ppm*	*ppm*	*ppm*	*ppm*	*ppm*	*ppm*	*ppm*	*ppm*	*ppm*	*ppb*
07-1222	LG206	4380	35	235	105	<2	420	44	120	<2	4	6	3	<0.1	2	<2	<4	4	148	16	<2	<2	1	22
07-1223	LG206	2780	28	451	500	5	690	98	94	185	4	<2	5	0.1	5	3	8	5	43	22	3	<2	1	37
07-1224	LG206	3130	33	227	260	7	510	115	105	9	2	<2	4	<0.1	<2	<2	<4	12	132	14	<2	30	1	5
07-1225	IS201	197	4530	106	76	11	140	100	20	45	6	<2	1	0.4	<2	<2	<4	<4	374	14	5	<2	1	65
07-1227	IS101	121	61	159	230	<2	170	45	24	34	13	<2	<1	<0.1	2	<2	<4	18	119	23	4	<2	1	6
07-1228	LG206	4100	122	270	110	5	470	92	125	20	4	6	4	0.1	<2	<2	<4	<4	85	15	<2	2	1	<1
07-1229	IS201	3930	64	156	120	17	320	66	115	6	9	<2	3	<0.1	4	4	6	<4	75	24	3	<2	1	2
07-1230	LG206	3540	50	203	100	<2	340	50	76	94	4	12	1	0.1	2	2	4	10	67	30	<2	<2	1	18
07-1231	LG206	3130	34	232	190	3	290	52	82	195	9	7	5	<0.1	<2	2	<4	<4	343	31	3	2	1	53
07-1232	IS201	196	63	287	185	<2	210	90	24	70	8	7	3	<0.1	3	3	<4	10	195	30	<2	<2	1	24
07-1233	IS101	151	51	249	370	<2	290	60	20	40	4	22	3	<0.1	<2	<2	4	24	11	26	3	<2	2	8
07-1234	IS111	420	28	119	200	<2	140	58	36	38	<2	<2	4	<0.1	<2	<2	<4	1100	151	14	<2	<2	1	16
07-1235	LG206	1650	64	584	170	9	280	52	68	390	3	<2	3	0.2	<2	<2	4	10	263	19	2	<2	1	81
07-1236	LG206	4160	47	471	100	2	185	75	110	16	<2	4	3	<0.1	3	6	<4	<4	1697	21	4	<2	1	19
07-1237	LG206	2520	58	267	140	<2	155	38	52	24	3	3	2	<0.1	4	<2	<4	4	607	21	2	<2	<1	34
07-1238	LG206	3790	53	213	100	<2	320	50	90	300	5	<2	1	<0.1	2	<2	5	8	429	26	2	<2	<1	14
07-1239	LG206	2480	48	182	110	4	340	78	88	175	8	4	2	<0.1	<2	2	<4	8	376	14	3	<2	1	3
07-1240	LG206	2900	40	209	105	<2	360	94	92	150	8	2	5	0.1	3	<2	<4	<4	104	19	<2	<2	<1	4
07-1241	IS201	3590	23	85	155	6	510	125	125	115	<2	3	1	0.5	<2	<2	<4	6	122	12	<2	<2	<1	29
07-1242	LG206	4320	47	190	380	<2	530	72	105	26	4	<2	1	<0.1	<2	2	8	<4	511	19	<2	<2	1	9
07-1243	IS100	3110	30	209	64	5	350	52	92	440	<2	<2	<1	<0.1	<2	<2	6	<4	3333	12	3	<2	<1	2
07-1244	LG206	4350	31	269	84	<2	290	62	88	340	2	<2	2	<0.1	3	<2	<4	<4	528	18	4	<2	91	3
07-1245	IS201	3500	80	178	98	6	310	68	88	130	4	5	3	0.1	2	<2	<4	<4	164	27	2	<2	<1	1
07-1246	LG206	3000	47	210	160	<2	350	68	88	110	5	6	4	0.1	3	2	6	<4	3373	16	<2	<2	<1	1
07-1247	LG206	3280	79	115	115	<2	370	78	100	52	2	<2	2	0.3	<2	2	<4	<4	106	19	4	<2	1	17
07-1248	LG206	3350	32	648	185	10	250	34	70	16	3	11	2	<0.1	2	7	6	10	1150	17	4	<2	<1	17
07-1253	IS201	1960	55	320	135	<2	140	120	85	115	9	11	2	<0.1	4	3	18	<4	14	32	2	<2	<1	12
07-1259	IS101	152	72	269	180	2	145	80	32	22	20	<2	5	<0.1	2	2	10	<4	50	33	3	<2	2	7
07-1262	IS101	271	75	248	290	<2	150	72	24	64	3	<2	5	0.2	2	<2	<4	10	145	46	6	<2	1	400
07-1265	IS100-gos	3180	<20	115	65	<2	280	58	92	3	2	<2	2	<0.1	<2	4	4	<4	308	19	2	<2	<1	31
07-1267	IS100-gos	2650	58	256	86	4	370	40	64	10	2	<2	3	<0.1	<2	3	8	<4	241	21	<2	<2	<1	43
07-1292	IS100	2100	19200	236	185	<2	195	6900	680	850	12	<2	7	<0.1	<2	<2	<4	<4	129	6	<2	<2	<1	23
07-1310	LG206	2640	956	394	180	<2	500	740	210	13	<2	<2	<1	<0.1	<2	<2	18	6	302	27	3	<2	1	<1
07-1343	LG206	336	482	1028	65	10	240	100	54	8	<2	<2	2	<0.1	3	<2	42	6	13	58	4	<2	1	1

Appendix II **Chemical Composition of Lawlers Samples.**

Sample Number	Sample Type	Box field	Map Reference	AMG Coordinates Easting	AMG Coordinates Northing	SiO2 wt %	Al2O3 wt %	Fe2O3 wt %	MgO wt %	CaO wt %	Na2O wt %	K2O wt %	TiO2 wt %
07-0819	sap-f	Fe-sap	SH-51-01	259619	6896850	32.60	16.00	39.32	0.121	0.113	0.037	0.06	1.316
07-1166	sap-f	Fe-sap	SH-51-01	259528	6896853	45.90	17.06	27.78	0.055	0.125	0.065	0.10	1.935
07-1170	sap-f	Fe-sap	SH-51-01	259511	6896824	33.80	16.67	37.94	0.064	0.112	0.038	<0.06	1.227
07-1174	sap-f	Fe-sap	SH-51-01	259508	6896810	30.30	14.04	44.53	0.079	0.113	0.034	<0.06	1.381
07-1175	sap-f	Fe-sap	SH-51-01	259551	6896872	25.10	13.49	52.17	0.046	0.085	0.033	<0.06	1.469
07-1180	sap-f	Fe-sap	SH-51-01	259700	6896775	52.80	11.07	26.60	0.037	0.076	0.049	<0.06	1.097
07-1183	sap-f	Fe-sap	SH-51-01	259511	6896824	18.90	11.64	59.23	0.033	0.051	0.016	<0.06	1.208
07-1195	sap-f	Fe-sap	SH-51-01	260128	6896452	36.90	16.57	33.44	0.153	0.116	0.018	<0.06	1.918
07-1202	sap-f	Fe-sap	SH-51-01	259714	6896740	49.30	17.14	20.84	0.435	0.273	0.036	<0.06	1.654
07-1203	sap-f	Fe-sap	SH-51-01	259643	6896811	25.10	18.16	45.33	0.046	0.076	0.021	<0.06	1.065
07-1204	sap-f	Fe-sap	SH-51-01	259584	6896849	20.90	15.49	50.57	0.094	0.119	0.038	<0.06	1.215
07-1266	sap-f	Fe-sap	SH-51-01	259708	6896751	48.00	18.54	20.69	0.080	0.123	0.038	<0.06	1.668
07-1268	sap-f	Fe-sap	SH-51-01	259619	6896839	23.70	16.42	47.15	0.068	0.089	0.017	<0.06	1.153
07-1269	sap-f	Fe-sap	SH-51-01	259619	6896839	32.90	22.18	33.28	0.055	0.089	0.018	<0.06	1.348
07-1270	sap-f	Fe-sap	SH-51-01	259619	6896839	22.20	14.28	55.17	0.075	0.113	0.016	<0.06	1.171
07-1279	sap-f	Fe-sap	SH-51-01	258310	6898800	13.50	11.71	58.29	0.505	0.063	0.014	<0.06	0.098
07-1280	sap-f	Fe-sap	SH-51-01	258310	6898800	9.50	6.50	67.93	0.561	0.052	0.013	<0.06	0.087
07-1281	sap-f	Fe-sap	SH-51-01	258310	6898800	10.00	6.07	67.69	1.018	0.054	0.013	<0.06	0.123
07-1282	sap-f	Fe-sap	SH-51-01	258310	6898800	24.90	7.90	47.09	4.477	0.234	0.023	<0.06	0.133
07-1289	sap-f	Fe-sap	SH-51-01	258300	6898825	14.20	13.28	56.52	0.244	0.087	0.023	<0.06	0.189
07-1290	sap-f	Fe-sap	SH-51-01	258300	6898825	13.10	5.97	65.54	0.737	0.127	0.026	<0.06	0.167
07-1291	sap-f	Fe-sap	SH-51-01	258300	6898825	27.40	6.33	50.20	1.415	0.254	0.045	<0.06	0.128
07-1296	sap-f	Fe-sap	SH-51-01	258312	6898850	34.00	23.52	26.40	0.552	0.339	0.324	0.08	0.404
07-1297	sap-f	Fe-sap	SH-51-01	258312	6898850	29.50	21.16	33.28	0.391	0.355	0.383	0.08	0.316
07-1298	sap-f	Fe-sap	SH-51-01	258312	6898850	17.40	7.90	59.22	0.943	0.351	0.291	0.07	0.208
07-1299	sap-f	Fe-sap	SH-51-01	258312	6898850	18.50	6.05	59.80	0.923	0.422	0.362	0.08	0.194

Note: Lower case terms in the Sample Type column are interim terms, i.e. not formal classification terms in Anand et al.(August 1989)

Appendix II **Chemical Composition of Lawlers Samples.**

Sample Number	Sample Type	Mn ppm	Cr ppm	V ppm	Cu ppm	Pb ppm	Zn ppm	Ni ppm	Co ppm	As ppm	Sb ppm	Bi ppm	Mo ppm	Ag ppm	Sn ppm	Ge ppm	Ga ppm	W ppm	Ba ppm	Zr ppm	Nb ppm	Se ppm	Be ppm	Au ppb
07-0819	sap-f	143	140	506	120	3	56	22	12	16	6	2	<1	<0.1	2	<4	34	18	165	97	8	3	2	680
07-1166	sap-f	66	118	462	72	<2	58	22	12	32	6	2	2	0.2	5	2	24	8	36	148	7	<2	1	100
07-1170	sap-f	229	164	536	78	<2	26	20	5	13	4	<2	2	0.2	<2	3	28	15	68	112	3	<2	1	120
07-1174	sap-f	940	100	497	270	<2	260	92	64	24	<2	5	3	<0.1	<2	3	20	8	72	99	4	<2	1	28
07-1175	sap-f	154	83	259	54	<2	46	10	8	11	6	12	4	0.2	<2	5	8	<4	378	101	6	<2	1	190
07-1180	sap-f	889	100	454	68	<2	210	48	46	10	5	<2	1	0.1	3	3	10	4	265	61	5	<2	<1	100
07-1183	sap-f	169	129	630	76	3	58	10	8	10	7	5	2	0.3	4	2	22	<4	72	109	2	<2	1	69
07-1195	sap-f	959	108	465	125	<2	390	88	62	32	5	10	1	<0.1	2	<2	24	5	18	101	7	<2	1	22
07-1202	sap-f	173	115	391	92	<2	54	28	10	7	4	<2	1	0.1	2	4	26	<4	29	86	3	<2	1	4
07-1203	sap-f	158	89	1000	230	8	40	44	6	48	5	3	3	0.3	<2	6	10	6	23	69	3	<2	1	110
07-1204	sap-f	183	119	751	220	<2	90	46	12	56	12	2	<1	0.1	6	<2	22	10	31	78	3	<2	1	8
07-1266	sap-f	246	203	693	160	<2	65	20	18	9	3	<2	<1	<0.1	5	<2	26	8	551	83	6	2	<1	250
07-1268	sap-f	180	265	809	160	6	42	22	10	40	6	<2	<1	0.2	<2	5	28	10	121	85	5	<2	1	470
07-1269	sap-f	183	570	1440	84	11	36	24	8	55	6	<2	<1	0.3	4	<2	42	<4	88	119	5	<2	<1	460
07-1270	sap-f	183	627	1290	80	14	40	32	10	74	6	10	2	0.2	3	<2	48	12	79	130	4	<2	<1	610
07-1279	sap-f	396	10100	360	330	3	60	2350	64	2100	30	32	4	0.1	3	4	<4	<4	<5	27	2	<2	1	5520
07-1280	sap-f	497	11000	234	440	<2	50	2800	62	2050	28	46	4	<0.1	6	<2	<4	<4	<5	15	<2	<2	1	3230
07-1281	sap-f	371	10800	280	610	<2	98	2350	88	2200	22	88	3	<0.1	<2	6	<4	<4	11	15	4	<2	1	2370
07-1282	sap-f	213	9200	29500	610	8	88	2350	82	1250	22	145	5	<0.1	2	2	<4	<4	13	17	<2	<2	1	2330
07-1289	sap-f	469	7820	522	270	8	55	2450	82	1960	24	26	6	<0.1	<2	<2	<4	<4	16	33	2	<2	<1	1420
07-1290	sap-f	681	15200	324	260	<2	135	4200	150	1980	16	8	2	<0.1	<2	2	20	<4	39	17	3	<2	<1	110
07-1291	sap-f	1080	210	248	230	26	165	5900	290	1440	11	<2	5	0.1	9	4	8	<4	97	10	2	<2	<1	270
07-1296	sap-f	147	6360	239	170	<2	38	1060	34	175	12	8	2	<0.1	<2	4	12	8	109	41	3	<2	<1	1140
07-1297	sap-f	267	7060	254	220	<2	34	1580	36	340	18	14	3	<0.1	2	<2	10	12	143	40	4	<2	<1	2050
07-1298	sap-f	255	4650	571	1080	<2	54	2550	60	1600	32	36	6	0.2	<2	5	15	<4	87	22	2	<2	1	2820
07-1299	sap-f	413	4640	602	790	15	68	2850	64	1480	25	140	11	0.2	<2	3	15	8	94	26	4	<2	<1	4020

APPENDIX III

Histograms of values of SiO_2, Al_2O_3, Fe_2O_3, MgO, TiO_2, V,
Cu, Pb, Ni, Co, Sb, Ag, Sn, Ga, W, Ba, Zr, and Nb

(Histograms of Cr, Mn, Zn, As, and Au in main text, Figs 44-48)

Dataset PR43 Sampletype: **Colluvium**

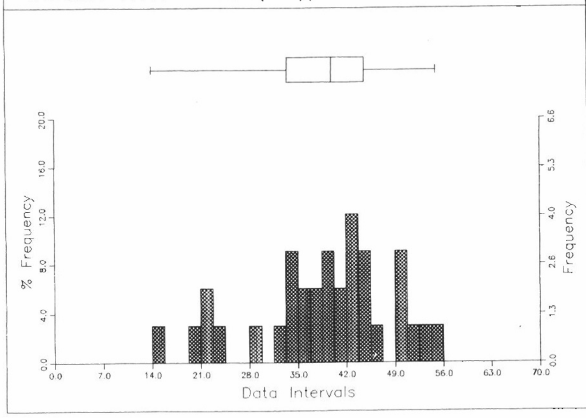

SiO2	
Samples	33.
Mean	38.57
Std. Dev.	10.07
Max	55.00
Min	14.00
Median	40.00
L Hinge	33.60
R Hinge	44.70

Dataset PR43 Sampletype: **Lateritic residuum**

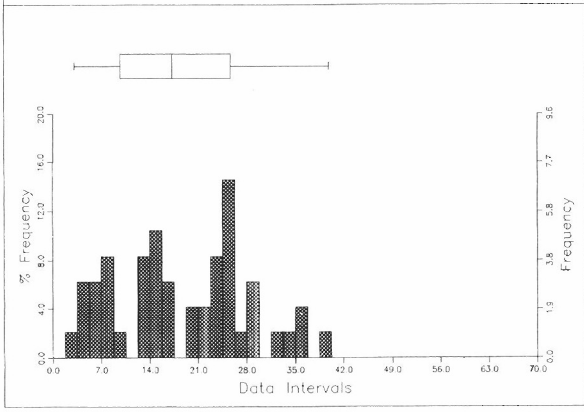

SiO2	
Samples	48.
Mean	18.83
Std. Dev.	9.60
Max	39.90
Min	3.20
Median	17.30
L Hinge	9.80
R Hinge	25.70

Dataset PR43 Sampletype: **Ferruginous saprolite**

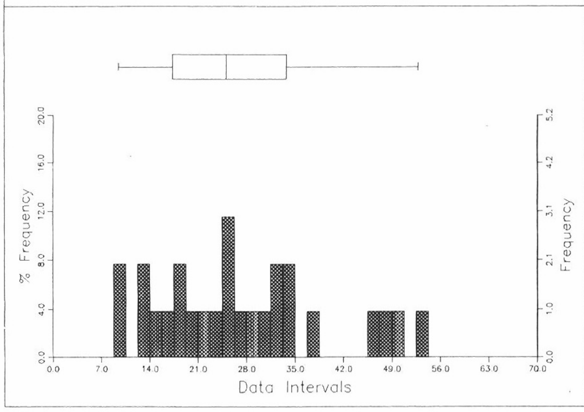

SiO2	
Samples	26.
Mean	27.32
Std. Dev.	12.14
Max	52.80
Min	9.50
Median	25.10
L Hinge	17.40
R Hinge	33.80

Dataset PR43 Sampletype: **Iron segregations**

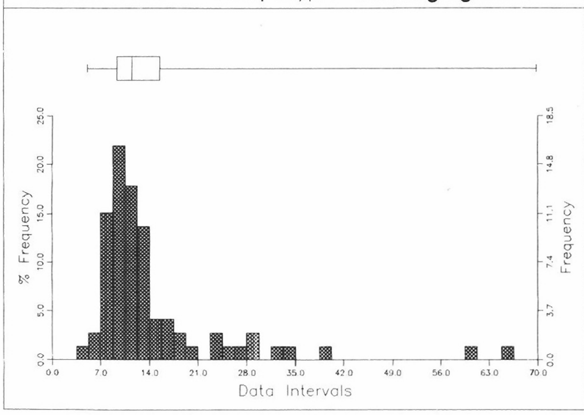

SiO2	
Samples	74.
Mean	15.53
Std. Dev.	12.30
Max	69.80
Min	5.10
Median	11.50
L Hinge	9.40
R Hinge	15.50

Dataset PR43 Sampletype: **Colluvium**

Al2O3

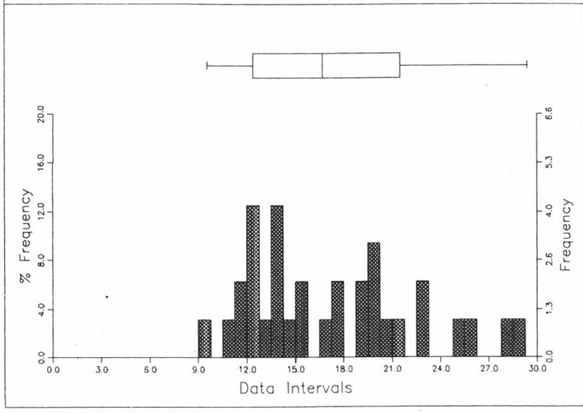

Samples	33.
Mean	17.57
Std. Dev.	5.63
Max	29.40
Min	9.56
Median	16.70
L Hinge	12.40
R Hinge	21.50

Dataset PR43 Sampletype: **Lateritic residuum**

Al2O3

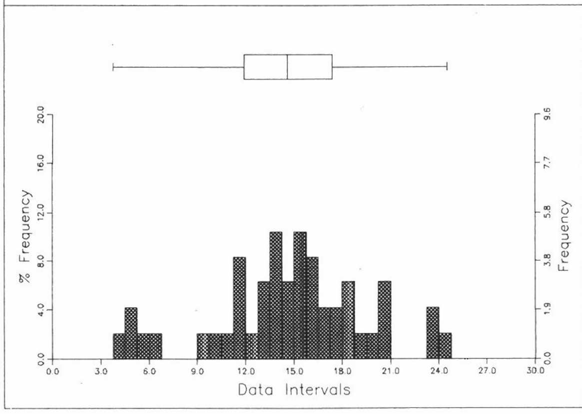

Samples	48.
Mean	14.67
Std. Dev.	4.74
Max	24.50
Min	3.76
Median	14.59
L Hinge	11.90
R Hinge	17.40

Dataset PR43 Sampletype: **Ferruginous saprolite**

Al2O3

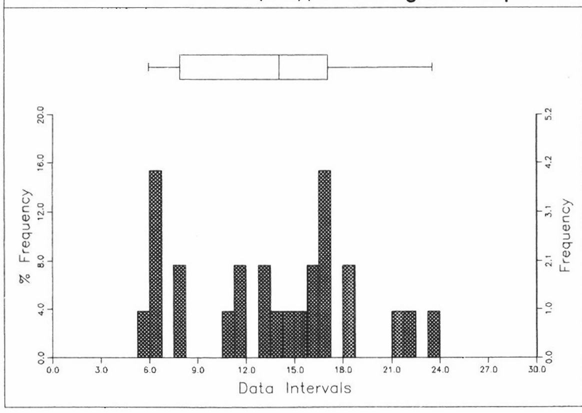

Samples	26.
Mean	13.66
Std. Dev.	5.25
Max	23.52
Min	5.97
Median	14.04
L Hinge	7.90
R Hinge	17.06

Dataset PR43 Sampletype: **Iron segregations**

Al2O3

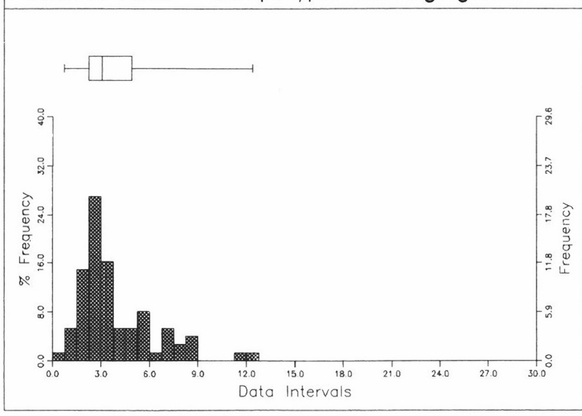

Samples	74.
Mean	3.87
Std. Dev.	2.38
Max	12.40
Min	0.72
Median	3.08
L Hinge	2.25
R Hinge	4.91

Dataset PR43 Sampletype: **Colluvium**

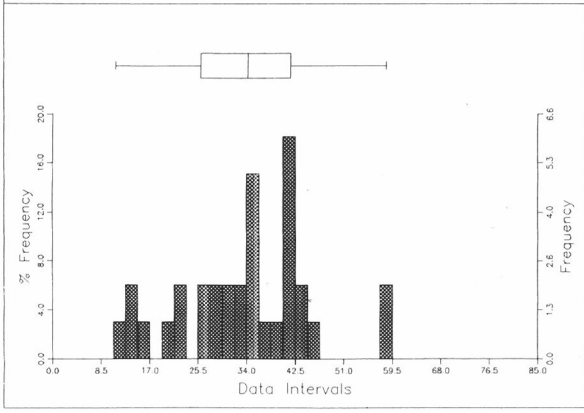

Fe2O3	
Samples	33.
Mean	33.54
Std. Dev.	11.41
Max	58.47
Min	11.14
Median	34.31
L Hinge	26.00
R Hinge	41.75

Dataset PR43 Sampletype: **Lateritic residuum**

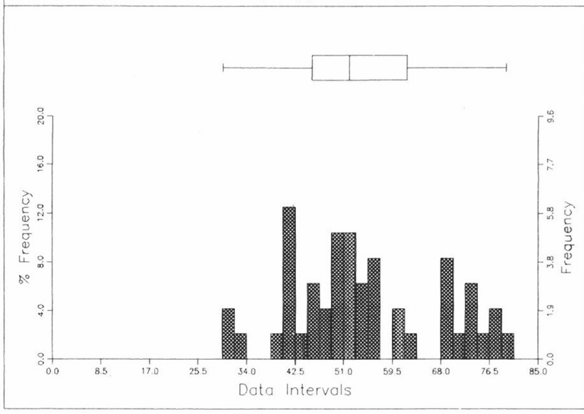

Fe2O3	
Samples	48.
Mean	54.44
Std. Dev.	12.92
Max	79.40
Min	29.88
Median	52.04
L Hinge	45.46
R Hinge	62.01

Dataset PR43 Sampletype: **Ferruginous saprolite**

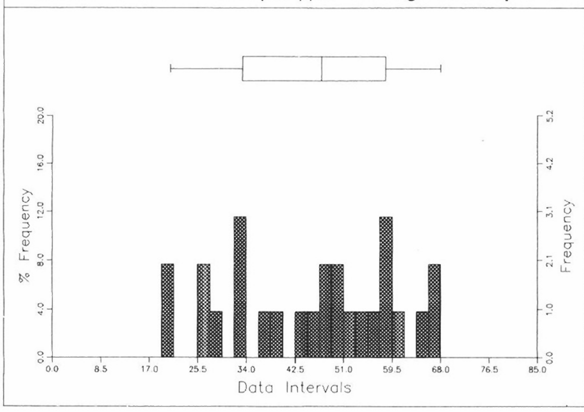

Fe2O3	
Samples	26.
Mean	45.62
Std. Dev.	14.50
Max	67.93
Min	20.69
Median	47.09
L Hinge	33.28
R Hinge	58.29

Dataset PR43 Sampletype: **Iron segregations**

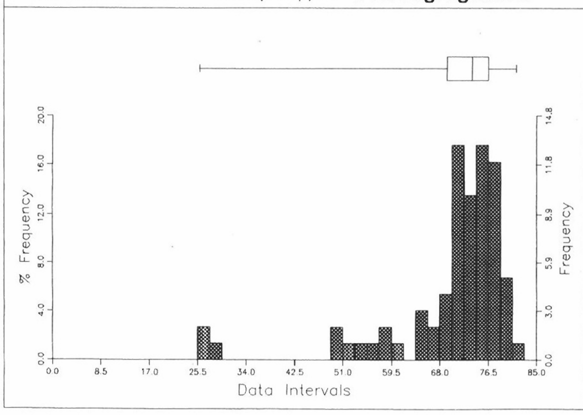

Fe2O3	
Samples	74.
Mean	69.96
Std. Dev.	11.32
Max	81.43
Min	25.88
Median	73.60
L Hinge	69.24
R Hinge	76.42

Dataset PR43 Sampletype: **Colluvium**

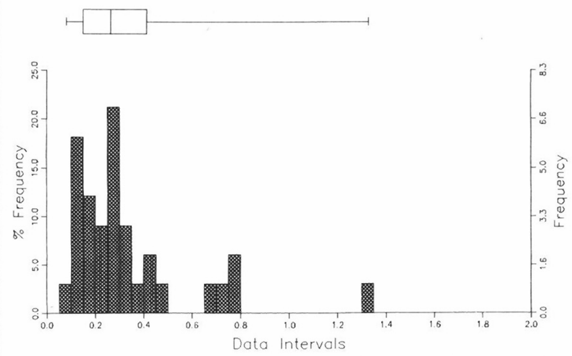

MgO	
Samples	33.
Mean	0.33
Std. Dev.	0.26
Max	1.33
Min	0.08
Median	0.26
L Hinge	0.15
R Hinge	0.41

Dataset PR43 Sampletype: **Lateritic residuum**

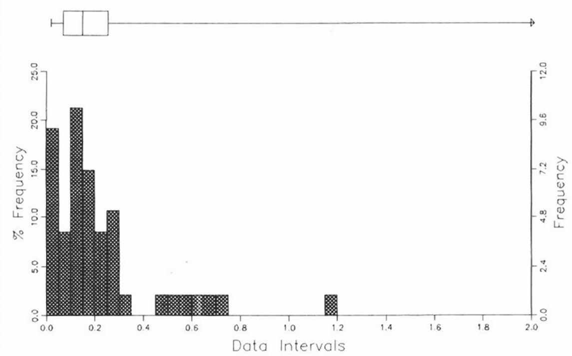

MgO	
Samples	48.
Mean	0.29
Std. Dev.	0.51
Max	3.42
Min	0.02
Median	0.15
L Hinge	0.07
R Hinge	0.26

Dataset PR43 Sampletype: **Ferruginous saprolite**

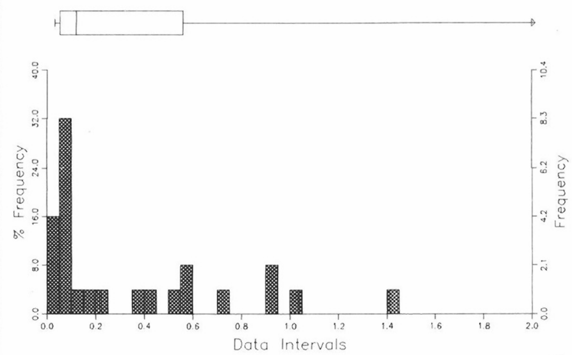

MgO	
Samples	26.
Mean	0.51
Std. Dev.	0.89
Max	4.48
Min	0.03
Median	0.12
L Hinge	0.05
R Hinge	0.56

Dataset PR43 Sampletype: **Iron segregations**

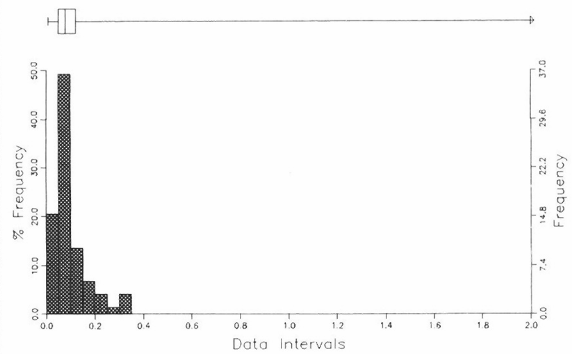

MgO	
Samples	74.
Mean	0.15
Std. Dev.	0.47
Max	4.09
Min	0.01
Median	0.08
L Hinge	0.05
R Hinge	0.12

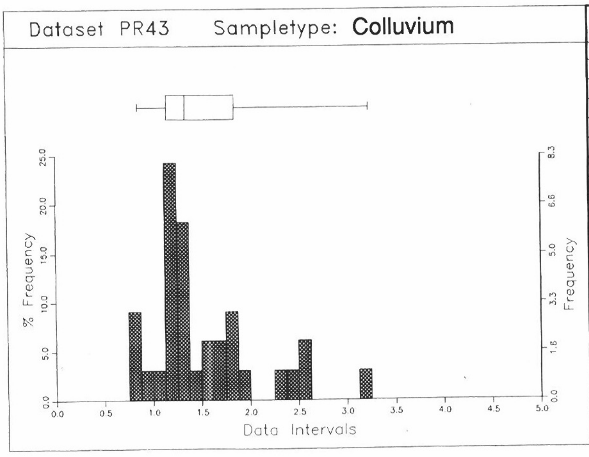

TiO2	
Samples	33.
Mean	1.53
Std. Dev.	0.56
Max	3.24
Min	0.85
Median	1.34
L Hinge	1.16
R Hinge	1.85

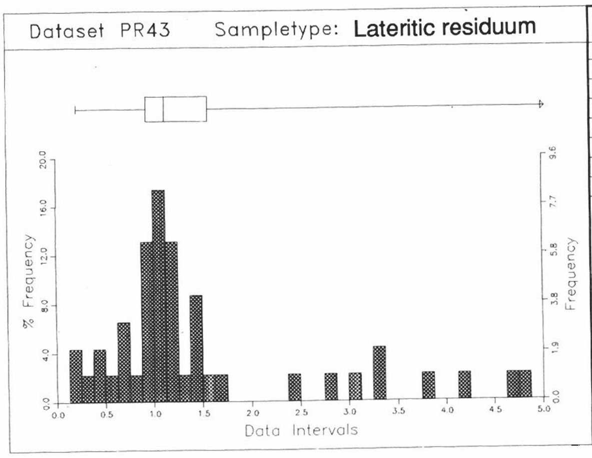

TiO2	
Samples	48.
Mean	1.72
Std. Dev.	1.58
Max	8.29
Min	0.22
Median	1.12
L Hinge	0.94
R Hinge	1.57

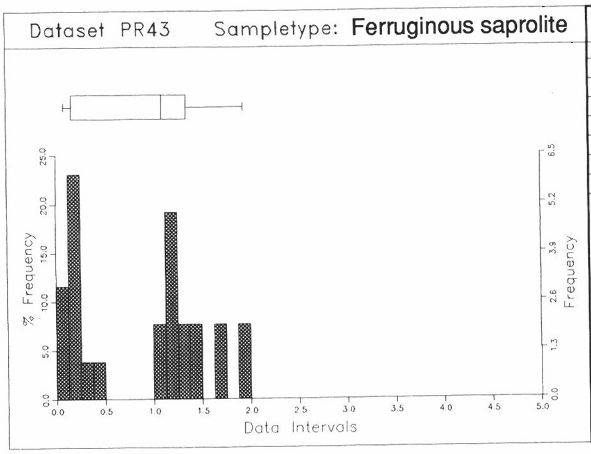

TiO2	
Samples	25.
Mean	0.88
Std. Dev.	0.64
Max	1.93
Min	0.09
Median	1.10
L Hinge	0.17
R Hinge	1.35

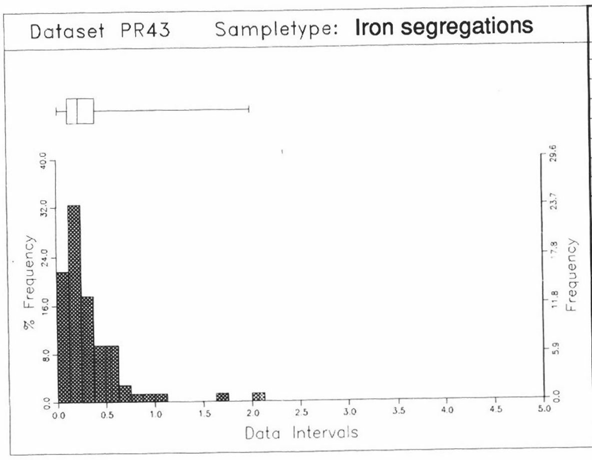

TiO2	
Samples	74.
Mean	0.33
Std. Dev.	0.34
Max	2.00
Min	0.02
Median	0.23
L Hinge	0.13
R Hinge	0.41

Dataset PR43 Sampletype: **Colluvium**

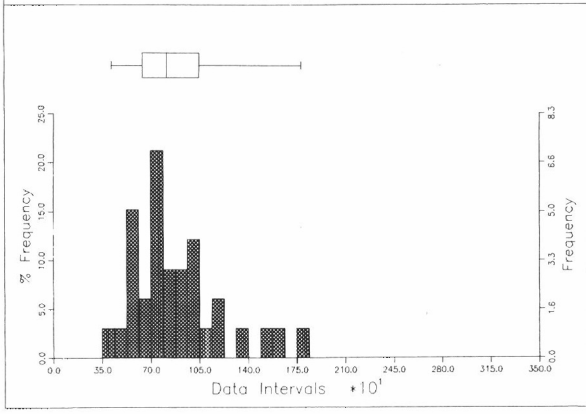

V	
Samples	33.
Mean	891.79
Std. Dev.	332.13
Max	1783.00
Min	417.00
Median	814.00
L Hinge	643.00
R Hinge	1047.00

Dataset PR43 Sampletype: **Lateritic residuum**

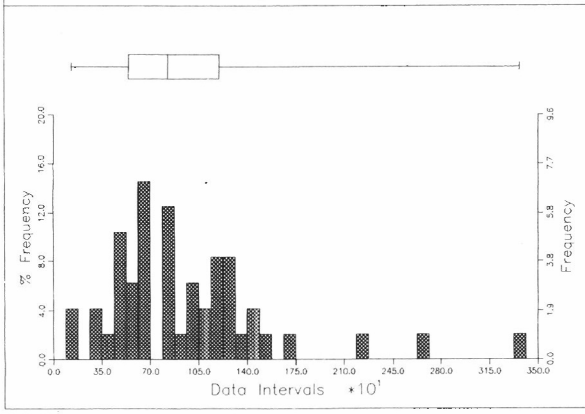

V	
Samples	48.
Mean	970.40
Std. Dev.	607.62
Max	3365.00
Min	132.00
Median	829.00
L Hinge	544.00
R Hinge	1199.00

Dataset PR43 Sampletype: **Ferruginous saprolite**

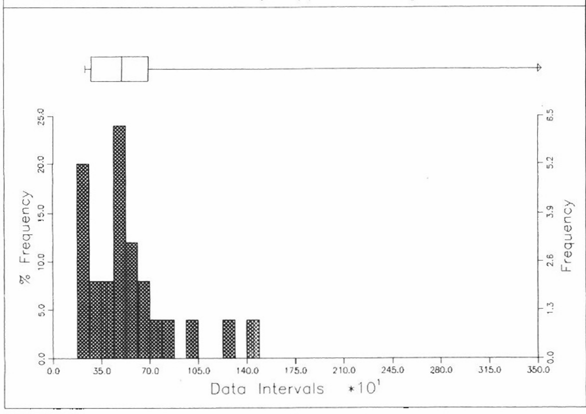

V	
Samples	26.
Mean	1666.04
Std. Dev.	5685.33
Max	29500.00
Min	234.00
Median	497.00
L Hinge	280.00
R Hinge	693.00

Dataset PR43 Sampletype: **Iron segregations**

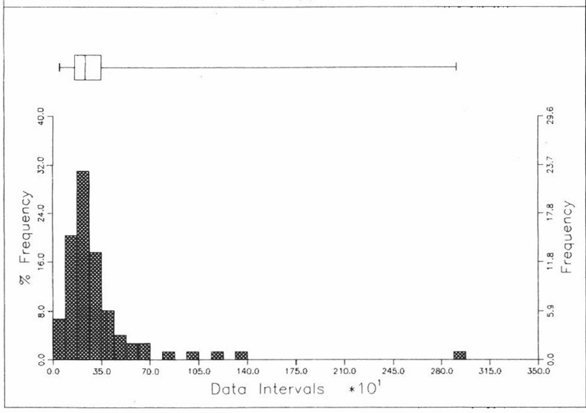

V	
Samples	74.
Mean	335.50
Std. Dev.	387.52
Max	2909.00
Min	47.00
Median	235.00
L Hinge	159.00
R Hinge	347.00

Dataset PR43 Sampletype: **Colluvium**

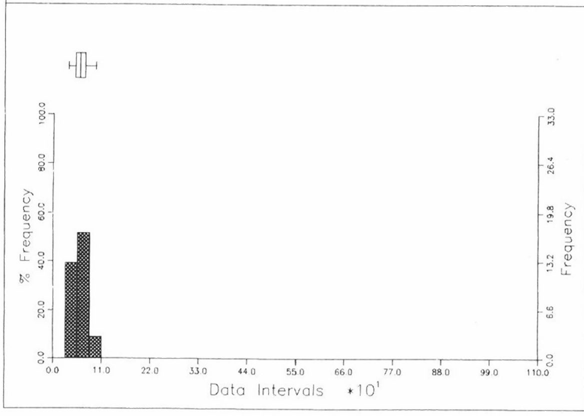

Cu	
Samples	33.
Mean	60.76
Std. Dev.	14.83
Max	96.00
Min	34.00
Median	60.00
L Hinge	50.00
R Hinge	72.00

Dataset PR43 Sampletype: **Lateritic residuum**

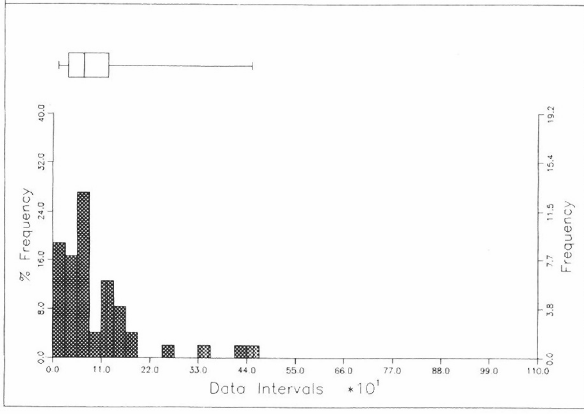

Cu	
Samples	48.
Mean	99.69
Std. Dev.	97.23
Max	450.00
Min	12.00
Median	70.00
L Hinge	34.00
R Hinge	125.00

Dataset PR43 Sampletype: **Ferruginous saprolite**

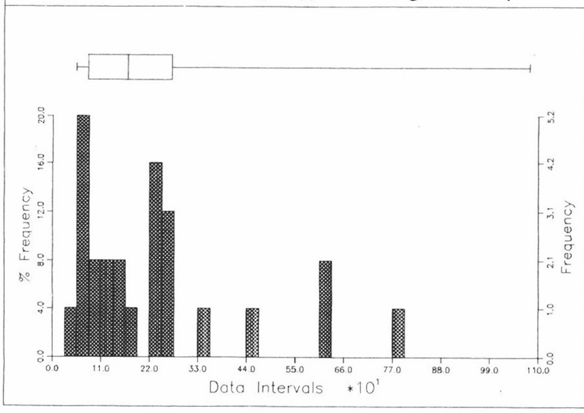

Cu	
Samples	26.
Mean	265.35
Std. Dev.	251.33
Max	1080.0
Min	54.00
Median	170.00
L Hinge	80.00
R Hinge	270.00

Dataset PR43 Sampletype: **Iron segregations**

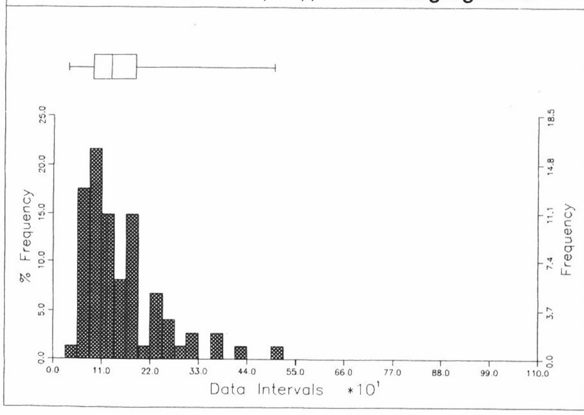

Cu	
Samples	74.
Mean	154.53
Std. Dev.	90.89
Max	500.00
Min	34.00
Median	130.00
L Hinge	90.00
R Hinge	185.00

Dataset PR43 Sampletype: **Colluvium**

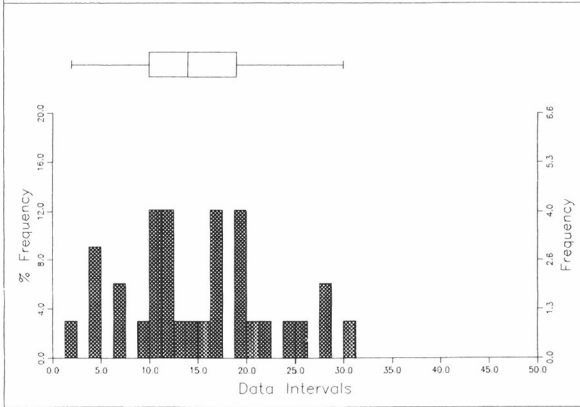

Pb	
Samples	33.
Mean	14.88
Std. Dev.	7.39
Max	30.00
Min	2.00
Median	14.00
L Hinge	10.00
R Hinge	19.00

Dataset PR43 Sampletype: **Lateritic residuum**

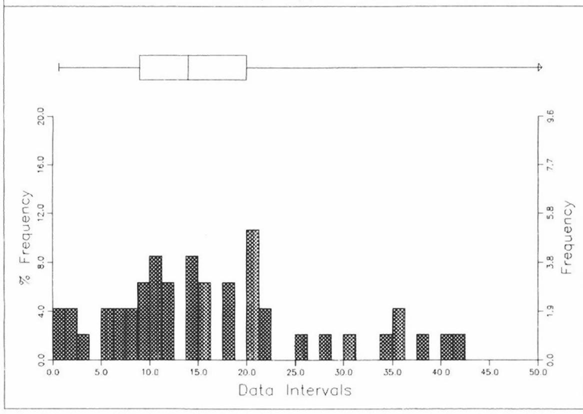

Pb	
Samples	48.
Mean	18.47
Std. Dev.	18.95
Max	125.00
Min	0.67
Median	14.00
L Hinge	9.00
R Hinge	20.00

Dataset PR43 Sampletype: **Ferruginous saprolite**

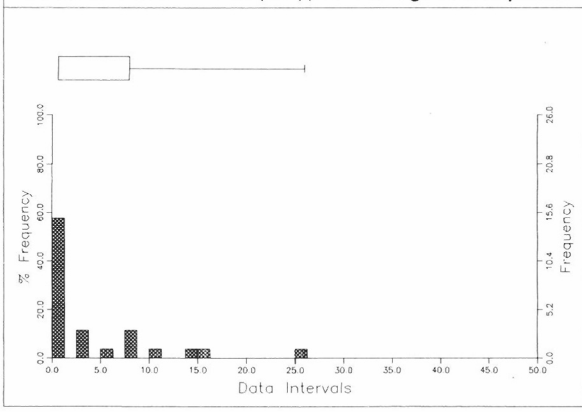

Pb	
Samples	26.
Mean	4.42
Std. Dev.	6.23
Max	26.00
Min	0.67
Median	0.67
L Hinge	0.67
R Hinge	8.00

Dataset PR43 Sampletype: **Iron segregations**

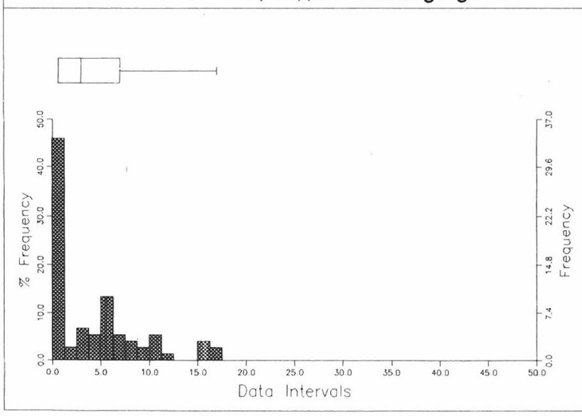

Pb	
Samples	74.
Mean	4.25
Std. Dev.	4.54
Max	17.00
Min	0.67
Median	3.00
L Hinge	0.67
R Hinge	7.00

Dataset PR43 Sampletype: **Colluvium**

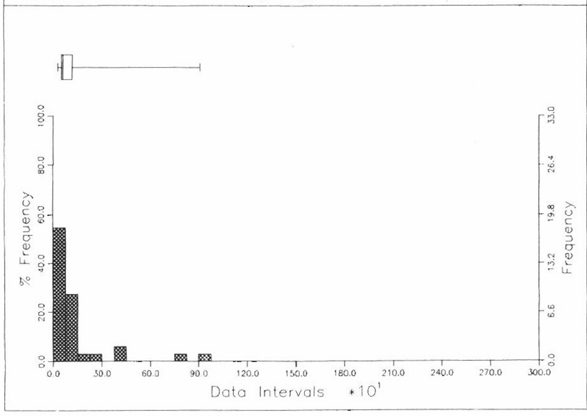

Ni	
Samples	33.
Mean	145.06
Std. Dev.	206.31
Max	910.00
Min	30.00
Median	62.00
L Hinge	52.00
R Hinge	120.00

Dataset PR43 Sampletype: **Lateritic residuum**

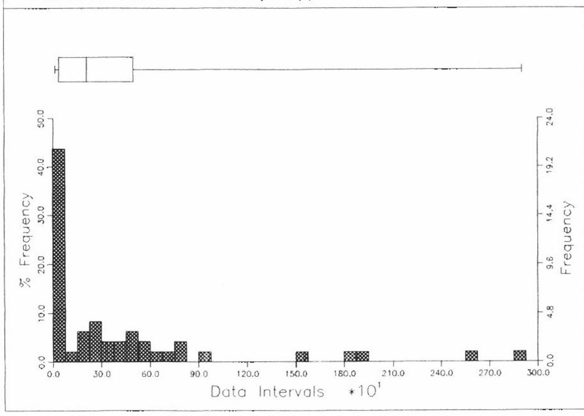

Ni	
Samples	48.
Mean	437.00
Std. Dev.	654.60
Max	2900.00
Min	16.00
Median	210.00
L Hinge	38.00
R Hinge	500.00

Dataset PR43 Sampletype: **Ferruginous saprolite**

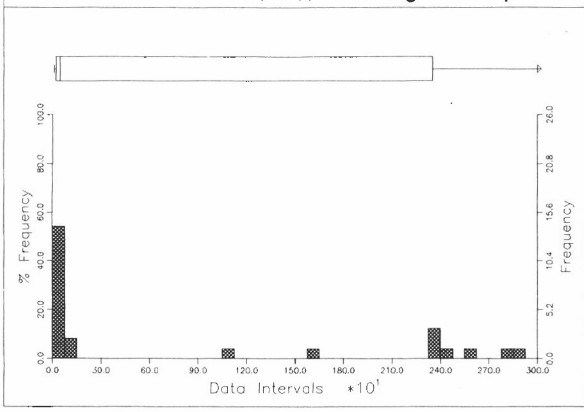

Ni	
Samples	26.
Mean	1191.08
Std. Dev.	1603.09
Max	5900.00
Min	10.00
Median	48.00
L Hinge	22.00
R Hinge	2350.00

Dataset PR43 Sampletype: **Iron segregations**

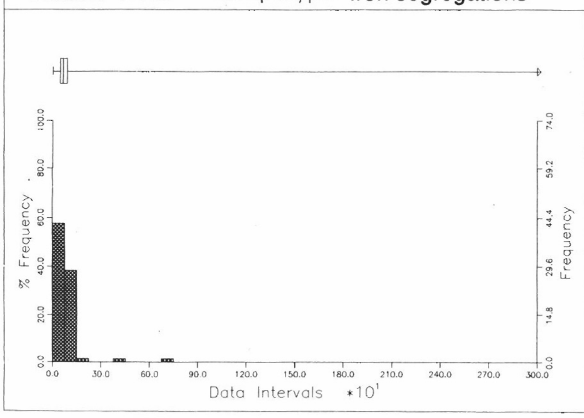

Ni	
Samples	74.
Mean	176.19
Std. Dev.	797.62
Max	6900.00
Min	4.00
Median	68.00
L Hinge	50.00
R Hinge	92.00

Dataset PR43 Sampletype: **Colluvium**

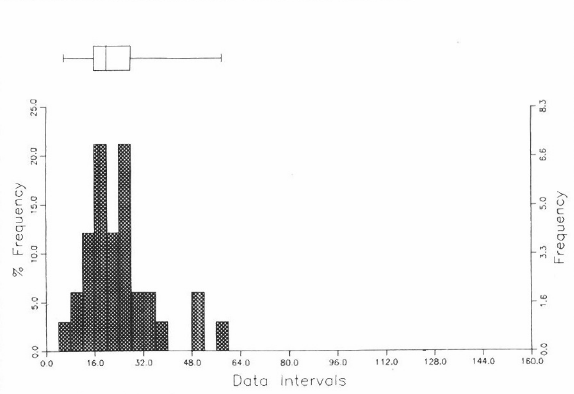

Co	
Samples	33.
Mean	23.67
Std. Dev.	11.77
Max	58.00
Min	6.00
Median	20.00
L Hinge	16.00
R Hinge	28.00

Dataset PR43 Sampletype: **Lateritic residuum**

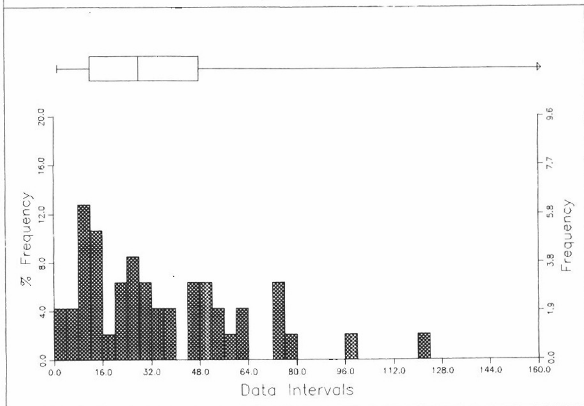

Co	
Samples	48.
Mean	38.24
Std. Dev.	36.41
Max	210.00
Min	1.33
Median	28.00
L Hinge	12.00
R Hinge	48.00

Dataset PR43 Sampletype: **Ferruginous saprolite**

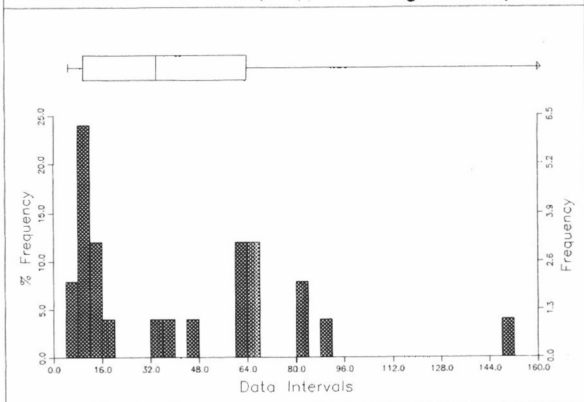

Co	
Samples	26.
Mean	50.12
Std. Dev.	60.64
Max	290.00
Min	5.00
Median	34.00
L Hinge	10.00
R Hinge	64.00

Dataset PR43 Sampletype: **Iron segregations**

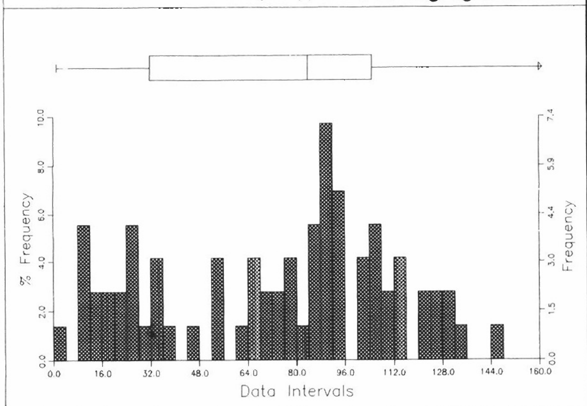

Co	
Samples	74.
Mean	82.09
Std. Dev.	81.61
Max	680.00
Min	1.33
Median	84.00
L Hinge	32.00
R Hinge	105.00

Dataset PR43 Sampletype: **Colluvium**

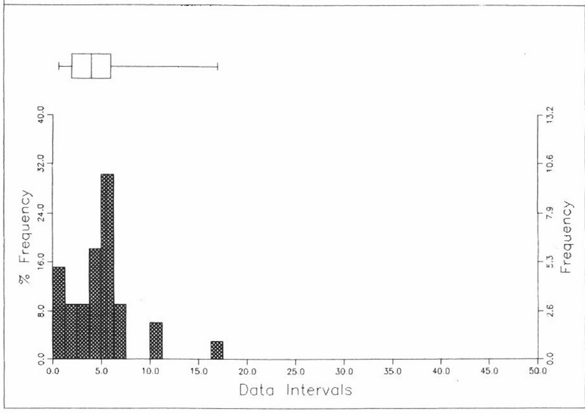

Sb	
Samples	33.
Mean	4.71
Std. Dev.	3.34
Max	17.00
Min	0.67
Median	4.00
L Hinge	2.00
R Hinge	6.00

Dataset PR43 Sampletype: **Lateritic residuum**

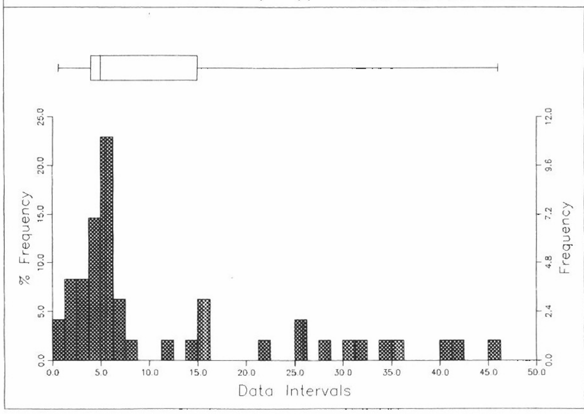

Sb	
Samples	48.
Mean	11.82
Std. Dev.	12.49
Max	46.00
Min	0.67
Median	5.00
L Hinge	4.00
R Hinge	15.00

Dataset PR43 Sampletype: **Ferruginous saprolite**

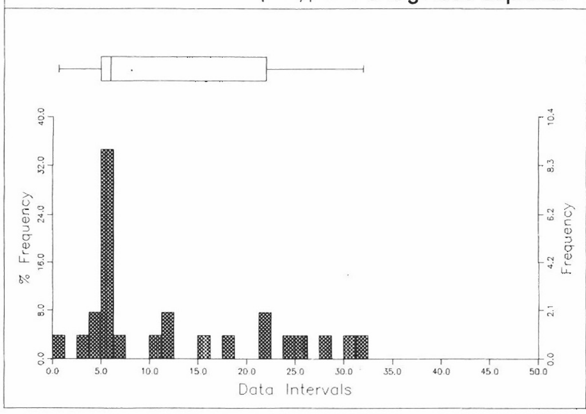

Sb	
Samples	26.
Mean	12.37
Std. Dev.	9.52
Max	32.00
Min	0.67
Median	6.00
L Hinge	5.00
R Hinge	22.00

Dataset PR43 Sampletype: **Iron segregations**

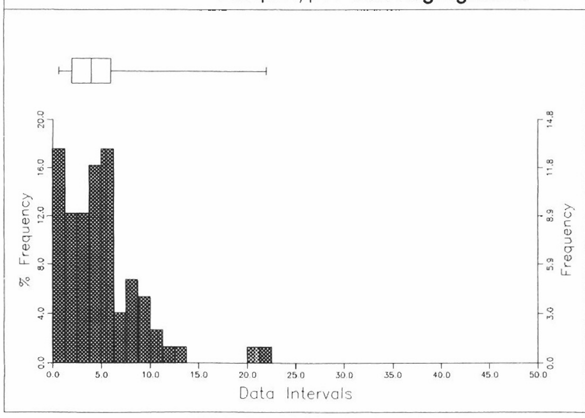

Sb	
Samples	74.
Mean	4.81
Std. Dev.	4.04
Max	22.00
Min	0.67
Median	4.00
L Hinge	2.00
R Hinge	6.00

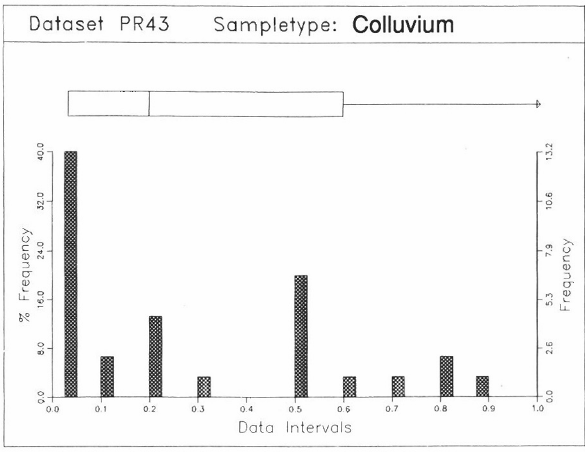

Ag	
Samples	33.
Mean	0.37
Std. Dev.	0.39
Max	1.50
Min	0.03
Median	0.20
L Hinge	0.03
R Hinge	0.60

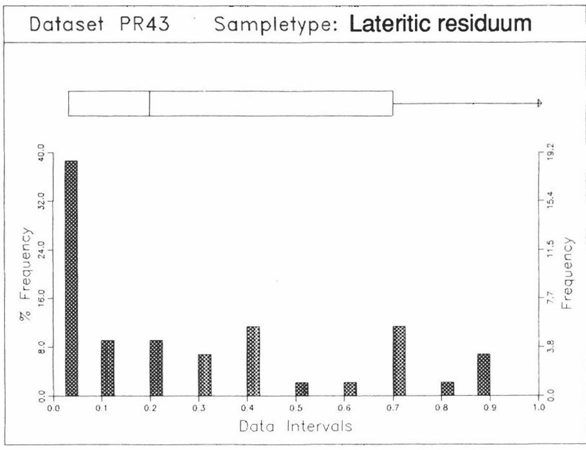

Ag	
Samples	48.
Mean	0.36
Std. Dev.	0.36
Max	1.20
Min	0.03
Median	0.20
L Hinge	0.03
R Hinge	0.70

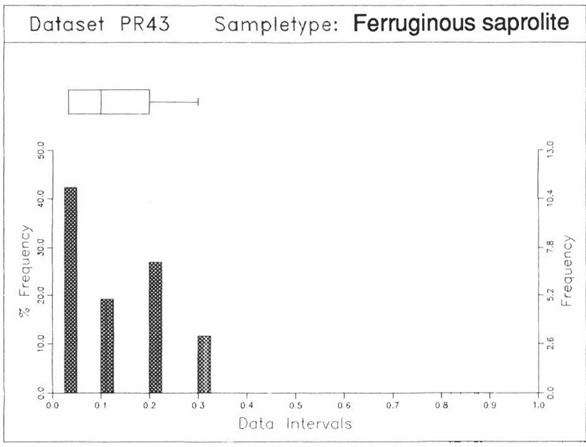

Ag	
Samples	26.
Mean	0.12
Std. Dev.	0.10
Max	0.30
Min	0.03
Median	0.10
L Hinge	0.03
R Hinge	0.20

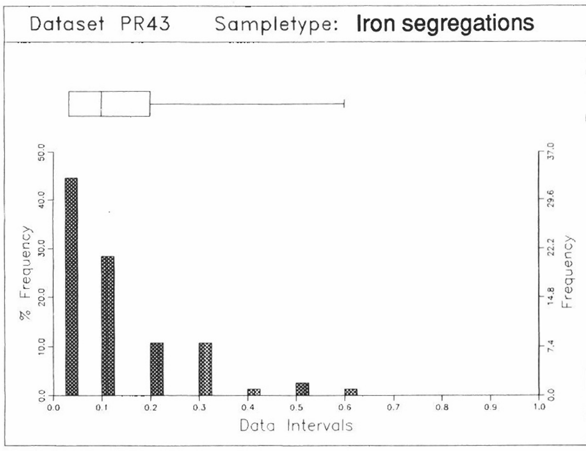

Ag	
Samples	74.
Mean	0.12
Std. Dev.	0.13
Max	0.60
Min	0.03
Median	0.10
L Hinge	0.03
R Hinge	0.20

Dataset PR43 Sampletype: **Colluvium**

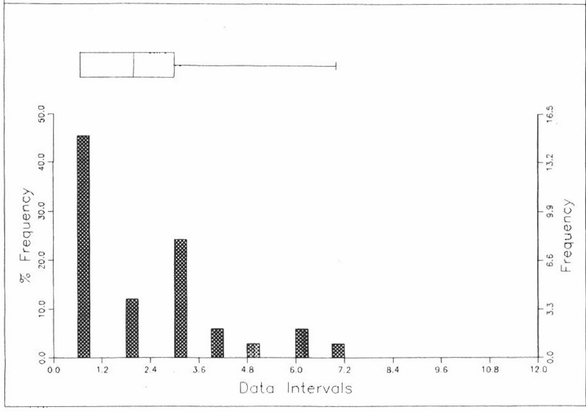

Sn	
Samples	33.
Mean	2.24
Std. Dev.	1.83
Max	7.00
Min	0.67
Median	2.00
L Hinge	0.67
R Hinge	3.00

Dataset PR43 Sampletype: **Lateritic residuum**

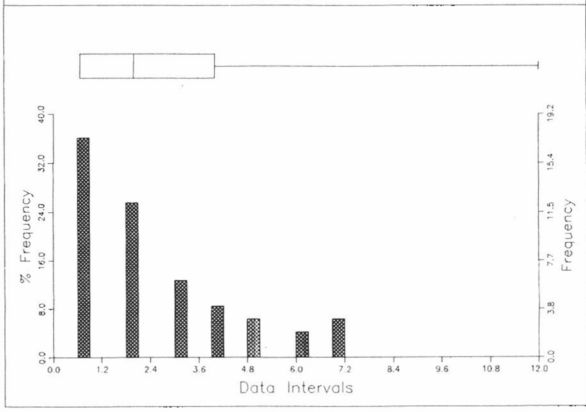

Sn	
Samples	48.
Mean	2.69
Std. Dev.	2.37
Max	12.00
Min	0.67
Median	2.00
L Hinge	0.67
R Hinge	4.00

Dataset PR43 Sampletype: **Ferruginous saprolite**

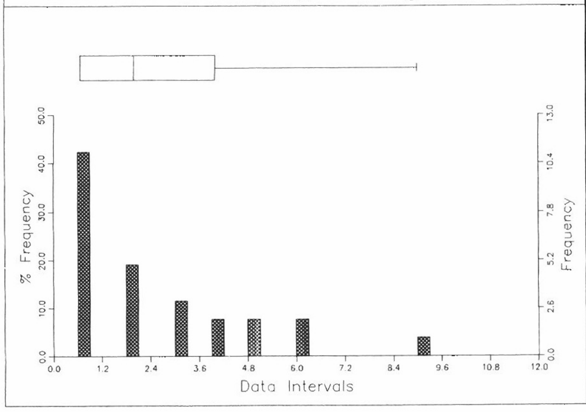

Sn	
Samples	26.
Mean	2.51
Std. Dev.	2.22
Max	9.00
Min	0.67
Median	2.00
L Hinge	0.67
R Hinge	4.00

Dataset PR43 Sampletype: **Iron segregations**

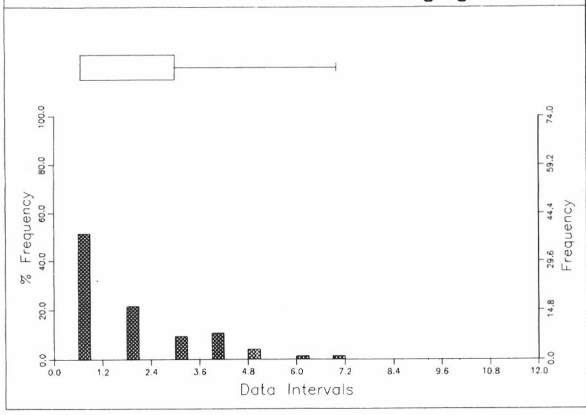

Sn	
Samples	74.
Mean	1.87
Std. Dev.	1.54
Max	7.00
Min	0.67
Median	0.67
L Hinge	0.67
R Hinge	3.00

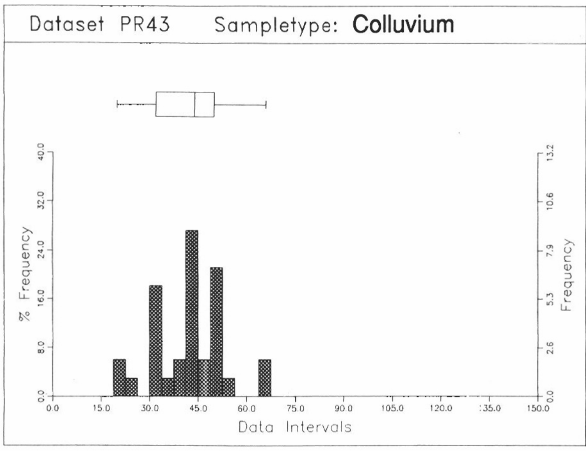

Ga	
Samples	33.
Mean	42.24
Std. Dev.	10.95
Max	66.00
Min	20.00
Median	44.00
L Hinge	32.00
R Hinge	50.00

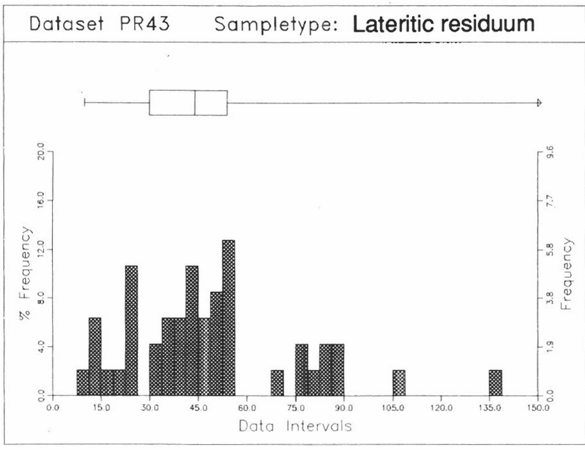

Ga	
Samples	48.
Mean	51.15
Std. Dev.	33.52
Max	195.00
Min	10.00
Median	44.00
L Hinge	30.00
R Hinge	54.00

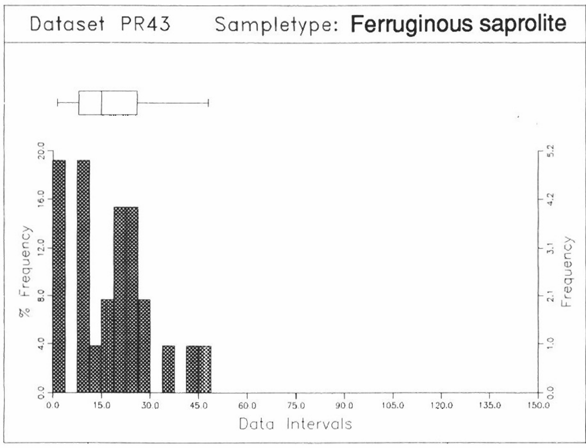

Ga	
Samples	26.
Mean	17.64
Std. Dev.	12.65
Max	48.00
Min	1.33
Median	15.00
L Hinge	8.00
R Hinge	26.00

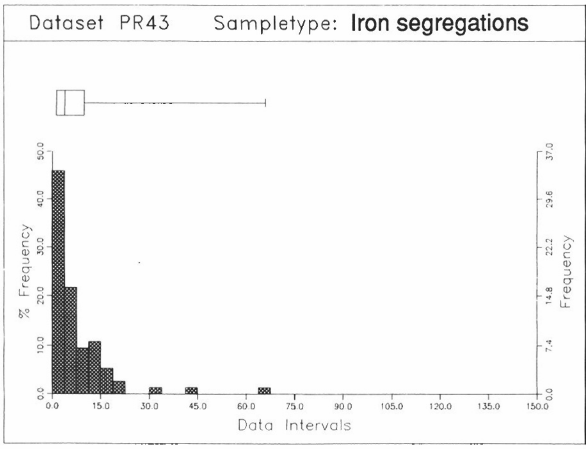

Ga	
Samples	74.
Mean	7.27
Std. Dev.	10.15
Max	66.00
Min	1.33
Median	4.00
L Hinge	1.33
R Hinge	10.00

Dataset PR43 Sampletype: **Colluvium**

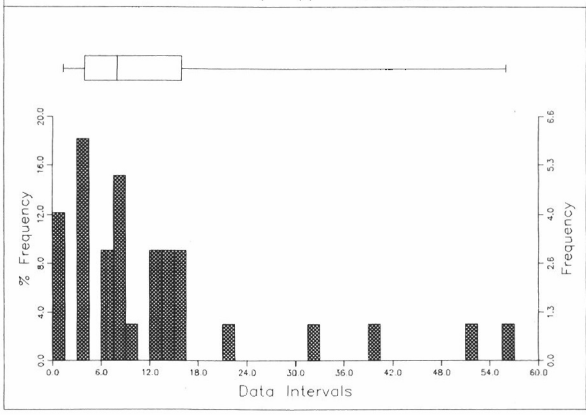

W	
Samples	33.
Mean	12.89
Std. Dev.	13.56
Max	56.00
Min	1.33
Median	8.00
L Hinge	4.00
R Hinge	16.00

Dataset PR43 Sampletype: **Lateritic residuum**

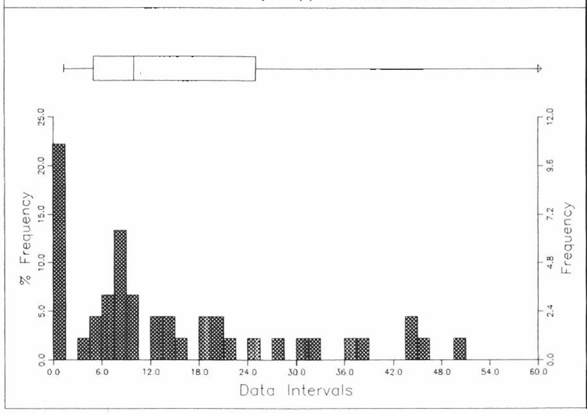

W	
Samples	48.
Mean	20.13
Std. Dev.	26.07
Max	130.00
Min	1.33
Median	10.00
L Hinge	5.00
R Hinge	25.00

Dataset PR43 Sampletype: **Ferruginous saprolite**

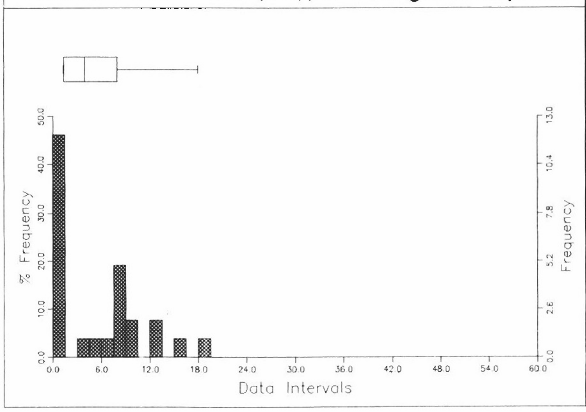

W	
Samples	26.
Mean	5.69
Std. Dev.	4.95
Max	18.00
Min	1.33
Median	4.00
L Hinge	1.33
R Hinge	8.00

Dataset PR43 Sampletype: **Iron segregations**

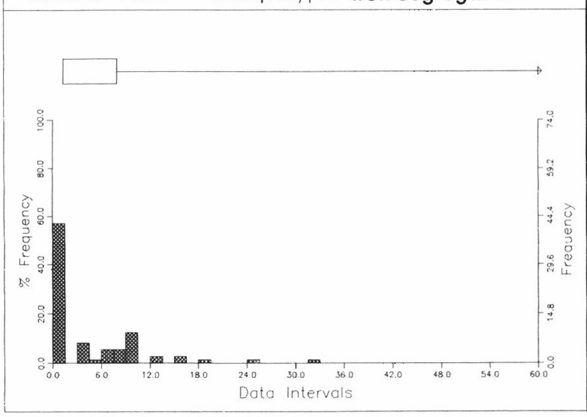

W	
Samples	74.
Mean	23.23
Std. Dev.	130.43
Max	1100.00
Min	1.33
Median	1.33
L Hinge	1.33
R Hinge	8.00

Dataset PR43 Sampletype: **Colluvium**

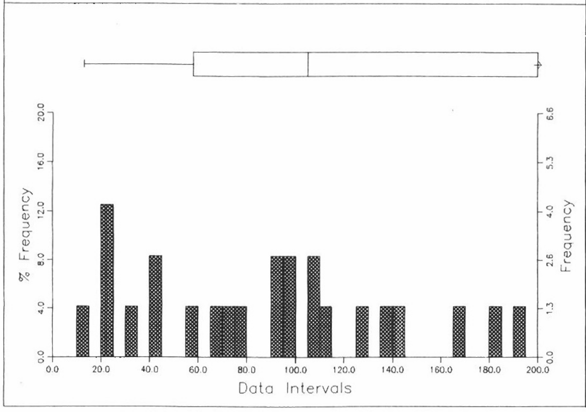

Ba	
Samples	33.
Mean	193.45
Std. Dev.	207.31
Max	894.00
Min	13.00
Median	105.00
L Hinge	58.00
R Hinge	329.00

Dataset PR43 Sampletype: **Lateritic residuum**

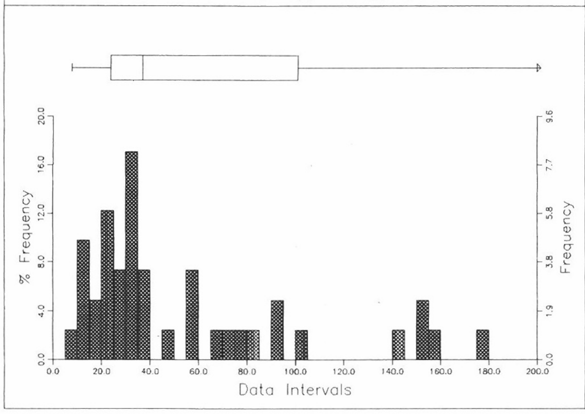

Ba	
Samples	48.
Mean	220.02
Std. Dev.	843.31
Max	5861.00
Min	8.00
Median	37.00
L Hinge	24.00
R Hinge	101.00

Dataset PR43 Sampletype: **Ferruginous saprolite**

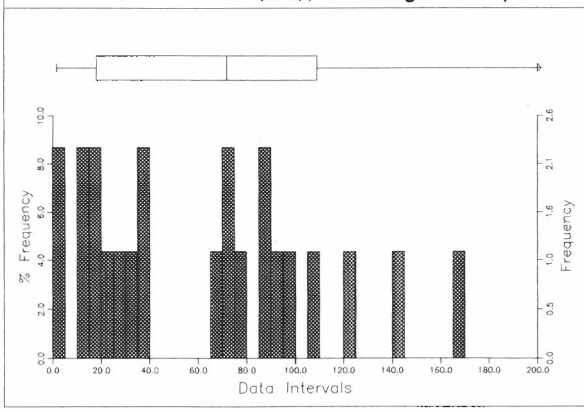

Ba	
Samples	26.
Mean	100.32
Std. Dev.	124.91
Max	551.00
Min	1.67
Median	72.00
L Hinge	18.00
R Hinge	109.00

Dataset PR43 Sampletype: **Iron segregations**

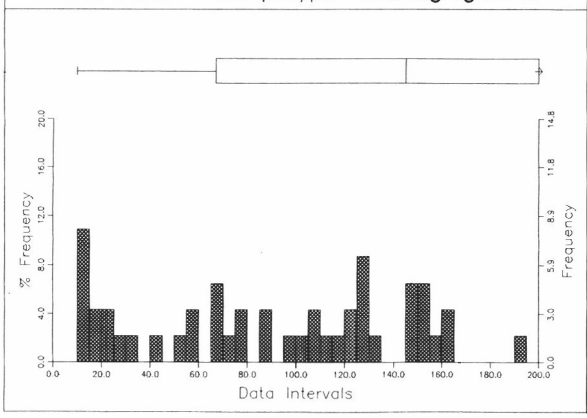

Ba	
Samples	74.
Mean	404.53
Std. Dev.	736.48
Max	3373.00
Min	10.00
Median	145.00
L Hinge	67.00
R Hinge	308.00

Dataset PR43 Sampletype: **Colluvium**

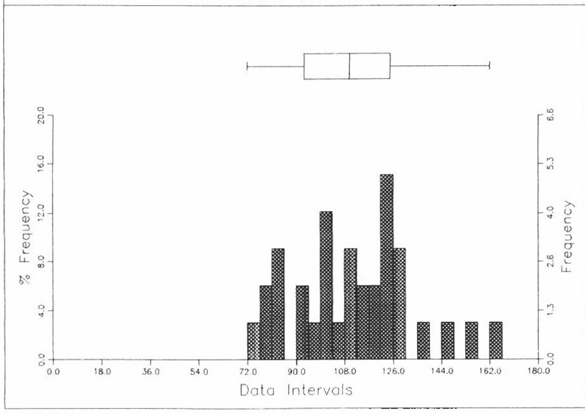

Zr	
Samples	33.
Mean	111.21
Std. Dev.	22.14
Max	162.00
Min	72.00
Median	110.00
L Hinge	93.00
R Hinge	125.00

Dataset PR43 Sampletype: **Lateritic residuum**

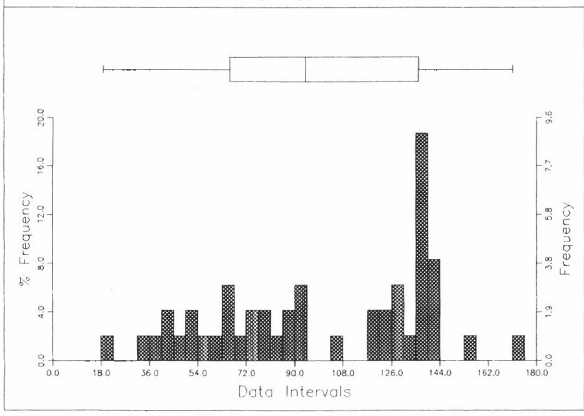

Zr	
Samples	48.
Mean	99.98
Std. Dev.	39.03
Max	171.00
Min	19.00
Median	94.00
L Hinge	66.00
R Hinge	136.00

Dataset PR43 Sampletype: **Ferruginous saprolite**

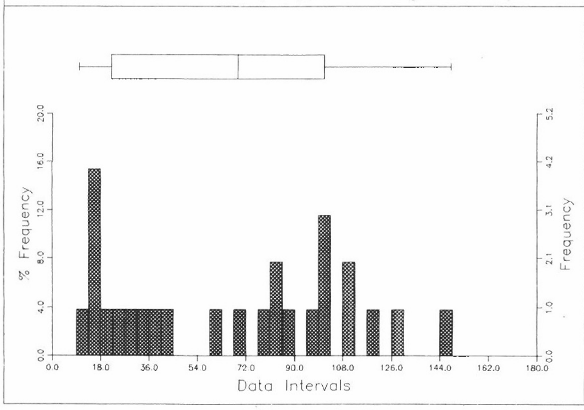

Zr	
Samples	26.
Mean	66.96
Std. Dev.	41.90
Max	148.00
Min	10.00
Median	69.00
L Hinge	22.00
R Hinge	101.00

Dataset PR43 Sampletype: **Iron segregations**

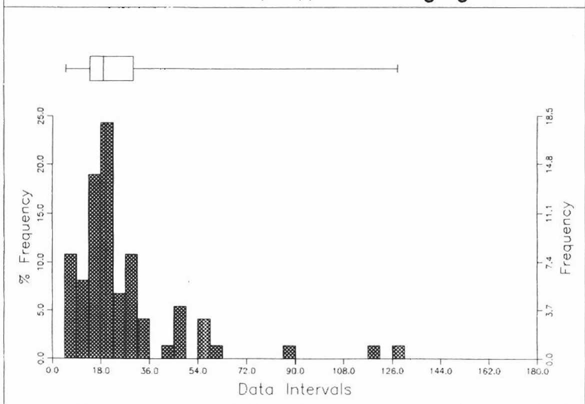

Zr	
Samples	74.
Mean	26.22
Std. Dev.	22.12
Max	128.00
Min	5.00
Median	19.00
L Hinge	14.00
R Hinge	30.00

Dataset PR43 Sampletype: **Colluvium**

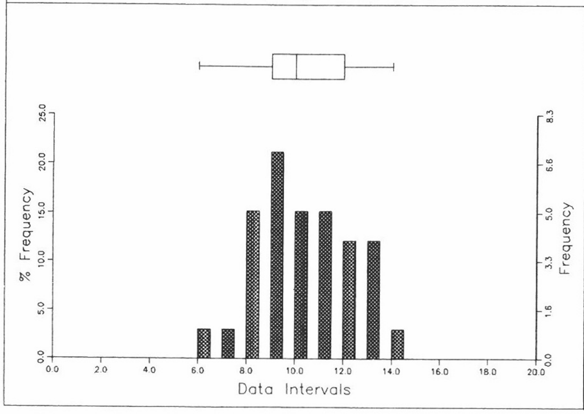

Nb	
Samples	33.
Mean	10.15
Std. Dev.	1.97
Max	14.00
Min	6.00
Median	10.00
L Hinge	9.00
R Hinge	12.00

Dataset PR43 Sampletype: **Lateritic residuum**

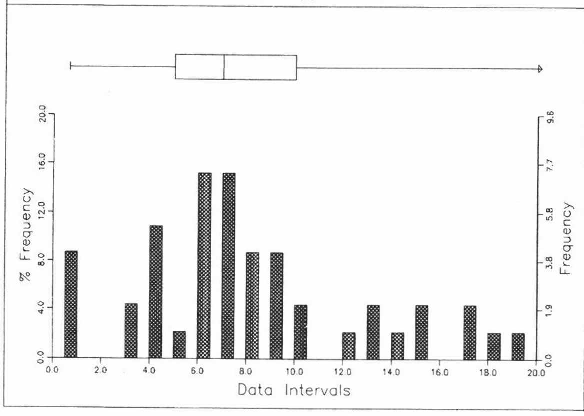

Nb	
Samples	48.
Mean	8.70
Std. Dev.	5.86
Max	28.00
Min	0.67
Median	7.00
L Hinge	5.00
R Hinge	10.00

Dataset PR43 Sampletype: **Ferruginous saprolite**

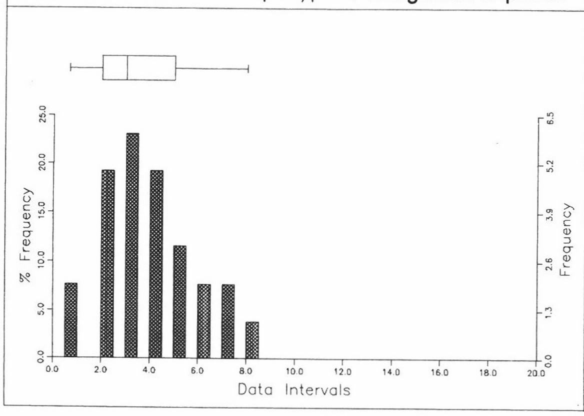

Nb	
Samples	26.
Mean	3.78
Std. Dev.	1.92
Max	8.00
Min	0.67
Median	3.00
L Hinge	2.00
R Hinge	5.00

Dataset PR43 Sampletype: **Iron segregations**

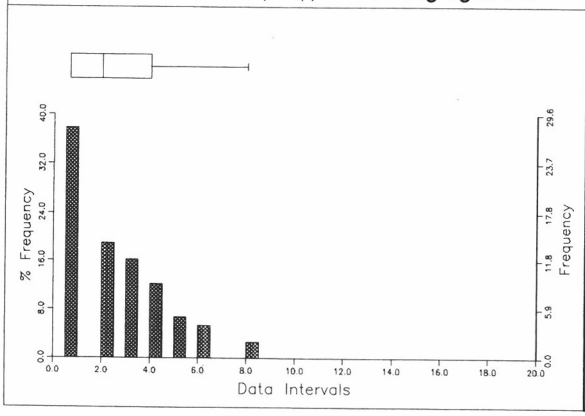

Nb	
Samples	74.
Mean	2.48
Std. Dev.	1.89
Max	8.00
Min	0.67
Median	2.00
L Hinge	0.67
R Hinge	4.00